University of Nebraska - Lincoln
DigitalCommons@University of Nebraska - Lincoln

Construction Systems -- Dissertations & Theses | Construction Systems

Summer 7-19-2012

Efficient Prestressed Concrete-Steel Composite Girder for Medium-Span Bridges

Yaohua Deng
University of Nebraska-Lincoln, jimdeng@iastate.edu

Follow this and additional works at: https://digitalcommons.unl.edu/constructiondiss

Part of the Construction Engineering and Management Commons

Deng, Yaohua, "Efficient Prestressed Concrete-Steel Composite Girder for Medium-Span Bridges" (2012). *Construction Systems -- Dissertations & Theses*. 9.
https://digitalcommons.unl.edu/constructiondiss/9

This Article is brought to you for free and open access by the Construction Systems at DigitalCommons@University of Nebraska - Lincoln. It has been accepted for inclusion in Construction Systems -- Dissertations & Theses by an authorized administrator of DigitalCommons@University of Nebraska - Lincoln.

EFFICIENT PRESTRESSED CONCRETE-STEEL COMPOSITE GIRDER FOR MEDIUM-SPAN BRIDGES

by

Yaohua Deng

A DISSERTATION

Presented to the Faculty of

The Graduate College at the University of Nebraska

In Partial Fulfillment of Requirements

For the Degree of Doctor of Philosophy

Major: Engineering

(Construction)

Under the Supervision of Professor George Morcous

Lincoln, Nebraska

August, 2012

Efficient Prestressed Concrete-Steel Composite Girder for Medium-Span Bridges

Yaohua Deng, Ph.D.

University of Nebraska, 2012

Adviser: George Morcous

In this dissertation, a new Prestressed Concrete-Steel Composite (PCSC) girder system is introduced. The PCSC girder is composed of a lightweight W-shape steel section with shear studs on its top and bottom flanges to achieve composite action with the pretensioned concrete bottom flange and the cast-in-place concrete deck. The PCSC girder is lightweight, economical, durable and easy to fabricate. To prove its feasibility and potential, this study is to investigate design and fabrication issues associated with the PCSC girder. A service design procedure is proposed using Age-adjusted Elasticity Modulus Method (AEMM) to evaluate the time-dependent stresses and strains in the PCSC girder due to creep and shrinkage effects of concrete and relaxation of strands. The strength design method, as a rational approach replacing the current working stress method, is proposed for the design of PCSC girders at prestress release, to assist engineers to accomplish economic design and production of PCSC girders. Finite Element Analysis (FEA) of PCSC girders at prestress release is performed to understand stress distributions and the transfer of the prestressing force from the strands to the composite section and investigate the influence of stud distribution on the stresses in the concrete bottom flange. A PCSC girder specimen was successfully fabricated and instrumented in the structural lab following the proposed fabrication procedure. Design

using AEMM and FEA were validated against the strain profiles at different sections, concrete surface strains and camber at mid-span. Flexural and shear tests were conducted to evaluate the flexural and shear capacities of the fabricated specimen. The crack moment, ultimate moment and ultimate shear obtained in tests satisfy the demand of bridge girders and well predicted using design calculations.

Dedication

To My Parents

Acknowledgements

I would like to thank Dr. George Morcous, my research advisor and chair of my dissertation committee, for his academic, financial and emotional support throughout my PhD's study at the University of Nebraska Lincoln. He has great influences on me not limited to technical writing, how to think in research, and how to give presentation. It has been a journey to accomplish this dissertation while Dr. Morcous has been an ideal traveling companion.

My appreciations go to a member of my doctoral committee, Dr. Christopher Y. Tuan, as my former advisor, due to his endless support, encouragement, and patience throughout my graduate study. Under his supervision, I extensively developed my writing skills of journal papers and made some academic achievements.

Special thanks go to Dr. Maher K. Tadros for always offering constructive suggestions during the journey of my dissertation. In addition, he sets an excellent example for me to be a good researcher and teacher and always shares his many years' wisdom.

I would like to thank Dr. Yong K. Cho, a member of my committee for reviewing my dissertation and giving useful suggestions.

Special thanks go to Prof. Foster for offering the assistantship and revising the Powerpoint of my presentation. Thanks to Dr. Terri Norton for providing the assistantship when I was really in need.

I would like to thank graduate colleagues and lab technicians for their assistance during experimental testing and study: Afshin Hatami, Jenna Hansen, Ibrahim Lotfy,

Eliya Henin, Peter Samir, Nathanael Toenies, Kelvin Lein, and Jeff Svatora. I will always cherish the memories of working together as a group.

I would like to express my gratitude to my parents, for their love, inspiration and unconditional support. I am indebted to my wife, Chuanli Zhou, for her love, patience and support. None of my graduate achievements would have been possible without their commitment and understanding at all times.

Table of Contents

Dedication ..... **i**

Acknowledgements ..... **ii**

List of Figures ..... **viii**

List of Tables ..... **xii**

Chapter 1 Introduction **1**

1.1 Problem Statement ***1***

1.2 Objectives ***3***

1.3 Organization ***4***

Chapter 2 Literature Review **6**

2.1 Introduction ***6***

2.2 Existing Prestressed Composite Girders ***6***

2.2.1 Type I Prestressed Composite Girder System *6*

2.2.2 Type II Prestressed Composite Girder System *13*

2.2.3 Type III Prestressed Composite Girder System *15*

2.2.4 Type IV Prestressed Composite Girder System *19*

2.3 Literature on Transfer and Development Lengths of Prestressing Strands ***27***

2.4 Literature on the Behavior of Stud Shear Connectors ***31***

2.5 Summary ***34***

Chapter 3 System Description and Design of PCSC Girders **36**

3.1 Introduction ***36***

3.2 System Description ***36***

3.2.1 Fabrication Procedure *37*

3.2.2 Advantages of PCSC girder *38*

3.3 System Design ***39***

3.4 Service Design Procedure for PCSC Girders ***41***

3.4.1 Effects of Creep and Shrinkage of Concrete and Relaxation of Strands *41*

3.4.2 Analytical Procedure for Calculating Stresses and Strains in PCSC Girders *45*

3.5 Design Examples of PCSC Girders and Comparisons ***49***

3.6 Summary and Conclusions ***64***

Chapter 4 Strength Design of PCSC Girders at Prestress Release **67**

4.1 Introduction ***67***

4.2 Formulation of Design Equations ***69***

4.3 Design Procedure and Examples ***78***

4.3.1 Proposed Procedure *78*

4.3.2 Design Examples and Comparison with Working Stress Design Method *80*

4.4 Summary and Conclusions ***82***

Chapter 5 Finite Element Analysis of PCSC Girders **83**

5.1 Introduction ***83***

5.2 Approaches of Finite Element Analysis ***83***

5.2.1 Material Models *83*

5.2.2 Element Models *88*

5.2.3 Loading, Boundary Conditions and Convergences *93*

5.3 Modeling and Validation of Bond between Concrete and Strand in Prisms ***94***

5.3.1 Tests by Morcous et al. (2011) *95*

5.3.2 Comparison between FEA Predictions and Test Results *96*

5.3.3 Comparison between FEA Predictions and Design Calculations 99

5.4 Examples of FEA of PCSC Girders 99

5.4.1 FEA of a PCSC Girder 99

5.4.2 FEA Predictions 101

5.5 Influences of Amount and Distribution of Studs 108

5.6 Summary and Conclusions 110

Chapter 6 Experimental Investigation and Validations 114

6.1 Introduction 114

6.2 Design of a PCSC Girder Specimen 114

6.3 Fabrication of a PCSC Girder Specimen and Measurements 116

6.3.1 Prestressing System and Devices 116

6.3.2 Girder Fabrication and Measurements 121

6.4 Flexural and Shear Tests 134

6.5 Test Results and Validation of Design Methods and FEA 139

6.5.1 Prestress Release and Measurements Afterwards 139

6.5.2 Flexural and Shear Tests 147

6.6 Summary and Conclusions 160

Chapter 7 Summary, Conclusions and Recommendations 163

7.1 Summary 163

7.2 Conclusions 164

7.3 Recommendations 165

References 167

Table of Contents for Appendices 173

Appendix A – Design Example of the PCSC-36 Girder for a Bridge 174

A.1 Calculations of Properties, Loads and Coefficients.....174

A.1.1 Section Properties and Materials 175

A.1.2 Calculating Loads.....177

A.1.3 Relaxation of Strands, Creep Coefficient, Shrinkage and Aging Coefficient ..179

A.2 Girder design 185

A.2.1 Service Strength Design.....185

A.2.2 Ultimate Strength Design.....206

A.2.3 Horizontal Shear Design 209

A.3 Deck Design.....211

A.4 Deflection Criteria.....211

Appendix B – Strength Design Example of the PCSC-36 Girder at Release 213

B.1 Strength Design at Release 214

B.2 Service Design at Release.....220

List of Figures

Fig. 1.1 – Stringer/multi-Girder Bridge System (FHWA, 2011) 1

Fig. 1.2 – Stringer/Multi-Girders 3

Fig. 2.1 – Type I Prestressed Composite Girder System 9

Fig. 2.2 – Typical Profiles of Corrugated Steel Plates (Yazeed and Ahmed, 2001) 10

Fig. 2.3 – Type II Prestressed Composite Girder 14

Fig. 2.4 – Type III Prestressed Composite Girder 19

Fig. 2.5 – Type IV Prestressed Composite Girder 20

Fig. 2.6 – Fabrication of Type IV Girder 21

Fig. 2.7 – U-shape Concrete Deck with the Preflex Girder (Staquet et al., 2004) 23

Fig. 2.8 – Preflex Girders with VPHC and HPC (Staquet et al., 2010) 26

Fig. 2.9 – Idealized Stress versus Distance from End of Member (AASHTO, 2007) 29

Fig. 3.1 – PCSC Girder System 37

Fig. 3.2 – Fabrication Procedure of the PCSC Girder System 38

Fig. 3.3 – Design Example of a Bridge 50

Fig. 3.4 – Sections of PCSC, Prestressed Concrete and Steel Girders (in.) 51

Fig. 3.5 – Concrete Ages at Different Stages and Intervals 53

Fig. 3.6 – Stress Profiles in the PCSC Girder at Different Stages and Intervals (Stress in ksi, Negative in Tension) 54

Fig. 3.7 – Stresses versus Time in Strands of PCSC Girder and Prestressed Concrete Girder 57

Fig. 3.8 – Stress Profile due to Total Creep and Shrinkage Effects (Stress in ksi, Negative in Tension) 58

Fig. 3.9 – Application of PCSC Girder Sections for Bridges with Different Spans..... 63

Fig. 3.10 – Summary Chart for PCSC Girder Sections with the Maximum Attainable Span versus Girder Spacing 64

Fig. 4.1 – Applied Load, Strains and Section Resistance of the Section 70

Fig. 4.2 – Cross-section of the PCSC-36 Girder (Span = 80 ft) 81

Fig. 5.1 – Stress-strain Curve of the Steel 84

Fig. 5.2 – Example of Compressive Stress-strain Curve of the Concrete..... 87

Fig. 5.3 – Geometry of Elements (ANSYS, 2009) 89

Fig. 5.4 – Example of the Bond-slip Relationships between Concrete and Prestressing Strands..... 91

Fig. 5.5 – Relationship between Shear Force and Displacement for One 7/8-in. Stud 93

Fig. 5.6 – Prism Specimens and Reinforcements (Morcous et al., 2011)..... 95

Fig. 5.7 –Model of One Fourth of the Prism..... 97

Fig. 5.8 – Strains at Different Locations Obtained using FEA Predictions and Test Measurements (1-day) 98

Fig. 5.9 – Stresses in the Strand of the Prism 98

Fig. 5.10 – Cross-section of the PCSC Girder 100

Fig. 5.11 –One-fourth Model of the PCSC Girder..... 101

Fig. 5.12 – Contours of Compressive Stresses in Concrete Bottom Flange 102

Fig. 5.13 – Locations in the PCSC Girder Section 103

Fig. 5.14 – Comparisons of Stresses and Strains in Concrete Bottom Flange and Steel Beam Obtained Using FEA Predictions and Design Calculations 105

Fig. 5.15 – Comparisons of Stresses in Strands Obtained Using FEA Predictions and Design Calculations 108

Fig. 5.16 – Stresses in FB and FT for PCSC Girders with Different Amounts of Studs 110

Fig. 6.1 – Cross-section of the PCSC Girder Bridge 114

Fig. 6.2 – Cross-section of the PCSC Specimen..... 115

Fig. 6.3 – Cross-section of the Prestressing Bed 117

Fig. 6.4 – Profiles of the North Abutment 118

Fig. 6.5 – Profile of Anchoring Steel Plate..... 119

Fig. 6.6 – Profiles of the South Abutment 120

Fig. 6.7 – Step 1: Welding Studs to Steel Beam, Pretensioning Strands, Placing Stirrups and Forming the Concrete Bottom Flange..... 122

Fig. 6.8 – Step 2: Placing Concrete into the Formwork and Finishing the Surface..... 123

Fig. 6.9 – Step 3: Placing the Steel Beam on Steel Chairs 124

Fig. 6.10 – Views of Specimen, Formwork and Supports 126

Fig. 6.11 – Specimen Instrumentation 127

Fig. 6.12 – Step 4: Stripping the Formwork and Releasing the Strands (7-day) 128

Fig. 6.13 – Step 5: Install Formwork and Reinforcement, Place Concrete, Finish Concrete Surface and Remove the Formwork for Concrete Deck 130

Fig. 6.14 – As-built Cross-section of the PCSC Specimen..... 131

Fig. 6.15 – Concrete Strengths of Concrete Bottom Flange and Deck at Different Ages 133

Fig. 6.16 – Test Setup for Flexural Test 135

Fig. 6.17 – Test Setup for Shear Test..... 136

Fig. 6.18 – Instrumentation for Flexural and Shear Tests 138

Fig. 6.19 – Strain Profiles in Sections at Mid-span and 48 in. from End 141

Fig. 6.20 – Concrete Surface Strain Plots at South and North Sides of the Specimen with Modified 95% AMS Method 143

Fig. 6.21 – Time Histories of Concrete Surface Strains at the Same Level of Centroid of Strands 145

Fig. 6.22 – Time History of the Camber of the Specimen at Mid-span 146

Fig. 6.23 – End Zone Cracking 147

Fig. 6.24 – Moment-deflection Relationship in Flexural Test 149

Fig. 6.25 – Strains-Moment Relationship in Flexural Test 150

Fig. 6.26 – Loading at Theoretical Ultimate Moment 150

Fig. 6.27 – Flexure Cracks in Flexural Test 151

Fig. 6.28 – Shear-Deflection Relationships in South and North Shear Tests 152

Fig. 6.29 –Moment-Deflection Relationships in South and North Shear Tests 152

Fig. 6.30 – Strains-Shear Relationships in South Shear Test 153

Fig. 6.31 – Strains-Shear relationships in North Shear Test 154

Fig. 6.32 – Relationships of Slips of Strands and Shear at Sections under Loading 155

Fig. 6.33 – Cracks at Crack Moment in South Shear Test 156

Fig. 6.34 – Shear Failure in the Specimen 157

Fig. 6.35 – Shear Failure in the Top of Deck 158

Fig. 6.36 – Shear Failure in Steel Beam 159

List of Tables

Table 2.1 – Analytical Transfer Length Formulae (in ksi and inch units)..... 30

Table 3.1 – Design Parameters of Different Girders 52

Table 3.2 – Ultimate Strength and Service Designs of Different Girders 59

Table 3.3 – Self-weight and Cost of Different Girders..... 61

Table 4.1 – Stress Limits at Prestress Release for Different Specifications..... 67

Table 4.2 – Comparisons of Strength Design and Working Stress Design for the end sections of PCSC Girders at Release 81

Table 5.1 – Concrete Material Table 86

Table 5.2 – Transfer Length Results from Prism Specimens (Morcous et al., 2011)..... 96

Table 5.3 – Comparison between Design Calculations and FEA Predictions..... 99

Table 5.4 – Maximum Stresses Obtained Using FEA Predictions and Design Calculations 107

Table 6.1 – Demand of the Bridge Girders..... 115

Table 6.2 – Specimen Properties 116

Table 6.3 – Concrete Strengths of Concrete Bottom Flange and Deck at Different Ages 132

Table 6.4 – Flexural and Shear Capacities of the PCSC Specimen..... 139

Table 6.5 – Calculated Loads to Reach the Theoretical Capacities of the PCSC Specimen 139

Table 6.6 – Summary of Transfer Length Measurement Estimation..... 143

Table 6.7 – Camber at Mid-span at Prestress Release 145

Table 6.8 – Test Loads on the PCSC Specimen 148

Table 6.9 – Test Moment and Shear of the PCSC Specimen 148

Chapter 1 Introduction

1.1 *Problem Statement*

The stringer/multi-girder bridge system consists of steel and prestressed concrete I-shaped girders with cast-in-place concrete deck as shown in Fig. 1.1(a). Fig. 1.1(b) indicates that about 55% of the bridges in United States are built using the stringer/multi-girder system, which is based on the statistics of national bridge inventory of Federal Highway Administration (FHWA, 2011). This system is popular due to its simplicity of fabrication, speed of construction, and ease of inspection, maintenance and replacement.

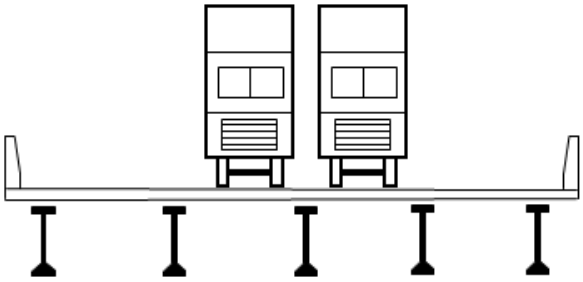

(a) Cross-section of the Stringer/Multi-Girder Bridge System

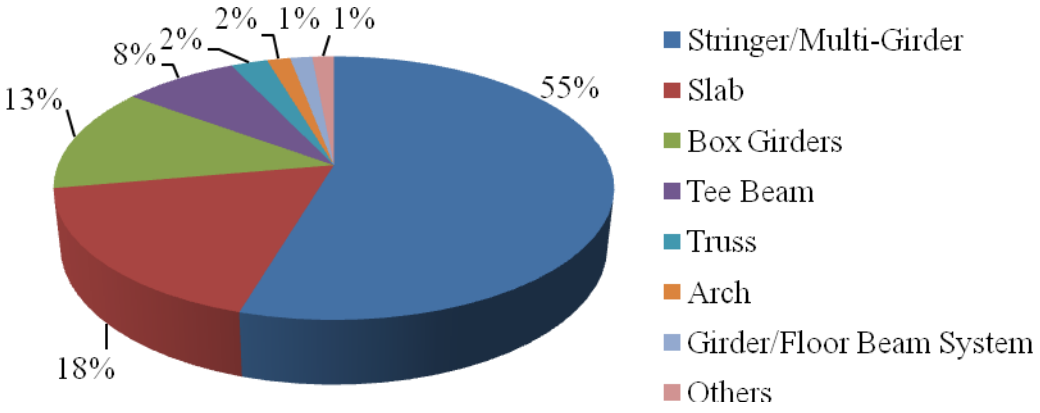

(b) Percentage of Bridges by Structural Type (FHWA, 2011)

Fig. 1.1 – Stringer/multi-Girder Bridge System (FHWA, 2011)

Steel girders (Fig. 1.2a) are preferred in continuous bridges, curved bridges, and long span bridges due to their lightweight, flexibility (i.e., curved and non-prismatic), and strength. The composite girder system consists of the steel girder connected to a concrete slab by shear connectors, as commonly found in bridge superstructures. Composite action between the steel girder and the top deck enhances structural efficiency by combining the structural elements to create a single composite section. The disadvantages of steel girders include high material cost, high maintenance cost and being susceptible to corrode due to chloride-contaminated splashes.

Prestressed concrete girders (Fig. 1.2b) are preferred in simple span, straight, and short-medium span bridges (i.e., span length less than 200 ft) due to their higher stiffness, durability and lower material cost compared to steel girders. The concept of prestressed concrete girders is to use initial prestress to counteract the tensile stresses induced by self-weight, deck weight and service loads. The strands embedded in the concrete are pre-tensioned under a high tensile stress to pre-compress the concrete. Prestressing greatly reduces both deflections and tensile cracks at service loads due to the pre-compression exerted by the prestressing steel (Nilson et al, 2010). Since the concrete protects the steel from corrosion, the durability of prestressed concrete girders is relatively high. The disadvantages of prestressed concrete girders encompass the concrete cracking at end zone and the top flange, depressing strands taken as a costly and dangerous operation, heavy sections limiting their span capacity and difficulty of making them continuous, curved, or non-prismatic.

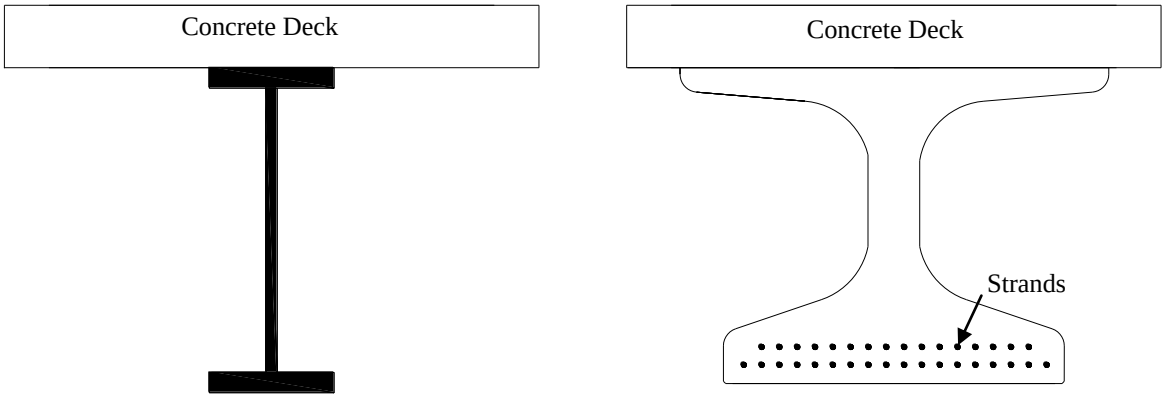

(a) Steel girder (b) Prestressed concrete girder

Fig. 1.2 – Stringer/Multi-Girders

1.2 *Objectives*

The main objective of this study is to develop a new Prestressed Concrete-Steel Composite (PCSC) girder system, which possesses the benefits including:

- A lightweight section
- An economical section
- Elimination of concrete cracking at prestress release
- Ease of fabrication
- Durability

This study is to investigate design and fabrication issues associated with the new PCSC girder. Examples of these issues are: fabrication procedure, service design, and strength design at release.

Specific tasks of this research are listed as follows:

- Perform detailed design of PCSC girders;

- Propose the strength design method and perform Finite Element Analysis (FEA) on PCSC girders at prestress release;
- Fabricate a girder specimen, investigate its performance and test its strength capacities;
- Evaluate and validate the adequacy of the design methods and FEA against the test results.

The outcome of this research is a new bridge girder system that has an excellent potential to change the way bridges are built today and result in safer, lighter, more durable and economical infrastructure.

1.3 *Organization*

The dissertation encompasses seven chapters:

Chapter 1 introduces the research conducted and includes problem statement, objectives and outcome of the study.

Chapter 2 reviews existing prestressed composite girders, and surveys the literature on the transfer development lengths of strands and stud shear connectors.

Chapter 3 describes the developed PCSC girder system and its fabrication sequences. A service design procedure using Age-adjusted Elasticity Modulus Method is proposed to design the PCSC girder for bridges and design examples are presented. Comparisons with steel and prestressed concrete girders are made based on design results.

Chapter 4 introduces the proposed strength design method for the PCSC girder at prestress release. Design equations are formulated for this method, the design procedure is proposed and design examples are presented.

Chapter 5 introduces detailed approaches of Finite Element Analysis of PCSC girders at prestress release. The model of bond between concrete and strand is validated against test results of prism specimens in the literature. And then FEA of PCSC girders at prestress release is presented.

Chapter 6 describes the experimental investigation on PCSC girders. The proposed fabrication sequences, design methods and FEA are validated against test results.

Chapter 7 presents summary and conclusions of research performed for the objectives of this dissertation. In addition, recommendations are given.

Chapter 2 Literature Review

2.1 *Introduction*

In this chapter, existing prestressed composite girders are categorized into four types. Cross-sections of those girders are introduced, the experimental and analytical studies on the girders' behavior are surveyed, and their advantages and disadvantages are also summarized. In addition, researches on the transfer and development lengths of prestressing strands and the behavior of stud shear connectors are surveyed in the literature, which have great influences on the behavior of prestressed composite girders.

2.2 *Existing Prestressed Composite Girders*

Several types of prestressed composite girders have been developed and investigated by researchers and designers. Four types of existing prestressed composite girders are found in the literature.

2.2.1 Type I Prestressed Composite Girder System

Type I prestressed composite girder system is constructed with corrugated steel web and top and bottom concrete flanges, as shown in Fig. 2.1. In this system, concrete bottom flange is usually prestressed, and corrugated steel webs sustain shear forces without taking any axial stresses due to flexure, prestressing, creep, etc. As illustrated by Yazeed and Ahmed (2001), the trapezoidal and zigzag profiles of corrugation are typically used for corrugated steel plates shown in Fig. 2.2(a) and Fig. 2.2(b), respectively.

This system using corrugated steel webs was adopted in several bridges in France and Japan (Yazeed and Ahmed, 2001; Jung et al., 2011). Cognac bridge, constructed in 1986 in France, has a box girder with top and bottom concrete flanges and trapezoidally corrugated web, whose cross-section is described in Fig. 2.1(a) (Yazeed and Ahmed, 2001). Maupré viaduct, completed in 1987, has seven spans varying from 40.95 to 53.55 m with a total length of 324.50 m. It has the box girder with an innovative triangular cross section, as shown in Fig. 2.1(b) (Yazeed and Ahmed, 2001). Hondani bridge, constructed in 1997 in Japan, has a box girder with the corrugated steel web and the concrete flanges as shown in Fig. 2.1(c) (Yazeed and Ahmed, 2001).

Recently, Ilsun bridge has been constructed in Korea, which is the world's longest (801m in total length) and widest (30.9m in maximum width) prestressed concrete box girder with corrugated steel web section (Jung et al., 2011). This bridge has fourteen spans, twelve of which were erected using an incremental launching method rarely applied in this type of bridges. Its overview and typical transverse cross section are as shown in Fig. 2.1(d). It has a composite superstructure of a one-piece tri-cellular cross section consisting of prestressed concrete slabs and corrugated steel webs as described in Fig. 2.1(d).

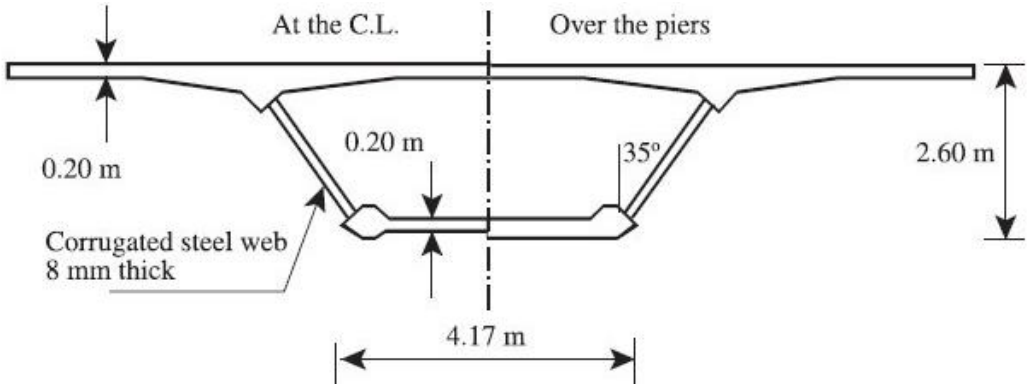

(a) Cross-section of the Box Girder of Cognac Bridge (Yazeed and Ahmed, 2001)

Fig. 2.1 – Type I Prestressed Composite Girder System (Continued)

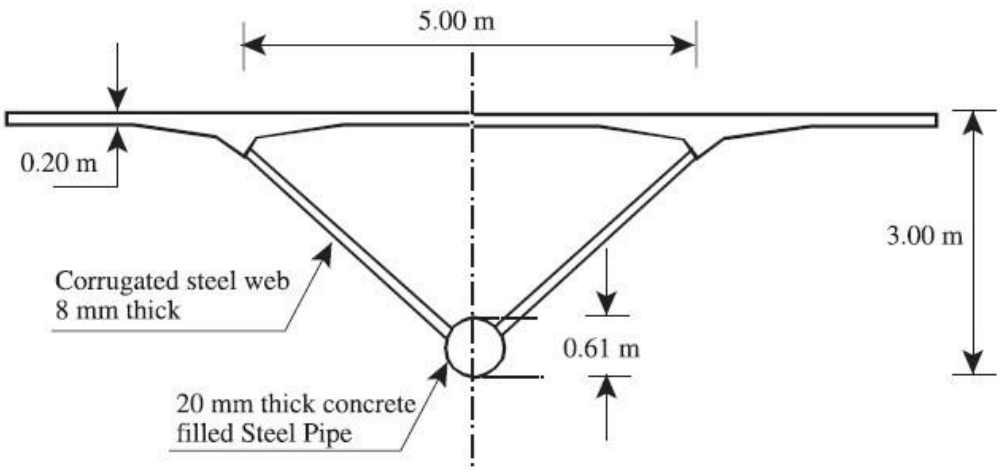

(b) Cross-section of the Box Girder of Maupré Viaduct (Yazeed and Ahmed, 2001)

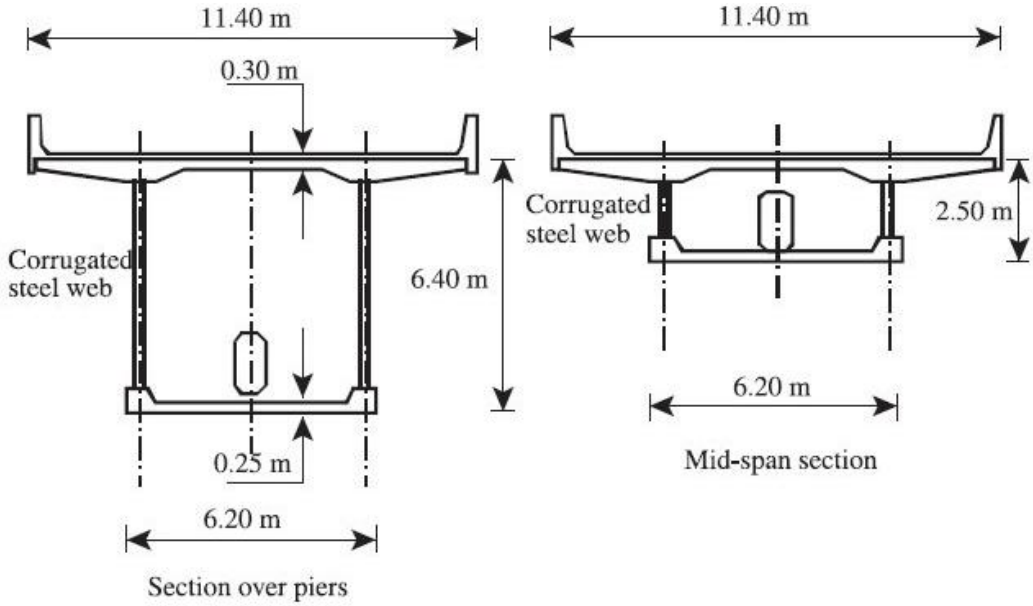

(c) Cross-section of the Box Girder of Hondani Bridge (Yazeed and Ahmed, 2001)

Fig. 2.1 – Type I Prestressed Composite Girder System (Continued)

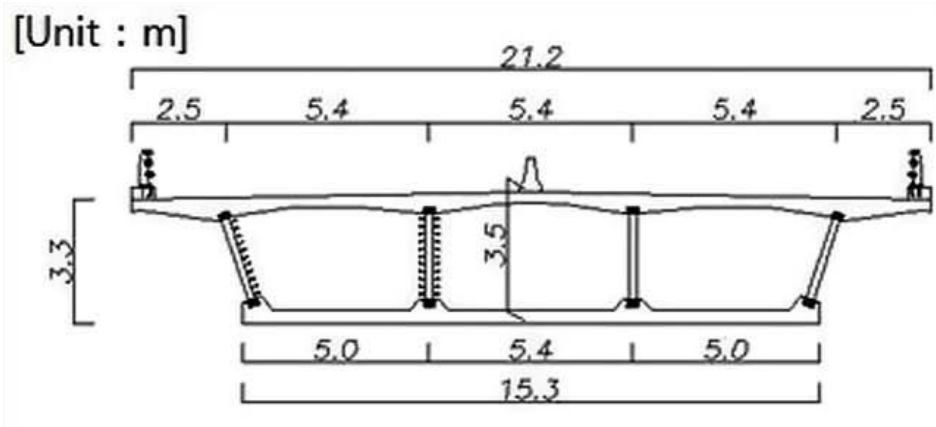

(d) Overview and Cross-section of Ilsun Bridge (Jung et al., 2011)

Fig. 2.1 – Type I Prestressed Composite Girder System

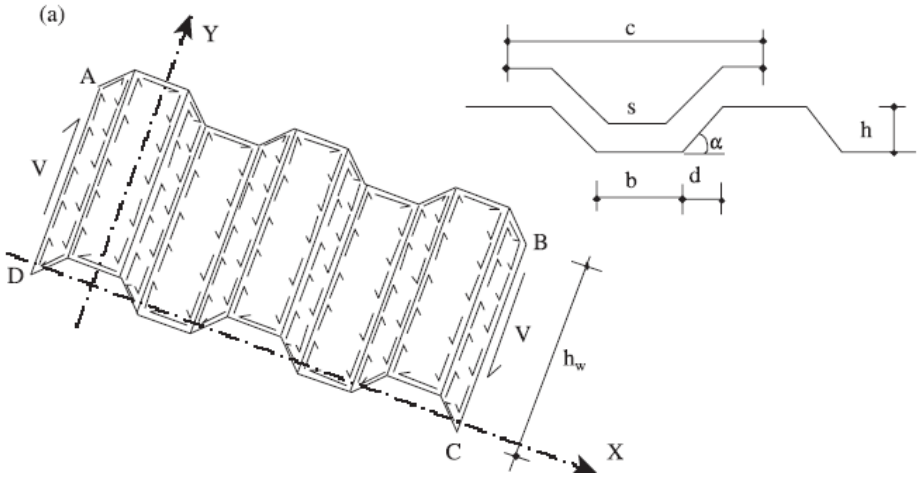

(a) Trapezoidal

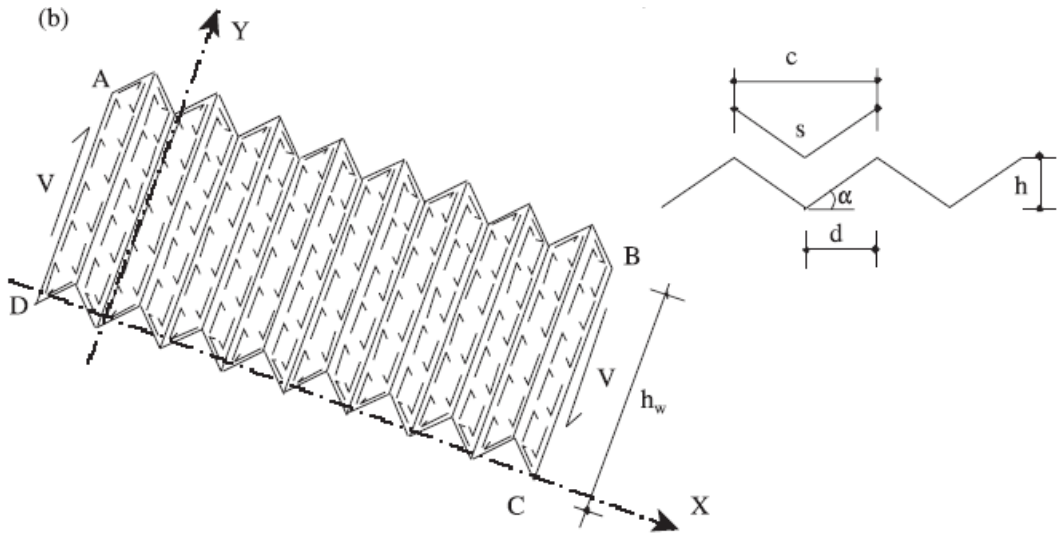

(b) Zigzag

Fig. 2.2 – Typical Profiles of Corrugated Steel Plates (Yazeed and Ahmed, 2001)

To understand behaviors of large-scale specimens of prestressed composites girders with corrugated steel webs, experimental and analytical studies were conducted by many researchers (Huang et al., 2004; Jung et al, 2010; Kim et al. 2011; Kim and Lee 2011; Ding et al., 2012). Pre-tension can be efficiently applied on the top and bottom concrete flanges due to the so-called ‘‘accordion effect’’ of corrugated webs. Huang et al.

(2004) presented a simple approach to account for three-dimensional phenomena of the accordion effect using link-type elements within a two-dimensional finite element model. Adequacy of the approach was validated through comparison of experimental and numerical results for a large-scale specimen of a prestressed concrete beam with corrugated steel web. Jung et al (2010) conducted the load tests on five prestressed concrete hybrid girders with steel web members, in order to fully understand the behaviors of the girders and the effects of steel web connection joints. The test results indicated that the serviceability issues such as cracking load and deflection and the safety issues such as stiffness and ultimate load capacity could be improved by modifying the steel web members and connection joints of concrete slabs and tendons.

Kim et al. (2011) performed a parametric study on the accordion effect of 24 corrugated webbed steel beams using the finite element analysis. Based on the analytical results, a simple method for estimating the accordion effect was proposed and a flexural behavior model was proposed for the prestressed composite beams with corrugated web. Kim and Lee (2011) presented an experimental study on the flexural behavior of three full scaled non-prestressed and prestressed composite beams with corrugated web, which had been developed by Kim et al. (2011). It was verified that the proposed flexural behavior model of the prestressed composite beams with corrugated web proposed by Kim et al. (2011) accurately estimated the flexural behavior before and after the composite with concrete. Besides, the horizontal shear capacities of the composite members were evaluated considering the horizontal shear failure observed in the test specimens.

Ding et al. (2012) established a three dimensional finite element model to investigate the behavior PC box-girder with corrugated steel webs under pure torsion taking material nonlinearity into consideration. The torque–twist curves and ultimate torsional strength predicted by FEA showed good agreement with test data. It was found that the ultimate torsional strength of specimens was in linear proportion to shear modulus and thickness of corrugated steel webs and to compressive strength of concrete.

The benefits of this system include (Yazeed and Ahmed, 2001; Huang et al., 2004):

(1) Light weight of webs in this system contributes to reduction of self-weight and thus leads to a reduction in prestress and an increase in span.

(2) Narrow spaced folds contribute to higher resistance to global and local buckling of the web.

(3) The number of intermediate diaphragms is reduced due to the increased transverse stiffness.

(4) The corrugated web only resists principal stresses caused by shear and decreases the effects induced by shrinkage, creep and temperature.

(5) Pre-tension can be efficiently applied on the top and bottom concrete flanges due to the so-called ‘‘accordion effect’’ of corrugated webs.

However, the complexity of fabricating corrugated steel webs and high cost of post-tensioning operations/hardware hindered the wide use of this system in North America.

2.2.2 Type II Prestressed Composite Girder System

Type II prestressed composite girder system is a prestressed composite floor slab, as shown in Fig. 2.3.

Bozzo and Torres (2004) proposed the prestressed composite slab made of semi-prefabricated prestressed composite steel-concrete beams, precast prestressed planks, and topping concrete. Its cross-section and lateral view are described in Fig. 2.3(a) and Fig. 2.3(b), respectively. This beam had recently been used to construct the library of the University of Lleida in Spain. Spans range from modules of 12 × 8 to 12 × 12 m, with total depths of only 300 mm. The composite steel–concrete beam was formed by cutting the steel skeleton of an HEB-320 mm, which allowed passing transversal reinforcement for the steel–concrete connection and was welded to an 800 × 10 mm plate at its bottom end. Two lateral angular L-shapes, 100 × 10 mm, were then welded to this bottom plate. The section was completed with 0.6″ diameter strands and pre-tensioned prior to casting the concrete. The number of strands varies along with different spans and loading.

Bozzo and Torres (2004) conducted the flexural tests on the prestressed composite beams and found that the structural element can be modeled under service conditions using the transformed section method. The metallic skeleton and the concrete worked perfectly together and no significant slip was observed, even at failure.

This is an excellent system for building floors where shallow depths are needed as the steel girder has to be fully embedded in concrete, which will result in a very heavy section if used in bridge applications.

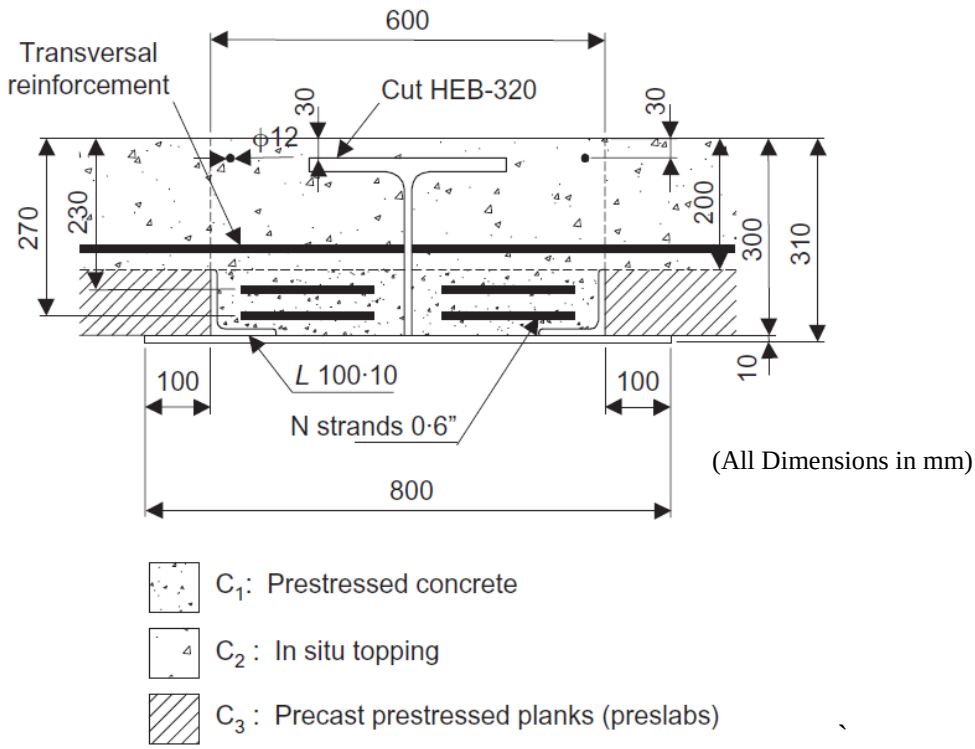

(a) Cross-section (Bozzo and Torres, 2004)

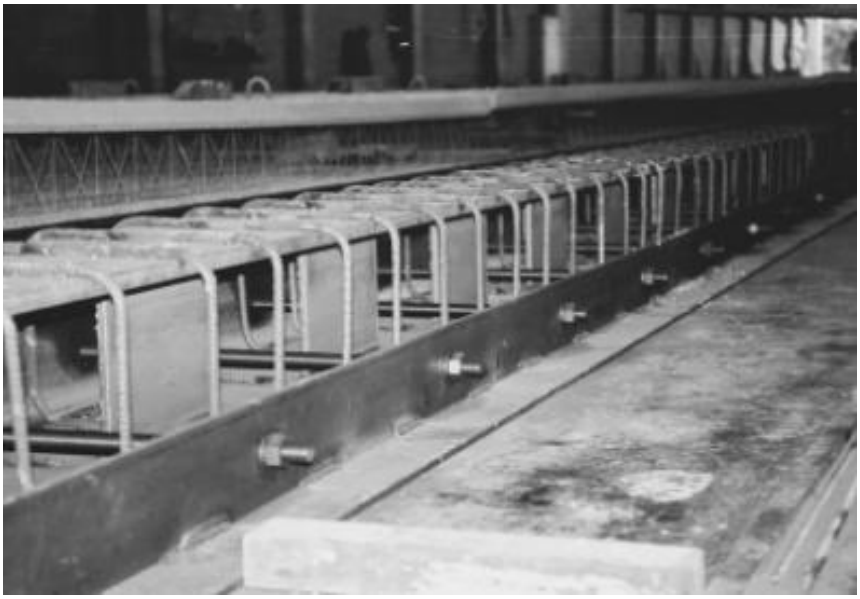

(b) Lateral View (Bozzo and Torres, 2004)

Fig. 2.3 – Type II Prestressed Composite Girder

2.2.3 Type III Prestressed Composite Girder System

Type III prestressed composite girder is composed of concrete deck and the steel beam and prestressed by embedded strands or external tendons as shown in Fig. 2.4.

Basu et al. (1987a-b) placed the prestressing strands into the negative moment regions of continuous composite beams while the slab acts compositely with the steel beam, as shown in Fig. 2.4(a). The concept of the beams is to eliminate the cracking of concrete by pre-tensioning the concrete slab in the negative moment regions near the interior supports prior to loading. The cracking of the concrete in the negative moment region has many drawbacks: (1) Cracking causes a reduction in the capacity of the section and partial loss of composite action; (2) In the case of bridges where continuous composite beams are used, this cracking and subsequent deterioration of the concrete slab and corrosion of reinforcements due to weathering effects lead to progressive serviceability failure. However, the concept is effective for crack prevention in the negative moment region while is not applicable in the positive moment region.

Saadatmanesh et al. (1989a) developed a prestressed composite girder system for new construction and bridge strengthening operations. In this system, steel beams are prestressed using high strength threaded bars anchored to the bottom or top flange at girder ends as shown in Fig. 2.4(b-c). The beam, shown in Fig. 2.4(b), was pre-tensioned with two 5/8-in. diameter high-strength threaded bars running below the bottom flange of the steel beam and subjected to positive bending moment. This beam was pre-tensioned before the concrete deck was placed so as to prevent the concrete from cracking in tension. The beam, shown in Fig. 2.4(c), was pre-tensioned after the concrete was placed

for applying compressive stresses in the concrete. It was used for the negative moment region of a continuous beam between the inflection points on each side of an interior support. Saadatmanesh et al. (1989b) tested two prestressed composite beams, one subjected to positive bending moment Fig. 2.4(b) and the other to negative bending moment Fig. 2.4(c). The relationships were established between the applied load and the deflection, and the strains in the concrete, steel beam, and prestressing bars. The values predicted by using force equilibrium and strain compatibility method between the deformations of the bars and the composite beam were found to agree well with the measured data.

Composite beams pre-tensioned by adding draped tendons can be applied to single span or continuous bridges (Fig. 2.4(d)). Lorenc and Kubica (2006) investigated the failure mechanisms and behavior of composite concrete-steel beams with the section shown in Fig. 2.4(d). The section was prestressed with external tendons and subjected to positive bending moment. Experimental tests were conducted on composite beams with straight and draped tendons as well as on a non-prestressed beam. Six simply supported beams subjected to a positive static bending moment were tested up to failure. It was found that the tendon shape (draped or straight without saddle points) has no significant influence on the behavior and ultimate resistance of composite beams as long as the tendons are located at the same eccentricity. It was also indicated that bond cohesion between steel and concrete can significantly affect the performance of the shear connection in composite beams. Chen and Gu (2005) conducted tests to investigate the ultimate moment and incremental tendon stress of steel–concrete composite beams

prestressed with draped external tendons under positive moment. It was found that adding prestressing by external tendons of the composite beams, the yield load and the ultimate resistance of the beams were significantly increased and the deflection at the serviceability state was also reduced. Based on the compatibility of the tendons and the composite beam, and equilibrium of the internal force, the simplified expressions for the ultimate incremental tendon stress related to the ultimate span/deflection value were developed. The results obtained from the simplified expressions were compared well with those obtained from tests and finite element analysis.

Although external tendons slightly improve the capacity and decrease the deflection of the system, its durability is not improved as the tendons and steel beam remained exposed.

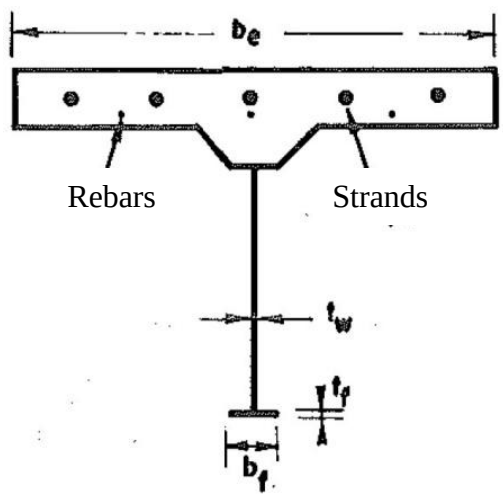

(a) Girder with Strands (Basu et al., 1987a-b)

Fig. 2.4 – Type III Prestressed Composite Girder (Continued)

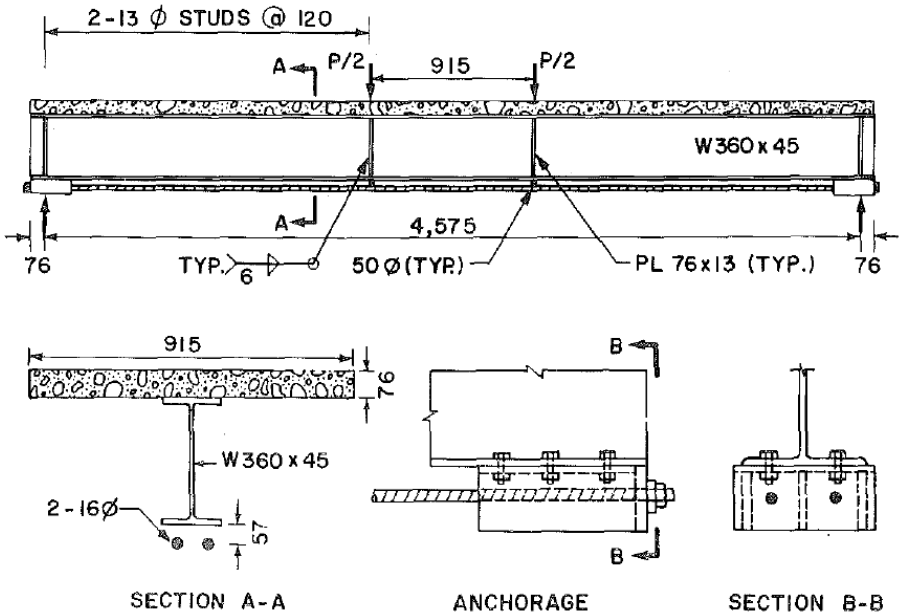

(b) Girder with External Tendons in Positive Moment Region (Saadatmanesh et al., 1989a-b)

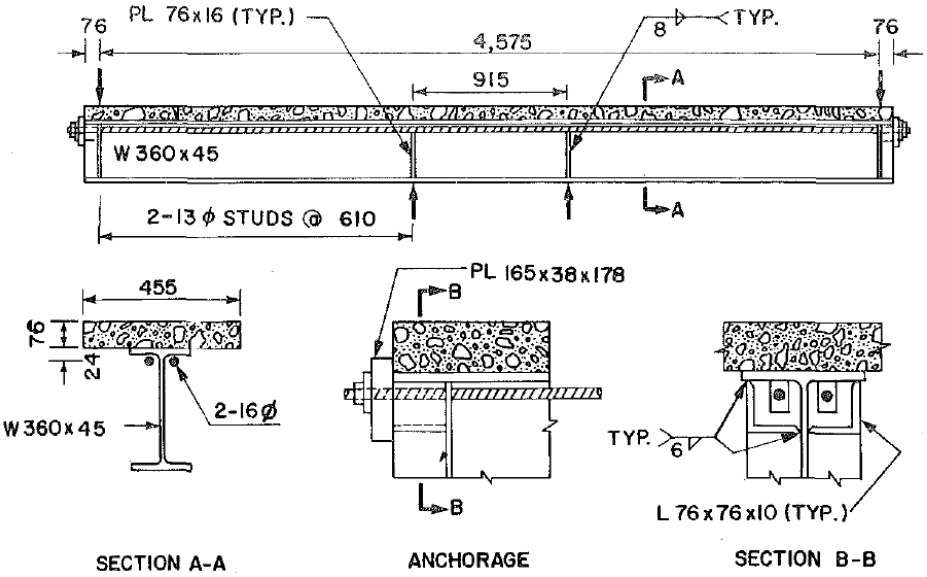

(c) Girder with External Tendons in Negative Moment Region (Saadatmanesh et al., 1989a-b)

Fig. 2.4 – Type III Prestressed Composite Girder (Continued)

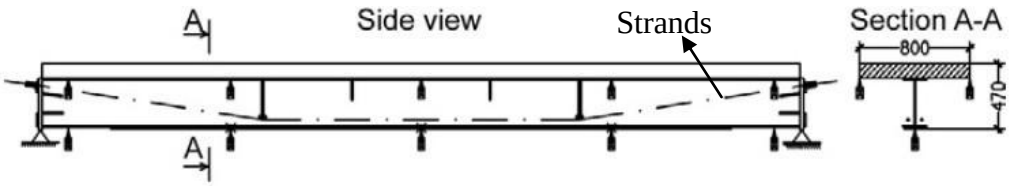

(d) Girder with Draped External Tendons (Lorenc and Kubica, 2006)

Fig. 2.4 – Type III Prestressed Composite Girder

2.2.4 Type IV Prestressed Composite Girder System

Type IV prestressed composite girder system is the Preflex girder as shown in Fig. 2.6. The technology of the Preflex girder was firstly introduced in Belgium since 1951, and then applied in Japan, Germany, Great Britain, and South Korea. The girder is a steel girder with the bottom flange encased by reinforced concrete, while the prestressing is applied by elastic bending of the steel girder and/or pre-tensioning strands. The steel girder is pre-bended by applying two concentrated loads at one-quarter and three-quarters of the span, which are removed when the concrete gains the desired strength (Morano and Mannini, 2006; Staquet et al., 2004; Hanswille, 2011). The typical section of the Preflex girder without and with prestressing strands are described in Fig. 2.6(a) and Fig. 2.6(b), respectively. The projects using the Preflex girder include buildings, e.g., the Southern Tower in Brussels has 144 Preflex beams with a span of 131 ft and the Berlaymont Building in Brussels has 319 Preflex beams; and bridges, e.g., the bridge over the Lixhe Dam across the Maas River has beams with a span of 154 ft and the bridge in Kerpen Horren in German has beams with a span of 135 ft (Morano and Mannini, 2006; Staquet et al., 2004). In addition, as stated by Hanswille (2011), the Preflex girder is usually used for railway and road bridges where the available structural depth is highly restricted and ratios of span to structural depth up to 45 can be achieved for road bridges.

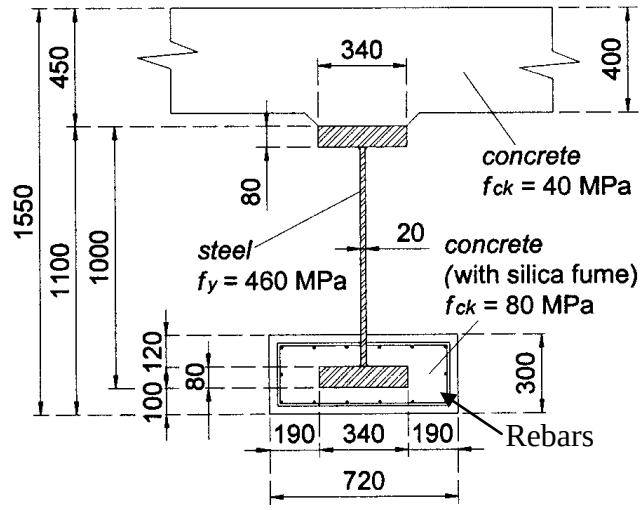

(a) Preflex Girder without Prestressing Strands (Morano and Mannini, 2006)

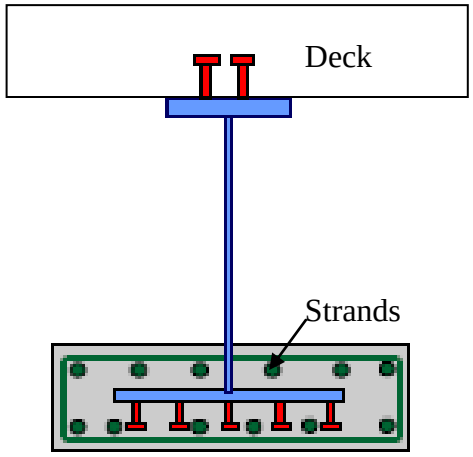

(b) Preflex Girder with Prestressing Strands (Hanswille, 2011)

Fig. 2.5 – Type IV Prestressed Composite Girder

The fabrication sequence of a Preflex beam is shown in Fig. 2.6(a) and described as follows (Morano and Mannini, 2006; Staquet et al., 2004):

(a) In the plant, place an I-shaped steel girder with an initial camber, which is supported at two ends.

(b) Pre-bend the steel girder by applying two concentrated loads at one-quarter and three-quarters of the span.

(c) Cast the concrete encasing the bottom flange of the steel girder, and keep in place the pre-bending loads in step (b).

(d) After the concrete gains the required strength, remove the pre-bending loads. The girder moves up with the camber smaller than the initial camber, and the concrete flange is subjected under compression.

(e) Place the concrete deck on the top of the steel girder.

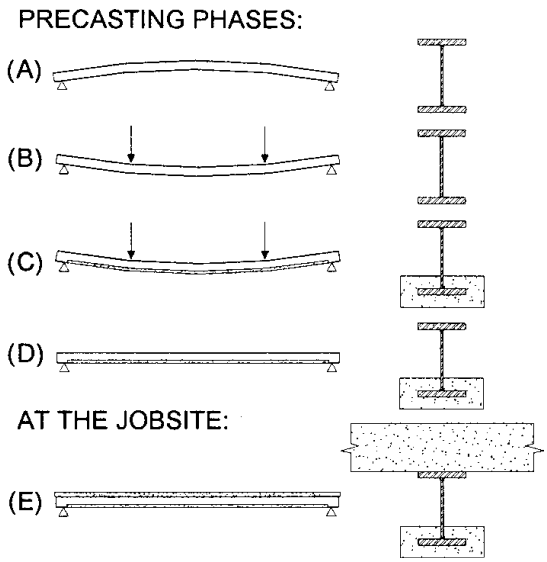

(a) Fabrication Sequence (Morano and Mannini, 2006)

(b) Stirrups for Concrete Bottom Flange (Portela et al., 2011)

Fig. 2.6 – Fabrication of Type IV Girder

Transverse reinforcement is placed into concrete bottom flange to account for shear stresses in concrete and stirrups are commonly placed at one quarter of the span from each support (Portela et al., 2011). However, it is noted that holes should be drilled in the web of the steel beam so that the stirrups can be installed in the place where the concrete bottom flange is located, as shown in Fig. 2.6(b).

In the literature, experimental and analytical studies of the Preflex girder under different loading conditions are performed by many researchers (Staquet et al., 2004; Staquet and Toutlemonde 2007; Toutlemonde and Staquet 2007; Staquet et al. 2010; Morano and Mannini, 2006; Portela et al., 2011).

Staquet et al. (2004) conducted experimental measurements of the U-shaped concrete deck with the Preflex girder, as shown in Fig. 2.7(a). The strains were measured by using vibrating wire strain gages and strain gages at mid-span and one-third-span sections, as described in Fig. 2.7(a). They used the age-adjusted elasticity modulus method (AEMM) and the step-by-step method to evaluate the time-dependent stresses and strains in preflex girders due to the effects of creep and shrinkage. Note that AEMM and the step-by-step method are very famous methods developed decades ago by researchers (Ghali et al, 2012). The strains measured at one-third-span section were compared with those calculated using the AEMM and the step-by-step method, as shown in Fig. 2.7(b-c). It was concluded that the experimental results agreed well with the calculated values and the step-by-step method predicted the strains in concrete section better than the AAMM when compared with test results.

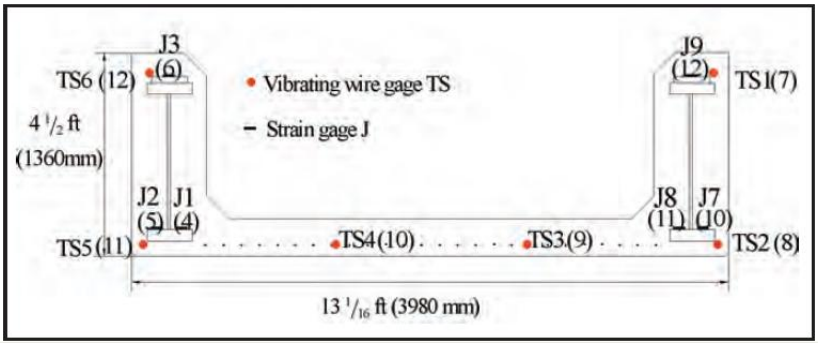

(a) Strain Measurement at Cross-section at Mid-span and One-third Span

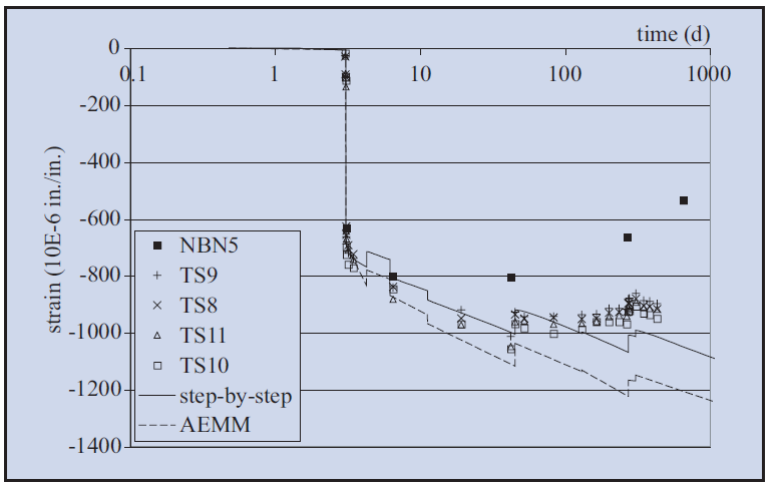

(b) Strains in Bottom Flange at Cross-section at One-third-span

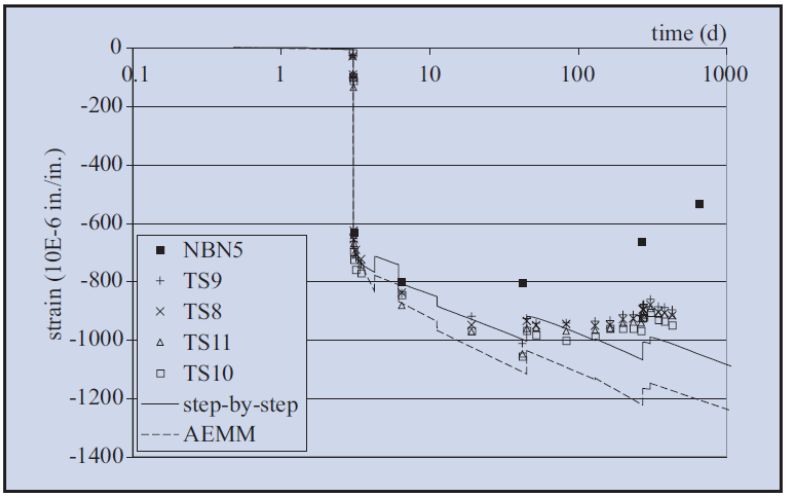

(c) Strain Measurement at Cross-section at One-third-span Span

Fig. 2.7 – U-shape Concrete Deck with the Preflex Girder (Staquet et al., 2004)

Staquet and Toutlemonde (2007) and Toutlemonde and Staquet (2007) found that serviceability limit state always dominates the design of the Preflex girder when service design, ultimate design, and fatigue design are considered, while the effects of creep and shrinkage are very important for the service design of the Preflex girder. Test results showed that the ultimate limit state taking into account warping of the steel beam and yielding of the top flange of the steel beam was always controlled by the serviceability limit state (Staquet and Toutlemonde, 2007). Test results indicated that the composite behavior of the Preflex girder was normally ensured without any fatigue degradation even under numerous live load cycles (Toutlemonde and Staquet, 2007).

For service design, it is required to control the compressive stress and eliminating cracking of concrete, taking into account the stress and prestress losses due to creep and shrinkage. Staquet and Toutlemonde (2007) used very high performance concrete (VHPC) for preflex girders due to the potential advantages of low delayed strains and high tensile stress. Low delayed strains due to significant decrease of the creep deformation and thus the decrease of the stress and prestress losses of the system. Staquet et al. (2010) demonstrated potential benefit of using VHPC (16 ksi concrete strengh) instead of high performance concrete (8 ksi concrete strengh). The magnitude of the total creep function (20°C, 50% relative humidity) of VHPC after 100 days of sustained loading was significantly lower than that of the HPC as illustrated in Fig. 2.8(a). The evolution of the stress at the level of the concrete bottom flange of the preflex girder was predicted by using the step-by-step method (Ghali et al, 2012) and the CEB90 model code (fib-CEB-FIP, 1999) for the modeling of the time-dependent strains of concrete. The cross-section

of the girder is shown in Fig. 2.8(b). It was found six months after the transfer of prestressing, the remaining compressive stress under permanent loading was 0.1 MPa and 3 MPa in the girders with HPC and VHPC, respectively, as shown in Fig. 2.8(c).

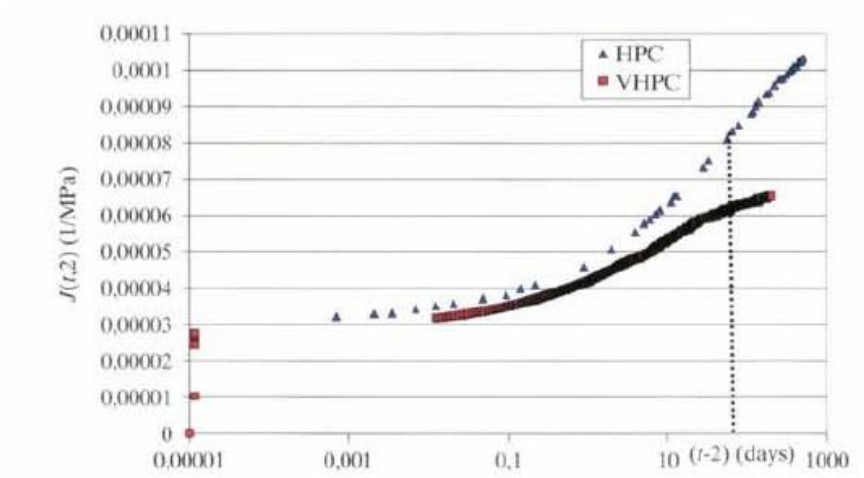

(a) Total Creep Function (20°C, 50% Relative Humidity) of HPC and VHPC Samples Loaded at Two Days.

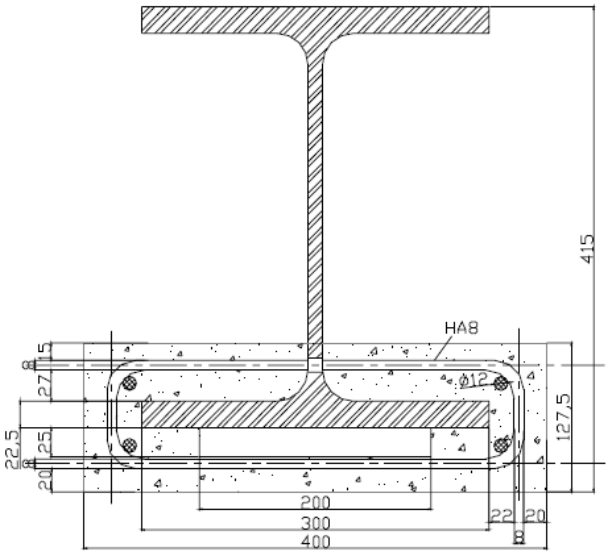

(b) Cross-section of the Girder

Fig. 2.8 – Prefelx girders with VPHC and HPC (Staquet et al., 2010, Continued)

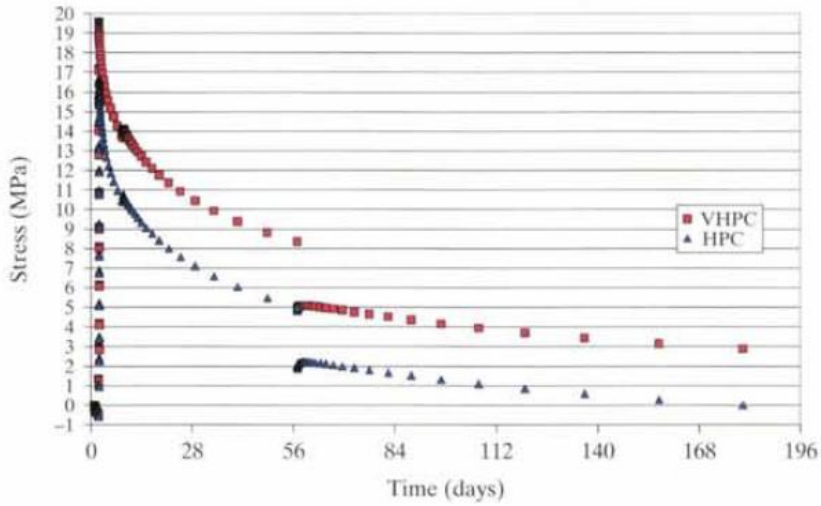

(c) Stress Predicted by CEB90-MC (1999) at the Level of the Concrete Bottom Flange for HPC with 8 ksi Concrete Strength and VHPC with 16 ksi Concrete Strength.

Fig. 2.8 – Preflex Girders with VPHC and HPC (Staquet et al., 2010)

Morano and Mannini (2006) proposed a method of calculating creep and shrinkage effects for Preflex beams. The proposed method using concrete age-adjusted modular ratios allows the calculation of time-dependent stresses in the concrete flange due to creep and shrinkage, with sufficient accuracy for practical applications and without carrying out cumbersome numerical computations. It was concluded that the simplified approach agreed very well with the results from the numerical approach. Portela et al. (2011) presents a procedure for evaluating simply supported pre-flex beams under dead load, superimposed dead load, and vehicular live loads taking into account the effects of creep and shrinkage by using the method proposed by Morano and Mannini (2006).

The Preflex girder has a light section, a very high moment capacity and a high span-to-depth ratio. However, the disadvantage of this system is the need for a loading

frame to pre-bend the steel girder and drilling holes in the web of steel beam for bottom flange reinforcement. The complexity of these operations increases the production cost significantly and limits the application of this system.

2.3 *Literature on Transfer and Development Lengths of Prestressing Strands*

Transfer length is the distance measured from the end of the prestressed concrete member over which the effective prestress is fully transferred from strands to the concrete. The force transferred along the transfer length increases from zero at the end of the member to the effective prestress at the end of the transfer length. The development length of prestressing strands is the minimum length of strands embeded in concrete for reaching the ultimate capacity of the section without strand slip. Namely, the ultimate stress in the strand could be reached without strand-concrete bond failure at the end of the development length.

Transfer and development lengths are both achieved due to the bond between concrete and strands. The bond between concrete and strands are induced by three factors, i.e., adhesion, Hoyer's effect, and mechanical interlocking. Adhesion is the chemical and physical bonding developed at the interface of the strands and concrete. Adhesion at prestress release could be assumed to be zero due to slip of strands (Guyon, 1960). Hoyer's effect and mechanical resistance mainly contribute to bond. Hoyer's effect is induced by the wedging action of strands. Strands contract in size when are initially stressed and attempt to return to their original size at release, resulting in high radial pressure and frictional resistance between concrete and strands. Mechanical resistance is

due to twisting of the outer wires of helical strands when the strands are released from tension while concrete surrounding the strands prevents twisting through mechanical interlock (Pozolo et al., 2010).

According to the AASHTO LRFD Bridge specifications (AASHTO, 2007), the transfer and development lengths for fully bonded prestressing strands can be expressed in Eqs. (2.1) and (2.2), respectively.

$$l_t = 60 d_b \tag{2.1}$$

where, l_t = transfer length (in.); d_b = nominal strand diameter (in.).

$$l_d \geq k[f_{ps} - \frac{2}{3} f_{pe}]d_b \tag{2.2}$$

where, l_d = development length (in); f_{ps} = average stress in prestressing steel (ksi); f_{pe} = effective stress in prestressing steel (ksi); k = factor equal to 1.0 for pretensioned panels, piling, and other pretensioned members with a depth of less than or equal to 24.0 in., and equal to 1.6 otherwise.

Eqs. (2.1) and (2.2) are applicable for bridge girders with minimum concrete strength of 4 ksi and a bottom flange reinforcement of at least no. 3 deformed bars with spacing not exceeding 6 in. enclosing the strands (AASHTO 2007). The equations were initially developed for prestressing strands with diameter up to 0.5 in, but later k factor was added to accommodate the use of 0.6 in. diameter strands as well as the new spacing requirements (AASHT, 2007). AASHTO (2007) requires that the distance between prestressing strands at member ends within the transfer length shall not be less than a clear distance taken as 1.33 times the maximum size of the aggregate nor less than the

center-to-center distances specified as 2 in. for 0.6-in.-diameter strands, and 1.75 in. for 0.5-in.-diameter strands. In addition, according to the AASHTO (2007), the total area of reinforcement located within the distance *h*/4 (where *h* is the overall height of the girder) from the end of the girder should not be less than 4% of the total prestressing force at transfer divided by 20 ksi. This reinforcement is required for crack control and resisting the splitting force at the girder ends due to prestressing.

Fig. 2.9 shows the relationship of stress versus the transfer and development length (AASHTO (2007). This relationship often gives conservative estimates of transfer and development length based on Kose and Burkett (2005).

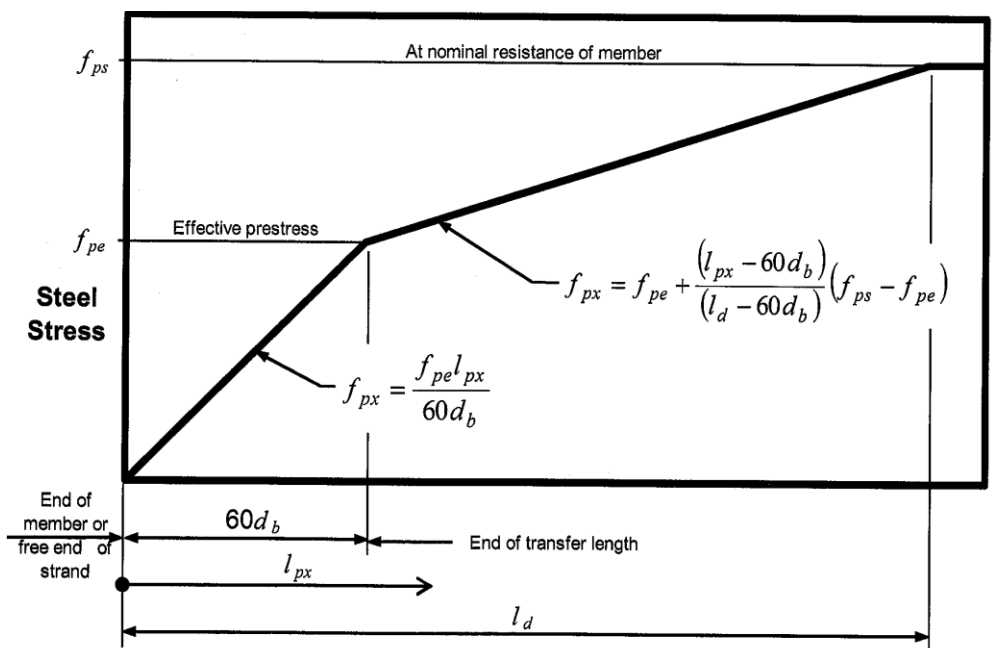

Fig. 2.9 – Idealized Stress versus Distance from End of Member (AASHTO, 2007)

In the last decades, large quantities of researches were conducted for the purpose of analytically predicting transfer and development length of steel strands, and many formulae are proposed (Pozolo et al., 2010; Morcous, 2011). For instance, Pozolo et al.

(2010) summarized analytical transfer length expressions from the literature over the past forty years, as shown in Table 2.1. It is noted that the equations summarized in Table 2.1 were mainly derived using the experimental data and used to suggest modifications to Eqs. (2.1) and (2.2).

Table 2.1 – Analytical Transfer Length Formulae (in ksi and inch units)

Reference	L_t Expression	Notes & Limitations
Based on Hanson and Kaar (1959)	$L_t = \frac{f_{pe} d_b}{3}$	
Olesniewicz (1975)	$L_t = \psi d_b \sqrt{\frac{f_{pe}}{f'_{ci}}}$	$\psi = 10$, average L_t
Zia and Mostafa (1977)	$L_t = \frac{1.5 f_{pi} d_b}{f'_{ci}} - 4.6$	f'_{ci} = 2-8 ksi
Nijhawam (1978)	$L_t = \frac{0.69 f_{pi} d_b}{f'_{ci}} + 10.3$	
Cousins et al. (1990)	$L_t = 0.5\left(\frac{U'_t \sqrt{f'_{ci}}}{B}\right) + \frac{f_{pe} A_p}{\pi d_b U'_t \sqrt{f'_{ci}}}$	Concrete strengths in psi; U'_t = 6.7 for uncoated strands; B = bond modulus (psi/in)
Bruggeling and Huyghe (1991)	$L_t = \frac{7 f_{pi} d_w}{12(0.13) f'_{ci}}$	$d_w = 0.33 d_b$ for 0.5-in., 7-wire strand
Balazs (1992)	$L_t = K d_b \sqrt[5]{\frac{f_{pi}^3}{f'^2_{ci}}}$	K = 4.64 ksi$^{(-1/5)}$, average L_t
Shahawy et al. (1992) Deatherage et al. (1994) Buckner (1995)	$L_t = \frac{f_{pi} d_b}{3}$	
Mitchell et al. (1993)	$L_t = 0.33 f_{pi} d_b \sqrt{\frac{3}{f'_{ci}}}$	f'_{ci} = 3.05-7.25 ksi
Russell and Burns (1996)	$L_t = \frac{f_{pe} d_b}{2}$	
Tadros and Baishya (1996)	$L_t = \frac{f_{pe} d_b}{0.8(3.04)}$	
Mahmoud et al. (1999)	$L_t = \frac{f_{pi} d_b}{\alpha_t f_{ci}'^{0.67}}$	α_t = 1.269 for steel strands
Marti-Vargas et al. (2007-b)	$L_t = \frac{\psi f_{pi} A_p}{0.282 \pi d_b f'^{0.67}_{ci}}$	$\psi = 1$, average L_t

In this dissertation, 0.7 in. diameter strands are used for the developed prestressed composite girder system. Morcous et al. (2011) strived to accommodate the use of 0.7 in. diameter strands in prestressed concrete girders. Morcous et al. (2011) conducted tests on several prestressed concrete girder sections, such as T-girder, Bridge Double Tee, NU900, and NU1100, as well as rectangular prism specimens. They made the following conclusions on transfer and development lengths of 0.7 in. diameter strands:

- The transfer length of 0.7 in. diameter strands ranged from 19 in. to 29 in, and is highly dependent on the concrete strength and the intensity of prestressing. These values are below the prediction using the Eq. (2.1) (AASHTO, 2007), i.e., 42 in. Also, neither the amount nor distribution of confinement reinforcement in the bottom flange had a significant effect on the transfer length of 0.7 in. diameter strands at release or at 28 days after release.
- The 0.7 in. diameter strands can be fully developed in high strength concrete (HPC) within the length predicted by the Eq. (2.1) (AASHTO, 2007) when spaced at 2 in. horizontally and vertically, based on the results of the experimental investigation with a minimum concrete strength of 10 ksi and no. 3 bars at 6 in. spacing at least distance 1.5*h* from the girder end. For a higher concrete strength (more than 15 ksi), shorter development length can be achieved.

2.4 *Literature on the Behavior of Stud Shear Connectors*

Composite members in bridges consist of a reinforced concrete deck supported on steel girders acting together as a unit under superimposed dead loads and live load. Stud

shear connectors are commonly used to transfer horizontal shear forces at the girder-deck interface, so as to achieve composite action. The headed steel stud is the most common type of shear connector used on steel girders and welded to the top flange using an arc-welding process (Badie et al., 2002). Note that 3/4 in. and 7/8 in. diameter studs are typically used. Badie et al. (2002) proved the feasibility of 1¼ in. studs and introduced its application in the first bridge built in the state of Nebraska. They also provided information on the development, welding, quality control, and testing of the 1¼ in. stud.

Ollgard et al. (1971) found the strength of stud shear connector is dependent on the concrete modulus of elasticity and concrete strength. According to AASHTO (2007), nominal shear resistance of one stud shear connector embedded in a concrete deck, Q_n, is determined by

$$Q_n = 0.5 A_{sc} \sqrt{f_c^{'} E_c} \leq A_{sc} F_u \tag{2.3}$$

where, A_{sc} = Area of cross-sectional area of the stud; f'_c= compressive strength of concrete; E_c = modulus of elasticity of concrete; F_u = minimum specified tensile strength of the stud.

Experimental push-off tests are usually used to investigate the load-slip behavior and the shear capacity of the shear stud in composite beam (Lam and El-Lobody, 2005). Ollgard et al. (1971) proposed the shear force-displacement relationship of shear studs under continuously loading based on the push-off testing results and an empirical formula can be expressed as

$$Q = Q_n(1 - e^{-\beta\Delta})^{\alpha} \tag{2.4}$$

where, Q = shear force in the stud; Δ = displacement at the weld point of the stud; and β and α = coefficients, equals 18 and 0.4, respectively.

Some researchers (Gattesco N. 1999; Queiroz et al. 2007) performed Finite Element Analysis (FEA) to investigate the behavior of composite girders. The studs were modeled using spring elements and the shear force-displacement relationship of shear studs proposed by Ollgard et al. (1971). However, the coefficients β and α were determined from the experimental results. Gattesco N. (1999) presented a numerical procedure for the analysis of steel and concrete composite beams, accounting for nonlinear behavior of concrete, steel and shear connectors. The adequacy of the program were validated against experimental data of four composite beams over the entire loading range up to failure. It was demonstrate that the numerical approach was a valid tool for extensive parametric studies on composite beams with complete or partial shear connection. Queiroz et al. (2007) evaluated full and partial shear connection in composite beams using the commercial finite element (FE) software ANSYS. The flexural behavior of simply supported composite beams subjected to either concentrated or uniformly distributed loads was simulated using proposed three-dimensional FE model. The investigated behavior encompasses load deflection behavior, longitudinal slip at the steel–concrete interface, distribution of stud shear force and failure modes. The reliability of the model was demonstrated in comparison with experiments and with alternative numerical analysis.

Lam and El-Lobody (2005) used three dimensional elements to model the load–slip behavior of studs. It was found at present the load–slip behavior and the shear capacity of the shear stud in composite beam were mainly based on data from the experimental push-off tests. They proposed an effective numerical model using the finite element method to simulate the push-off test. The model was validated against test results and compared with the predictions using the current codes of practices. The finite element model assists in understanding the different failure modes found in experimental testing and hence shear capacity of headed shear studs in the concrete deck.

2.5 *Summary*

Four types of existing prestressed composite girders developed and investigated by researchers and designers are summarized:

- Type I – Corrugated steel web girders constructed with top and bottom concrete flanges.
- Type II – Prestressed composite floor slab
- Type III – Concrete deck on the top of steel beam prestressed by embedded strands or external tendons
- Type IV – Preflex girders

Experimental and analytical studies were conducted by researchers to understand behaviors of prestressed composites girders are surveyed. The advantages and disadvantages of the four types of the prestressed composite girders are summarized.

Transfer and development lengths are both achieved due to the bond between concrete and strands. The bond between concrete and strands are induced by three factors, i.e., adhesion, Hoyer's effect, and mechanical interlocking. Statements on transfer and development lengths in AASHTO LRFD Bridge specifications (AASHTO, 2007) are introduced. Large quantities of researches were conducted for the purpose of analytically predicting transfer and development length of steel strands and many formulae are proposed in the literature. Researchers strived to accommodate the use of 0.7 in. diameter strands in prestressed concrete girders.

Stud shear connectors are commonly used to transfer horizontal shear forces at the girder-deck interface, so as to achieve composite action. Note that 3/4 in. and 7/8 in. diameter studs are typically used and application of 1¼ in. studs in the bridge is also found in the state of Nebraska. The researches on the shear capacity and load-slip behavior the shear studs using experimental tests and Finite Element Analysis are surveyed in the literature.

Chapter 3 System Description and Design of PCSC Girders

3.1 *Introduction*

In this chapter, the Prestressed Concrete Steel Composite (PCSC) girder system is introduced in detail. The components, the fabrication procedure and advantages of the system are described. The design for all the components of the system is presented and the design procedure taking into account creep and shrinkage effects is introduced in detail. Design examples for single span bridges are presented and design results including prestress losses, stresses in the section, section strength, and deflection are thus summarized and compared against design requirements in AASHTO LRFD Bridge Design Specifications (AASHTO, 2007). In order to prove the advantages of the developed PCSC girders, comparisons among the PCSC girder, prestressed concrete girder and steel girder are then made.

3.2 *System Description*

The PCSC girder system is composed of a pre-tensioned concrete bottom flange, reinforced concrete deck and a rolled steel section (usually W-shaped) in between, as described in Fig. 3.1. Shear studs are used to connect the rolled steel section to the bottom flange and later to the deck creating a fully composite section. As shown in Fig. 3.1, trapezoidal shape is an alternative option for concrete bottom flange so as to prevent accumulation of water, bird nests and debris. However, a rectangular shape will be used for the concrete bottom flange in this study for simplification.

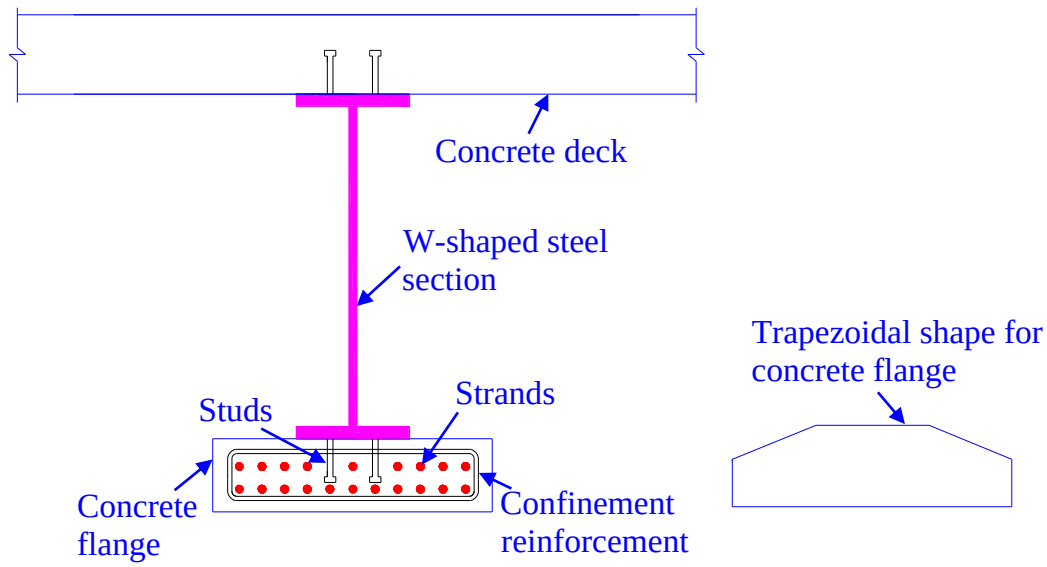

Fig. 3.1 – PCSC Girder System

3.2.1 Fabrication Procedure

The PCSC girders can be fabricated using a procedure of five steps as shown in Fig. 3.2:

- Step 1 is to weld studs to steel beam, pre-tension strands, place reinforcements and install formwork;
- Step 2 is to place concrete into the formwork and finish the top surface of concrete;
- In Step 3, the steel beam is placed on the top of fresh concrete and supported by the supported chairs, and the studs at bottom penetrate into the fresh concrete.
- Step 4 is to strip the formwork, release and cut the strands.
- Step 5 is to install formwork and reinforcement and place concrete for the reinforced concrete deck.

It is noticed that this fabrication procedure is simple, convenient, and similar to the standard procedure of producing prestressed concrete girders and does not need specialized equipment, materials and forms.

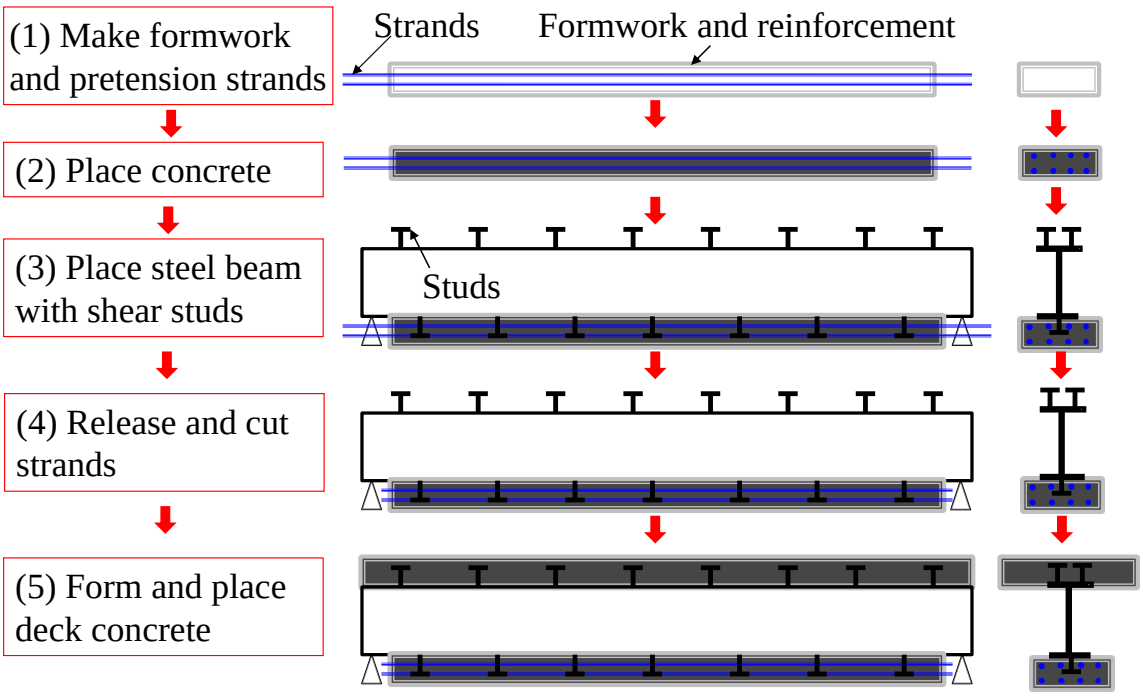

Fig. 3.2 – Fabrication Procedure of the PCSC Girder System

3.2.2 Advantages of PCSC girder

The advantages of the PCSC girder are summarized as follows:

- Using pre-tensioned bottom flange and rolled steel section greatly simplifies the fabrication and results in a very economical and lightweight section.
- The prestressing force in strands significantly improves the moment capacity of the section, while the web of steel section maintains the shear capacity.

- Using rolled steel section eliminates the problems associated with prestress release, such as concrete cracking which is common in prestressed concrete girders and draping strands which is taken as a costly and dangerous operation and is not required in the fabrication of the PCSC girder. Thus, it allows using a smaller concrete section and higher prestressing force.
- The PCSC girder is as durable as prestressed concrete girders because it uses concrete to protect bottom flange from chloride-contaminated splashes and top flange from applied de-icing chemicals.
- The PCSC girder can be made continuous by splicing the steel web and top flange.
- Efficiency of the PCSC girder can be further enhanced by using 0.7″ diameter strands and ultra-high performance concrete, which have been immensely studied in earlier research by Morcous et al. (2011), Hatami et al. (2011) and Patzlaff et al. (2009). Note that ultra-high performance concrete has high tensile stress and low delayed strains due to significant decrease of the creep deformation.

3.3 *System Design*

The design of a PCSC girder includes calculations of section properties and different loads, service design, strength design at release, ultimate strength design, vertical shear design, horizontal shear design, deck design and design check for deflection and camber. Service design is used to check service requirements of the section and materials and should take into account the effects of creep, shrinkage and relaxation of strands. Note that service design for a PCSC girder is significantly different

from a prestressed concrete girder, and will be discussed in detail later in Section 3.4. Strength design at release, which is taken as a rational method replacing the current working stress method, is used to check the strength requirement at prestress release. Ultimate strength design, which is based on strain compatibility and plane section assumption, are used to check strength requirements of the section and materials at the final stage. Vertical shear design is to check the shear strength of the section, which is mainly provided by the steel section. Horizontal shear design is to determine the number of shear studs sustaining the interface shear forces between the concrete deck and the steel section, and between the concrete bottom flange and the steel section. The deck is designed using empirical design method.

Due to the construction sequence of the PCSC girder, three stages of service design are performed as follows:

- Stage 1: At prestress release

  Structure: Girder sections only

  Loads: Self-weight of girder

- Stage 2: During construction

  Structure: Girder sections only

  Loads: Super-imposed dead loads of haunch and deck

- Stage 3: In service

  Structure: Girder sections with deck

  Loads: Super-imposed dead loads of wearing surface and railing, and moving live loads (truck + impact and lane load).

In addition to self-weight of the girder and dead loads, the following loads are considered:

- Jacking stress for strands is assumed to be 0.75 × 270 = 202.5 ksi. Prestress losses should be determined in term of elastic shortening, long-term shrinkage and creep of concrete and relaxation of strands, and prestress gains due to dead and live loads.
- Vehicular live load includes the design truck in addition to a lane load of 0.64 klf uniformly distributed over 10 ft width (AASHTO, 2007). Multiple presence factors are used based on the number of loaded lanes (maximum of 4 traffic lanes and 2 pedestrian lanes) and dynamic load allowance of 33% is used according to AASHTO (2007).

3.4 *Service Design Procedure for PCSC Girders*

As mentioned before, service design for a PCSC girder is significantly different from that for a prestressed concrete girder due to the effects of creep and shrinkage of concrete and relaxation of strands. In this section, a review on those effects is performed and then an analytical procedure is proposed to evaluate the time-dependent stresses and strains in the PCSC girder.

3.4.1 Effects of Creep and Shrinkage of Concrete and Relaxation of Strands

Due to gradual development of creep and shrinkage of concrete and relaxation of prestressing strands, the stresses and strains in prestressed concrete members varies over a life-long period (Ghali et al., 2012). For prestressed composite girders, the stress and strain redistributions between the concrete and the steel section and between the concrete

and strands will simultaneously occur along with the change of the time-dependent stresses and strains in the concrete and strands. To evaluate the time-dependent stresses and strains and their redistributions, the time functions for the stress or strain should be used for each component of PCSC girders.

For concrete, when a stress is applied on concrete, a strain will be instantaneously induced; if the stress is sustained, the strain will continue increasing with time due to creep. Consequently, the magnitude of the instantaneous strain and strain due to creep have to be determined by the age of concrete at loading and duration of loading. The relationship between sustained stress and strain can be expressed as (Ghali et al., 2012)

$$\varepsilon_c(t) = \frac{\sigma_c(t_0)}{E_c(t_0)}\left[1+\psi(t,t_0)\right] \tag{3.1}$$

where t_0 and t = ages of concrete when the initial stress is applied and when the strain is considered; $\sigma_c(t_0)$ and $E_c(t_0)$ = the concrete stress and the modulus of elasticity of concrete at age t_0; $\varepsilon_c(t)$ = concrete strain at age t; $\psi(t,t_0)$ = the creep coefficient. The creep coefficient is the ratio of strain due to creep to the instantaneous strain and can be expressed in term of age t_0 and age t. As recommended by AASHTO (2007), the creep coefficient may be taken as

$$\psi(t,t_0) = 1.9k_{vs}k_{hc}k_f k_{td}t_0^{-0.118} \tag{3.2}$$

where,

$$k_{vs} = 1.45 - 0.13\left(\frac{V}{S}\right) \geq 0.0 \tag{3.3}$$

$$k_{hc} = 1.56 - 0.008H \tag{3.4}$$

$$k_f = \frac{5}{1 + f_{ci}^{'}} \tag{3.5}$$

$$k_{vs} = \left(\frac{t - t_0}{61 - 4 f_{ci}^{'} + t - t_0} \right) \tag{3.6}$$

where, H = relative humidity (%); k_{vs} = factor for the effect of the volume-to-surface ratio of the component; k_{hc} = humidity factor for creep; k_f = factor for the effect of concrete strength; k_{td} = time development factor; $\frac{V}{S}$ = volume-to-surface ratio (in.); f'_{ci} = specified compressive strength of concrete at time of prestressing for pretensioned members. It is noted that one day of accelerated curing by steam or radiant heat is equivalent to seven days of normal curing (AASHTO, 2007).

Shrinkage occurs due to the hydration reactions taking place inside the cement matrix and moisture loss when exposed to the environment. When the volume change due to shrinkage is restrained, stresses will be generated. For concretes without shrinkage-prone aggregates, the strain due to shrinkage occurring between the ages t_0 and t, may be taken as (AASHTO, 2007)

$$\varepsilon_{sh}(t, t_0) = -k_{vs} k_{hs} k_f k_{td} \, 0.48 \times 10^{-3} \tag{3.7}$$

where, k_{hs} is humidity factor for shrinkage and can be expressed as

$$k_{hs} = 2.00 - 0.014H \tag{3.8}$$

Within the range of stresses in service conditions, the superposition is allowed for the instantaneous strain due to stress increments or decrements, the strain due to creep,

and the strain due to shrinkage. Namely, with the changes of the applied stresses, the total strain of concrete is given by (Ghali et al., 2012)

$$\varepsilon_c(t) = \sigma_c(t_0)\frac{1+\psi(t,t_0)}{E_c(t_0)} + \int_0^{\Delta\sigma_c(t)} \frac{1+\psi(t,t_0)}{E_c(\tau)} \mathrm{d}\sigma_c(\tau) + \varepsilon_{sh}(t,t_0) \tag{3.9}$$

where, τ = an intermediate age between t_0 and t; $\sigma_c(\tau)$ =initial stress applied at age t_0; $E_c(\tau)$ = modulus of elasticity of concrete at age τ; $\psi(t,t_0)$ = coefficient of creep at time t for loading at age τ. In the Eq. (3.9), $\Delta\sigma_c(t)$ can be introduced as an increment in concrete stress during the period from age t_0 to age t, but the creep coefficient $\psi(t,t_0)$ is replaced by a reduced value which equals $\chi(t,t_0)\psi(t,t_0)$, where $\chi(t,t_0)$ is defined as the aging coefficient. Thus, the Eq. (3.9) can be simplified as (Ghali et al., 2012)

$$\varepsilon_c(t) = \sigma_c(t_0)\frac{1+\psi(t,t_0)}{E_c(t_0)} + \Delta\sigma_c(t)\frac{1+\chi(t,t_0)\psi(t,t_0)}{E_c(t_0)} + \varepsilon_{sh}(t,t_0) \tag{3.10}$$

Introducing the aging coefficient greatly simplifies the strain calculations with regard to the stress increments or decrements. As stated by Ghali et al. (2012), $\chi(t,t_0)$ is usually used as a multiplier to $\psi(t,t_0)$ and rarely accurately determined, and high accuracy in the derivation of $\chi(t,t_0)$ is hardly justified. Thus, in the calculations of this dissertation, the value of aging coefficient $\chi(t,t_0)$ is directly obtained by referring to the graphs in the Appendix A given by Ghali et al. (2012). It depends on compressive strength of the concrete at 28 days, relative humidity and notional size ($h_0 = \frac{2V}{S}$).

When a strand is stretched between two fixed points, the stress will decrease progressively if the strain is maintained constant, i.e., the constant-length. The relaxation

of strands is due to the effect of creep on strands and the relaxation under constant strain is defined as intrinsic relaxation, $\Delta\sigma_{pr}$. Note that the relaxation of strands results in the time-dependent prestress loss. The stress in strands of prestressed concrete members decreases gradually due to shrinkage and creep of concrete. Thus, the relaxation value used to predict the prestress loss should be smaller than the intrinsic relaxation (Ghali et al., 2012). Due to no significant influence of relaxation on the prestress loss, the relaxation loss is evaluated based on AASHTO (2007). That is, the prestress losses due to relaxation of prestressing strands between time of transfer and deck placement, Δf_{pr1}, and between time of deck placement and final time, Δf_{pr2}, are determined as

$$\Delta f_{pr1} = \Delta f_{pr2} = 1.25 \text{ ksi} \tag{3.11}$$

3.4.2 Analytical Procedure for Calculating Stresses and Strains in PCSC Girders

To evaluate the time-dependent stresses and strains in the prestressed concrete structures, two methods are commonly used, i.e., the step-by-step numerical method and the age-adjusted elasticity modulus method (AEMM) (Ghali et al., 2012). Recently, Age-Adjusted Modular Ratio Method was also developed by Morano and Mannini (2006). Due to time-consuming computations, the step-by-step numerical method is intended for computer use and can be achieved effectively by using computer program. However, the AEMM can be performed similarly to conventional elastic analysis and can be carried out by manual computations. In this dissertation, the AEMM is used for analysis and design of PCSC girders.

When using the AEMM to determine the time-dependent stress and strain, age-adjusted transformed section properties should be obtained by using age-adjusted modulus ratios among different materials. And the elasticity modulus of concrete should be adjusted by aging coefficient and creep coefficient, i.e., age-adjusted elasticity modulus, $\bar{E}_c(t,t_0)$, which can be expressed as

$$\bar{E}_c(t,t_0) = \frac{E_c(t_0)}{1+\chi(t,t_0)\psi(t,t_0)} \tag{3.12}$$

With substitution of Eq. (3.12), Eq. (3.10) may be re-written as follows:

$$\varepsilon_c(t) = \sigma_c(t_0)\frac{1+\psi(t,t_0)}{E_c(t_0)} + \frac{\Delta\sigma_c(t)}{\bar{E}_c(t_0)} + \varepsilon_{sh}(t,t_0) \tag{3.13}$$

The three terms in Eq. (3.13) can be explained respectively as: strain due to the stress at age t_0 and creep during the period $(t-t_0)$; strain due to a stress increment of magnitude of zero at t_0 increasing gradually to a final value $\Delta\sigma_c(t)$ at age *t*; and strain due to free shrinkage occurring during the period $(t-t_0)$ (Ghali et al., 2012).

The analytical procedure to derive the time-dependent strain and stress was demonstrated in four analytical steps by Noppakunwijai et al. (2002) and Ghali et al. (2012). In this dissertation, the analytical procedure is further elaborated in terms of PCSC girders. Due to no significant effect of strand relaxation, strand relaxation is considered separately, and the prestress losses due to strand relaxation are simply evaluated by Eq. (3.11). In order to analyze the creep and shrinkage effects, the total time of loading is divided into several intervals based on different construction stages and loading stages as introduced in Section 3. In each interval, the stress and strains due to

different loads and effects of creep and shrinkage should be derived in four analytical steps as follows:

Step 1:

To calculate the stresses and instantaneous strains induced by sustained loads at the start of concerned period (such as the initial prestressing force, self-weight and dead load), the transformed section of the composite section should be determined by using conventional modulus elasticity at different ages. Note that components of the transformed section include steel section, strands and concrete section. It should also be noted that live load is not a sustained load and induces no time-dependent stresses/strain. Determine the stresses/strains in the top and bottom fibers of each concrete component, the stresses/strains in the top and bottom fibers of each steel component, and presstress losses in the prestressing strands, due to the sustained loads applied in the start of the concerned interval.

Detach all the components of steel section, strands and concrete section and allow them to deform freely. Determine the axial strain and the curvature of each concrete component induced by the creep and shrinkage in the concerned interval based on Eq. (3.1-3.8), taking into account the influences of all the sustained loads applied in and before the concerned interval. The time-dependent stresses obtained in Step 4 should also be considered as “sustained loads” and included into the calculations of the axial strain and the curvature of each concrete component due to creep and shrinkage, and the start of the “sustained loads” is assumed at the middle of the interval in which the “sustained loads” was derived.

Step 2:

Artificially restrain all the concrete components to counteract the axial strain and the curvature due to creep and shrinkage in Step 1. Calculate the restraining axial force and the corresponding stress/strain in each concrete component, and the restraining moment and the corresponding stresses/strians in the top and bottom fibers of each concrete component. In this step, the age-adjusted effective modulus for each concrete component should be used and can be determined by Eq. (3.12). The creep coefficient can be derived by Eq. (3.2) and the value of the aging coefficient can be obtained referring to the graphs in the Appendix A given by Ghali et al. (2012).

Step 3:

When the artificial restraint is removed, all the components are re-attached, and equilibrium is restored by applying the total restraining axial force and the total restraining moment of all the components to the age-adjusted transformed section in reversed directions, which are obtained in Step 2. The age-adjusted transformed section properties are obtained by using age-adjusted effective modulus for each concrete component. Determine the stresses/strains in the top and bottom fibers of each concrete component, the stresses/strains in the top and bottom fibers of each steel component, and presstress losses in the prestressing strands.

Step 4:

The time-dependent stresses and strains due to creep and shrinkage in the concerned interval can be obtained by summing up all the time-dependent values determined in Step 1 to Step 3. The time-dependent stresses should also be considered as

"sustained loads" and included into the calculations of the axial strain and the curvature of each concrete component due to creep and shrinkage in Step 1 for the next intervals. The total increment/decrement of stresses and strains generated in the concerned interval can be obtained by summing up all the values calculated in step 1 to step 3. The total stresses and strains at the end of the concerned interval can be obtained by summing up all the values calculated in and before the concerned interval.

In each interval, increment/decrement of deflection/camber at mid-span of a simply supported girder can be estimated using the values of curvature at three sections. The three sections consist of two sections at one-fourth span and one section at mid-span. Parabolic variation is assumed between these sections. The deflection/camber at mid-span, Δ, can be expressed as (Gahli et al., 2012)

$$\Delta = \frac{L^2}{24}(2\kappa_1 + \kappa_2) \tag{3.14}$$

where, L = span of the girder; κ_1 = curvature of the sections at one-fourth span; and κ_2 = curvature of the section at mid-span.

3.5 *Design Examples of PCSC Girders and Comparisons*

An 80 ft long simple span bridge, as shown in Fig. 3.3, was designed using the PCSC girder by following the design methods introduced in Section 3.3 and 3.4, based on AASHTO LRFD Bridge Design Specifications (AASHTO, 2007). The bridge has a width of 38′8″ and is composed of five girders with the center-to-center spacing of 8 ft and 7 in thick deck. For the purpose of comparison, a steel girder and a prestressed concrete girder

were also alternatively designed for this bridge, while keeping the identical structural depth of the bridge, i.e., around 43 in.

The cross-sections of the PCSC girder, the steel girder and the prestressed concrete girder are shown in Fig. 3.4. Design parameters of the girders are summarized in Table 3.1. For the PCSC girder, the concrete bottom flange has dimension of 24″×6.5″, and 18-0.7″ diameter strands, and the steel beam has the W30×90 rolled section (AISC, 2010). Confinement reinforcement of #3 bars is spaced at less than 6″ in the concrete bottom flange, based on AASHTO (2007). The detailed design calculations are attached in the Appendix A.

(a) Span of the Bridge

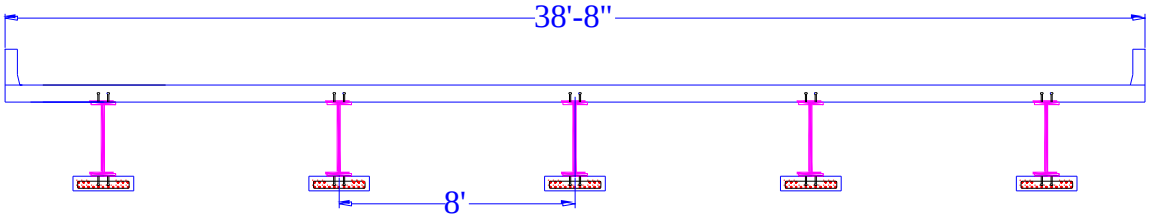

(b) Cross-section of the Bridge

Fig. 3.3 – Design Example of a Bridge

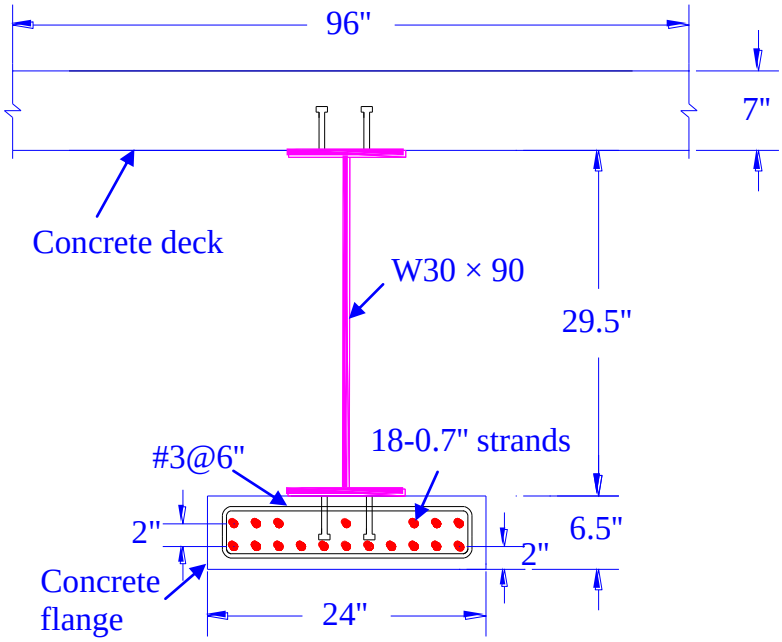

(a) PCSC Girder (PCSC-36)

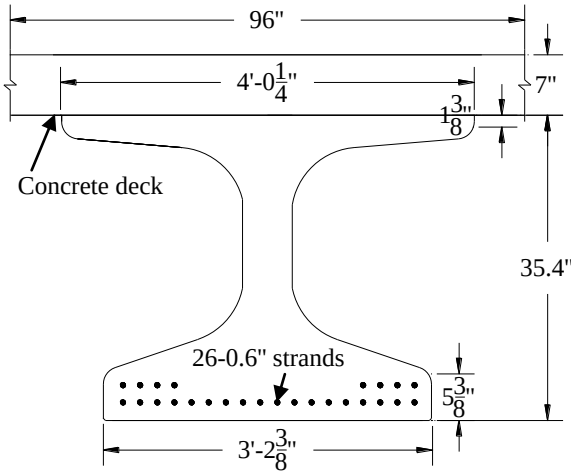

(b) Prestressed Concrete Girder (NU900)

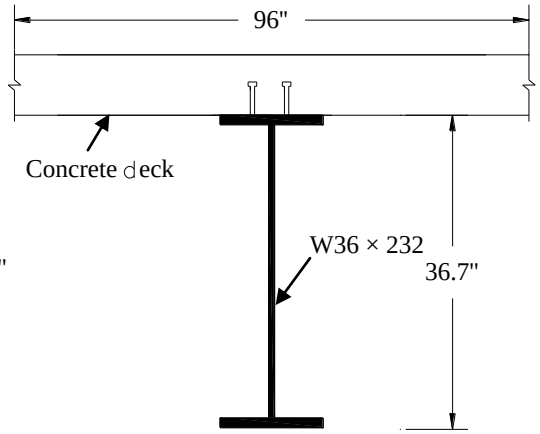

(c) Steel Girder

Fig. 3.4 – Sections of PCSC, Prestressed Concrete and Steel Girders (in.)

Table 3.1 – Design Parameters of Different Girders

	PCSC girder (PCSC-36)					Prestressed concrete girder			Steel girder		
Dimensions	Concrete bottom flange		W30×90			NU900			W36×232		
	Depth (in)	Width (in)	Height (in)	Flange (in)	Width of Web (in)	Height (in)	Flange (in)	Width of Web (in)	Height (in)	Flange (in)	Width of Web (in)
	6.5	24	29.5	10.4×0.61	0.47	35.375	48×1.375	5.875	37.1	12.1×1.57	0.87
Strands	Numbers				18-0.7"	Numbers		26-0.6"	none		
	Area (in^2)				5.292	Area (in^2)		5.642			
Steel	f_y (ksi)				50	f_y (ksi)		50	f_y (ksi)		50
Concrete	f'_{ci} (ksi)				8	f'_{ci} (ksi)		5	$f'_{c.slab}$ (ksi)		4
	f'_c (ksi)				10	f'_c (ksi)		7			
	$f'_{c.slab}$ (ksi)				4	$f'_{c.slab}$ (ksi)		4			
Span (ft)	80					80			80		
Deck depth (in.)	7					7			7		
Girder spacing (ft)	8					8			8		

The design consists of three stages: stage 1 at prestress release, stage 2 during deck placement and stage 3 in service. Since one day of accelerated curing by steam or radiant heat may be taken as seven days of normal curing, day 7 at stage 1 ($t_{0f} = 7$) is used as the age of the concrete of the bottom flange. The stage 2 and 3 is at day 30 ($t_{1f} = 30$) and day 60 ($t_{2f} = 60$), respectively. The interval 1, interval 2 and interval 3 are defined between stage 1 and stage 2, between stage 2 and stage 3, and between stage 3 and time infinity (t_{3f} = 100,000), respectively. The creep and shrinkage effects are calculated separately during different intervals, because additional loads are applied on the PCSC girder at the start of each interval.

Because the deck is placed at stage 2, day 1 at stage 2 ($t_{0f} = 1$) is used as the age of the concrete of the deck, and day 30 ($t_{1f} = 30$) and day 100,000 ($t_{3d} = 100,000$) are used as the ages of the concrete of the deck at stage 3 and time infinity, respectively, as illustrated in Fig. 3.5. At the start of the interval 2, the deck is composite with the PCSC girder, however, due to the self-weight of the deck is only applied on the PCSC girder, no stresses are induced in the deck and only shrinkage effects of deck should be considered during interval 2.

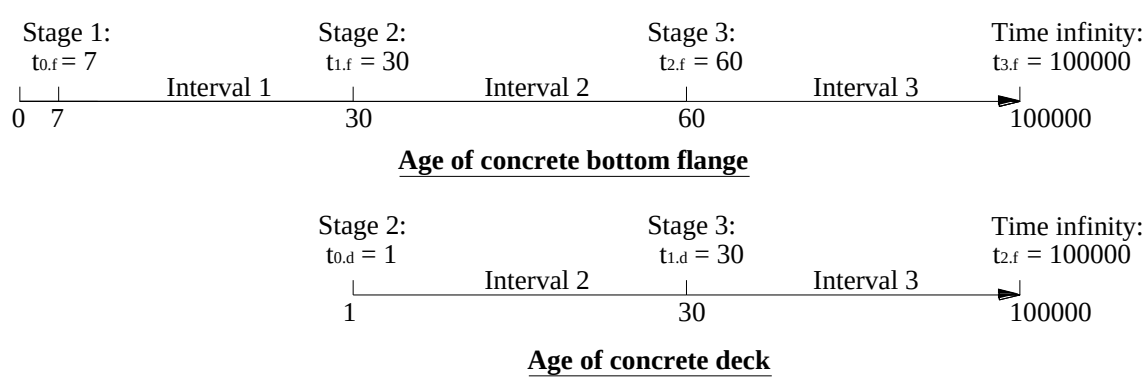

Fig. 3.5 – Concrete Ages at Different Stages and Intervals

Interval 1: From Stage 1 at release to Stage 2 during construction ($t_{0.f}$ = day 7 to $t_{1.f}$ = day 30)

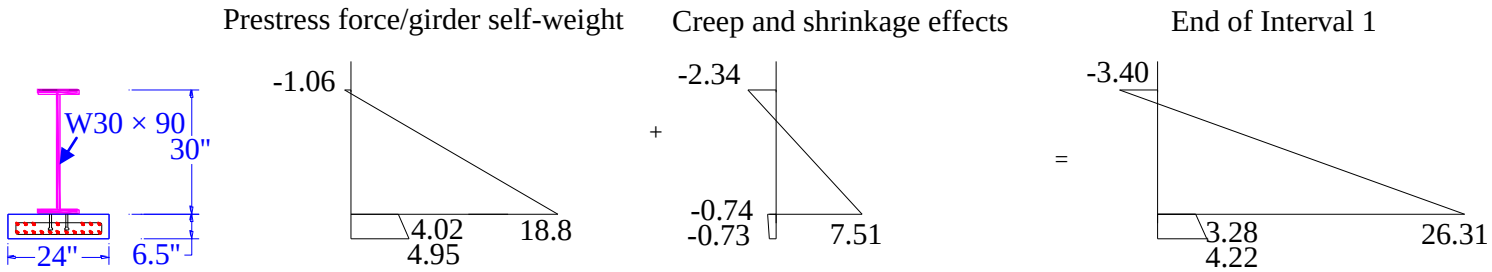

Interval 2: From Stage 2 during construction to Stage 3 in service ($t_{1.f}$ = day 30 to $t_{2.f}$ = day 60)

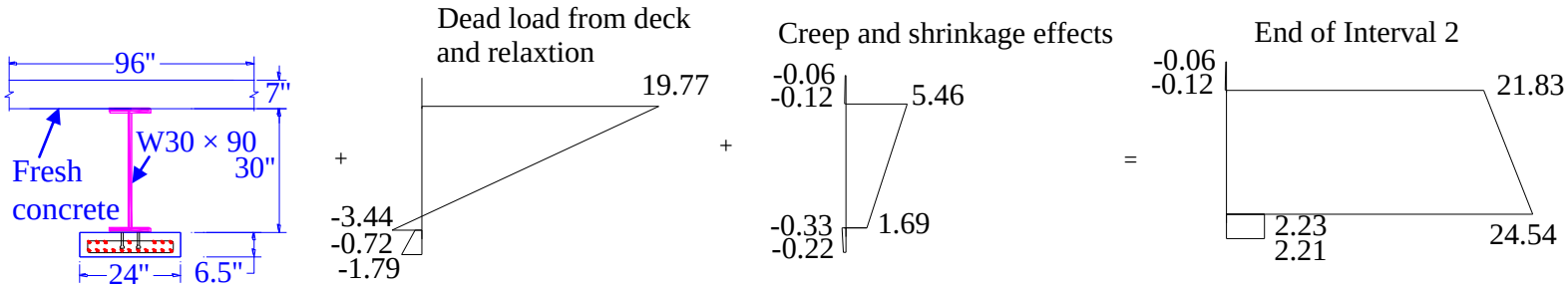

Interval 3: From Stage 3 in service to time infinity ($t_{2.f}$ = day 60 to $t_{3.f}$ = day 100000)

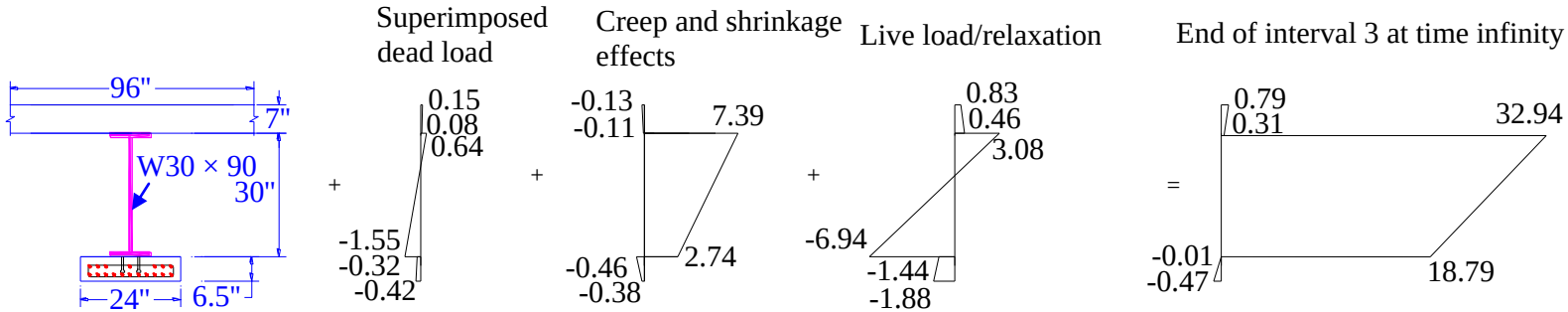

Fig. 3.6 – Stress Profiles in the PCSC Girder at Different Stages and Intervals (Stress in ksi, Negative in Tension)

Stress profiles in the PCSC girder at different stages and intervals are described in detail in Fig. 3.6. During interval 1, the stress profiles due to prestress force/girder self-weight and creep and shrinkage effects are separately shown in Fig. 3.6, and the stress profile at the end of interval 1 is thus obtained by summing up all those stress profiles. During interval 2, the stress profiles due to dead load from deck/relaxation and creep and shrinkage effects are separately described in Fig. 3.6, and the stress profile at the end of interval 2 is thus obtained by summing up all those stress profiles and the stress profile at the end of interval 1. During interval 3, the stress profiles due to superimposed dead load, creep and shrinkage effects and live load/relaxation are separately shown in Fig. 3.6, and the stress profile at the end of interval 2 is thus obtained by summing up all those stress profiles and stress profile at the end of interval 2.

Stresses versus time in strands of PCSC girder and prestressed concrete girder are described in Fig. 3.7. As illustrated in Fig. 3.7(a), prestress losses can be evaluated by taking into account elastic shortening due to prestress force/girder self-weight and losses induced by creep, shrinkage and relaxation during interval 1; elastic gain due to deck placement and losses induced by creep, shrinkage and relaxation during interval 2; elastic gain due to superimposed dead load and live load and losses induced by creep, shrinkage and relaxation during interval 3. Fig. 3.7(b) also indicates that the prestress losses of the PCSC girder due to creep and shrinkage at different stages and intervals are less than those of the prestress concrete girder. This is due the confinement of steel beam to the prestressed concrete bottom flange and higher concrete strength of the PCSC girder.

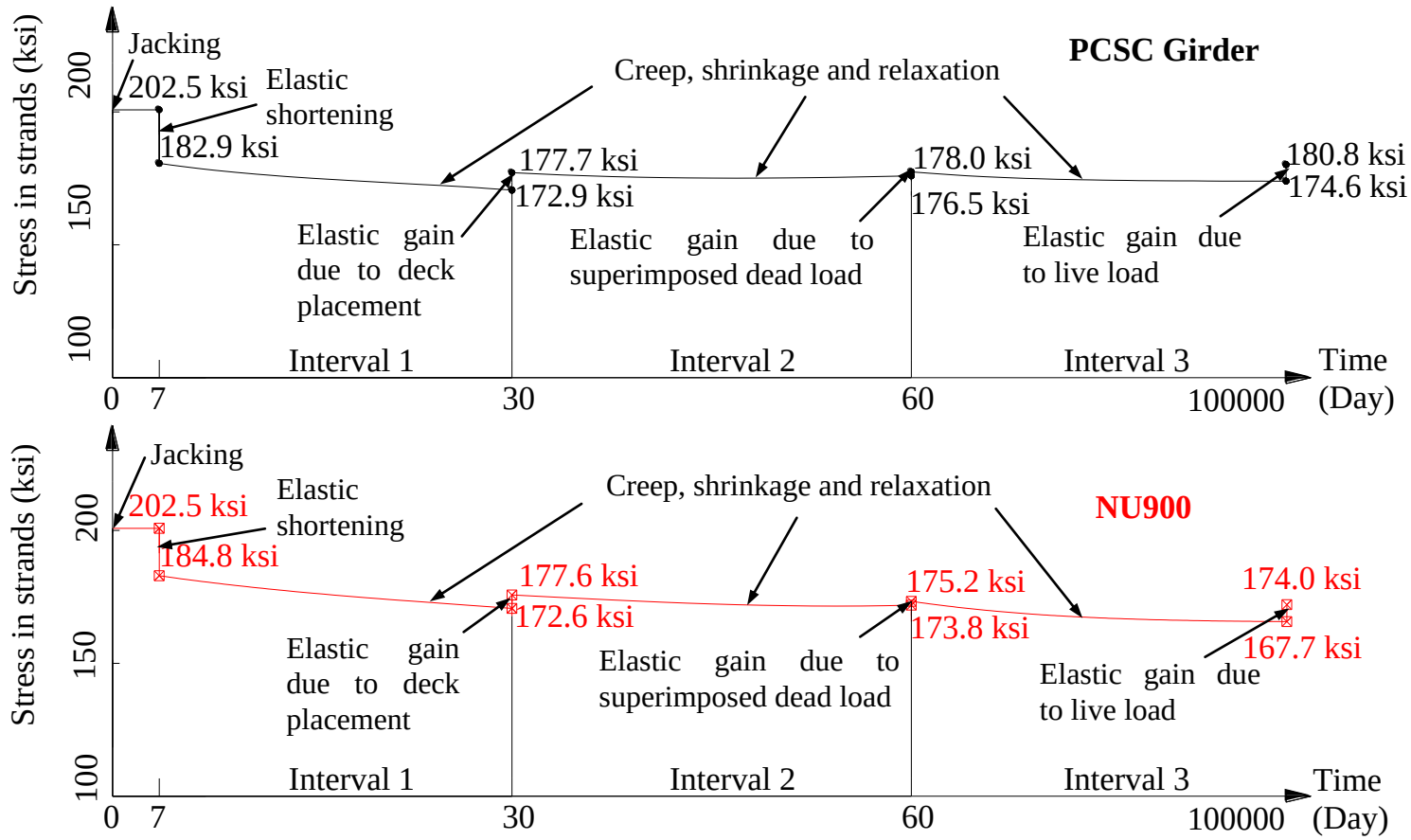

(a) Separately in PCSC Girder and NU900 Girder

Fig. 3.7 – Stresses versus Time in Strands of PCSC Girder and Prestressed Concrete Girder (Continued)

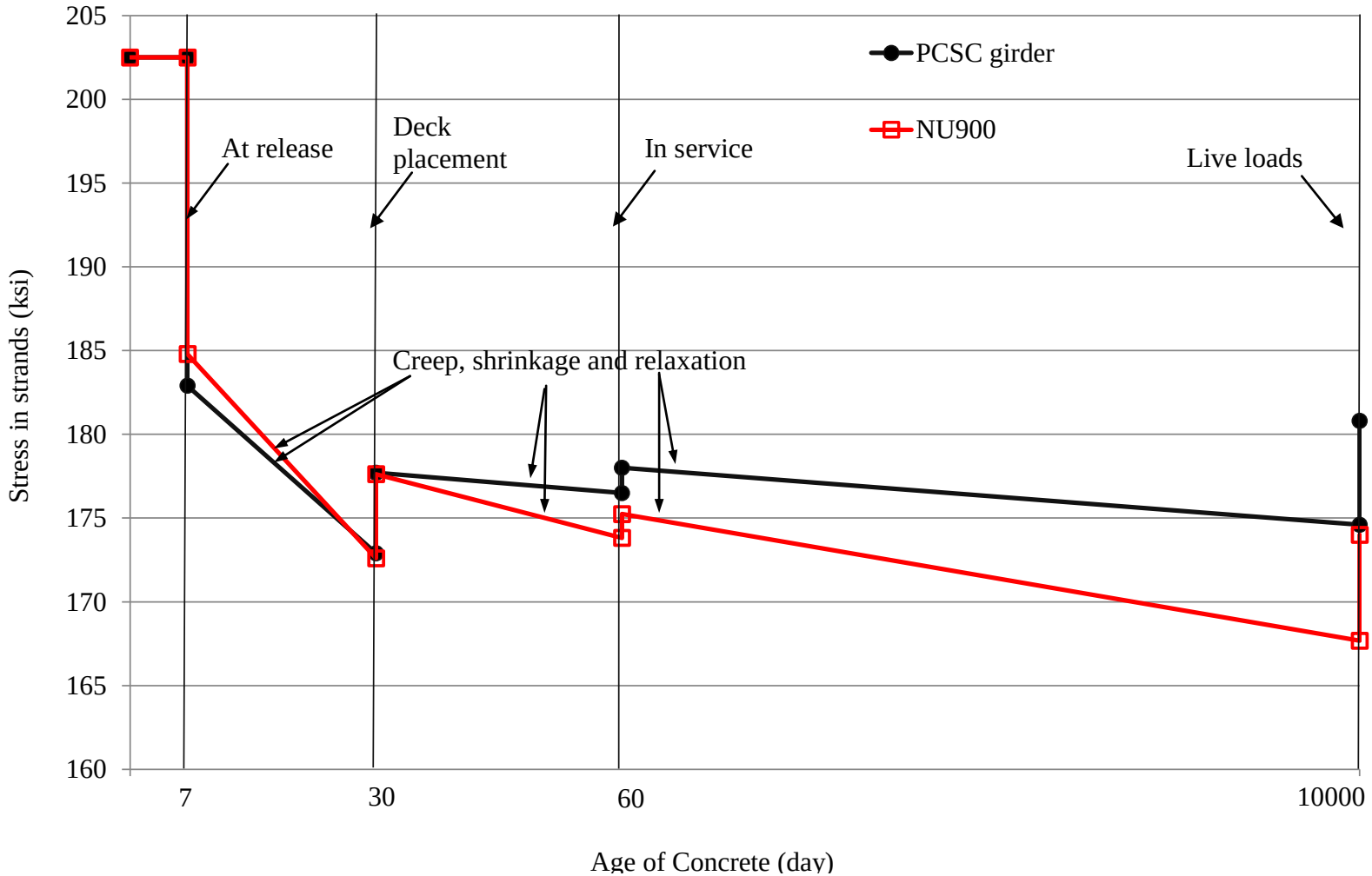

(a) Comparisons between PCSC Girder and NU900 Girder

Fig. 3.7 – Stresses versus Time in Strands of PCSC Girder and Prestressed Concrete Girder

The stress profile due to the total effects of creep and shrinkage in all intervals is described in Fig. 3.8. Fig. 3.8 indicates that average stresses of –1.4 ksi, 11.2 ksi, –0.21 ksi (Negative in tension) are induced by those effects in concrete bottom flange, steel beam and top deck, respectively. Due to the significant tensile stress generated in the concrete bottom flange, service III design is always dominant over other design considerations such as ultimate strength design and vertical shear design. In other words, the stresses in concrete bottom flange induced by creep and shrinkage should be recognized very well during the design of the PCSC girder.

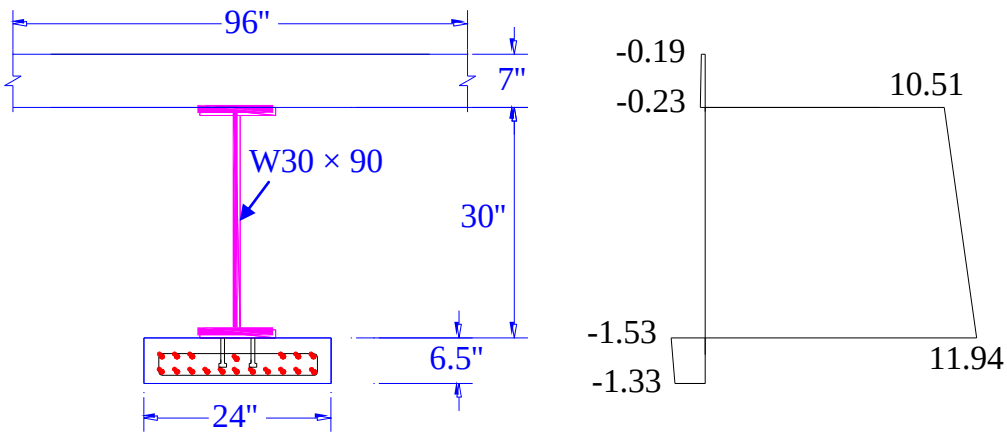

Fig. 3.8 – Stress Profile due to Total Creep and Shrinkage Effects (Stress in ksi, Negative in Tension)

Ultimate strength and service designs of the PCSC girder are compared with those of prestressed concrete and steel girders, as shown in Table 3.2. As evidenced in Table 3.2, the PCSC girder has much higher flexural strength than those of prestressed concrete and steel girders. Actually, ultimate strength design does not dominate the girder design.

Table 3.2 – Ultimate Strength and Service Designs of Different Girders

		PCSC girder (PCSC-36)			Prestressed concrete girder			Steel girder	
Ultimate strength design		ϕM_n (kip-ft)		M_u (kip-ft)	ϕM_n (kip-ft)		M_u (kip-ft)	ϕM_n (kip-ft)	M_u (kip-ft)
		6146		3707	4719		4236	5924	3634
		ϕV_n (kip)		V_u (kip)	ϕV_n (kip)		V_u (kip)	ϕV_n (kip)	V_u (kip)
		402		223	> 234 (2-#4@8in)		234	857	221
Service strength design (Mid-span section)		Stress (ksi)		Stress Limits (ksi)	Stress (ksi)		Stress Limits (ksi)	N/A	
	Stage 1	$\boldsymbol{f_{f.b}}$	**4.95**	$\mathbf{0.6f'_{ci} = 4.8}$	$f_{g.b}$	2.74	$0.6f'_{ci} = 3.0$		
		$f_{f.t}$	4.02						
		$f_{s.b}$	18.8	$0.7f_y = 35$	$f_{g.t}$	0.27	$-0.24\sqrt{f'_{ci}} = -0.54$		
		$f_{s.t}$	–1.06	$-0.7f_y = -35$					
	Stage 2	$f_{f.b}$	2.44	$0.45f'_c = 4.5$	$f_{g.b}$	1.37	$0.45\ f'_c = 2.25$		
		$f_{f.t}$	2.56						
		$f_{s.b}$	22.9	$0.7f_y = 35$	$f_{g.t}$	1.67	$0.45\ f'_c = 2.25$		
		$f_{s.t}$	16.4						
	Stage 3 to time infinity	$\boldsymbol{f_{f.b}}$	**–0.47**	$-0.19\sqrt{f'_c} = -0.60$	$\boldsymbol{f_{g.b}}$	**-0.33**	$-0.19\sqrt{f'_c} = -0.50$		
		$f_{f.t}$	–0.01						
		$f_{s.b}$	32.9	$0.7f_y = 35$	$f_{g.t}$	2.28	$0.6f'_c = 4.2$		
		$f_{s.t}$	18.8						
		$f_{d.b}$	0.31	$0.6f'_{c.slab} = 2.4$	$f_{d.t}$	0.85	$0.6f'_{c.slab} = 2.4$		
		$f_{d.t}$	0.79						
Deflection check	LL (in.)	0.88			0.81			**1.01**	
	span/800 (in.)	1.2							

Note: $f_{f.b}$ ($f_{f.t}$) = stress at bottom (top) fiber of concrete bottom flange; $f_{s.b}$ ($f_{s.t}$) = stress at bottom (top) fiber of steel beam; $f_{d.b}$ ($f_{d.t}$) = stress at bottom (top) fiber of deck; $f_{g.b}$ ($f_{g.t}$) = stress at bottom (top) fiber of prestressed concrete girder.

The service design at the mid-span section is demonstrated in Table 3.2. The stresses in the mid-span section of the prestressed concrete girder satisfy the compressive and tensile limits at all stages. No stress limit is required for the design of the steel girder. The stress at the bottom fiber of concrete bottom flange is the most critical design value and always dominates the PCSC girder design. It is found that that the stresses in the mid-span section of the PCSC girder satisfied the compressive and tensile limits at stage 2 and stage 3 to time infinity. However, at stage 1 (at prestress release), the stress in the bottom fiber of concrete flange does not satisfy the compressive stress limit as shown in Table 3.2. Actually, it is not reasonable to design the PCSC girder at prestress release using service design method. The author will propose a rational design method, i.e., strength design method for the design of the PCSC girder at prestress release, which will be presented and discussed in Chapter 4. Concrete strength of 8 ksi at prestress release is a safe design for the PCSC-36 girder. Deflection check indicates that the mid-span deflections of the three girders induced by live load satisfy the deflection limit (span/800), as shown in Table 3.2. Note that the design of the steel girder is dominated by the deflection limit as indicated in Table 3.2.

In terms of self-weight, it can be easily noticed in Table 3.3 that the self-weight of PCSC girder is 0.252 kip/ft, which is much less than that of the prestressed concrete girder, i.e., 0.675 kip/ft, and is close to that of the steel girder, i.e., 0.232 kip/ft. The unit cost of shear stud is estimated to be $4/one stud including labor cost according to Bonenfant (2009). According to (FDOT, 2012), the unit cost of prestressed concrete solid flat slab (< 48" × 12") and the straight steel beam with rolled wide flange sections is 150 $/ft-section and 1.35 $/lb., respectively. The unit cost of NU girder is estimated 250 $/ft

based on estimation of the Precasters in Omaha. Note that the labor cost is included into all the unit cost. Calculations in Table 3.3 indicate that the fabrication cost of the PCSC girder is estimated 284 $/ft, which is little larger than that of presstressed concrete girder, i.e., $250, and cheaper than that of steel girder, i.e., $321.

Table 3.3 – Self-weight and Cost of Different Girders

		PCSC girder (PCSC-36)			Prestressed concrete girder	Steel girder	
Components		Concrete bottom flange (24″×6.5″)	W30×90	Studs (3/ft)	NU900	W36×232	Studs (2/ft)
Self-weight (klf)	Separate	0.162	0.090	---	0.675	0.232	---
	Total	0.252			0.675	0.232	
Approx. Cost ($/ft)	Separate	150	122	12	250	313	8
	Total	284			250	321	

In order to further prove the feasibility of PCSC girders, different PCSC girder sections are designed for bridges with different spans, as shown in Fig. 3.9. The bridges have the identical cross-section as shown in Fig. 3.3(b). The bridges have a width of 38′8″ and are composed of five girders with the center-to-center spacing of 8 ft and 7 in thick deck. The concrete strength of concrete bottom flange is 8 ksi and 10 ksi at prestress release and 28 days, respectively. The deck has the 28-day strength of 4 ksi. The PCSC girder sections, PCSC-38, PCSC-44, PCSC-53, for 95 ft span, 125 ft span and 155 ft span are shown in Fig. 3.9(a), Fig. 3.9(b) and Fig. 3.9(c), respectively. The maximum span-to-depth ratio is up to 29.6. It is found that if the higher span is designed, more strands, and higher depth of the steel beam are required for the PCSC girder section.

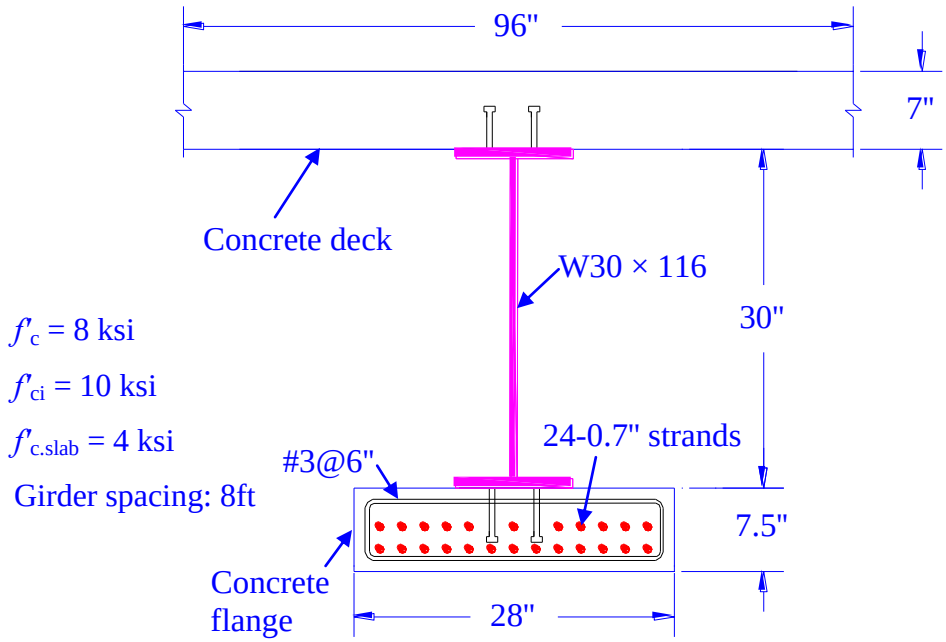

(a) PCSC-38: 95 ft Span (Span-to-depth ratio: 25.6)

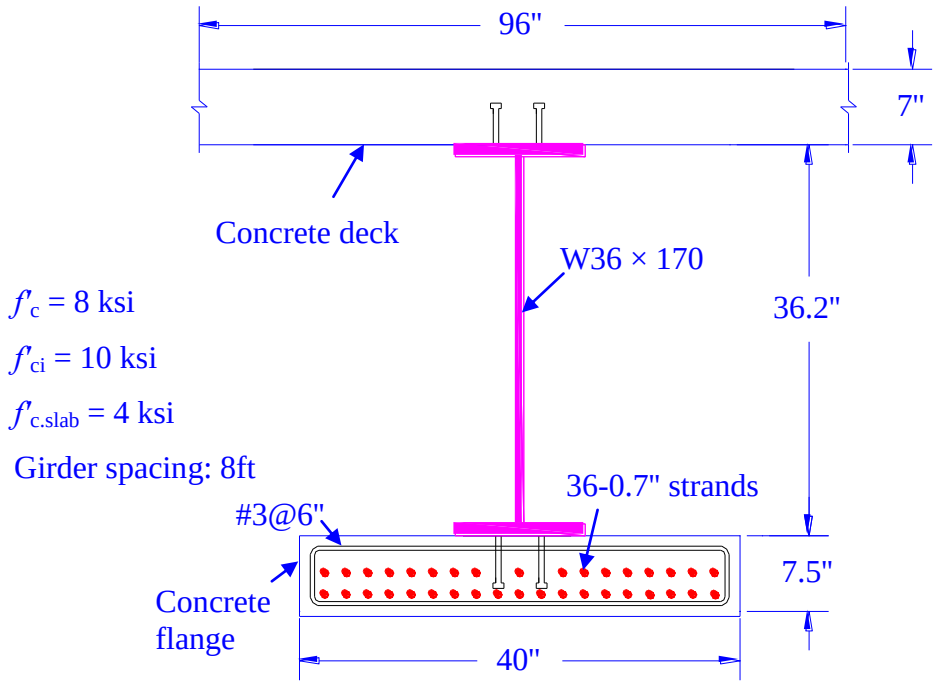

(b) PCSC-44: 125 ft Span (Span-to-depth ratio: 29.6)

Fig. 3.9 – Application of PCSC Girder Sections for Bridges with Different Spans

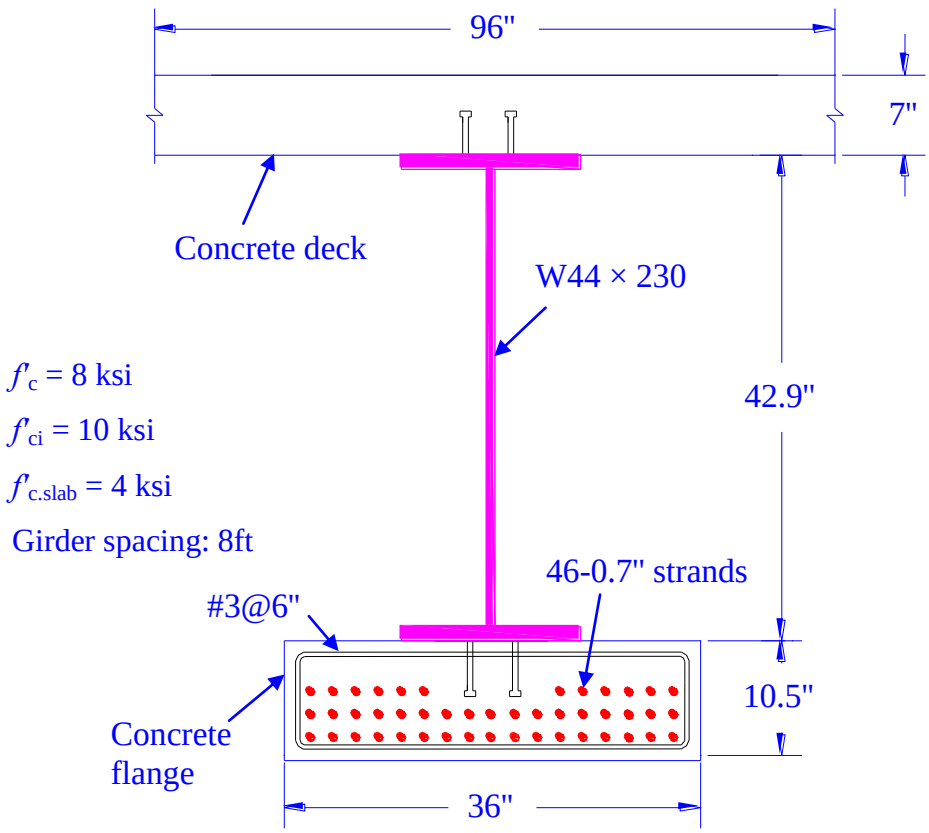

(c) PCSC-53: 155 ft Span (Span-to-depth ratio: 29.1)

Fig. 3.9 – Application of PCSC Girder Sections for Bridges with Different Spans

In order to provide the designer with an excellent starting point for preliminary design, a summary chart display the maximum attainable span versus girder spacing (6, 8, 10, and 12 ft.) for different girder sections, PCSC-38, PCSC-44, and PCSC-53, as shown in Fig. 3.10. The chart shows the largest possible span length allowed when girder spacing, concrete strength, and PCSC girder sections are given.

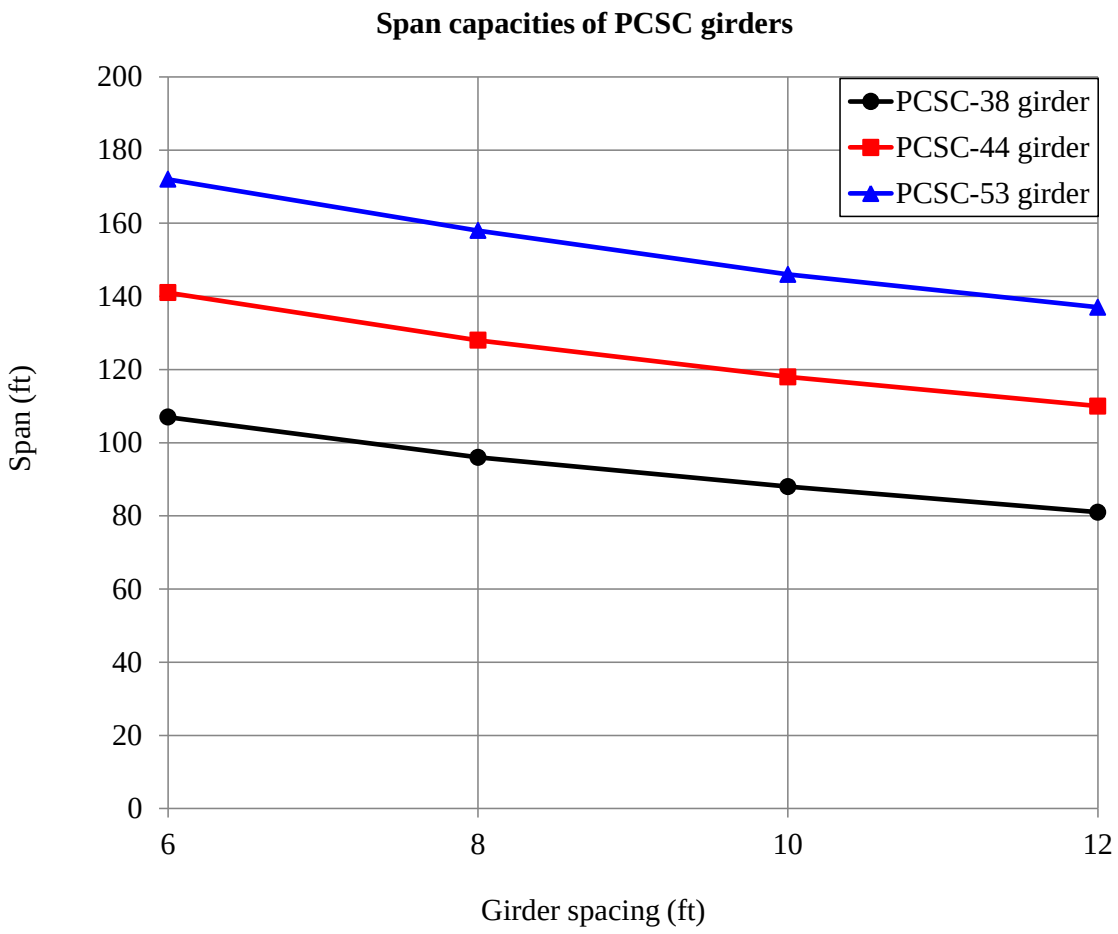

Fig. 3.10 – Summary Chart for PCSC Girder Sections with the Maximum Attainable Span versus Girder Spacing

3.6 *Summary and Conclusions*

The PCSC girder system is composed of a precast rectangular pre-tensioned concrete bottom flange, a rolled steel section (usually W-shaped), and reinforced concrete deck. Shear studs are used to connect the rolled steel section to the bottom flange and later to the deck creating a fully composite section. The fabrication procedure is proposed for PCSC girders and it is simple, convenient, and similar to that of producing prestressed concrete girders.

Due to the effects of creep and shrinkage of concrete and relaxation of strands, a design procedure to evaluate the time-dependent stresses and strains in the PCSC girder is proposed using AEMM. Design examples are presented for bridges with different spans. In order to provide the designer with an excellent starting point for preliminary design, a design summary chart showing the maximum attainable span versus girder spacing is developed for different girder sections. Some conclusions are made in the design examples:

- Prestress losses in the PCSC girder induced by creep and shrinkage at different stages and intervals are less than those of the prestress concrete girder due the confinement of steel beam to the prestressed concrete bottom flange.
- Due to the significant tensile stress generated in the concrete bottom flange, service III design is always dominant over other design considerations such as ultimate strength design and service design at other stages. The stresses in concrete bottom flange induced by the effects of creep and shrinkage are significant, and should be well designed using the proposed design procedure.
- At prestress release, the stress in the bottom fiber of concrete flange may not satisfy the compressive stress limit. However, it is not reasonable to design the PCSC girder at prestress release using service design method. Strength design method is a rational method for designing the PCSC girder at prestress release and will be introduced in the Chapter 4.
- Ultimate strength and service designs and deflection check show that PCSC girders are applicable for bridges based on AASHTO (2007).

- When designing a bridge, the PCSC girder is lighter than the prestressed concrete girder and is cheaper than that of the steel girder.
- PCSC girders are designed for single span bridges with the span up to 155 ft and span-to-depth ratio up to 29.6. It is found that if the higher span is designed, more strands, and higher depth of the steel beam are required for the PCSC girder section.

Chapter 4 Strength Design of PCSC Girders at Prestress Release

4.1 *Introduction*

Current design specifications such as ACI 318 (ACI, 2011), AASHTO LRFD (AASHTO, 2007) and PCI Design Handbook (PCI, 2010) generally only adopt working stress design method for designing pretensioned flexural concrete members. Table 4.1 lists the compressive and tensile stress limits according to those specifications at different sections immediately after prestress release (i.e., before time-dependent prestress losses). Table 4.1 indicates that current design specifications are not in a full agreement with respect to compressive and tensile stress limits.

Table 4.1 – Stress Limits at Prestress Release for Different Specifications

Specifications	Compressive stress limits (psi)		Tensile stress limits (psi)	
	Mid sections	End sections	Other sections	End sections
ACI 318 (ACI, 2011)	$0.6f'_{ci}$	$0.7f'_{ci}$	$3\sqrt{f'_{ci}}$	$6\sqrt{f'_{ci}}$
AASHTO LRFD (AASHTO, 2007)	$0.6f'_{ci}$	$0.6f'_{ci}$	$3\sqrt{f'_{ci}}$	$3\sqrt{f'_{ci}}$
PCI Design Handbook (PCI, 2010)	$0.7f'_{ci}$	$0.7f'_{ci}$	$7.5\sqrt{f'_{ci}}$	$7.5\sqrt{f'_{ci}}$
PCI Bridge Design Manual (PCI, 2011)	$0.6f'_{ci}$	$0.6f'_{ci}$	$3\sqrt{f'_{ci}}$	$3\sqrt{f'_{ci}}$

Note: 1000 psi = 6.895 MPa.

These allowable stress limits are used to satisfy the serviceability criteria, such as deflection, camber, and cracking (Noppakunwijai et al., 2001). However, it is a common perception among design engineers that compressive stress limits are provided to prevent the crushing of concrete at release, which is in fact a strength requirement not a serviceability requirement. This is especially true for PCSC girders, since no tensile stress is induced in the concrete bottom flange. In addition, an earlier study by Noppakunwijai et al. (2001) has indicated that the factor of safety provided by compressive stress limits

can vary significantly with parameters, such as reinforcement ratio, concrete strength, and section geometry, and it is not justified to use a constant stress limit at release as the basis for controlling compression failure.

Strength design method as a rational alternative to the working stress design method was developed for pretensioned flexural concrete members at prestress release by Noppakunwijai et al. (2001). Load and resistance factors of the proposed method were obtained from similar applications without calibration or reliability analysis. Later, the values of load and resistance factors have evolved over time after the evaluation and justification by Noppakunwijai, et al (2003). Recently, Deng and Morcous (2012) further calibrated the strength design of pretensioned flexural concrete members at release using reliability analysis. Load factors are selected based on the load combinations of ACI 318-11 (2011) and resistance factors are calibrated to achieve target reliability index of 3.5. Reliability analysis was conducted for several rectangular and inverted-T sections and resistance factors of 0.75 and 0.70 were recommended for 3 ksi (20.7 MPa) and 5 ksi (34.5 MPa) concrete strengths at prestress release, respectively.

Developing a rational method for evaluating the structural capacity of precast/pre-tensioned flexural concrete members at prestress release is crucial in the design and production of those members. Using the strength design method provides the designer with a rational approach replacing the current working stress method. To assist engineers to accomplish economic design and production of PCSC girders, this chapter extends the strength design method for the design of PCSC girders at prestress release. The design equations are formulated using the strain compatibility approach. Design procedure is developed to assist the engineers in applying the strength design method in an efficient

and accurate manner. Design examples are also presented and compared against those designed using the working stress method.

4.2 *Formulation of Design Equations*

The formulation of design equations for strength design at release was conducted using the strain compatibility approach and based on all the assumptions of the ultimate strength design of reinforced concrete. These assumptions include:

(1) Plane sections remain plane. Sections perpendicular to the axis of bending keep plane under bending.

(2) A perfect bond exists between the concrete and strands, and between the concrete and steel. The strains in the strands and steel are equal to those in the concrete at the same level.

(3) The stresses can be derived from the strains in the concrete, strands and steel by using their stress-strain relationships, respectively.

Due to the shallow section of the concrete bottom flange and the deep W-shaped steel section, the bottom of web and the bottom flange of the steel section always yield when using strength design of PCSC girders at prestress release. Thus, it is assumed that the neutral axis of the girder section is located at the web of the steel section and the bottom flange of the steel section yields.

The concrete strength at release, f'_{ci}, and distant from extreme compression fiber to neutral axis, c, are the only two unknown variables. The solutions for f'_{ci} and c can be derived based on the formulation of design equations of axial force and bending moment

for both applied load and section resistance. Applied axial force and bending moment as shown in Fig. 4.1 can be formulated as follows

$$Q_{sP} = A_{ps} f_{pj} \tag{4.1}$$

$$Q_{sM} = A_{ps} f_{pj} d_p \tag{4.2}$$

$$Q_{swM} = M_{sw} \tag{4.3}$$

where, Q_{sP} = axial force due to prestressing strands; Q_{sM} = bending moment due to eccentricities of prestressing strands; Q_{swM} = bending moment due to self-weight; A_{ps} = area of prestressing strands; f_{pj} = jacking stress of strands; d_p = centroidal distance of strands from bottom fiber; and M_{sw} = moment due to self-weight.

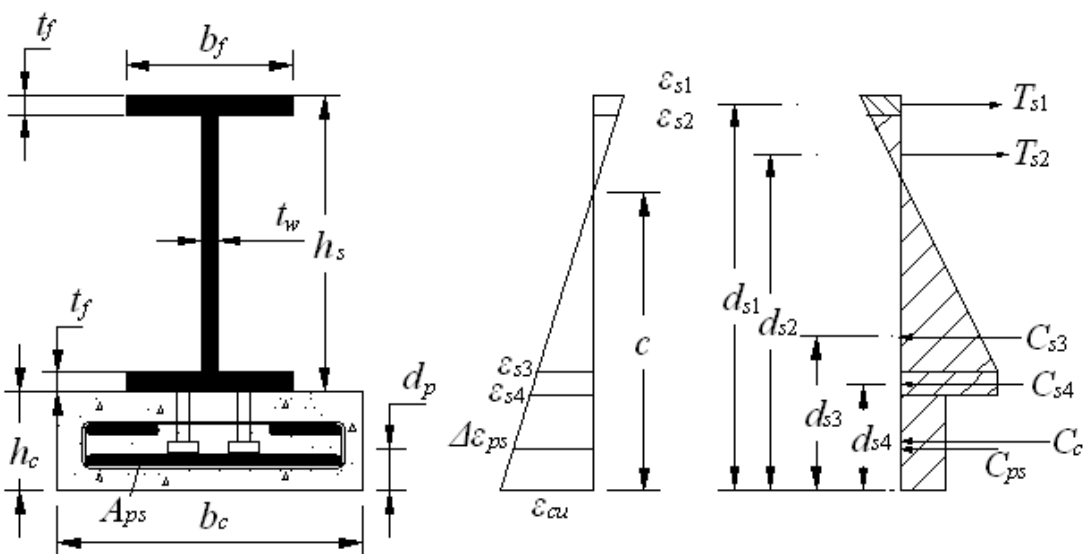

Fig. 4.1 – Applied Load, Strains and Section Resistance of the Section

Section resistance is defined as the total axial force and moment that the section can resist. Fig. 4.1 shows the components of the section resistance for the section. Based on Fig. 4.1, the strain changes in strands and the strains of fibers in steel beam can be derived as

$$\Delta\varepsilon_{ps} = \frac{c - d_p}{c}\varepsilon_{cu} \tag{4.4}$$

$$\varepsilon_{s1} = \frac{h_s + h_c - c}{c}\varepsilon_{cu} \tag{4.5}$$

$$\varepsilon_{s2} = \frac{h_s + h_c - c - t_f}{c}\varepsilon_{cu} \tag{4.6}$$

$$\varepsilon_{s3} = \frac{c - h_c - t_f}{c}\varepsilon_{cu} > \varepsilon_s \tag{4.7}$$

$$\varepsilon_{s4} = \frac{c - h_c}{c}\varepsilon_{cu} > \varepsilon_s \tag{4.8}$$

where, c = distance from extreme compression fiber to neutral axis; h_s = depth of steel section; h_c = depth of concrete bottom flange; t_f = thickness of flanges of steel section; ε_{cu} = ultimate concrete compression strain, equals 0.003; $\Delta\varepsilon_{ps}$ = strain change in strands. ε_{s1} = strain at the top fiber of top flange of steel section; ε_{s2} = strain at the bottom fiber of top flange of steel section; ε_{s3} = strain at the top fiber of bottom flange of steel section; ε_{s4} = strain at the bottom fiber of bottom flange of steel section; ε_s = yielding strain of steel, i.e., equals 0.00172 for 50 ksi (345 MPa) steel. Note that ε_{s3} and ε_{s4} should be verified and should be larger than ε_s. Since yielding stress should be used for the value of stresses in bottom flange of the steel section, the following equations are used for ε_{s2} and ε_{s3}

$$\varepsilon_{s3} = \varepsilon_s \tag{4.9}$$

$$\varepsilon_{s4} = \varepsilon_s \tag{4.10}$$

Meanwhile, due to the small thickness of the steel web, the strain in the steel web is assumed to be linear and the strain in the bottom fiber of the steel web is equal to yielding strain of steel, ε_s. The stress in steel web is calculated by using strains ε_{s2} and ε_{s3} from Eq. (4.6) and (4.9), respectively.

Distances from the force components on the steel beam section to the bottom fiber can be expressed as follows

$$d_{s1} = h_s + h_c - \frac{t_f}{2} \tag{4.11}$$

$$d_{s2} = \frac{2(h_s + h_c - t_f) + c}{3} \tag{4.12}$$

$$d_{s3} = \frac{c + 2(h_c + t_f)}{3} \tag{4.13}$$

$$d_{s4} = h_c + \frac{t_f}{2} \tag{4.14}$$

where, d_{s1} = distance from T_{s1} to bottom fiber of section; d_{s2} = distance from T_{s2} to bottom fiber of section; d_{s3} = distance from C_{s3} to bottom fiber of section; d_{s4} = distance from C_{s4} to bottom fiber of section.

Force components of the resistance can be derived as follows

$$T_{s1} = b_f t_f E_s \frac{(\varepsilon_{s1} + \varepsilon_{s2})}{2} \tag{4.15}$$

$$T_{s2} = t_w (h_s + h_c - c - t_f) E_s \frac{\varepsilon_{s2}}{2} \tag{4.16}$$

$$C_{s3} = t_w (c - h_c - t_f) E_s \frac{\varepsilon_{s3}}{2} \tag{4.17}$$

$$C_{s4} = b_f t_f E_s \frac{(\varepsilon_{s3} + \varepsilon_{s4})}{2} \tag{4.18}$$

$$C_c = \alpha f_{ci}^{'} h_c b_c \tag{4.19}$$

$$C_{ps} = A_{ps} \left(\Delta\varepsilon_{ps} E_{ps} - \alpha f_{ci}^{'} \right) \tag{4.20}$$

where, T_{s1} = tensile force on the top flange of steel section; T_{s2} = tensile force on the web of steel section; C_{s3} = compressive force on the web of steel section; C_{s4} = compressive force on the bottom flange of steel section; b_f = width of flange; E_s = elastic modulus of steel; E_{ps} = elastic modulus of strands; t_w = thickness of web; A_{ps} = area of strands; α = factor relating to compressive stress, f'_{ci}. For f'_{ci} = 3~5 ksi (28~48 MPa), α equals 0.90; for f'_{ci} = 5~10 ksi (48~69 MPa), α equals 0.85. Note that the values of α are developed based on the expression for the stress-strain curve of concrete proposed by Wee et al. (1996) as

$$f_c = f'_{ci}\left[\frac{k_1\beta\left(\dfrac{\varepsilon}{\varepsilon_o}\right)}{k_1\beta - 1 + \left(\dfrac{\varepsilon}{\varepsilon_o}\right)^{k_2\beta}}\right] \tag{4.21}$$

where, f_c and ε are stress and strain on concrete respectively; strain at peak stress is expressed as

$$\varepsilon_o = 0.00078(f'_{ci})^{1/4} \qquad \text{(in MPa)} \tag{4.22}$$

$$\beta = \frac{1}{1 - f'_{ci}/(\varepsilon_o E_{it})} \tag{4.23}$$

where, initial tangent modulus is expressed as

$$E_{it} = 10200(f'_{ci})^{1/3} \qquad \text{(in MPa)} \tag{4.24}$$

and when $f'_{ci} \leq 50$ MPa (7.25 ksi), k_1 = 1and k_2 = 1; when $f'_{ci} > 50$ MPa (7.25 ksi), for ascending branch of the curve, k_1 = 1and k_2 = 1, and for descending branch of the curve, the following equations should be used as

$$k_1 = \left(\frac{50}{f'_{ci}} \right)^{3.0} \tag{4.25}$$

$$k_2 = \left(\frac{50}{f'_{ci}} \right)^{1.3} \tag{4.26}$$

As previously assumed, the strain of the top fiber of concrete bottom flange is larger than the yielding strain of steel, ε_s. For conservative consideration, the yielding strain is used at the top fiber. The strain of the bottom fiber of concrete bottom flange equals to ultimate concrete compression strain, 0.003. Substitution of strains on the top and bottom fibers of concrete bottom flange into Eq. (4.26) gives stresses. Factor, α, is used to simplify the stresses on concrete bottom flange as a rectangular stress block. The average stress of the top and bottom fibers of concrete bottom flange divided by f'_{ci} yields the value of α.

Axial force resistance and moment resistance are found as follows

$$R_P = C_c + C_{ps} + C_{s3} + C_{s4} - T_{s1} - T_{s2} \tag{4.27}$$

$$R_M = C_c \frac{h_c}{2} + C_{ps} d_p + C_{s3} d_{s3} + C_{s4} d_{s4} - T_{s1} d_{s1} - T_{s2} d_{s2} \tag{4.28}$$

According to ACI 318-11 design code (ACI 318, 2011), the design strength at the sections shall not be less than the required strength with combinations of factored loads. The strength design requirement can be expressed as follows

$$\phi R_{P_n} \geq Q_{P_u} \tag{4.29}$$

$$\phi R_{M_n} \geq Q_{M_u} \tag{4.30}$$

where, ϕR_{P_n} & ϕR_{M_n} = the design strength; R_{P_n} = nominal values for axial force strength; R_{M_n} = nominal bending moment strength; ϕ = resistance factor (or strength reduction factor), as suggested by Deng and Morcous (2012), ϕ = 0.75 for f'_{ci} = 3 ksi and ϕ = 0.70 for f'_{ci} = 5 ksi; and Q_{P_u} & Q_{M_u} = the required strength calculated from factored load effect. The required axial force strength and bending moment strength, i.e., Q_{P_u} and Q_{M_u}, can be expressed with load factors as follows

$$Q_{P_u} = \gamma_p Q_{sP_n} \tag{4.31}$$

$$Q_{M_u} = \gamma_p Q_{sM_n} + \gamma_m Q_{swM_n} \tag{4.32}$$

where, Q_{sP_n} = nominal axial force due to prestressing strands; Q_{sM_n} = nominal bending moment due to prestressing strands; Q_{swM_n} = nominal bending moment due to self-weight; γ_p = initial prestress load factor, equals 1.2; and γ_m = self-weight moment load factor, equals 0.9 when self-weight moment counteracts the moment due to prestress relative to neutral axis of the section, or 1.2 when the self-weight moment is in the same direction as the moment due to prestress relative to neutral axis of the section. However, the moments in the formulation of design equations are calculated relative to the bottom fiber of the section. For calculation purpose, self-weight moment is positive when it induces compressive stress on the top fibers and negative when it induces compressive stress on the bottom fibers.

It is worth noting that the values of load factors (i.e., γ_p and γ_m) are adopted from those of the dead load according to load factor combinations of ACI 318-11 design code

(ACI 318, 2011). The factor of 1.2 is commonly used for the dead load. However, it is specified to be 0.9 for the case where a higher dead load reduces the effects of other loads.

(a) Simplified solutions

The unknown variables, f'_{ci} and c, can thus be determined by substitutions of Eqs. (4.4-6) and (4.9-14) into Eqs. (4.15-20), Eqs. (4.15-20) into Eqs. (4.27-28), Eqs. (4.1-3) into Eqs. (4.31-32) and substitution of Eqs. (4.27-28) and (4.31-32) into Eq. (4.29-30). To derive the solutions to f'_{ci} and c, the following two equations need to be solved:

$$f_{ci}^{'} = \frac{A_{ps}\left(\frac{\gamma_p}{\phi} f_{pj} - \Delta\varepsilon_{ps} E_{ps}\right) + \frac{E_s t_w}{2}\left[\left(c - h_c - t_f\right)\varepsilon_s - \left(h_s + h_c - c - t_f\right)\varepsilon_{s2} + \frac{b_f t_f}{t_w}\left(2\varepsilon_s - \varepsilon_{s1} - \varepsilon_{s2}\right)\right]}{\alpha\left(h_c b_c - A_{ps}\right)} \tag{4.33}$$

$$f_{ci}^{'} = \frac{A_{ps} d_p\left(\frac{\gamma_p}{\phi} f_{pj} - \Delta\varepsilon_{ps} E_{ps}\right) + \frac{\gamma_m}{\phi} M_{sw} + \frac{E_s t_w}{2}\left\{\left(c - h_c - t_f\right)\varepsilon_s d_{s3} - \left(h_s + h_c - c - t_f\right)\varepsilon_{s2} d_{s2} + \frac{b_f t_f}{t_w}\left[2\varepsilon_s d_{s4} - \left(\varepsilon_{s1} + \varepsilon_{s2}\right) d_{s1}\right]\right\}}{\alpha\left(h_c b_c \frac{h_c}{2} - A_{ps} d_p\right)} \tag{4.34}$$

The distances of bottom fiber and top fiber of steel web to the bottom fiber of section are taken as the lower bound and upper bound for c, respectively. Trials of different values of c into Eqs. (4.33) and (4.34) give the two values of f'_{ci}. The correct value of c is the one that results in the same value of f'_{ci}.

(b) Closed form solutions

To derive the closed form solution to c from Eqs. (4.33) and (4.34), the following cubic equation needs to be solved:

$$Ac^3 + Bc^2 + Cc + D = 0 \tag{4.35}$$

where the following notation is used,

$$A = \frac{1}{6} w_1 E_s t_w \left(\varepsilon_{cu} - \varepsilon_s\right) \tag{4.36}$$

$$B = -\frac{1}{2} E_s t_w \left[w_2 \left(\varepsilon_{cu} - \varepsilon_s \right) + \frac{1}{3} w_1 \varepsilon_s \left(h_c + t_f \right) \right] \tag{4.37}$$

$$C = r_4 + r_5 - w_2 \frac{\gamma_p A_{ps} f_{pj}}{\phi} + w_1 \frac{\gamma_p A_{ps} f_{pj} d_p + \gamma_m M_{sw}}{\phi} \tag{4.38}$$

$$D = r_1 + r_2 + r_3 \tag{4.39}$$

where,

$$w_1 = h_c b_c - A_{ps} \tag{4.40}$$

$$w_2 = \frac{1}{2} h_c{}^2 b_c - A_{ps} d_p \tag{4.41}$$

$$r_1 = A_{ps} E_{ps} \varepsilon_{cu} h_c b_c d_p \left(d_p - \frac{1}{2} h_c \right) \tag{4.42}$$

$$r_2 = \frac{1}{2} E_s \varepsilon_{cu} t_w \left\{ w_2 \left[t_f \left(2h_c + 2h_s - t_f \right) - \left(h_c + h_s \right)^2 \right] + w_1 \left[\frac{2}{3} (h_c{}^3 + h_s{}^3 - t_f{}^3) + (h_c + h_s)(2h_c h_s + 2t_f{}^2) - 2t_f (h_c + h_s)^2 \right] \right\} \tag{4.43}$$

$$r_3 = \frac{1}{2} E_s \varepsilon_{cu} b_f t_f \left\{ w_2 \left(-2h_c - 2h_s + t_f \right) + w_1 \left[2 \left(h_c + h_s \right)^2 - t_f (2h_c + 2h_s - \frac{1}{2} t_f) \right] \right\} \tag{4.44}$$

$$r_4 = \frac{1}{2} E_s t_w \left\{ w_2 \left[2\varepsilon_{cu} \left(h_c + h_s - t_f \right) - \varepsilon_s (h_c + t_f) \right] + w_1 \left[\varepsilon_{cu} \left(-(h_c + h_s)^2 + t_f (2h_c + 2h_s - t_f) \right) + \frac{2}{3} \varepsilon_s (h_c + t_f)^2 \right] \right\} \tag{4.45}$$

$$r_5 = -\frac{r_1}{d_p} + \frac{1}{2} E_s b_f t_f \left\{ 2w_2 \left(\varepsilon_{cu} + \varepsilon_s \right) + w_1 \left[-2h_c \left(\varepsilon_{cu} + \varepsilon_s \right) - 2h_s \varepsilon_{cu} + t_f \left(\varepsilon_{cu} - \varepsilon_s \right) \right] \right\} \tag{4.46}$$

Assume,

$$p = 9AC - 3B^2 \tag{4.47}$$

$$q = 2B^3 - 9ABC + 27A^2 D \tag{4.48}$$

$$U = -\frac{q}{2}\sqrt{\left(\frac{3}{|p|}\right)^3} \tag{4.49}$$

According to Oswald (2009), the solutions of real values to c are found as

$$c = \begin{cases} \frac{1}{3A}\left(\sqrt[3]{-q} - B\right) & \text{if } p = 0 \quad (4.50a) \\ \frac{1}{3A}\left[2\sqrt{\frac{|p|}{3}}\sinh\left(\frac{1}{3}\operatorname{arcsinh}U\right) - B\right] & \text{if } p > 0 \quad (4.50b) \\ \frac{1}{3A}\left\{2(-1)^n\sqrt{\frac{|p|}{3}}\cosh\left[\frac{1}{3}\operatorname{arccosh}\left((-1)^n U\right)\right] - B\right\} & \text{if } p < 0 \text{ and } U \leq -1,\ n = 1;\ \text{if } p < 0 \text{ and } U \geq 1,\ n = 2 \quad (4.50c) \\ \frac{1}{3A}\left\{2\sqrt{\frac{|p|}{3}}\cos\left[\frac{1}{3}\arccos U + (k-1)\cdot\frac{2\pi}{3}\right] - B\right\} & \text{if } p < 0 \text{ and } |U| \leq 1 \text{ where } k = 1, 2, 3 \quad (4.50d) \end{cases}$$

Note that if the value of c is solved by Eq. (4.50d), two of the three solutions can be easily abandoned due to the meaning of engineering for each design. And f'_{ci} is determined by

$$f'_{ci} = \frac{\frac{\gamma_p}{\phi}Q_{sP_n} - A_{ps}\Delta\varepsilon_{ps}E_{ps} - E_s t_w\left((c - h_c - t_f)\frac{\varepsilon_s}{2} - (h_s + h_c - c - t_f)\frac{\varepsilon_{s2}}{2}\right) - E_s b_f t_f\left(\varepsilon_s - \frac{(\varepsilon_{s1} + \varepsilon_{s2})}{2}\right)}{\alpha(h_c b_c - A_{ps})} \tag{4.51}$$

4.3 *Design Procedure and Examples*

4.3.1 Proposed Procedure

In order to assist designers use the developed formulae for strength design of PCSC girders at release, the following procedure is proposed:

(1) Determine the following parameters: b_f, h_s, t_f, t_w, b_c, h_c, d_p, A_{ps}, f_{pj}, f_y, w_{ow} and L.

(2) Calculate self-weight moment, M_{sw} and determine the value of load factor γ_m for M_{sw}. γ_m equals 0.9 when M_{sw} counteracts the moment due to prestress or 1.2 when M_{sw} is in

the same direction as the moment due to prestress both relative to neutral axis of the section. Select the value for resistance factor, ϕ, which equals 0.75 and 0.70 for the concrete strength at release of 3 ksi (20.7 MPa) and 5 ksi (34.5 MPa), respectively.

(3) Two methods can be adopted as follows:

- Simplified solutions

Trials of different values of c may be required to obtain the solution f'_{ci}. Choose a value of c, which is larger than the distance from bottom fiber of steel web to bottom fiber of section (i.e., $h_c + t_f$) and less than the distance from top fiber of steel web to bottom fiber of section (i.e., $h_c + h_s - t_f$). Substitute the value of c into Eqs. (4.33-34) to find two solutions for f'_{ci}. If the solutions of f'_{ci} obtained from Eqs. (4.33) and (4.34) are almost identical, the correct solution of f'_{ci} is obtained. If the solutions of f'_{ci} obtained from Eqs. (4.33) and (4.34) are significantly different, another trial is made using a different value of c.

- Closed form solutions

Calculate w_1, w_2, r_1, r_2, r_3, r_4, r_5 by Eqs (4.40-46) and substitute into Eqs (4.36-39) giving A, B, C and D. Subsequently calculate p, q and U by Eqs. (4.47-49), respectively. According to the range of p and U, an appropriate equation in Eqs. (4.50a-d) should be chosen to calculate the design solution of c. The design solution of f'_{ci} is obtained by Eq. (4.51).

(4) Design the required amount of shear studs between steel beam and concrete bottom flange from end to transfer length, which is determined based on the horizontal shear force.

(5) Check the design results.

4.3.2 Design Examples and Comparison with Working Stress Design Method

To help the designers understand the proposed design procedure, design examples are developed using the PCSC girder sections designed for bridges in Section 3.5. Concrete bottom flanges of the girders were designed with the concrete strength of 8 ksi at prestress release. Girder sections, PCSC-36, PCSC-38, PCSC-44, and PCSC-53, were shown in Fig. 3.4(a), Fig. 3.9(a), Fig. 3.9(b), Fig. 3.9(c), respectively, and designed for bridges with spans of 80 ft, 95 ft, 125 ft, and 155 ft, respectively. For instance, the dimensions of PCSC-36 girder section are shown in Fig. 4.2. For the purpose of comparisons, those girders are designed using strength design method and working stress design method. An example with detailed design calculations for the girder section PCSC-36 is attached in Appendix B, including strength design method with simplified solutions and closed form solutions and working stress design method.

The required concrete strength at release, f'_{ci}, end sections of those girders at transfer length, are summarized in Table 4.2. This is because the end section is the critical section due to self-weight of the girders when using strength design method. Table 4.2 indicates that the required concrete strength at release, f'_{ci}, at end sections using strength design method are no more than those using working stress design method. It is noted that the lower required concrete strength at release benefits the production of the PCSC girder. Based on the required concrete strength at release using strength design method shown in Table 4.2, it can be concluded that concrete strength of 8 ksi at release was safely designed for concrete bottom flanges of girder sections, PCSC-36, PCSC-38, PCSC-44, and PCSC-53 in Section 3.5.

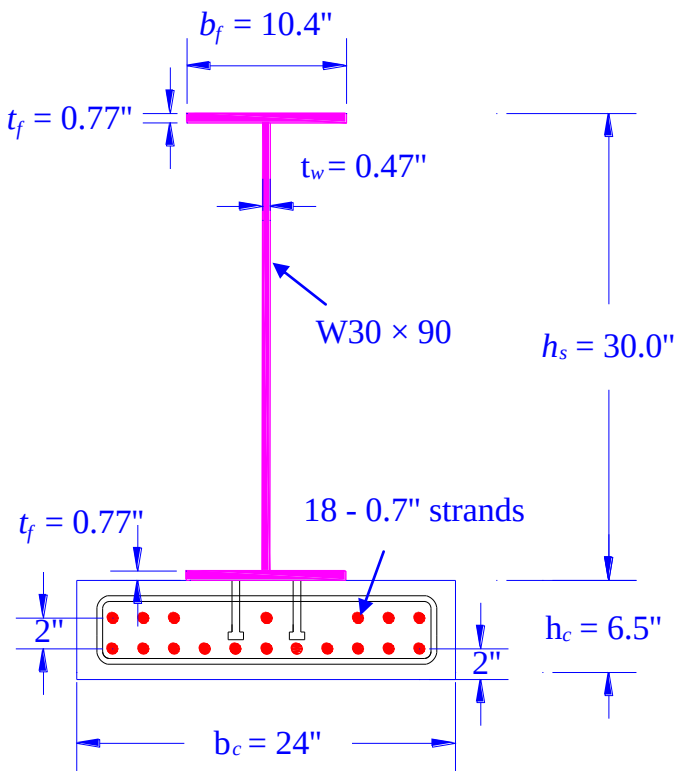

Fig. 4.2 – Cross-section of the PCSC-36 Girder (Span = 80 ft)

Table 4.2 – Comparisons of Strength Design and Working Stress Design for the end sections of PCSC Girders at Release

Girder sections	Span (ft)	f'_{ci} (ksi)			
		Strength design	Working stress design using different compressive stress limits		
			ACI (2011)	AASHTO (2007) or PCI (2011)	PCI (2010)
			$0.7f'_{ci}$	$0.6f'_{ci}$	$0.7f'_{ci}$
PCSC-36	80	7.6	7.8	9.1	7.8
PCSC-38	95	7.7	8.0	9.3	8.0
PCSC-44	125	8.0	8.0	9.3	8.0
PCSC-53	155	8.0	8.2	9.6	8.2

Note: 1 ksi = 6.895 MPa.

4.4 *Summary and Conclusions*

Developing a rational method for evaluating the structural capacity of pretensioned concrete members at prestress release is crucial in the design and production of flexural precast/prestressed members. Using the strength design method provides the designer with a rational approach replacing the current working stress method. The strength design method for PCSC girders at prestress release is introduced in detail.

The design equations were formulated for strength design at release using the strain compatibility approach and based on all the assumptions of the ultimate strength design of reinforced concrete. Note that both simplified solutions and closed form solutions were derived for the design formula. For applying the strength design method in an efficient and accurate manner, a design procedure was proposed.

To help the designers understand the proposed design procedure, design examples are developed for different PCSC girder sections of bridges with spans ranging from 80 ft, to 155 ft, using strength design method and working stress design method. End section is the critical section when using strength design method The required concrete strength at release, f'_{ci}, at end sections using strength design method are no more than those using working stress design method, and the lower required concrete strength at release benefits the production of the PCSC girder.

Chapter 5 Finite Element Analysis of PCSC Girders

5.1 *Introduction*

The purpose of Finite Element Analysis (FEA) of PCSC girders at prestress release is to understand the transfer of the prestressing force from the strands to the composite section and stress distribution at prestress release, and to investigate the impact of stud distribution on the stresses in the concrete bottom flange.

In this Chapter, the approaches of Finite Element Analysis (FEA) of PCSC girders are discussed for material models of steel, concrete and strands, element models of steel, concrete, strands, bond between concrete and strand and shear studs, loading, boundary conditions, and convergence issues. The approach to model the bond between concrete and strand is validated against the results of prism tests in the literature. Then, the FEA of a PCSC girder is performed and its predictions are compared with the results of design calculations, in terms of strain and stress distributions in the cross-section of the PCSC girder and initial camber at prestress release. Finally, parameter studies of the influences of amount and distribution of studs on the performance of the PCSC girder are conducted.

5.2 *Approaches of Finite Element Analysis*

5.2.1 Material Models

The elastic–perfectly plastic uniaxial material model is used for the steel, which is provided with bilinear kinematic hardening using von Mises plasticity. Note the strain hardening modulus equals zero. The yield strength of rolled steel section equals 50 ksi

(345 GPa), elastic modulus equals 29000 ksi (200 GPa), and Poisson's ratio equals 0.3. the stress-strain Curve of the Steel is described in Fig. 5.1.

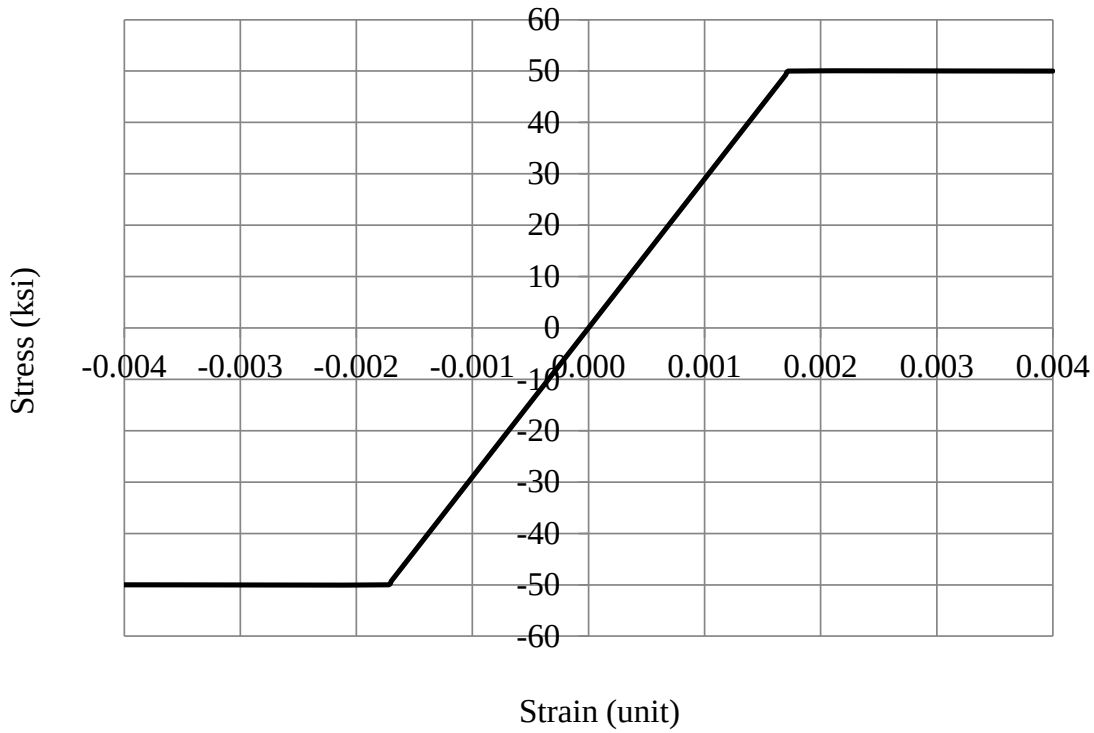

Fig. 5.1 – Stress-strain Curve of the Steel

Willam-Warnke constitutive model (Willam and Warnke, 1975) is used as the concrete material model. This model takes into account both cracking and crushing failure modes and predicts the failure of brittle materials. The criterion for failure of concrete due to a multiaxial stress state can be expressed as follows (ANSYS, 2009)

$$\frac{F}{f_c^{'}} - S \geq 0 \tag{5.1}$$

where, F = a function of the principal stress state (σ_{xp}, σ_{yp}, σ_{zp}); (σ_{xp}, σ_{yp}, σ_{zp}) = principal stresses in principal directions; S = failure surface expressed in terms of principal stresses; f'_c = uniaxial crushing strength. If Eq. (5.1) is satisfied, the concrete material will crack or

crush. A total of five input strength parameters (Constant 3-5 and 7-8) and an ambient hydrostatic stress state parameter (Constant 6) are needed to define the failure surface, as shown in Table 5.1. Hydrostatic stress state (σ_h) is defined by

$$\sigma_h = \frac{1}{3}(\sigma_{xp} + \sigma_{yp} + \sigma_{zp}) \tag{5.2}$$

And low hydrostatic stress state is defined by

$$|\sigma_h| = 0.3 f_c^{'} \tag{5.3}$$

When applied to stress situations with a low hydrostatic stress component, the failure surface can be specified with a minimum of two constants f'_t and f'_c. Constant 5, 7 and 8 default to the values suggested by Willam and Warnke (1975) as follows (ANSYS, 2009)

$$f_{cb} = 1.2 f_c^{'} \tag{5.4}$$

$$f_1 = 1.45 f_c^{'} \tag{5.5}$$

$$f_2 = 1.725 f_c^{'} \tag{5.6}$$

Shear transfer coefficients of 0.3 and 0.6 are used for an open crack (Constant 1) and a closed crack (Constant 2), respectively. Since the crush is not expected in the analytical models, the crushing capability is deactivated in the analysis and Constant 4 is set to –1.

Table 5.1 – Concrete Material Table

Input on TBDATA Commands with TB,CONCR			
Constant	Parameters	Description	Value
1	N/A	Shear transfer coefficients for an open crack	0.3
2	N/A	Shear transfer coefficients for a closed crack	0.6
3	f'_t	Ultimate uniaxial tensile strength	Input
4	f'_c	Ultimate uniaxial compressive strength	–1
5	f_{cb}	Ultimate biaxial compressive strength	Default
6	σ_h^a	Ultimate biaxial compressive strength	Default
7	f_1	Ultimate compressive strength for a state of biaxial compression superimposed on hydrostatic stress state	Default
8	f_2	Ultimate compressive strength for a state of uniaxial compression superimposed on hydrostatic stress state	Default
9	N/A	Stiffness multiplier for cracked tensile condition	Default

Elastic–perfectly plastic uniaxial material model with bilinear isotropic hardening is used for the concrete model. The yielding stress is equal to the concrete compressive strength and tangent modulus equals zero. The modulus of elasticity, E_c, may be takne as (AASHTO, 2007)

$$E_c = 33000 K_1 w_c^{1.5} \sqrt{f_c^{'}} \quad \text{(ksi)} \tag{5.7}$$

where, K_1 = correction factor for source of aggregate to be taken as 1.0; w_c = unit weight of concrete (kcf). The Poisson's ratio equals 0.3. Tensile strength can be derived by (AASHTO, 2007)

$$f_t^{'} = 0.19\sqrt{f_c^{'}} \quad \text{(ksi)} \tag{5.8}$$

For instance, the stress-strain curve of the concrete with compressive strength of 6000 psi is shown in Fig. 5.2.

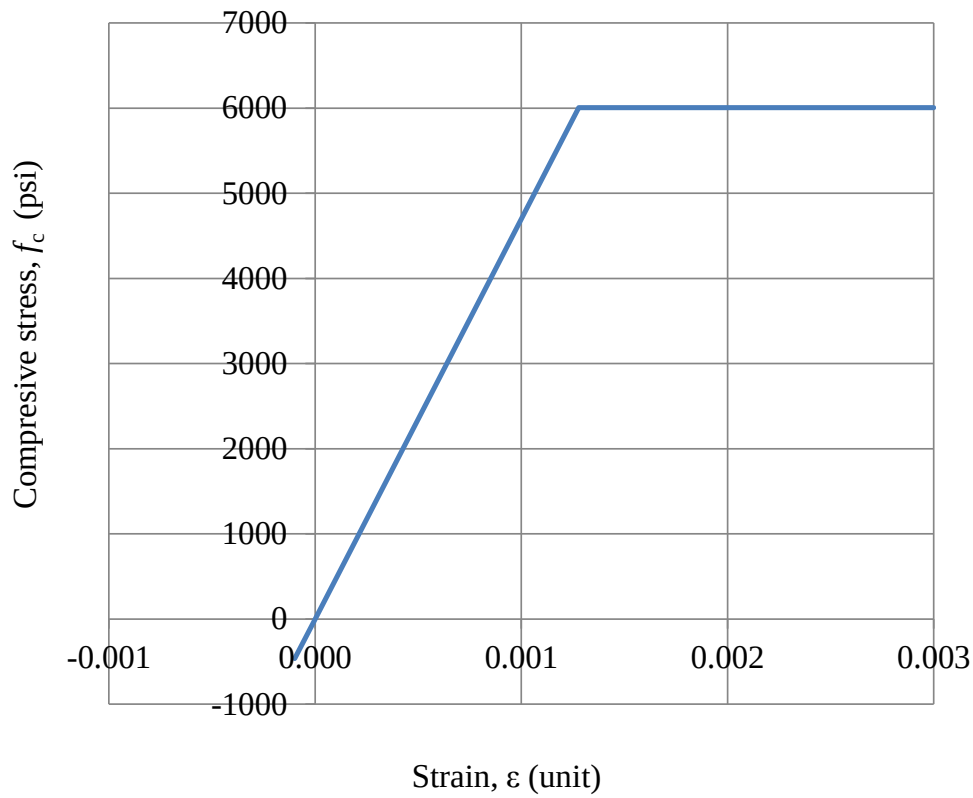

Fig. 5.2 – Example of Compressive Stress-strain Curve of the Concrete

The strand model is provided with multi-linear kinematic hardening using von Mises plasticity. The stress-strain curve of the 270-ksi (1862 MPa) strand is available from the PCI design handbook 7th edition (PCI, 2010):

$$\varepsilon_{ps} \le 0.0085: \; f_{ps} = 28800\varepsilon_{ps} \text{ (ksi)} \tag{5.9}$$

$$\varepsilon_{ps} > 0.0085: \; f_{ps} = 270 - \frac{0.04}{\varepsilon_{ps} - 0.007} \text{ (ksi)} \tag{5.10}$$

where, ε_{ps} and f_{ps} = the strain and the stress in the strand, respectively.

5.2.2 Element Models

Concrete is modeled by using 8-node SOLID65 element as shown in Fig. 5.3(a), which has three translational degrees of freedom (d.o.f.) at each node, in addition to capabilities of cracking (in three orthogonal directions) and crushing. The element has one solid material and up to three rebar materials in three directions. Thus, this element is commonly used to accommodate nonlinear material properties (ANSYS, 2009).

Prestressing strands are modeled by using LINK8 element as shown in Fig. 5.3(b), which is a uniaxial tension-compression element with three translational degrees of freedom at each node and no bending stiffness (ANSYS, 2009).

The rolled steel section is modeled using 4-node SHELL181 element as shown in Fig. 5.3(c) with six degrees of freedom at each node: translations in the *x*, *y*, and *z* directions, and rotations about the *x*, *y*, and *z*-axes (ANSYS, 2009).

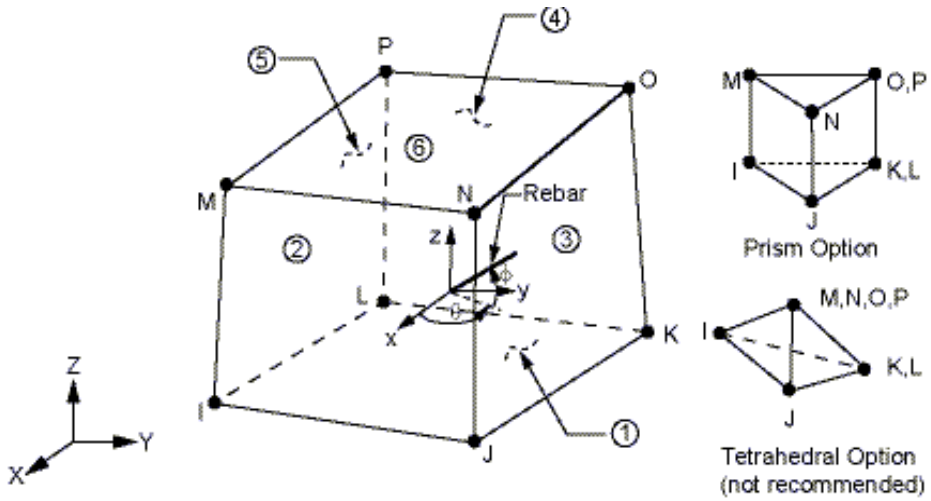

(a) SOLID65 Element (ANSYS, 2009)

Fig. 5.3 – Geometry of Elements (ANSYS, 2009, Continued)

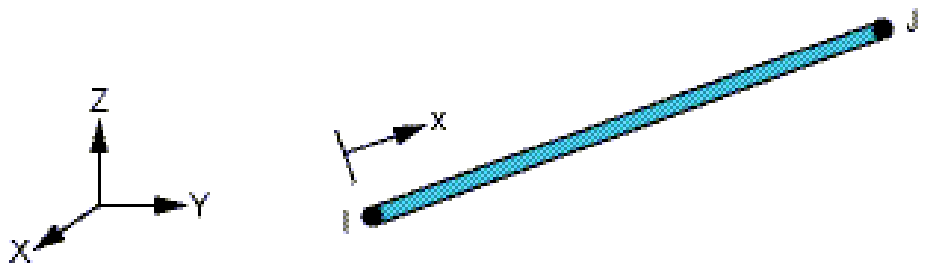

(b) LINK8 Element (ANSYS, 2009)

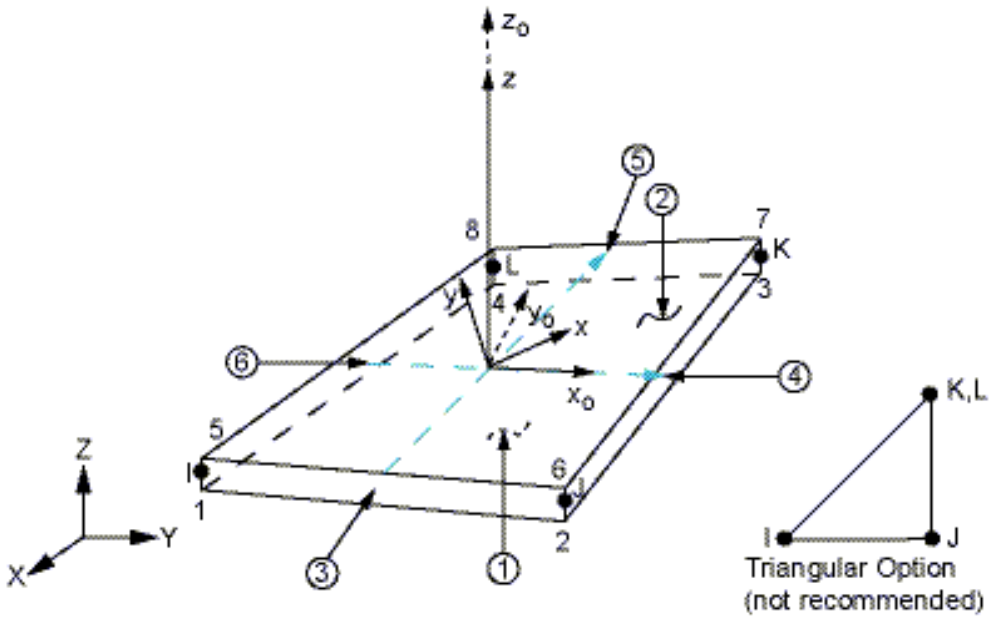

(c) SHELL181 Element (ANSYS, 2009)

Fig. 5.3 – Geometry of Elements (ANSYS, 2009)

The bond between concrete and prestressing strands is modeled by using COMBIN39 element, which is a unidirectional element with nonlinear generalized force-deflection capability and possesses longitudinal or torsional capability in 1-D, 2-D, or 3-

D applications. This element is placed between two coincident nodes of the concrete element and the prestressing strand element along the slip direction (*z*-axis coordinate). The other two coordinates (*x* and *y*-axis) are coupled together for those coincident nodes.

The bond-slip relationship between concrete and seven-wire strands, proposed by Balázs (1992), can be expressed as

$$\tau_b = c\sqrt{f_c^{'}\sqrt{\delta}} \tag{5.11}$$

where τ_b = the bond stress along the slip direction; c = 0.783 ksi$^{1/2}$ (5.4 MPa$^{1/2}$); f'_c = concrete compressive strength; δ = the slip of strands to concrete.

It is noted that the bond stress in this relationship is only dependent on the concrete strength. Therefore, the lower transfer length of strands is expected for higher concrete strength. To adopt this relationship into the FE model, the distributed bond stress is transformed into the concentrated force between coincident nodes between the components of the model, where the COMBIN39 element is established. This force between each couple of the coincident nodes is simply determined by the product of the bond stress, circumference of strand and element size along the strands.

For instance, for 6 ksi concrete and 0.7 in. diameter strands, the bond stress-slip relationship is calculated as shown in Fig. 5.4(a). When the elements are sized with 3 in. along the strands, and force-slip relationship between the concrete and a 0.7 in. diameter strand can be determined as shown in Fig. 5.4(b). It is noted that this relationship was not used for Finite Element Analysis by other researchers in the literature, so its adequacy should be validated against test results.

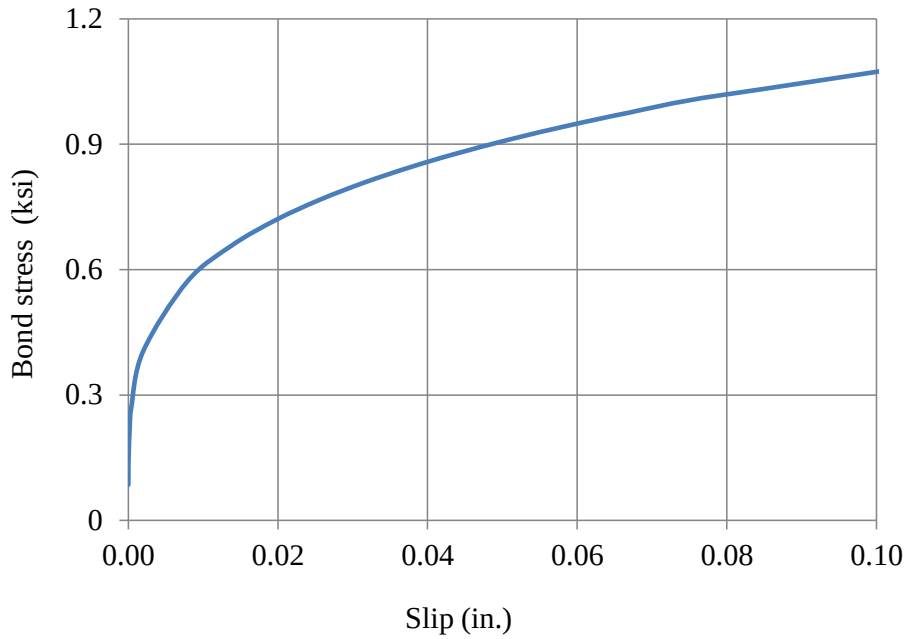

(a) Bond stress-slip relationship

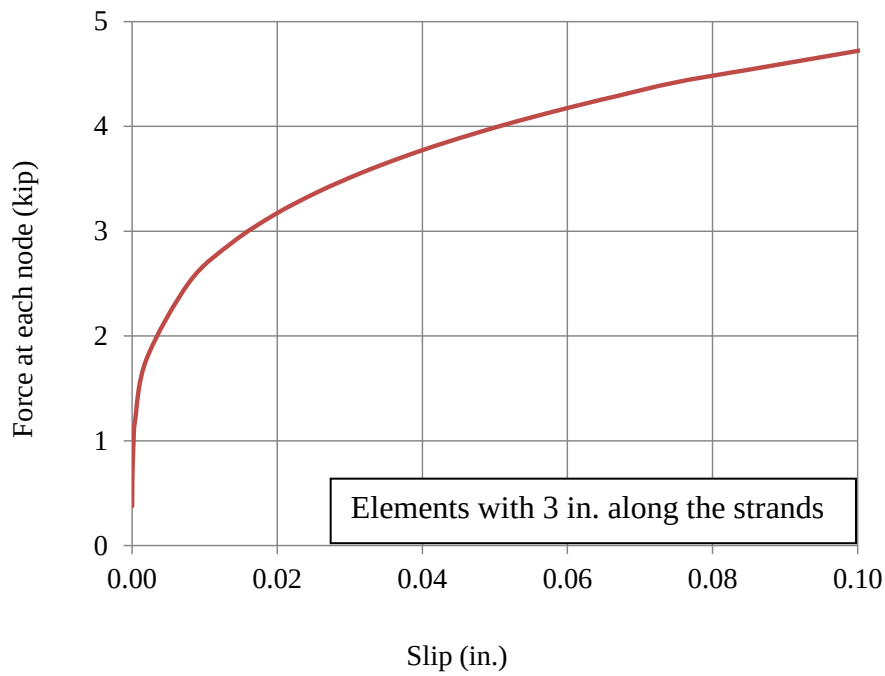

(b) Bond force-slip relationship between the concrete and a 0.7 in. diameter strand

Fig. 5.4 – Example of the Bond-slip Relationships between Concrete and Prestressing Strands

The shear studs between concrete flange and steel beam are modeled by using COMBIN39 element. This element is placed at the locations of studs and between two coincident nodes of the concrete element and the steel beam element along the slip direction (z-axis coordinate). The other two coordinates (*x* and *y*-axis) are coupled together. When sustaining shear forces, the studs were rotated through angles at the weld (Ollgard et al., 1971). It seems that slip happens at the interface between concrete flange and steel beam. For the purpose of FEA, it is assumed that a displacement happens at weld points of studs, and COMBIN39 element is placed at the coincident nodes of concrete and steel beam at those weld points. Ollgard et al. (1971) proposed the shear force-displacement relationship of shear studs under continuously loading based on the push-off testing results and an empirical formula can be expressed as

$$Q = Q_n (1 - e^{-18\Delta})^{\frac{2}{5}} \tag{5.12}$$

where, Q = shear force in the stud; Δ = displacement at the weld point of the stud; and according to AASHTO (2007), nominal shear resistance, Q_n, is determined by

$$Q_n = 0.5 A_{sc} \sqrt{f_c^{'} E_c} \le F_u A_{sc} \tag{5.13}$$

where, A_{sc} = Area of cross-sectional area of the stud; f'_c= compressive strength of concrete; E_c = modulus of elasticity of concrete; F_u = minimum specified tensile strength of the stud. When f'_c = 9 ksi, the relationship between shear force and displacement for one 7/8-in. stud is depicted in Fig. 5.5.

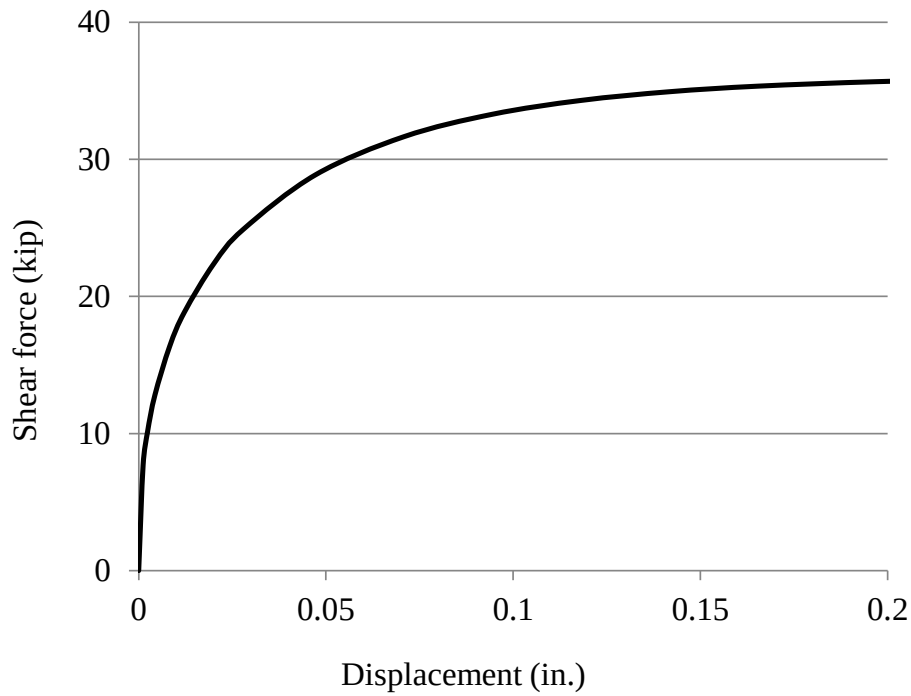

Fig. 5.5 – Relationship between Shear Force and Displacement for One 7/8-in. Stud

5.2.3 Loading, Boundary Conditions and Convergences

The initial prestress of strand is imposed by assigning a temperature drop to the strand elements, which generates the equivalent pre-stress. Note that the initial prestress equals the jacking stress, i.e, 75% of f_{pu} for low relaxation strand (f_{pu} = 270 ksi). Because the elastic shortening occurs in the FE models along with applying jacking force, the initial prestress loss is not separately accounted for. And the long-term prestress losses due to creep, shrinkage, relaxation of strands, and prestress gains are not considered, because the model is only established for prestressed members at prestress release. A line load is applied on the top of steel beam to simulate the body load due to the self-weight of the girder.

The boundary conditions are defined by taking into account two planes of symmetry, and simply supported conditions were imposed on the nodes at two ends of the specimen such that the beam is free to rotate at the supports.

CNVTOL command is adopted to set convergence values for the nonlinear analysis and L2 norm is selected to check square root sum of the squares (SRSS). The convergence tolerances are set for both displacement and forces. Parameters are set to facilitate the convergence of the nonlinear problem solutions:

- Suppress extra displacement shapes and include tensile stress relaxation after cracking for SOLID65 elements;
- Set appropriate interval and number of load steps and substeps;
- Open auto-step and predictor to solve potential computational problem;
- Check reasonable element sizes and shapes;
- The COMBIN39 elements placed at the interfaces between concrete and strands and between concrete and steel section may induce unexpected crush of concrete, the crushing capability is deactivated in the analysis, which also facilitates the convergence of computations.

5.3 *Modeling and Validation of Bond between Concrete and Strand in Prisms*

As mentioned in Section 4.2.2, the bond-slip relationship between concrete and strands was rarely used for FEA, so tests conducted by Morcous et al. (2011) are used to validate its adequacy.

5.3.1 Tests by Morcous et al. (2011)

Morcous et al. (2011) fabricated four concentrically prestressed rectangular prisms for transfer length measurements. The dimensions of the prisms were 96×7×7 in., with a single 0.7 in. diameter strand placed at the center of the prism. Each prism contained confining ties at varying spacing, as shown in Fig. 5.6. Confining ties with an outside to outside dimension of 5 in. were placed at 12, 9, 6 and 3 in. on center, respectively. Note that the first stirrup placed at half of the inner stirrup spacing from the end. The strand was tensioned to $0.75f_{pu}$, and the specified concrete strength at release was 6 ksi. The four specimens were instrumented with DEMEC strain gages on two sides, starting from each end and ending at the middle of the specimen. Then, several readings were taken at 1-day, 7 days, 14 days, and 28 days after release.

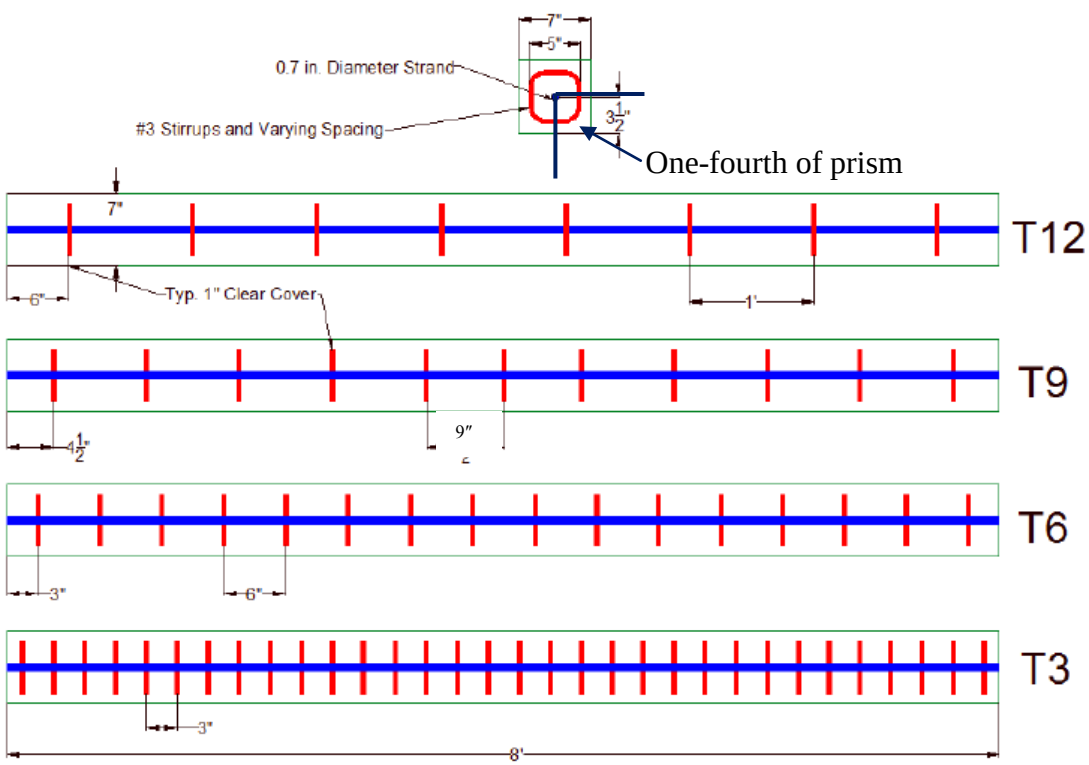

Fig. 5.6 – Prism Specimens and Reinforcements (Morcous et al., 2011)

The 95% Average Measured Strain (AMS) method was performed on each prism's sides at North and South ends for a total of eight transfer regions. Table 5.2 lists transfer lengths for prism specimens obtained using AMS method. Transfer lengths are also predicted using equations in codes ACI 318 (ACI, 2011) and AASHTO LRFD (AASHTO, 2007) as shown in Table 5.2. Table 5.2 indicates that the measured transfer lengths are shorter than those predicted using equations of codes.

Table 5.2 – Transfer Length Results from Prism Specimens (Morcous et al., 2011)

Prism	Stirrup spacing (in.)	l_t		ACI, $50d_b$ (in.)	AASHTO, $60d_b$ (in.)
		1-day (in.)	28-day (in.)		
T12	12	27.6	27.9	35	42
T9	9	25.8	27.2		
T6	6	25.6	26.2		
T3	3	27.4	28.2		
Average	---	26.6	27.4	---	--

Note: l_t – Transfer length of the strand; d_b – Diameter of the strand

5.3.2 Comparison between FEA Predictions and Test Results

The test results in Table 5.2 indicate that confining ties have no significant influence on the transfer length of strands. Therefore, the confining ties are not included in the FE model. Due to double symmetries in geometry, loading and boundary conditions, only one fourth of the prism is modeled using ANSYS (ANSYS, 2009), as shown in Fig. 5.7.

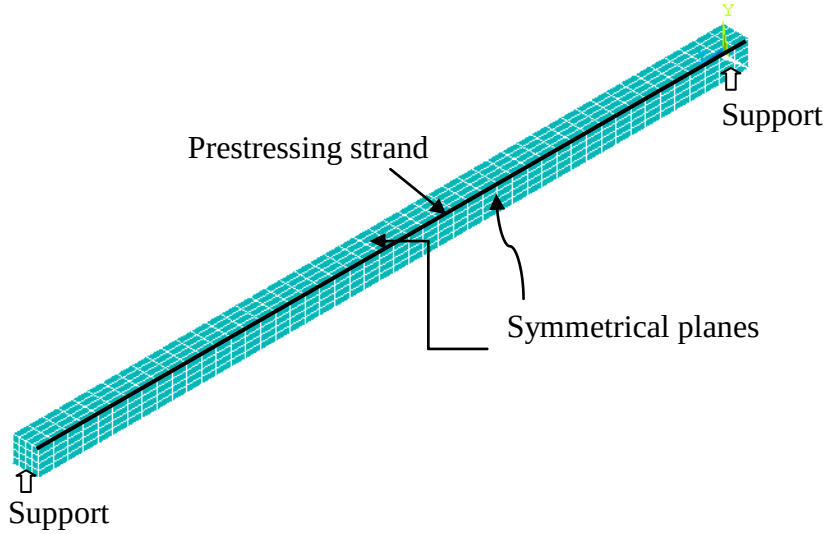

Fig. 5.7 –Model of One Fourth of the Prism

Only the strain data at 1-day after release were used to validate the FEA results in order to minimize the influences of shrinkage and creep of concrete. As shown in Fig. 5.8, the strains in prism T9 predicted using FEA follow the same order as those measured from the four prisms. However, due to the creep and shrinkage of concrete during 1-day after prestress release (which is not included in the FEA), the strain values predicted by FEA is generally less than experimental results.

The stresses in the strand of the prism are shown in Fig. 5.9. The stresses gradually increase to a constant value at 40 in. from end, and then almost keep constant until mid-span. It can be concluded that the transfer length of the strand equals 40 in. compared to 26.6 in., the average transfer length obtained from test data at 1-day using ASM method.

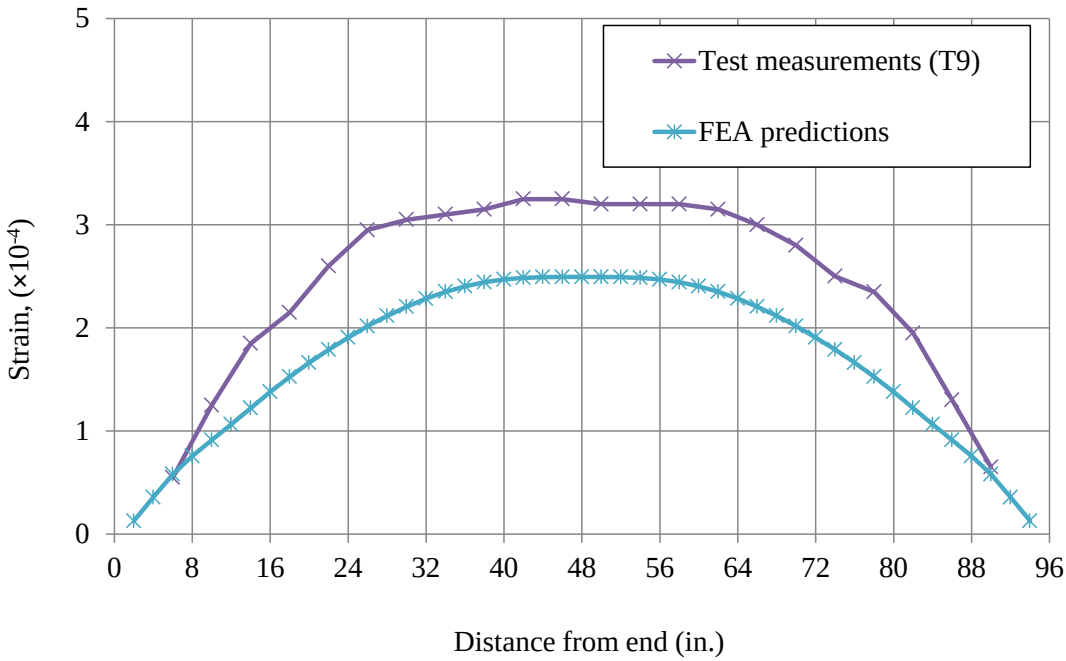

Fig. 5.8 – Strains at Different Locations Obtained using FEA Predictions and Test Measurements (1-day)

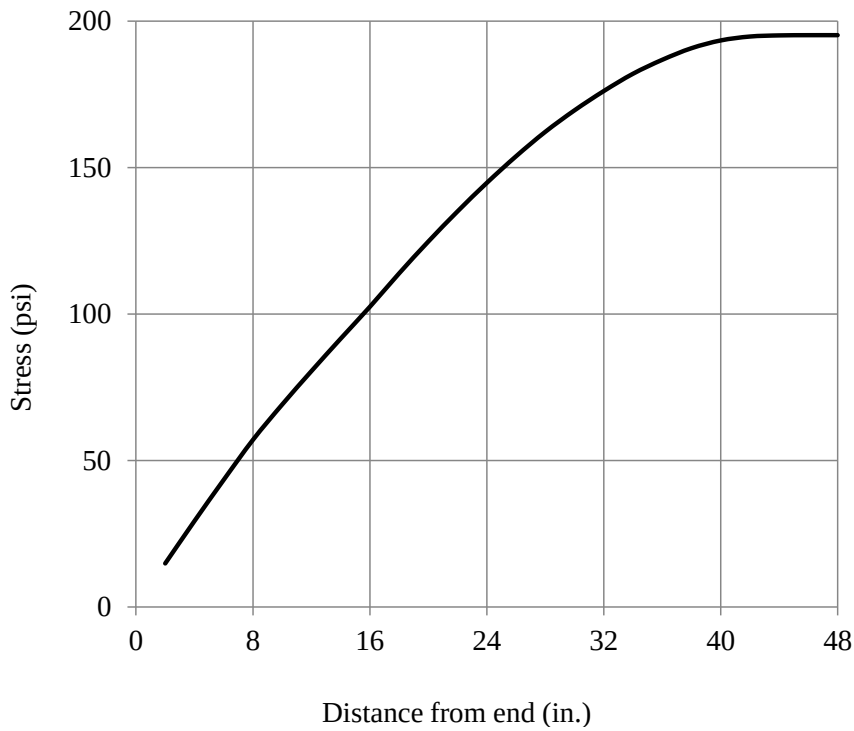

Fig. 5.9 – Stresses in the Strand of the Prism

5.3.3 Comparison between FEA Predictions and Design Calculations

The design calculations based on strain compatibility and full bond assumption are also performed and compared with the results obtained from FEA. Table 5.3 indicates that the compressive stress in concrete at mid-span and the effective stress in strands obtained from FEA are compared well with those obtained by using design calculations.

Table 5.3 – Comparison between Design Calculations and FEA Predictions

	Compressive stress in concrete at mid-span (ksi)	Effective stress in strands (ksi)
Design calculations	1.179	195.3
FEA predictions	1.171	195.2

5.4 *Examples of FEA of PCSC Girders*

5.4.1 FEA of a PCSC Girder

As an example, Finite Element Analysis (FEA) is performed for a PCSC girder with the cross-section as shown in Fig. 5.10. The information for steel beam, concrete bottom flange, studs and strands of the PCSC girder are also described in Fig. 5.10. The steel beam has the rolled shaped section W18×86 and the length of 50 ft. Concrete bottom flange has a length of 49 ft and the dimension of 24 × 6.375 in. The concrete strength at release is 11 ksi. Twelve 0.7-in. strands are placed in concrete bottom flange, i.e., 8 strands at bottom layer and 4 strands at top layer. Strands are spaced on center at 2 in. and the centroidal spacing between the bottom and top layers of strands is 2.75 in. One hundred and four 7/8-in. shear studs are placed between the concrete bottom flange and the steel section. The studs are spaced on center at 6 in. along 2.5 ft from ends and then spaced at 12 in until the mid-span.

Due to double symmetries in geometry, loading and boundary conditions, only one fourth of the PCSC girder is modeled, as shown in Fig. 5.10. That is, only half section and half span are established for the FE model, as illustrated in Fig. 5.10 and Fig. 5.11. The model includes the steel beam, prestressed concrete flange including the concrete flange and prestressing strands, the bond between the concrete and strands, and shear studs between the steel beam and the concrete flange. Note that the stirrups are ignored in the model. The steel beam, concrete bottom flange, and strands are sized with 6 in., 3 in., and 3 in. along the length, respectively.

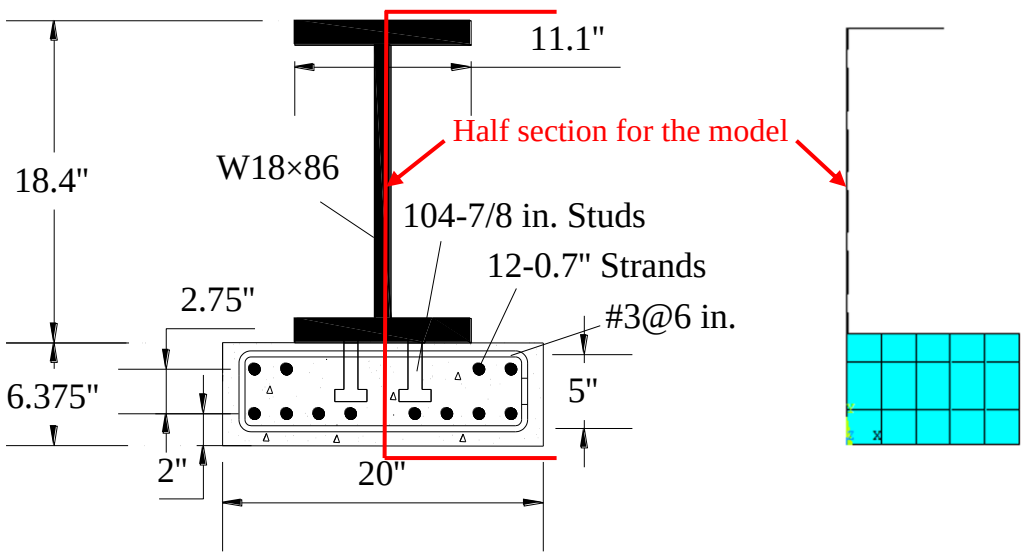

Fig. 5.10 – Cross-section of the PCSC Girder

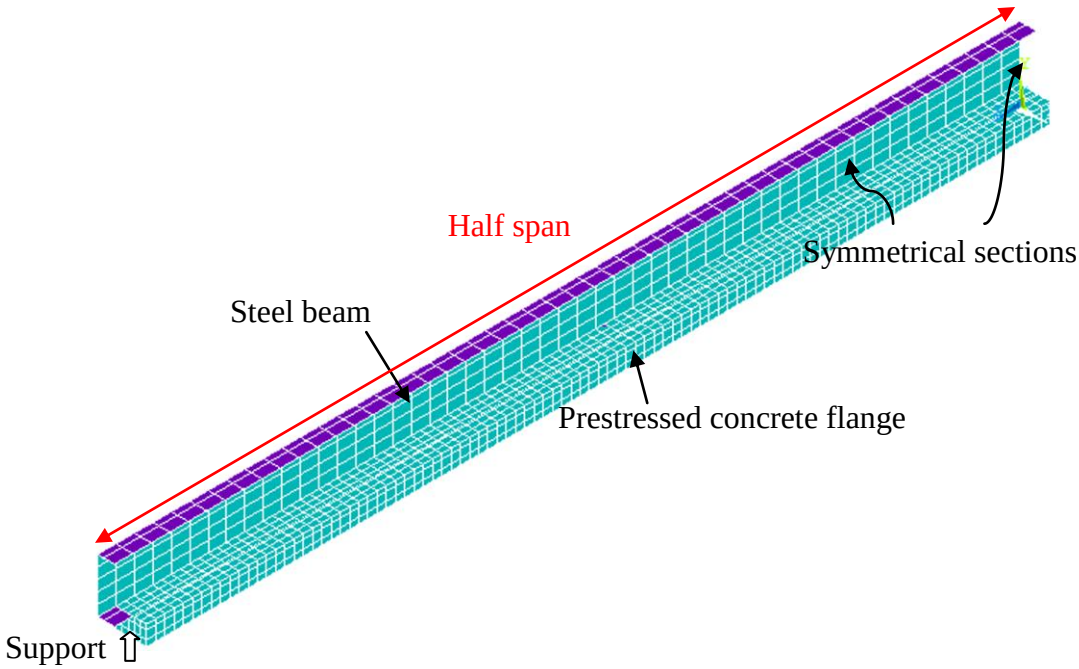

Fig. 5.11 –One-fourth Model of the PCSC Girder

5.4.2 FEA Predictions

The contours of compressive stresses in concrete bottom flange for the sections at mid-span and 30 in. from end are shown in Fig. 5.12(a) and Fig. 5.12(b), respectively. Fig. 5.12(a) indicates that the stresses in the mid-span section gradually increase from the bottom fiber to the top fiber and no significant difference of stresses is found between middle and side of the section. The stresses in the section at 30 in. from end also gradually increase from bottom fiber to the top fiber, but are significantly influenced by the stud connected to the concrete, as shown in Fig. 5.12(b). Further, the most critical stress is located in the section far away from the studs. Thus, due to the influences of studs in the local region, the stresses/strains in the region close to studs will be avoided for the analysis. In this dissertation, the stresses in the side of the section are used for further analysis.

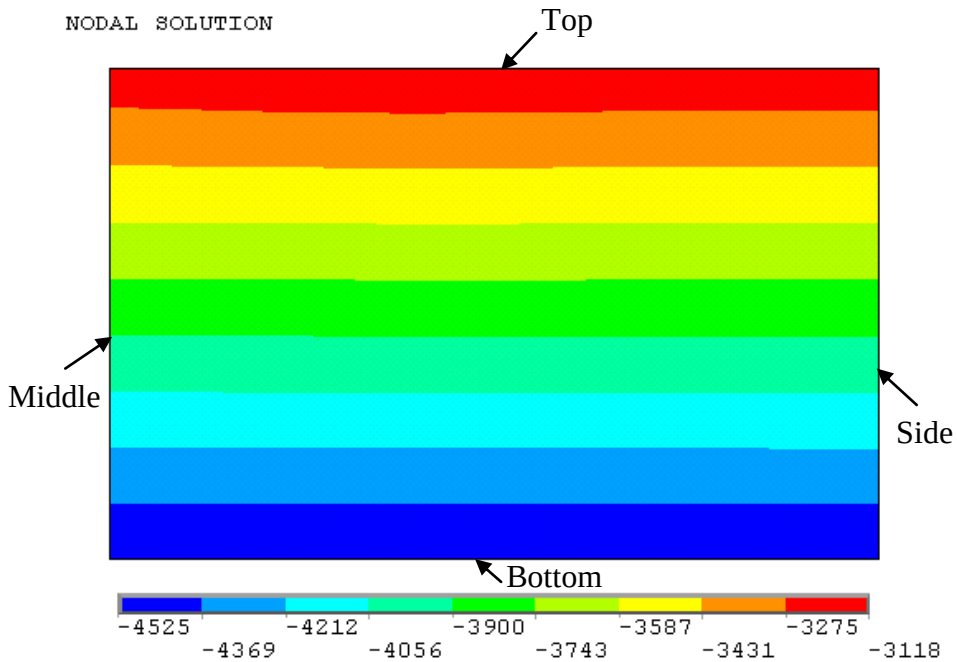

(a) Section at Mid-span

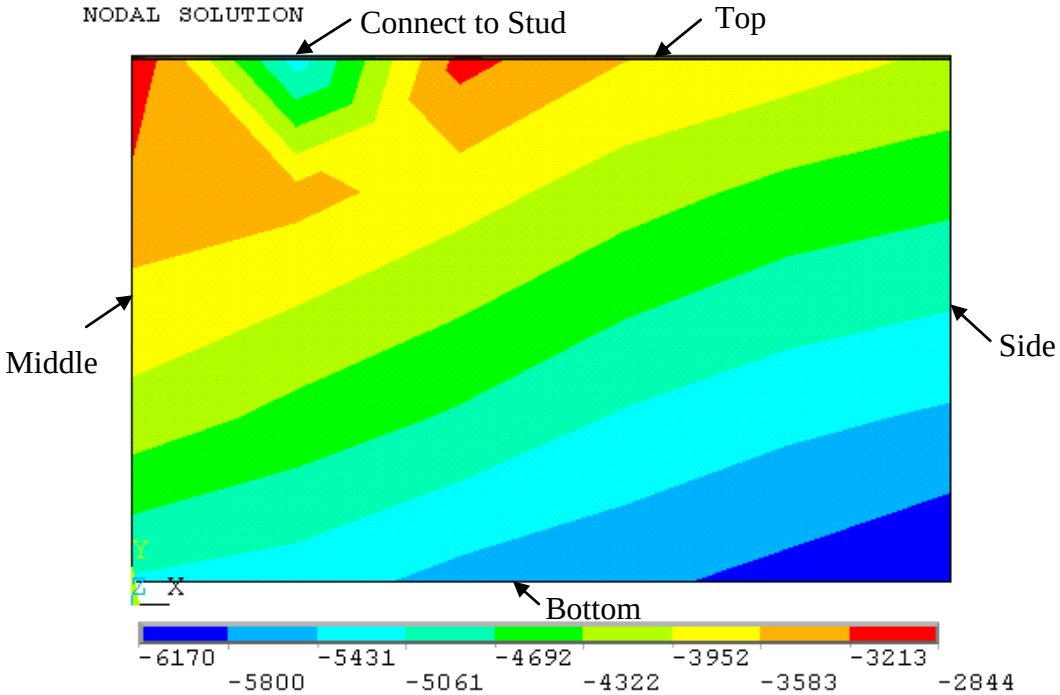

(b) Section at 30 in. from End

Fig. 5.12 – Contours of Compressive Stresses in Concrete Bottom Flange

In the following analysis, the letters “S” and “F” are an abbreviation of the location at the steel beam and the concrete bottom flange, respectively. The letters “T” and “B” refer to the locations at the top and the bottom of each component, respectively. The “ST”, “SB”, “FT”, and “FB” represent locations in the PCSC girder section as shown in Fig. 5.13.

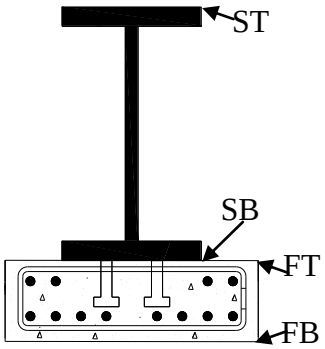

Fig. 5.13 – Locations in the PCSC Girder Section

The stresses and strains in concrete bottom flange and steel beam at different locations from end to mid-span of the PCSC girder are obtained using FEA Predictions, as shown in Fig. 5.14(a) and Fig. 5.14(b). Fig. 5.14(a) describes that the stresses in FB and FT (Bottom and Top of concrete bottom flange) gradually increase from end to 27 in. from end, and reach the maximum values of 6.1 and 4.0 ksi, respectively. Fig. 5.14(b) describes that the strains in FB and FT gradually increase from end to 27 in., and reach the maximum values of 961 and 638 macros, respectively. However, the stresses and strains in SB and ST (Bottom and top of steel beam) increase to their maximum value at 150 and 78 in. from end as shown in Fig. 5.14(a) and Fig. 5.14(b), respectively. After reaching the maximum values, all the stresses and strains slightly decrease to the values at the mid-span. Fig. 5.14(b) also indicates that the strains in FT have the same values as

those in SB from 150 in. to mid-span. This indicates that the no slip happens between steel beam and concrete bottom flange for the sections from 105 in. to mid-span.

The stresses and strains at different locations from end to mid-span of the PCSC girder are also obtained using design calculations, as shown in Fig. 5.14(a) and Fig. 5.14(b). The transfer length is determined by $60d_b$ (d_b is diameter of the strand) according to AASHTO (2007), i.e., 42 in for 0.7 in. diameter strand. It is assumed that the prestress linearly increases from zero at end to the value of effective prestress at transfer length. As shown in Fig. 5.14, the stresses and strains in FB, FT, SB and ST increase to their maximum values at the transfer length, and decrease to the values at mid-span due to self-weight of the PCSC girder. Note that the strain curves for FT and ST coincide together due to the assumption of full bond between concrete bottom flange and steel beam for the design, as shown in Fig. 5.14(b).

Fig. 5.14 indicates that stresses and strains in FB, FT, SB and ST from 105 in. to mid-span predicted using FEA agree well with those obtained using design calculations. This stresses and strains in the middle region predicted using FEA agree well with those obtained using the design calculations with the assumption of the fully composite action between concrete bottom flange and steel beam. However, the stresses/strains in FB and FT, and SB and ST from end to 105 in. predicted using FEA are generally higher and lower than those obtained using design calculations, respectively. This is due to the local influence of shear studs on the stresses and the slip between concrete bottom flange and steel beam.

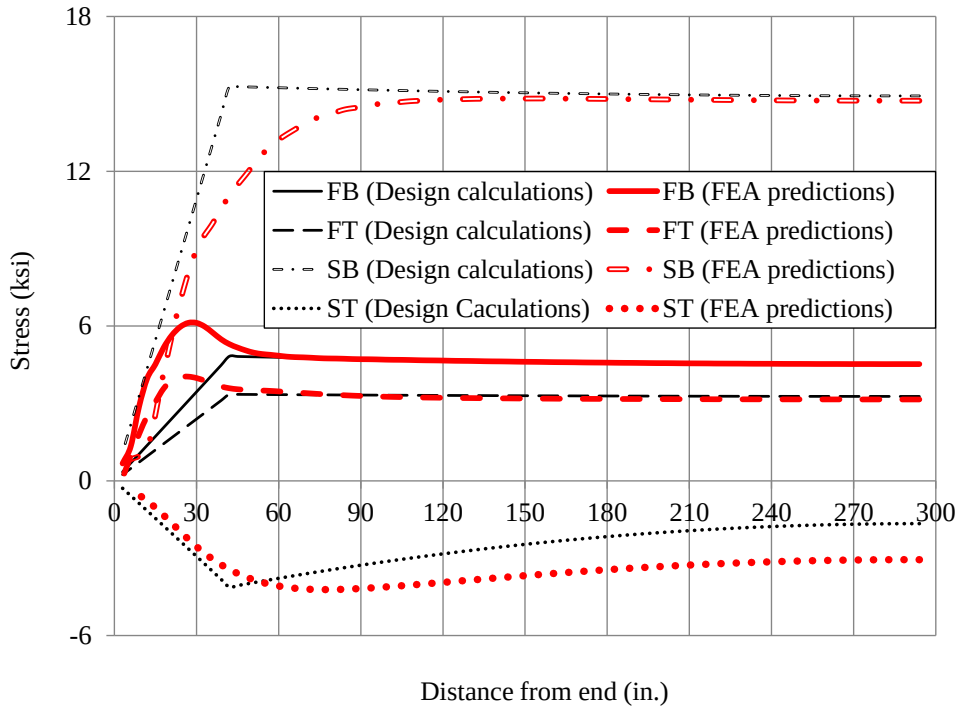

(a) Stresses at Different Locations

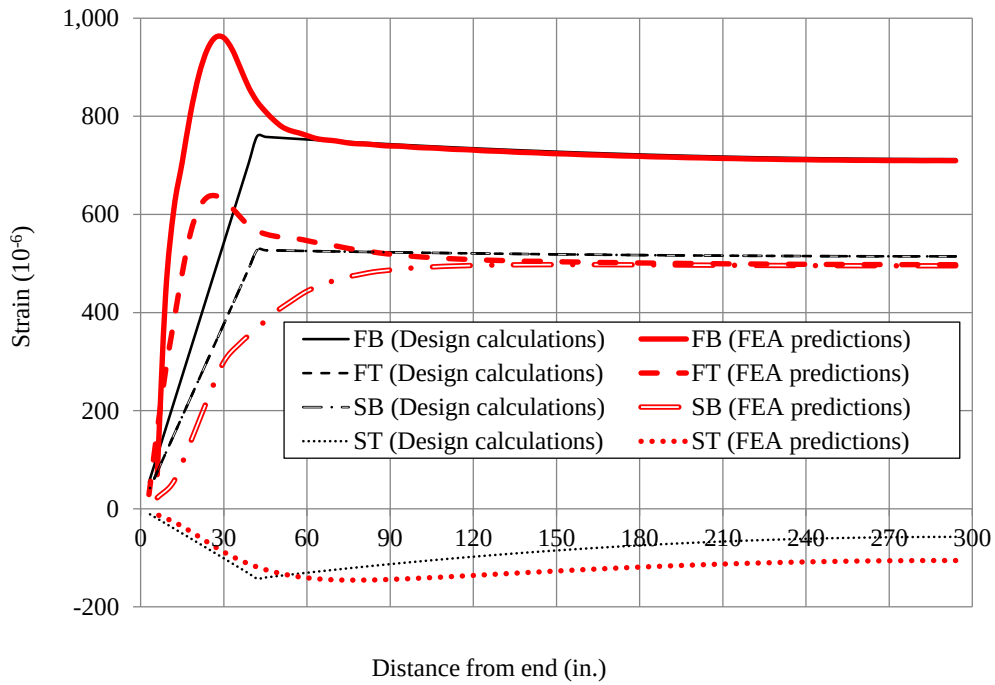

(b) Strains at Different Locations

Fig. 5.14 – Comparisons of Stresses and Strains in Concrete Bottom Flange and Steel Beam Obtained Using FEA Predictions and Design Calculations

The maximum stresses in FB, FT, SB and ST predicted using FEA are compared with those obtained using design calculations, as tabulated in Table 5.4. The maximum stresses in FB, FT, SB and ST of mid-span section and SB and ST of end sections predicted using FEA agree well with those using design calculations, although the stress in ST (tensile stress in steel beam) shows a little difference. It should be noted that the tensile stress in steel beam will not be of concern for the PCSC girder design at prestress release. The maximum stresses in FB and FT of end sections predicted using FEA are 26.7% and 20.6% larger than those obtained using design calculations. This is due to the local influence of shear studs on the stresses and the slip between concrete bottom flange and steel beam.

Based on the discussion above, the full bond assumption is applicable for the section at mid-span. Thus, it is reasonable to use AEMM for Service III design at mid-span which dominates other design considerations as mentioned in Chapter 3. Although FEA predictions indicates that design calculations with full bond assumption do not give good predictions on the stresses in end sections, end sections are only concerned at prestress release and designed using strength design method at release as introduced in Chapter 4.

Table 5.4 – Maximum Stresses Obtained Using FEA Predictions and Design Calculations

	Design calculations		FEA predictions	
	End sections	Mid-span section	End sections	Mid-span section
f_{fb} (ksi)	**4.83**	4.53	**6.12**	4.52
f_{ft} (ksi)	**3.35**	3.27	**4.04**	3.15
f_{sb} (ksi)	14.5	14.2	14.8	14.7
f_{st} (ksi)	–4.12	–1.66	–4.22	–3.06

Note: f_{fb} – Maximum compressive stress in FB; f_{ft} – Maximum compressive stress in FT; f_{sb} – Maximum compressive stress in SB; f_{st} – Maximum tensile stress in ST.

As shown in Fig. 5.15, the stresses in strands predicted using FEA gradually increase to a constant value at 30 in. from end, and then almost keep constant until mid-span, which represents that the transfer length of the strand equals 30 in. compared to 40 in. of the transfer length of the prism specimen predicted using FEA in Fig. 5.9. This is mainly due to higher strength of concrete in PCSC girder, 11 ksi, compared to 6 ksi of concrete of the prism.

The stress in strands predicted using FEA is compared with design calculations as shown in Fig. 5.15. The stress in strands at 27 in. from end, 185.0 ksi, is lower than that at transfer length (42 in.) predicted using design calculation, 188.5 ksi. This further proves that the higher stresses in FB and FT of end sections predicted using FEA are due to local influence of shear studs and the slip between concrete bottom flange and steel beam instead of higher prestress at ends. The stress in strands at mid-span, 195.9 ksi, is higher than that predicted using design calculation, 187.6 ksi.

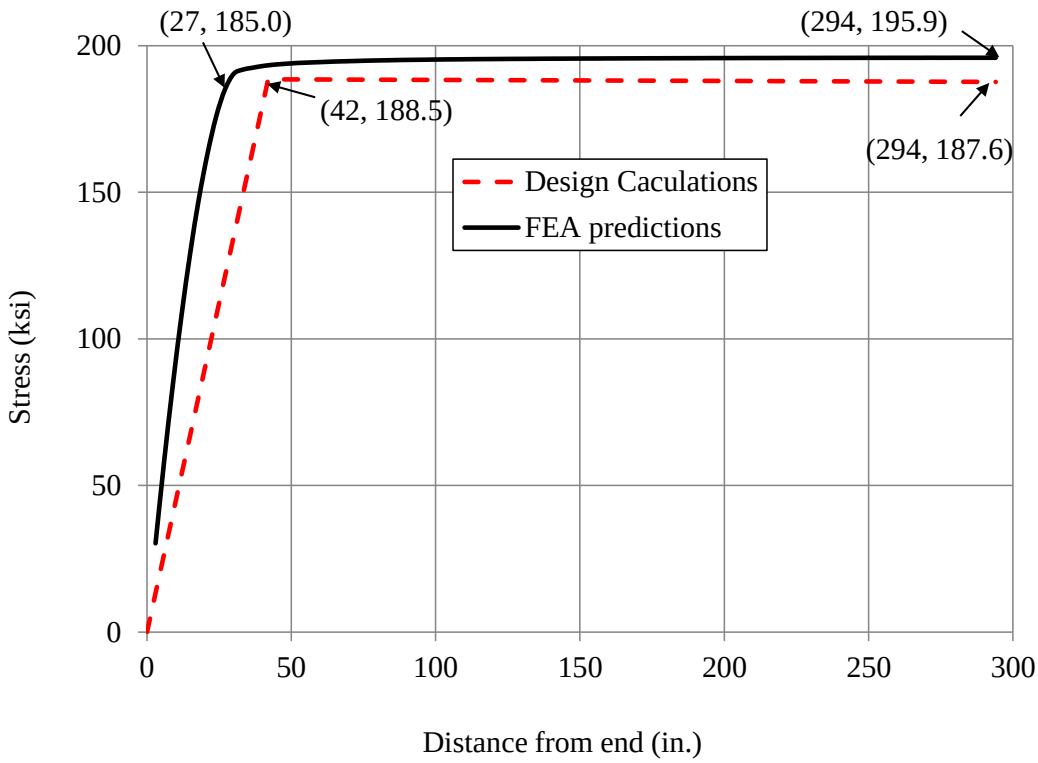

Fig. 5.15 – Comparisons of Stresses in Strands Obtained Using FEA Predictions and Design Calculations

5.5 *Influences of Amount and Distribution of Studs*

In order to investigate the influences of the amount and distribution of studs, five PCSC girders with the identical cross-section as shown in Fig. 5.10 are used for parameter studies. For the girders with this cross-section, the required amount of studs is 60, which is determined based on the ultimate strength design. The shear studs are used to transfer all the prestress force in strands at the interface between the concrete bottom flange and steel beam, because the concrete takes no tensile stress at the ultimate state.

The five PCSC girders have the same components except shear studs as those described in Section 4.4.1. Five types of distribution of shear studs are used for the five

PCSC girders respectively: 192, 96, 64, 48, and 24 studs are spaced on center at 6, 12, 18, 24, and 48 in. between the steel beam and the concrete bottom flange, respectively. Note that two studs are assigned in one row.

Fig. 5.16 shows stresses in FB and FT (top and bottom fibers of the concrete bottom flange) from end to mid-span for the five girders with different amounts of studs. For the five girders, the stresses in both FB and FT increase to the maximum values from end to 30 in. from end and then gradually decrease to the values at mid-span. The lower amount of studs is placed into the PCSC girder, the higher peak values of stresses are found in FB and FT, although the differences are not significant.

For the two PCSC girders with the amount of studs less than 60, i.e., 48 and 24 studs, the curves of stresses in FB and FT are not smooth due to the large spacing of the studs, as shown in Fig. 5.16. It can be also seen in Fig. 5.16 that for the three girders with the amount of studs larger than 60, i.e., 64, 96 and 192 studs, no significantly difference is found among the peak values of stresses in FB or FT. It can be concluded that the shear studs have no significant influences on the stresses in the concrete bottom flange as long as the amount of studs placed in the PCSC girder is more than the required number.

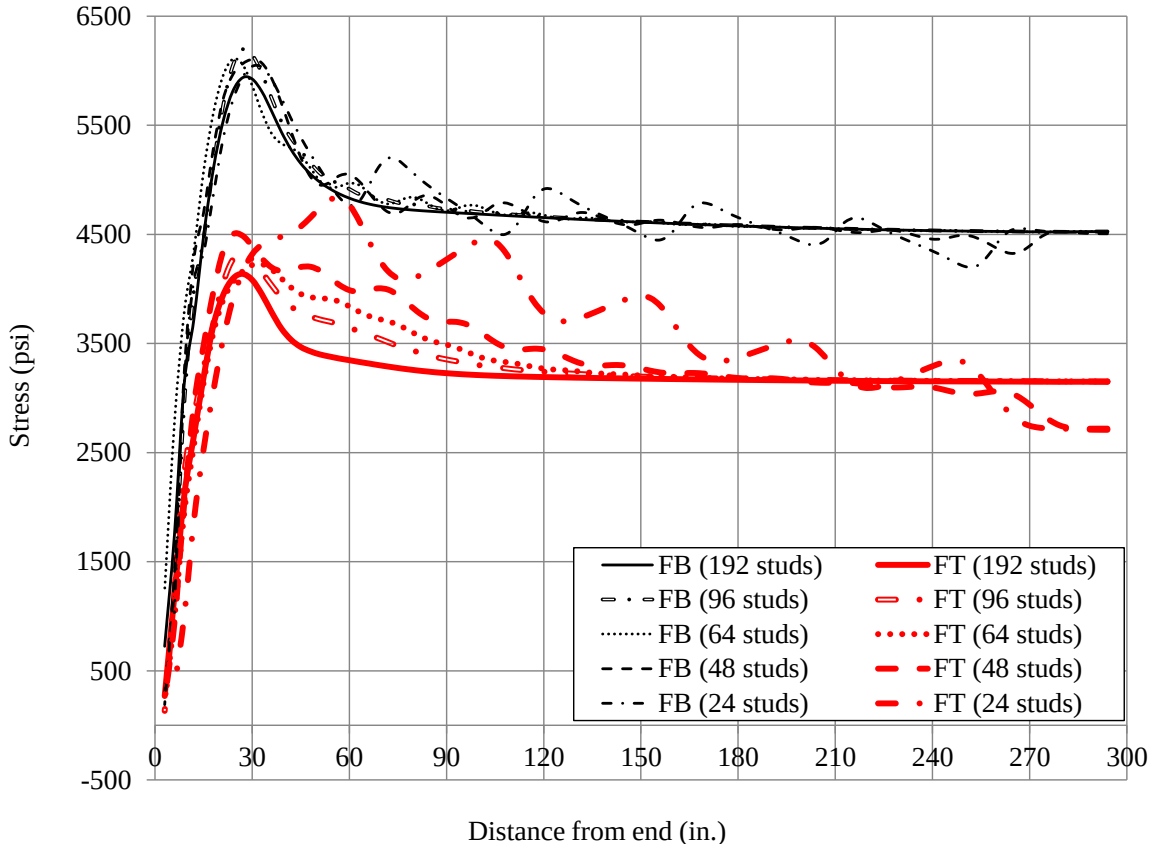

Fig. 5.16 – Stresses in FB and FT for PCSC Girders with Different Amounts of Studs

5.6 *Summary and Conclusions*

The approaches of Finite Element Analysis (FEA) of PCSC girders are introduced for material models of steel, concrete and strands, element models of steel, concrete, strands, bond between concrete and strand and shear studs, loading, boundary conditions, and convergence issues.

FEA of prism specimens are performed and adequacy of the bond-slip relationship between concrete and strands are validated against test data and design calculations.

After validating the adequacy of the bond-slip relationship between concrete and strands, Finite Element Analysis (FEA) is thus performed for a PCSC girder. The model includes the steel beam, prestressed concrete flange including the concrete flange and prestressing strands, the bond between the concrete and strands, and shear studs between the steel beam and the concrete flange. Note that the stirrups are ignored in the model. FEA predictions are compared with design calculations and parameter studies are performed to investigate the influences of studs on the stresses in concrete bottom flange. Some conclusions can be made as follows:

- The stresses in each section gradually increase from the bottom fiber to the top fiber. No significant change of stresses is found between middle and side of the mid-span section. The stresses in the end section slightly changed due to the stud connected to the concrete but the most critical stress is located far away from the studs.
- For FEA predictions, the stresses/strains in concrete bottom flange reach the maximum values at different location from those in steel beam. No slip happens between concrete bottom flange and steel beam from 105 in. to mid-span.
- For design calculations, the stresses and strains in concrete bottom flange and steel beam reach their maximum values at the transfer length.
- This stresses and strains predicted using FEA do not agree well with those obtained using the design calculations with the assumption of the fully composite action until

105 in. to mid-span. This is due to the local influence of shear studs and the slip between concrete bottom flange and steel beam.

- The maximum stresses in mid-span section and steel beam of end sections predicted using FEA agree well with those using design calculations. The maximum stresses in FB and FT of end sections predicted using FEA are 26.7% and 20.6% larger than those obtained using design calculations, due to local influence of shear studs and the slip between concrete bottom flange and steel beam.
- The full bond assumption is applicable for the section at mid-span and it is reasonable to use AEMM for Service III design at mid-span. Although FEA predictions indicates that design calculations with full bond assumption do not give good predictions on the stresses in end sections, end sections are only concerned at prestress release and designed using strength design method at release.
- FEA predictions show a lower transfer length in the strands of PCSC girder compared to that in the strands of the prism, due to higher concrete strength.

In order to investigate the influences of the amount and distribution of studs, five PCSC girders with the identical cross-section are used for parameter studies. The five PCSC girders have the same components but different distributions of shear studs. Some conclusions can be drawn as follows:

- The lower amount of studs is placed into the PCSC girder, the higher peak values of stresses are found in the concrete bottom flange, although the differences are not significant.
- For the PCSC girders with the amount of studs less than 60, the curves for stresses in the concrete bottom flange are not smooth due to the large spacing of the studs.

- The shear studs have no significant influences on the stresses in the concrete bottom flange as long as the amount of studs placed in the PCSC girder is more than the required number.

Chapter 6 Experimental Investigation and Validations

6.1 *Introduction*

A PCSC girder specimen was designed using the bridge design procedures introduced in Sections 3.3 and 3.4. The prestressing system located in structural testing lab at the University of Nebraska Lincoln, Omaha, NE, was introduced. The specimen was fabricated in the prestressing system following the fabrication steps presented in Section 3.2, and measurements were also performed. Flexural and shear tests were conducted to evaluate the flexural and shear capacities of the fabricated specimen. Finally, the test results were presented in detail, and design procedures and Finite Element Analysis (FEA) were validated against those results.

6.2 *Design of a PCSC Girder Specimen*

In order to design a PCSC girder specimen, a bridge is designed with a single span of 50 ft, girder spacing of 8 ft and a 7 in. reinforced concrete deck, as described in Fig. 6.1. The bridge has a width of 38ft 8 in. and consists of five girders. Design of the PCSC girders was performed following the design procedures introduced in section 3.3-3.4. Demand of the bridge girders including unfactored service moment, factored ultimate moment, and factored ultimate shear is summarized in Table 6.1.

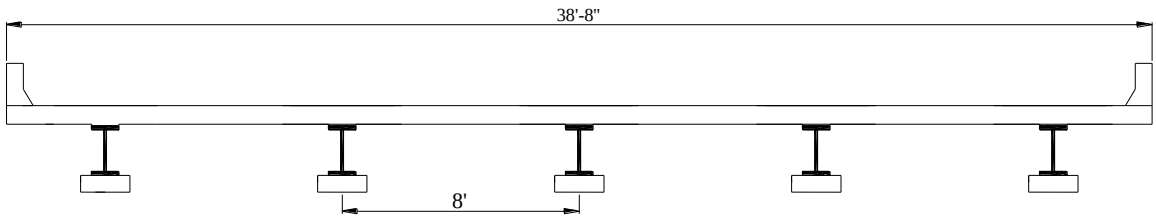

Fig. 6.1 – Cross-section of the PCSC Girder Bridge

Table 6.1 – Demand of the Bridge Girders

Unfactored service moment (kip-ft)	Factored ultimate moment (kip-ft)	Factored ultimate shear (kip)
1109	1759	174

Due to the lab limitations and material availabilities, a 50-ft long steel beam with the rolled shaped section W18×86 and 12 strands are used for the design of PCSC girder specimen. The cross-section of the PCSC girder specimen is shown in Fig. 6.2. Deck and concrete bottom flange both have a length of 49 ft. The dimension of the concrete bottom flange is 24 × 6.75 in. The concrete strengths at release and at final are 8 ksi and 10 ksi, respectively. Twelve 0.7-in. strands are placed in concrete bottom flange, i.e., 8 strands at bottom layer and 4 strands at top layer. The strands are spaced on center at 2 in., and the centroidal spacing between the bottom and top layers of strands is 2.75 in.

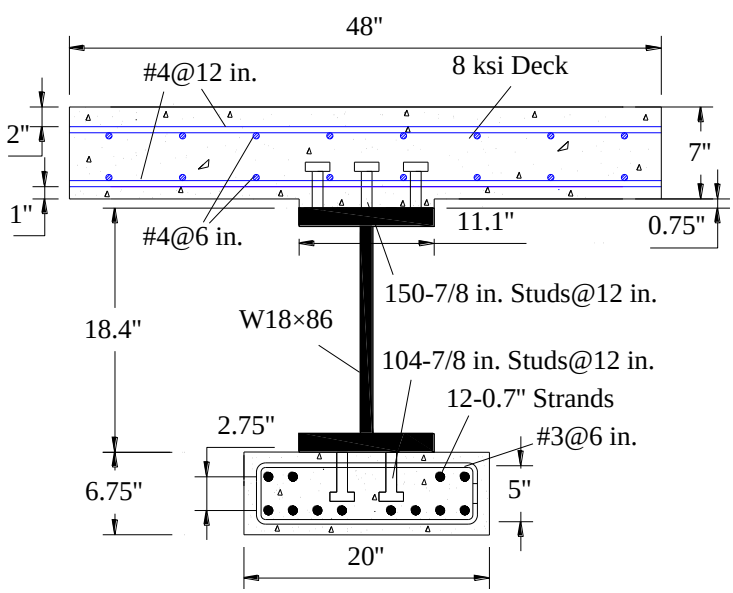

Fig. 6.2 – Cross-section of the PCSC Specimen

One hundred fifty 7/8-in. stud shear connectors are placed at 12 in. between the concrete deck and the steel section; One hundred and four 7/8-in. stud shear connectors are placed at 12 in. between the concrete bottom flange and the steel section. The studs at top and bottom of the steel beam are transversally spaced on center at 4 in. The studs at the bottom of steel beam are spaced on center at 6 in. along 2.5 ft from ends and then spaced at 2 in until the mid-span. In order to compare to girder spacing of 96 in and concrete compressive strength of 4 ksi, the dimension of deck is 7 in. depth and 48 in. width, the concrete strength of deck is 8 ksi, and deck is designed with #4@6 in. (instead of #4@12 in. in bridge deck) for top and bottom layer reinforcements and the clear cover of reinforcement is 2 in. for the top layer and 1 in. for bottom layer. The section properties are listed in Table 6.2.

Table 6.2 – Specimen Properties

Deck		Steel section		Concrete bottom flange			
Dimensions	f'_c	Section	Yield strength	Section	f'_{ci}	f'_c	Strands
48"×7"	8 ksi	W18×86	50 ksi	20"×6.75"	8 ksi	10 ksi	12-0.7"

6.3 *Fabrication of a PCSC Girder Specimen and Measurements*

6.3.1 Prestressing System and Devices

The PCSC girder specimen was fabricated in the prestressing system located in structural testing lab at the University of Nebraska-Lincoln, Omaha, NE. Prestressing system provides anchoring for prestressing strands and casting bed for specimens. The prestressing system comprises prestressing bed, end abutments, anchoring devices and jacks.

The cross-section of the prestressing bed is described in Fig. 6.3. The main framework of the prestressing bed is the U-shaped concrete bed around 60 ft long and with dimensions of cross-section as shown in Fig. 6.3. Wood floor is placed on the top of the flange of the concrete bed, assuring even surface and facilitating installment of the formwork. Steel plates are embedded into the flanges of the concrete bed at end sections, so as to distribute applied loading and prevent localized damage/failure.

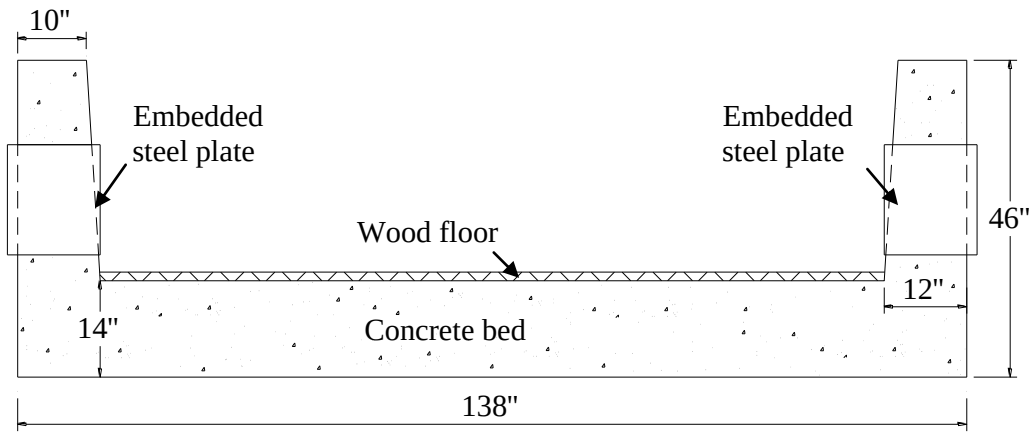

Fig. 6.3 – Cross-section of the Prestressing Bed

End abutments, used to restrain the prestressing strands, are assembled at the north end and the south end of the prestressing bed. Longitudinal and transverse profiles of the north abutment are depicted in Fig. 6.4(a) and Fig. 6.4(b), respectively. As shown in the Fig. 6.4(a-b), the stacked steel plates functioning as beam members distribute the prestress force into embedded steel plates of the prestressing bed. Each stacked steel plate has thickness of1 in., width of 24 in. and length of 144 in. Chucks are used to anchor strands for each strand and are supported by the anchoring steel plate. Anchoring steel plate distributes the prestress force into the stacked steel plates. The anchoring steel plate has the thickness of 2.4 in. and its profile is shown in Fig. 6.5. As shown in Fig. 6.5,

holes are drilled in the anchoring steel plate in a way of following the same pattern of the strand distribution.

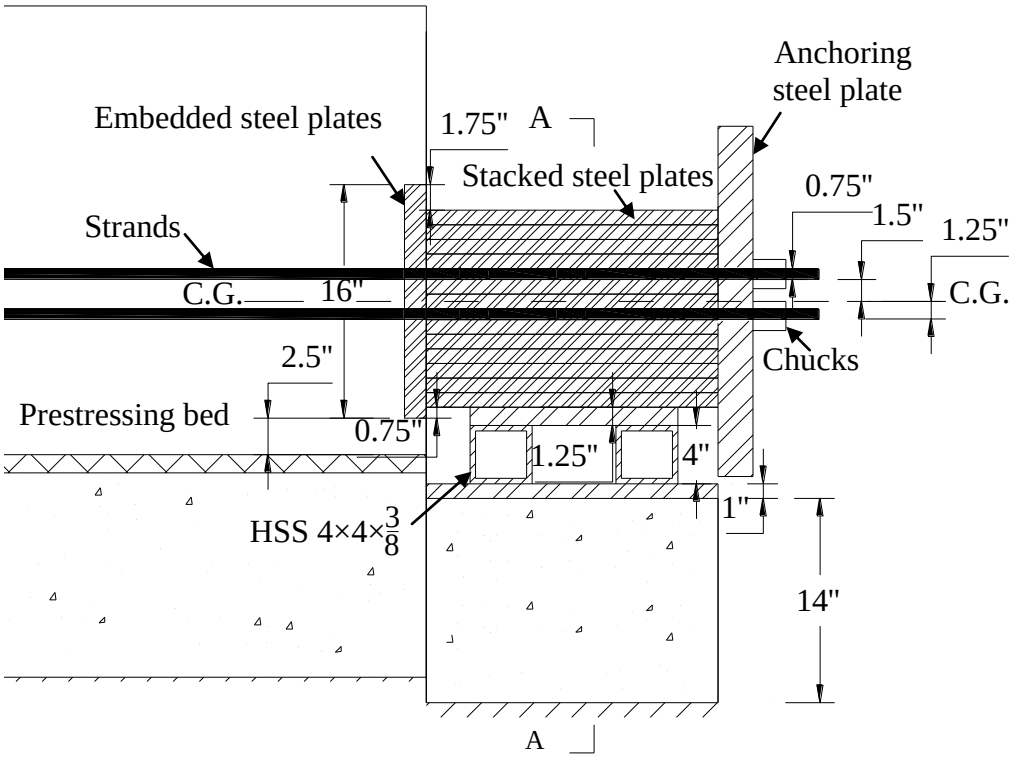

(a) Longitudinal Profile of the North Abutment

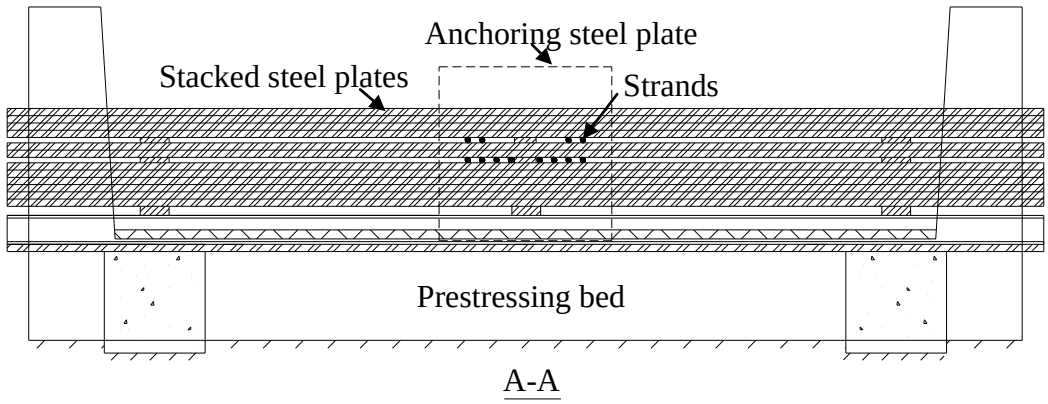

(a) Transverse Profile of the North Abutment (A-A)

Fig. 6.4 – Profiles of the North Abutment

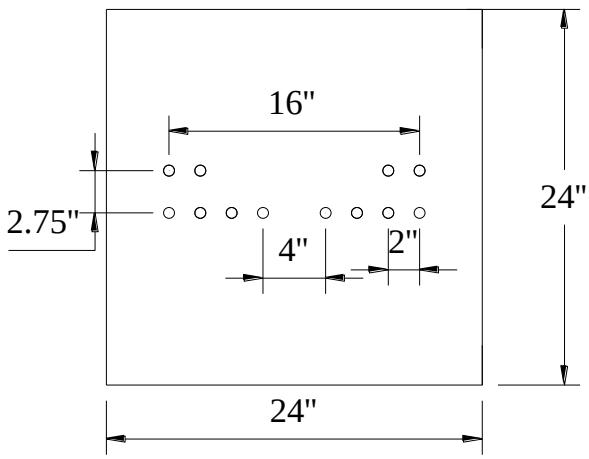

Fig. 6.5 – Profile of Anchoring Steel Plate

Longitudinal and transverse profiles of the south abutment are depicted in Fig. 6.6(a) and Fig. 6.6(b), respectively. The anchoring steel plate, stacked steel plates, chucks of the south abutment are installed in the same way as those of the north abutment. Rollers are mounted at the bottom of the south abutment in order to fit the deformation of strands when applying and releasing prestress force on strands. For applying the identical prestress force to each strand, a hydraulic jack is used to symmetrically pre-tension strands one by one. Two jacks are placed between the south abutment and prestressing bed as shown in Fig. 6.6(a) and are used for the release of prestressing strands in the future.

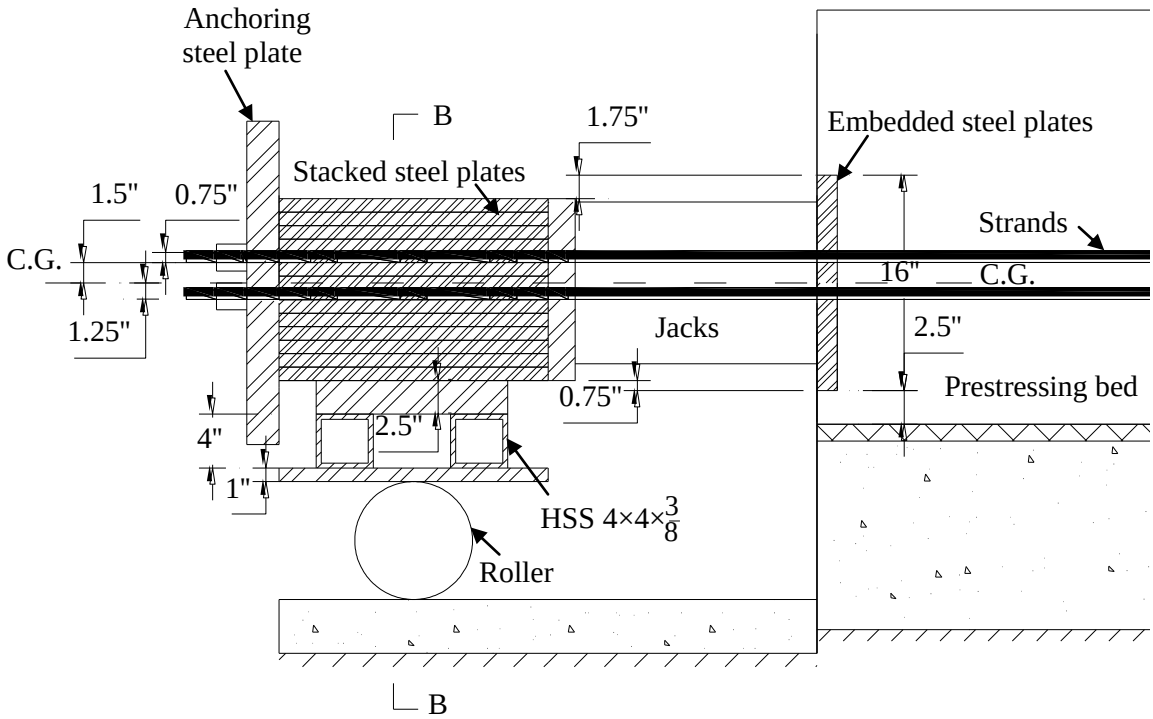

(a) Longitudinal Profile of the South Abutment

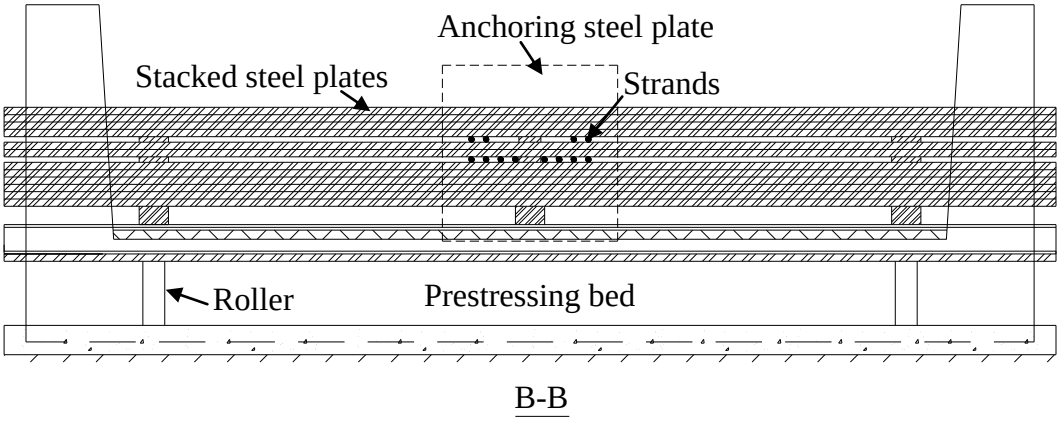

(b) Transverse Profile of the South Abutment (B-B)

Fig. 6.6 – Profiles of the South Abutment

6.3.2 Girder Fabrication and Measurements

The PCSC girder specimen was fabricated by following the procedure of five steps as presented in Section 3.2 and illustrated in Fig. 3.2:

- Step 1 consists of welding studs to steel beam, pre-tensioning strands, placing stirrups and forming the concrete bottom flange, as shown in Fig. 6.7(a). The studs were initially welded to the bottom flange of steel beam and then the top flange of steel beam after being flipped over. The 12-0.7″ diameter strands were threaded through the south abutment plates, through the steel support chairs and confinement reinforcement, then finally through the north abutment plates. Each strand was chucked at both ends and the 12-0.7″ diameter strands were symmetrically pre-tensioned to $0.75f_{pu}$ one by one using a hydraulic hand jack. The stirrups were tied to strands and staggered against the studs at the required spacing as shown in Fig. 6.7(a). Compatibility of stirrups and studs are checked by supporting the steel beam on the support chairs as shown in Fig. 6.7(b).

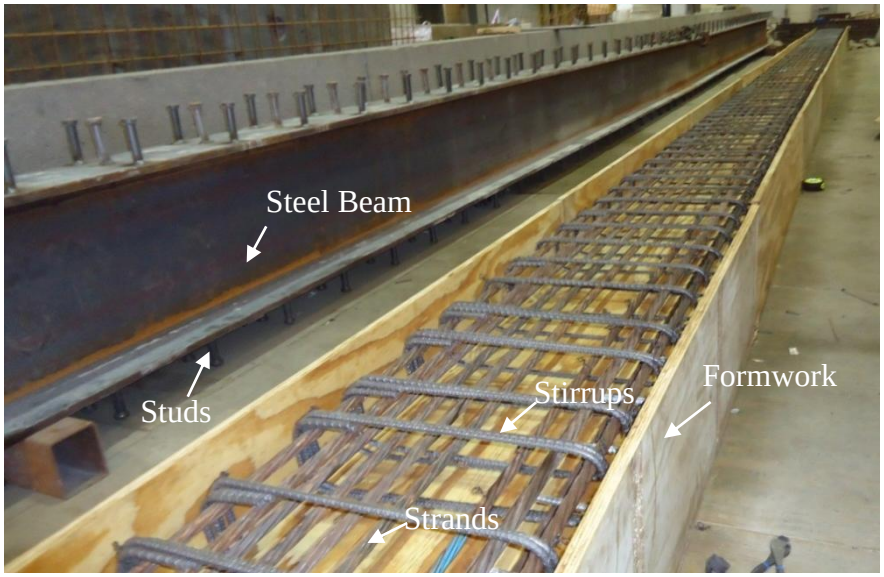

(a)Welding Studs to Steel Beam, Pretensioning Strands, Placing Stirrups and Forming the Concrete Bottom Flange

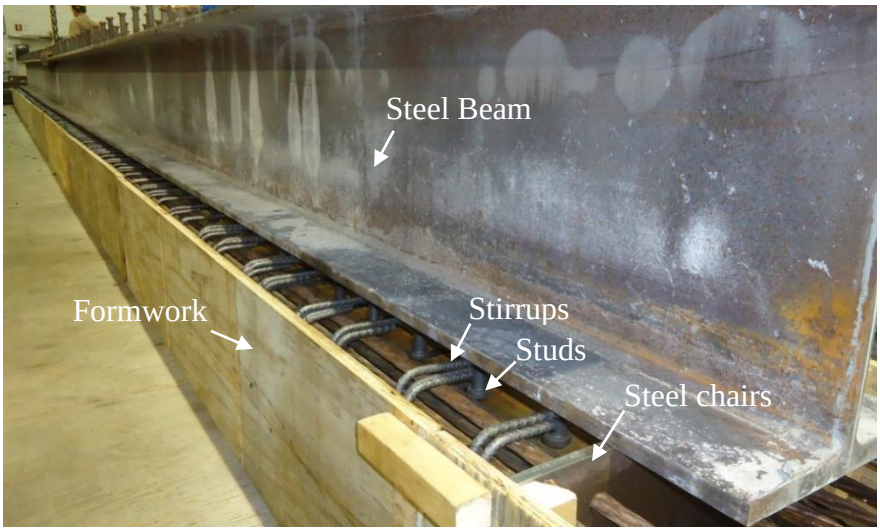

(b) Check Compatibility of Stirrups and Studs

Fig. 6.7 – Step 1: Welding Studs to Steel Beam, Pretensioning Strands, Placing Stirrups and Forming the Concrete Bottom Flange

- In Step 2, Self-consolidating concrete (SCC) was then delivered by the Ready Mix truck. After adding additional dosage of HRWRA, slump flow test showed a concrete spread of 22 in. Cylinder samples were taken and SCC was poured into the formwork

without vibration and the top surface of concrete was finished, as described in Fig. 6.8(a) and Fig. 6.8(b), respectively.

(a) Pour Concrete into Formwork (b) Finish the Concrete Surface

Fig. 6.8 – Step 2: Placing Concrete into the Formwork and Finishing the Surface

- In Step 3, the steel beam was placed on the top of fresh concrete and supported by the supported chairs, and the studs at bottom penetrated into the fresh concrete, as shown in Fig. 6.9(a). The support chairs are shown in Fig. 6.9(b). For achieving good interfacial contact between concrete and bottom flange of the steel beam, the bottom flange of the steel beam was vibrated using a vibrator, as shown in Fig. 6.9(c). Afterwards, the concrete flange were covered with burlap and kept wet for three days. The steel beam has initial deflection of 0.75 in. at mid-span due to fabrication accuracy and own weight, which is close to the thickness of the bottom flange of steel beam. After placement, the steel bottom flange was just located at the top of concrete bottom flange at supports, and was embedded into the concrete bottom flange with the same top surface at mid-span.

(a) Steel Beam Sits on Steel Chairs

(b) Steel Support Chairs

(c) Vibrating the Bottom Flange of Steel Beam

Fig. 6.9 – Step 3: Placing the Steel Beam on Steel Chairs

The set-up sketch of specimen, formwork and supports is described in Fig. 6.10(a). The profiles of support chairs are illustrated in Fig. 6.10(b). Note that holes were drilled in the support chairs with the same pattern as the distribution of strands, allowing the strands to be placed into the formwork and between the end abutments. The formwork fits between the support chairs and its cross-section is shown in Fig. 6.10(c). The distribution of studs and stirrups were well arranged so that the studs could fit into the concrete between stirrups. Detailed distribution of studs and stirrups are described in Fig. 6.10(d).

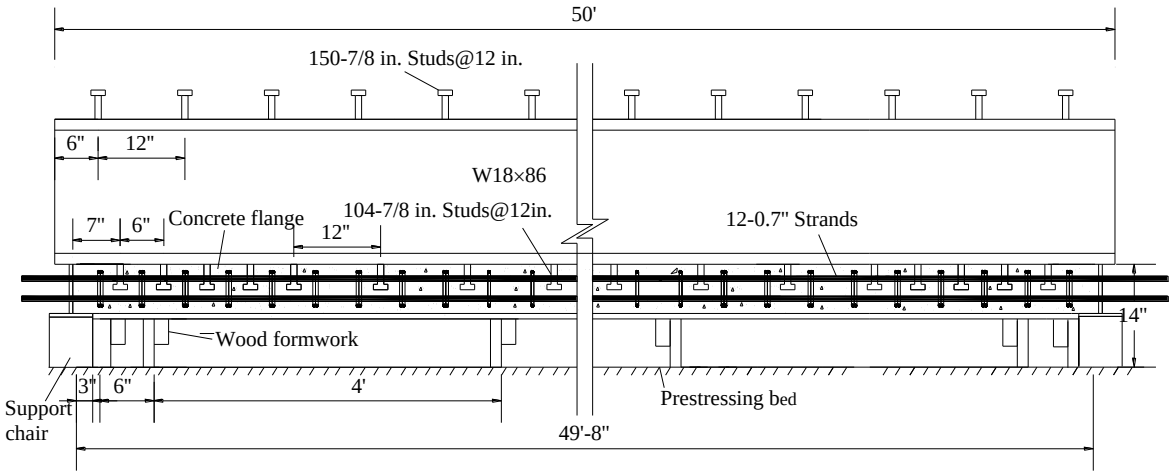

(a) Specimen Elevation View

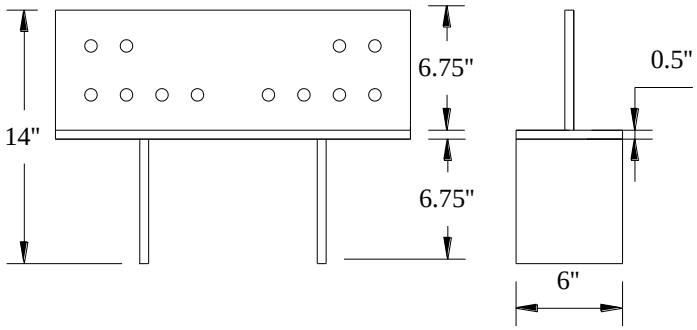

(b) Profiles of Support Chairs

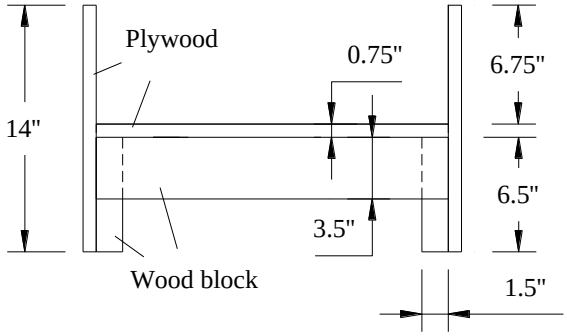

(c) Cross-section of Formwork

Fig. 6.10 – Views of Specimen, Formwork and Supports (Continued)

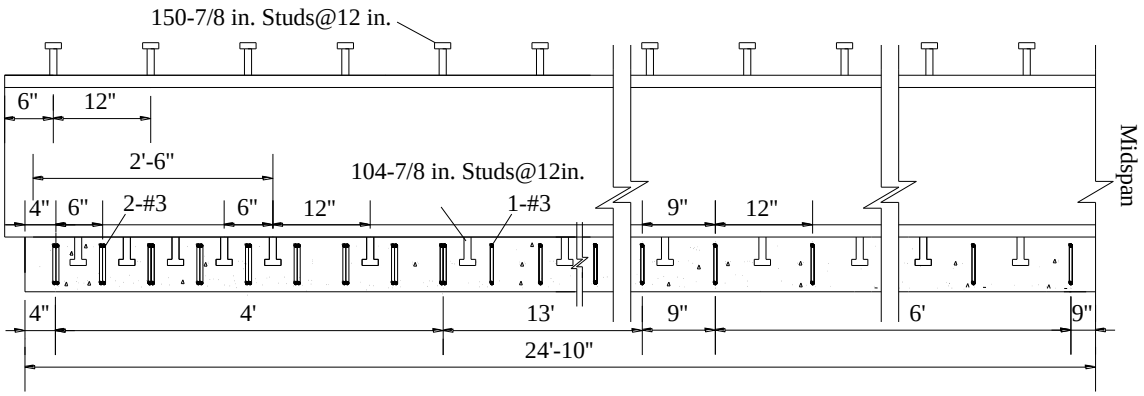

(d) Detailed Distribution of Studs and Stirrups

Fig. 6.10 – Views of Specimen, Formwork and Supports

- Step 4 includes stripping the formwork, releasing and cutting the strands. At the concrete age of 3-day, the formwork was removed. The specimen was placed on two supports with the span of 49 ft. The strain gages and detachable mechanical strain gages (DEMEC) were glued on cross-sections at mid-span and 48 in. from end. Note the section at 48 in. from end was selected based on the transfer length found as 42 in. in light of AASHTO (2007). The strain gages of the type FLA-6-11 and the type PL-60-11 were glued on the top and bottom of the steel beam and the concrete flange respectively, as illustrated in Fig. 6.11(a). The letters “S”, and “F” are an abbreviation of the strain gage’s location at the steel beam and the concrete bottom flange, respectively. The letters “T” and “B” refer to strain gage’s location at the top and the bottom of each component, respectively. DEMEC strain gages were glued on the concrete bottom flange at the same level of the centroid of prestressing strands, as shown in Fig. 6.11(a). Fig. 6.11(b) shows DEMEC strain gages were glued on concrete flange from the end to 8 ft from the end. Readings from strain gages will be recorded using an automated data-acquisition system consisting of a multiplexer and

a datalogger controlled by a computer interface. Readings from DEMEC strain gages will be obtained using a digital indicator.

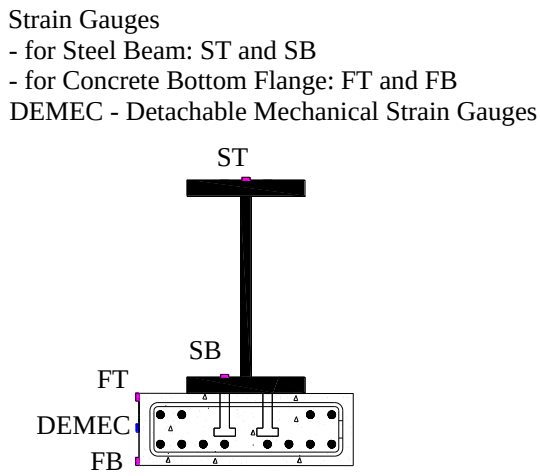

(a) Locations of Strain Gages at Sections at 48 in. from end and Mid-span

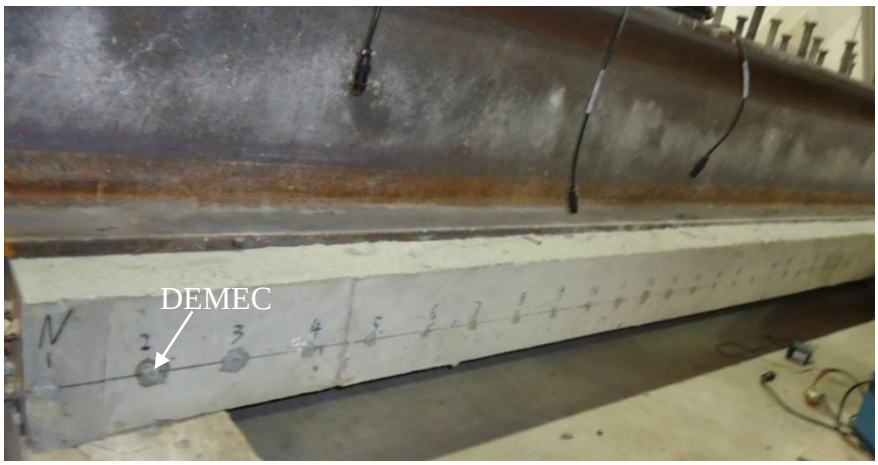

(b) DEMEC Strain Gages along 8 ft from Girder Ends

Fig. 6.11 – Specimen Instrumentation

Compressive testing of cylinders showed that the concrete strength was 10.1 ksi and 11.0 ksi at the ages of 3-day and 7-day, respectively, which are higher than the required 8 ksi at prestress release. The prestress force was gradually released by adjusting the hydraulic jacks located between the prestressing bed and the south

abutment, as shown in Fig. 6.12(a). The strands were cut using flame cutting machine, as shown in Fig. 6.12(b). The strain data were immediately recorded by strain gages and DEMEC strain gages due to the prestress force, and the camber was measured by a ruler. Readings from DEMEC strain gages and the camber will be continuously recorded after prestress release.

(a) Release the Strands (b) Cut the Strands

Fig. 6.12 – Step 4: Stripping the Formwork and Releasing the Strands (7-day)

- Step 5 includes installation of formwork and reinforcement and placement concrete. Formwork was constructed to provide concrete deck with depth of 7 in. and width of 49 in. and length of 29.5 ft. The deck reinforcement consisted of two layers were installed into the formwork as shown in Fig. 6.13(a). At the age of 43-day of concrete bottom flange, SCC was delivered by ready mix truck and the slump flow testing

showed SCC had a spread of 22 in. The cylinders were taken, the SCC was poured into the deck formwork as shown in Fig. 6.13(b) and the concrete was finished as shown in Fig. 6.13(c). The concrete deck were covered with burlap and kept wet for three days. Later, immediately after the formwork was removed, the strains on the concrete flange were measured by DEMEC strain gages and the camber was measured by a ruler. After removing the formwork, the complete girder specimen is shown in Fig. 6.13(d).

(a) Install the Formwork and Place the Reinforcement

(b) Place Concrete into Formwork (43-day)

Fig. 6.13 – Step 5: Install Formwork and Reinforcement, Place Concrete and Finish Concrete Surface for Concrete Deck (Continued)

(c) Finish Concrete Surface (43-day)

(d) Remove Formwork

Fig. 6.13 – Step 5: Install Formwork and Reinforcement, Place Concrete, Finish Concrete Surface and Remove the Formwork for Concrete Deck

Strain readings from DEMEC strain gages and the camber will be continuously monitored until the age of the concrete bottom flange reaches 60 days.

Differences between the designed section and the fabricated section are:

1) Due to initial deflection, the bottom flange of steel beam was located at the top of concrete bottom flange at supports and embedded into the concrete bottom flange with the same top surface at mid-span.
2) The width of deck is 49 in.
3) The concrete strengths of the concrete bottom flange and concrete deck.

Average of the depth of concrete bottom flange is found as (6.0 + 6.75) = 6.375 in. For simplicity, a constant depth, 6.375 in., is assumed for concrete bottom flange from end to mid-span. The as-built cross-section of the PCSC girder specimen is shown in Fig. 6.14.

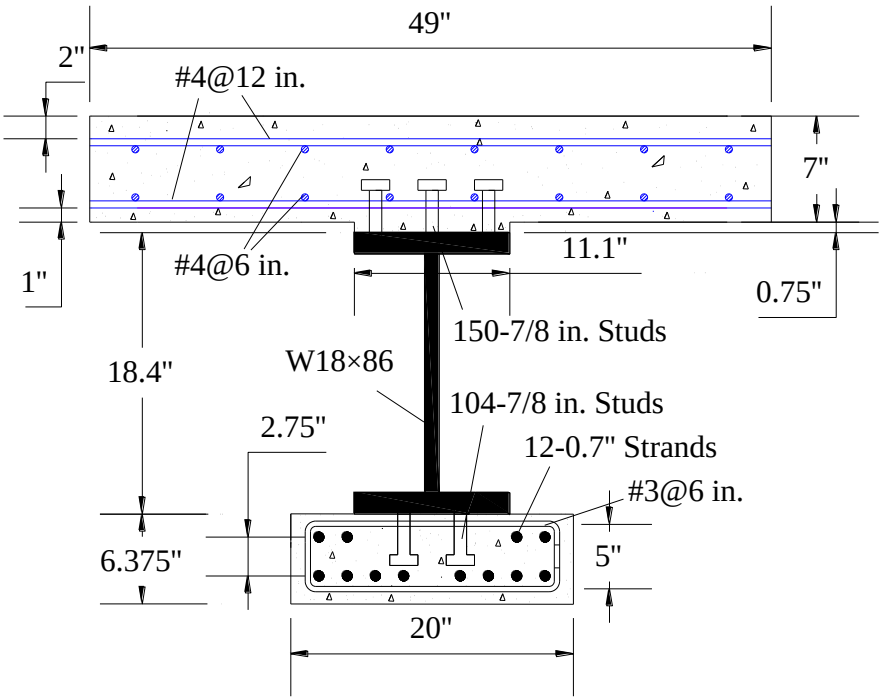

Fig. 6.14 – As-built Cross-section of the PCSC Specimen

Concrete strengths of concrete bottom flange and deck at different ages are summarized in Table 6.3. The concrete strengths of concrete bottom flange at prestress

release and 28-day are 11 ksi and 13.3 ksi, compared to 8 ksi and 10 ksi according to the design of the PCSC girder specimen, respectively. The concrete strength of concrete deck at 28-day is 10.6 ksi compared to 8 ksi according to the design of the PCSC girder specimen. As described in Fig. 6.15, prestress release, deck placement, flexural test and shear test were performed at ages of concrete bottom flange, 7-day, 43-day, 71-day and 81-day. Flexural test and shear test were performed at ages of concrete deck, 28-day and 38-day.

Table 6.3 – Concrete Strengths of Concrete Bottom Flange and Deck at Different Ages

Concrete bottom flange		Concrete deck	
Concrete age (day)	Concrete strength (ksi)	Concrete age (day)	Concrete strength (ksi)
3	10.1	5	8.2
7	11.0	28	10.6
11	11.7	38	11
14	12.1	---	---
28	13.3	---	---
71	13.9	---	---

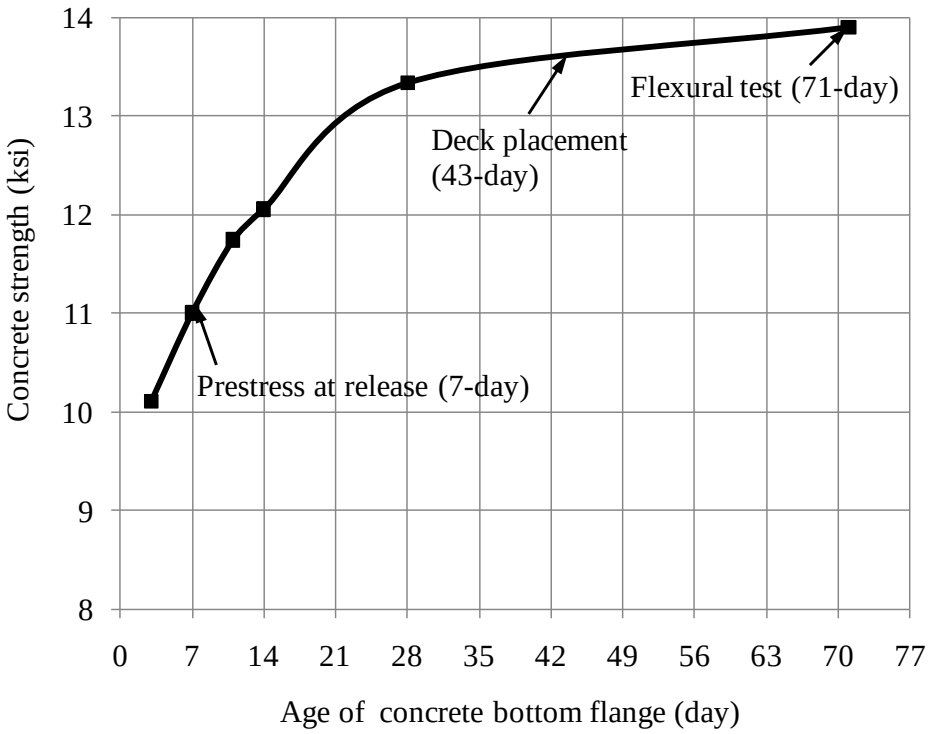

(a) Concrete Bottom Flange

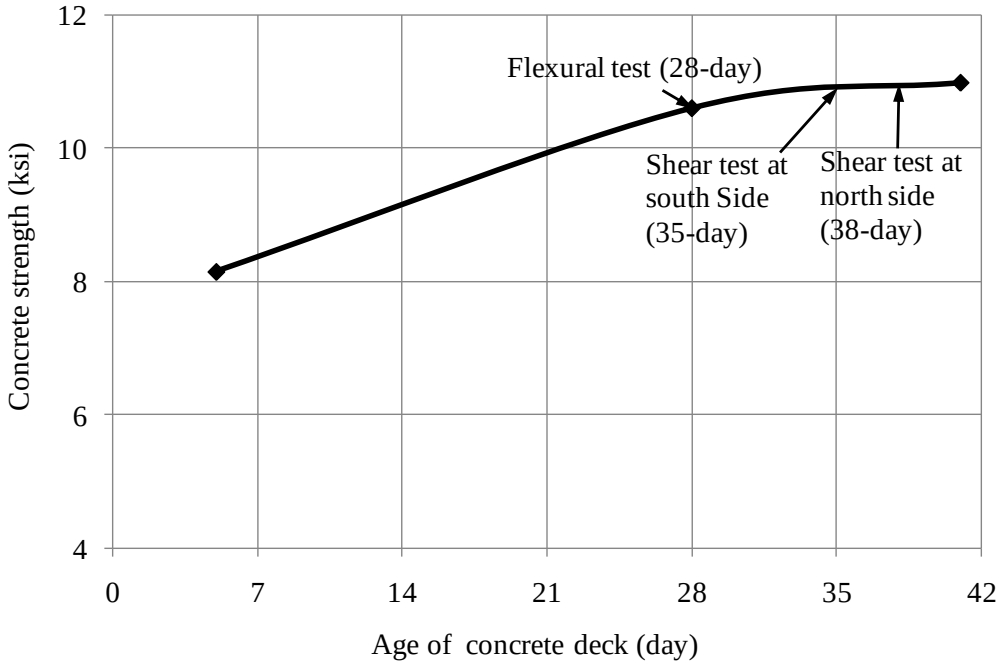

(b) Concrete Deck

Fig. 6.15 – Concrete Strengths of Concrete Bottom Flange and Deck at Different Ages

6.4 *Flexural and Shear Tests*

The flexural test was conducted to evaluate the moment capacity of the PCSC girder specimen, and the test setup is shown in Fig. 6.16(a). The PCSC girder specimen was simply supported on the roller supports with the span of 48 ft. The spread beam was used to apply two point loads on the top of the deck of the specimen. Two point loads were spaced at 14 ft to simulate the HS-20 truck load and used to create pure bending in the middle sections of the specimen between the two loads. The elevation view of the flexural test setup is described in Fig. 6.16(b). The steel frame was installed to hold the jack for loading and fixed by threaded rods which were screwed into the floor inserts as shown in Fig. 6.16(b).

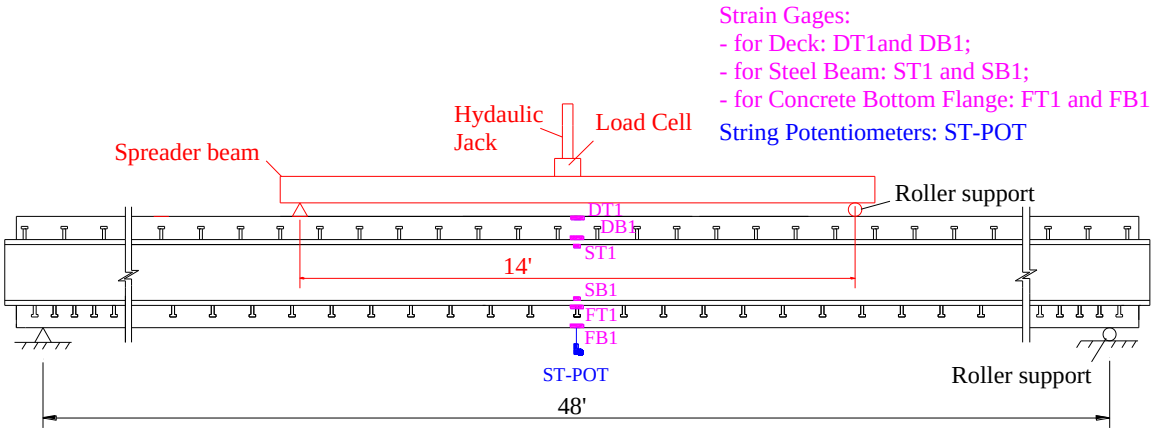

(a) Flexural Test Setup

Fig. 6.16 – Test Setup for Flexural Test (Continued)

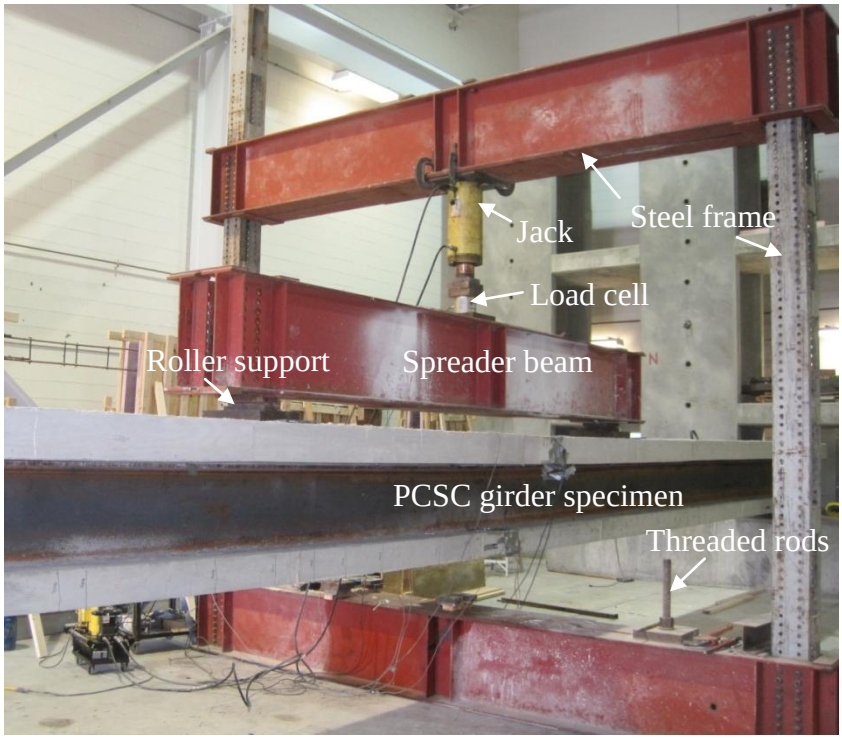

(b) Elevation View of Flexural Test Setup

Fig. 6.16 – Test Setup for Flexural Test

After the flexural test, the shear tests were conducted to evaluate the shear capacity of the PCSC girder specimen, and the test setup is shown in Fig. 6.17(a). Two shear tests were conducted for the south and north sides of the specimen. For each test, one point load was applied on the section at 9 ft from the support. The bearing plate with dimensions 8″ × 17″× 2¼″ was placed on the top of deck so as to distribute the load to the specimen and avoid local damage of the deck. The view of the shear test setup is described in Fig. 6.17(b).

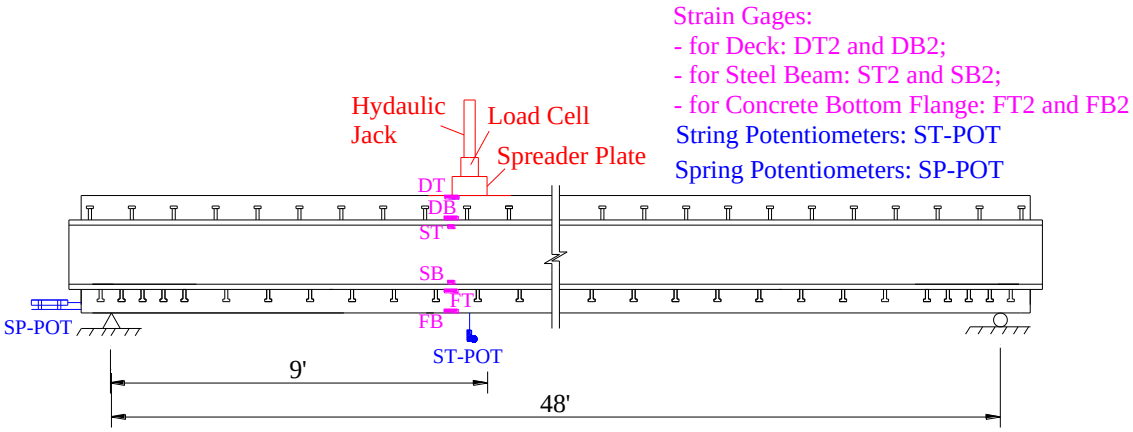

(a) Shear Test Setup

(b) Elevation View of Shear Test Setup

Fig. 6.17 – Test Setup for Shear Test

As shown in Fig. 6.16(a) and Fig. 6.17(a), strain profiles were measured on the sections at mid-span and 9ft from support for the flexural test and the shear test, respectively. Note that the strain gages for shear tests were installed at the section along the edge of the bearing plate as described in Fig. 6.17(a). Twelve strain gages were used to record the strain distribution at the concrete deck, the steel beam, and the concrete bottom flange, as shown in Fig. 6.18(a). The letters “D”, “S”, and “F” are an abbreviation of the strain gage’s location at the concrete deck, the steel beam, and the concrete bottom flange, respectively. The letters “T” and “B” refer to strain gage’s location at the top and the bottom of each component, respectively. The numbers “1” and “2” of the identification for strain gages refer to the west and east sides of the specimen, respectively.

String Potentiometers (ST-POT) were attached to the bottom of the concrete bottom flange in order to record the deflections of the sections at mid-span and 9 ft from support for the flexural test and the shear test, respectively. The strand slip was measured at the end of the specimen using Spring Potentiometers (SP-POT). Only the slip of the bottom layer of the strands was monitored and the locations of 4 instrumented strands are illustrated in Fig. 6.18(b).

Readings will be recorded using an automated data-acquisition system consisting of a multiplexer and a data logger controlled by a computer interface.

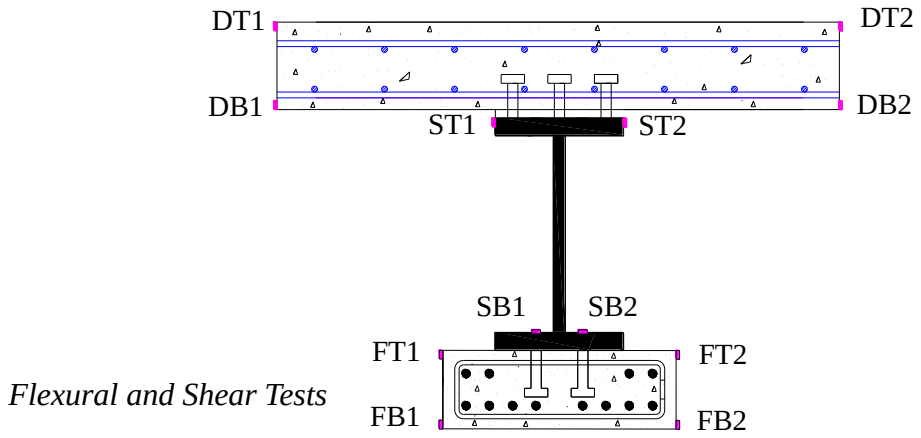

(a) Strain Gages on the Cross-sections at Mid-span and 9 ft from the Support

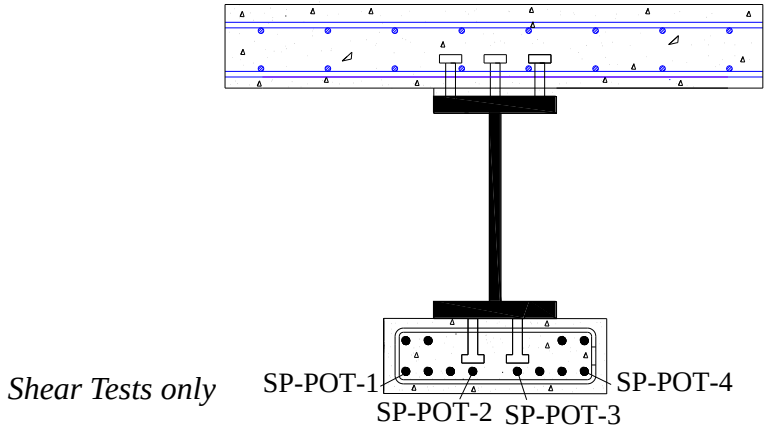

(b) Spring-Potentiometers (SP-POT)

Fig. 6.18 – Instrumentation for Flexural and Shear Tests

The PCSC girder specimen was designed to satisfy the demand of bridge girders in Section 6.3. However, due to higher concrete strengths for concrete bottom flange and deck and some changes in the section dimensions, the flexural and shear capacities of the fabricated specimen section in Fig. 6.14 differed slightly from the designed specimen in Fig. 6.2. Table 6.4 indicates that, for the fabricated specimen, the theoretical values of crack moment, nominal moment and nominal shear are larger than unfactored service moment, factored ultimate moment, and factored ultimate shear in demand, respectively.

The loads for testing were determined based on theoretical flexural and shear capacities and no safety factors were used. Due the self-weight of the specimen and the spreader beam, the initial moment in the mid-span section, 236 kip-ft, should be considered in the flexural test. Likewise due to self-weight of the specimen, initial shear in the section at 9 ft from support, 11.4 kip, should be considered in the shear test. Thus, by excluding self-weight, the calculated loads to reach theoretical crack, moment nominal moment, and nominal shear are summarized in the Table 6.5.

Table 6.4 – Flexural and Shear Capacities of the PCSC Specimen

Demand of Bridge Girders			**Theoretical Values**		
Unfactored service moment (kip-ft)	Factored ultimate moment (kip-ft)	Factored ultimate shear (kip)	Crack moment (kip-ft)	Nominal moment (kip-ft)	Nominal Shear (kip)
1110	1759	174	1257	3360	235

Table 6.5 – Calculated Loads to Reach the Theoretical Capacities of the PCSC Specimen

Calculated Loads Excluding Self-weight		
Flexural test		Shear test
For crack moment (kip)	For nominal moment (kip)	For nominal shear (kip)
120	368	275

6.5 *Test Results and Validation of Design Methods and FEA*

6.5.1 Prestress Release and Measurements Afterwards

Immediately after prestress release, the strains were measured in sections at mid-span and 48 in. from end as shown in Fig. 6.11(a). The strain gages “FT” and “FB” gave

error data which were discarded. Strain profiles in sections at mid-span and 48 in. from end are described in Fig. 6.19(a) and Fig. 6.19(b), respectively. Based on the assumption that full bond exists between the steel section and the concrete bottom flange, design calculations are performed and linear strain profiles are derived in the sections as shown in Fig. 6.19. In addition, the strain profiles are also predicted using FEA as plotted in Fig. 6.19. Fig. 6.19 indicates that the strain profiles obtained in the tests agree well with those using FEA and design calculations. The small differences are mainly due to a little slip between the steel section and the concrete bottom flange.

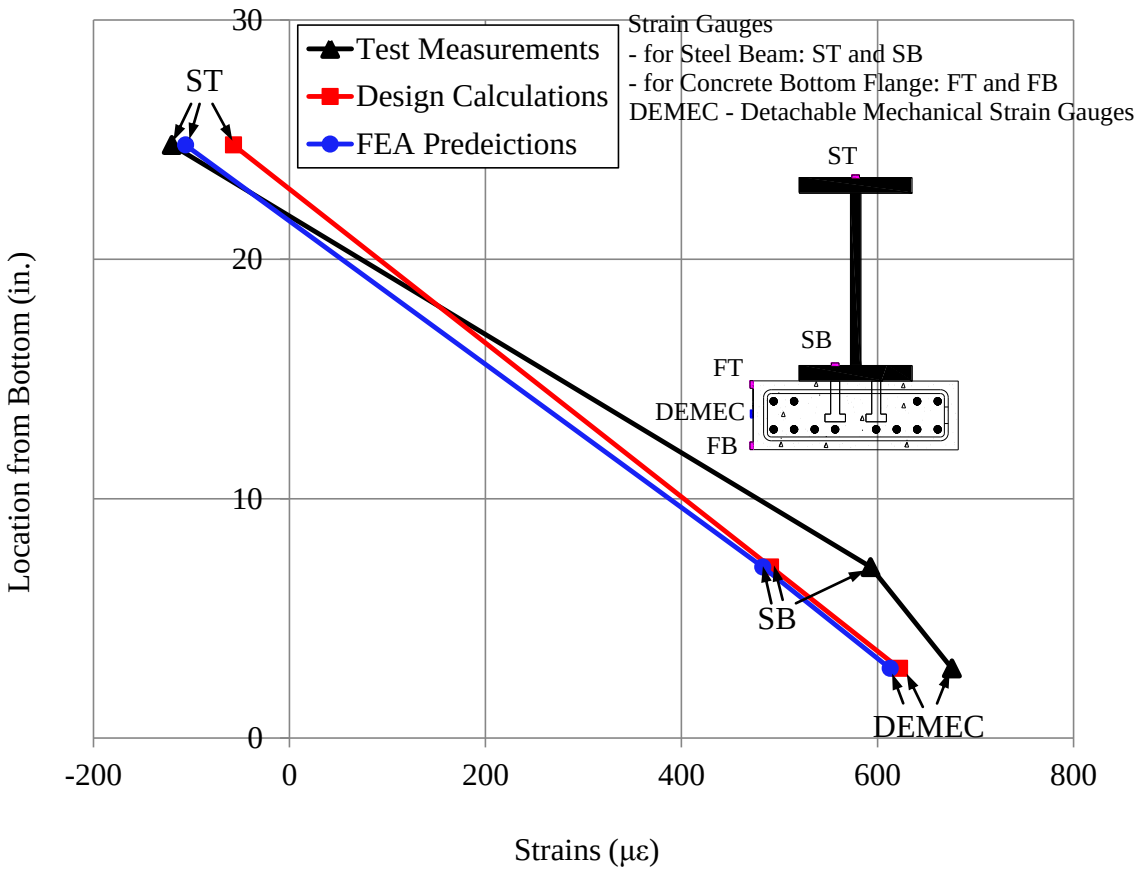

(a) Section at Mid-span

Fig. 6.19 – Strain Profiles in Sections at Mid-span and 48 in. from End (Continued)

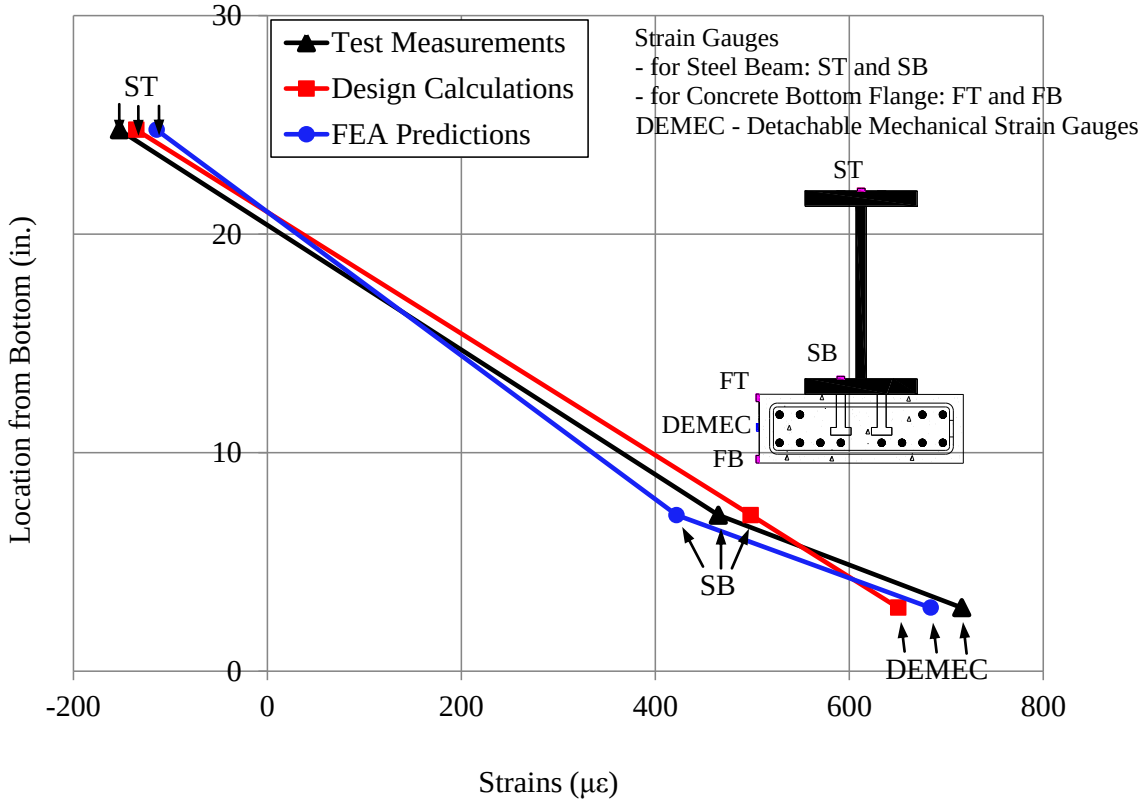

(b) Section at 48 in. from End

Fig. 6.19 – Strain Profiles in Sections at Mid-span and 48 in. from End

Concrete surface strains at 7-day and 28-day were monitored using DEMEC strain gages at transfer zones of south and north sides of the specimen and plotted in Fig. 6.20. The transfer lengths were estimated using a modified 95% Average Maximum Strain (AMS) method as described in Fig. 6.20. Regarding this method, the apex at the start of the strain plateau is visually identified, and a linear ascending trend line is plotted by fitting the data from the point at the end of the specimen to the apex. The constant strain region beyond the apex is visually identified in the plots, average maximum strain is reduced to 95% and a horizontal line is plotted. The intersection of the 95% AMS line and the linear ascending trend line is then calculated using the general slope intercept equation (Carrol, 2009). The transfer length values determined using modified 95% AMS

method and predicted using ACI and AASHTO equations, are tabulated in Table 4.7. Table 4.7 indicates that the transfer length for 0.7 strands is over-estimated using ACI and AASHTO equations. The low value of transfer length is mainly due to high concrete strength at release and rusted surface condition of strands.

Concrete surface strains at the same level of strands at 7-day are also predicted using FEA and design calculations and are plotted in Fig. 6.20. It is found that strains predicted using FEA follow exactly the same order as those obtained from tests at south and north sides and the adequacy of FEA is thus validated. However, only the strains from end to transfer length obtained using design calculations agree well with those obtained from tests. This means that the strains are not well predicted using design calculations from end to transfer length.

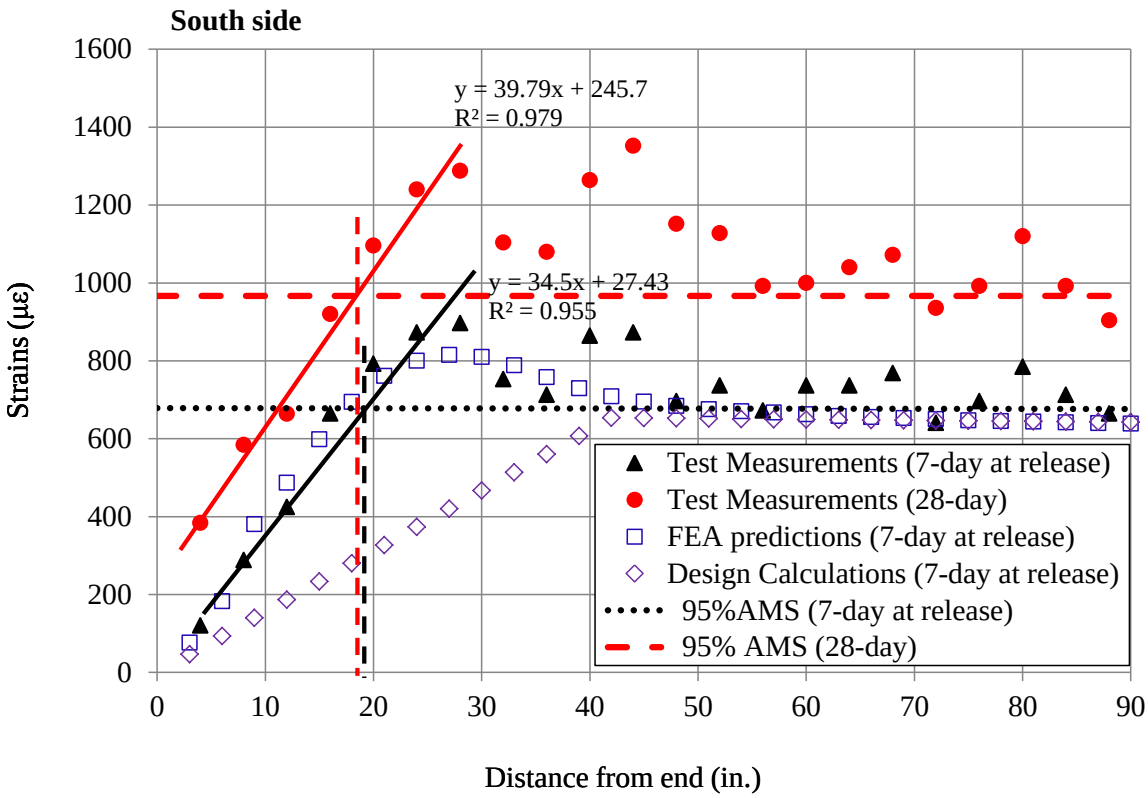

(a) South Side

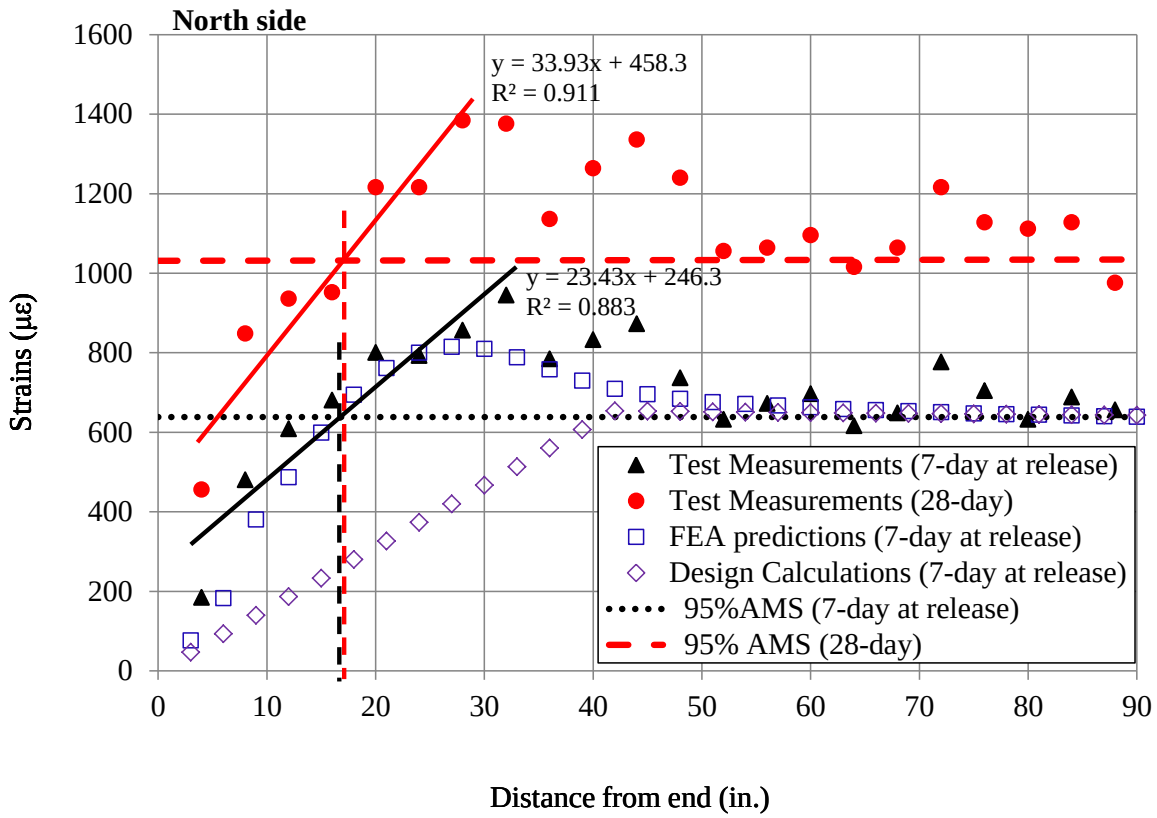

(b) North Side

Fig. 6.20 – Concrete Surface Strain Plots at South and North Sides of the Specimen with Modified 95% AMS Method

Table 6.6 – Summary of Transfer Length Measurement Estimation

	7-day at release	28-day	$(f_{se}/3)d_b$	ACI, $50d_b$	AASHTO, $60d_b$
South side (in.)	19.0	18.5	33.1	35.0	42.0
North side (in.)	16.8	17.0			
Average (in.)	**17.9**	**17.8**			

Concrete surface strains at the same level of centroid of strands were continuously monitored from 7-day at release to 60-day. The time histories of those strains at mid-span

and 48 in. from end are plotted in Fig. 6.21(a) and Fig. 6.21(b), respectively. It should be noted that the strain drop at 43-day is due to self-weight of the deck. The changes of concrete surface strains with time were also predicted using Age-adjusted Elasticity Modulus Method (AEMM) introduced in Section 3.4. Note that full bond is assumed between steel section and concrete bottom flange. As described in Fig. 6.21, the time histories of strains predicted using AEMM compare fairly with those obtained from the tests.

(a) At Mid-span

Fig. 6.21 – Time Histories of Concrete Surface Strains at the Same Level of Centroid of Strands (Continued)

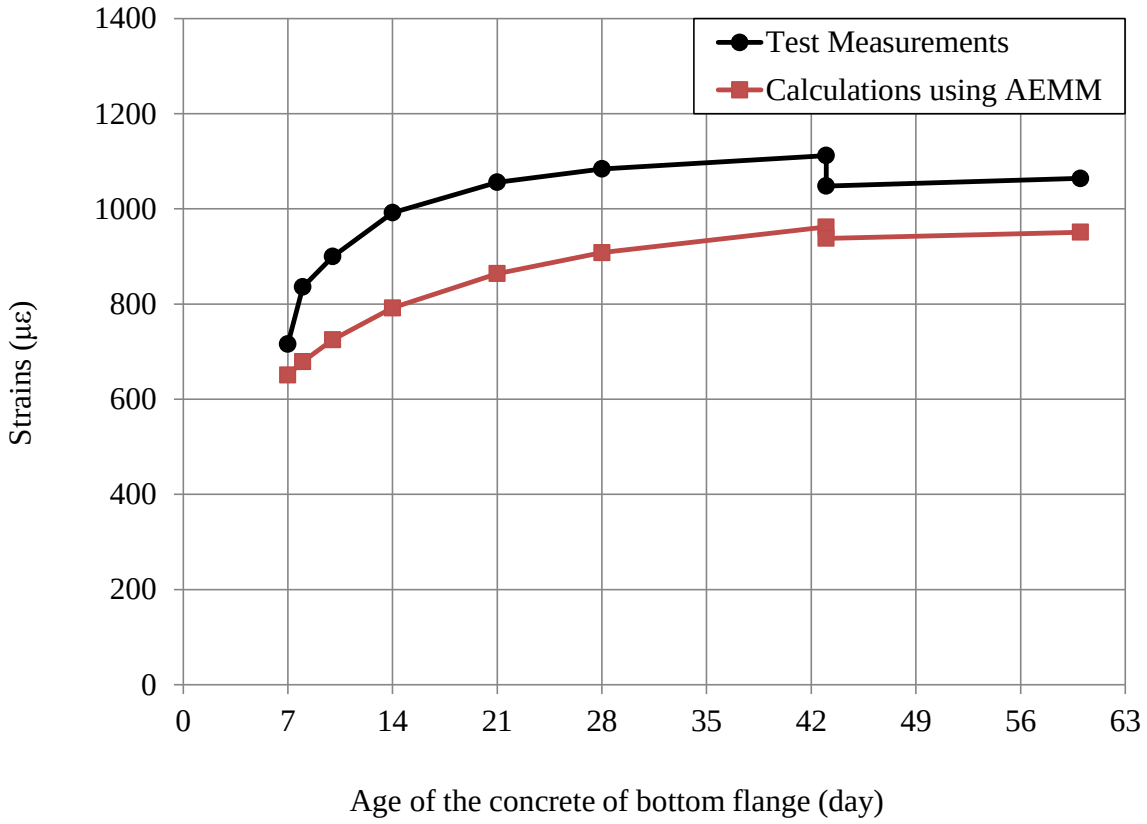

(b) At 48 in. from End

Fig. 6.21 – Time Histories of Concrete Surface Strains at the Same Level of Centroid of Strands

The camber of the specimen at mid-span was continuously monitored from 7-day at prestress release to 60-day. The initial camber at mid-span at prestress release is predicted using design calculations and FEA. As shown in Table 6.7, both methods give a good prediction within 12.5% and 7.5 margin of error, respectively.

Table 6.7 – Camber at Mid-span at Prestress Release

	Test measurement	Design calculations	FEA predictions
Camber at mid-span (in.)	1.6	1.40	1.48
Error	---	–12.5%	–7.5%

The time histories of the camber are plotted in Fig. 6.22. It should be noted that the camber drop at 43-day is due to the deflection induced by the deck placement. The change of the camber with time was also predicted using Age-adjusted Elasticity Modulus Method (AEMM) introduced in Section 3.4. As described in Fig. 6.21, the time history of the camber predicted using AEMM compare fairly with that obtained from the test measurement.

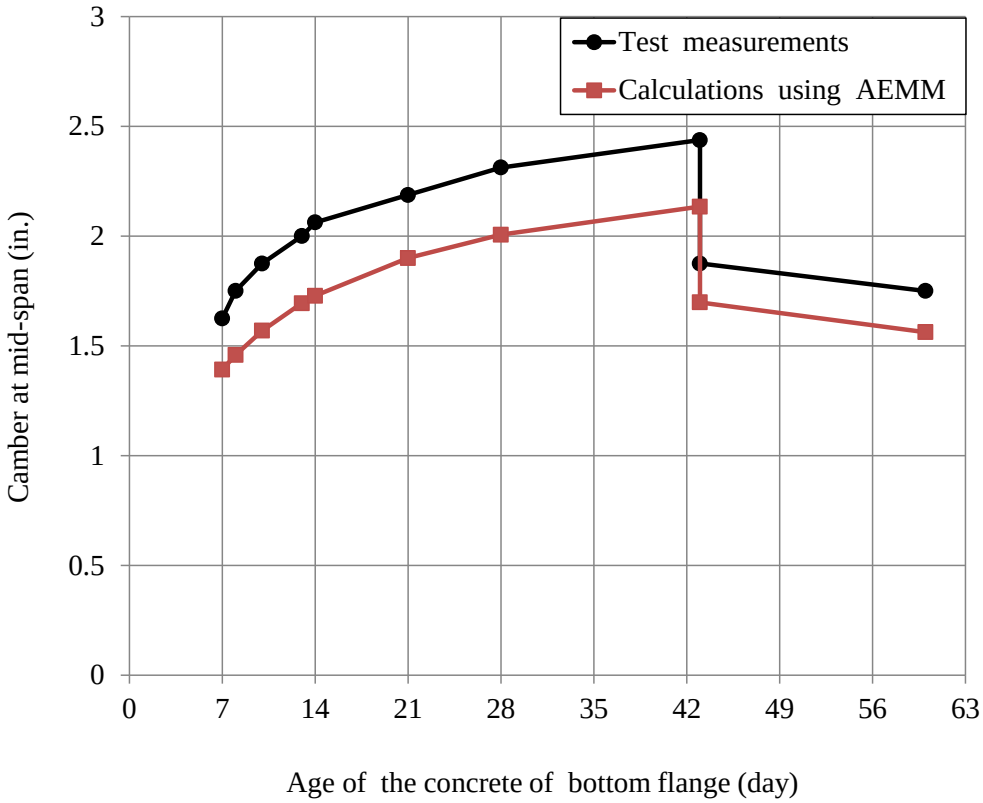

Fig. 6.22 – Time History of the Camber of the Specimen at Mid-span

Because the stirrups were placed in the concrete bottom flange at 4 in. from the ends of the specimen and bearing plates with embedded studs were not used at ends as shown in Fig. 6.10(d), end zone cracking was found as shown Fig. 6.23. Vertical and inclined cracks are shown in Fig. 6.23(a) and Fig. 6.23(b), respectively. Due to end zone

cracking, the supports were moved inside and the span decrease to 48 ft during the flexural and shear tests so as to avoid local damage at ends and slip of strands. Note that the distance from each support to each end of the specimen is 10 in.

(a) Vertical Cracks

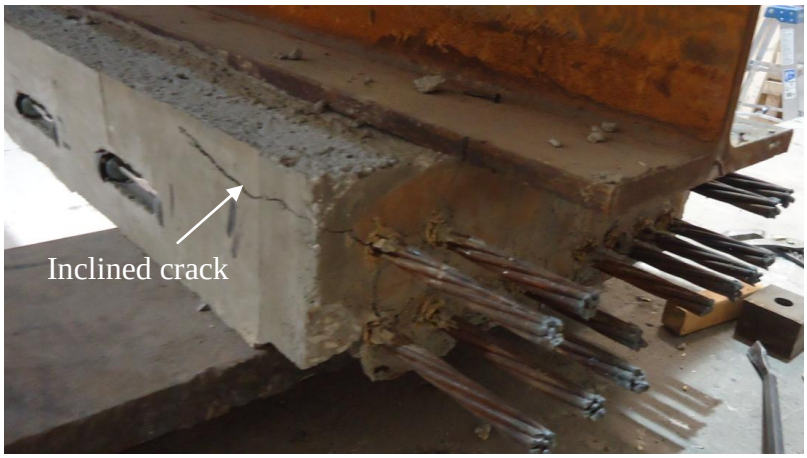

(b) Inclined Cracks

Fig. 6.23 – End Zone Cracking

6.5.2 Flexural and Shear Tests

A summary of applied loads compared with calculated loads for flexural and shear tests is tabulated in Table 6.8. Test moment and shear of the PCSC specimen

compared with the demand of bridge girders and theoretical values along with safety of factors are summarized in Table 6.9. The crack moment is determined based on tensile strength of concrete, $0.19\sqrt{f_c^{'}}$, based on AASHTO (2007). Table 6.9 indicates that the crack moment in flexural test has the factor of safety, 1.06, and the ultimate moment in flexural test and ultimate shear in shear tests both have the factor of safety of around 1.9, compared to the demand of bridge girders.

Table 6.8 – Test Loads on the PCSC Specimen

Calculated loads excluding self-weight			**Test loads excluding self-weight**			
Flexural test		Shear test	Flexural test		Shear test	
For crack moment (kip)	For nominal moment (kip)	For nominal shear (kip)	For crack moment (kip)	For nominal moment (kip)	For nominal shear (kip)	
					South	North
120	368	275	111	377	384	391

Table 6.9 – Test Moment and Shear of the PCSC Specimen

Demand of bridge girders			**Theoretical values**			**Test results**			
Unfactored service moment (kip-ft)	Factored ultimate moment (kip-ft)	Factored ultimate shear (kip)	Crack moment (kip-ft)	Ultimate moment (kip-ft)	Ultimate Shear (kip)	Crack moment (kip-ft)	Ultimate moment (kip-ft)	Ultimate shear (kip)	
								South test	North test
1110	1759	174	1257	3360	256	1180	3441	324	329
---			Ratio of values to demand			Ratio of results to demand			
---	---	---	1.13	1.91	1.47	1.06	1.96	1.86	1.89

The moment-deflection relationship for the flexural test is shown in Fig. 6.24. The initial moment due to self-weight of the specimen is included in Fig. 6.24. The deflection at mid-span increased linearly to 1.29 in. as the moment at mid-span reached the crack moment, 1180 kip-ft. Note that the deflection at mid-span was predicted to be 0.86 in. at

theoretical crack moment, 1257 kip-ft. The errors of predicting deflection and crack moment at mid-span are 33.3% and 6.5%, respectively. After the crack moment, the deflection went exponentially to 8.9 in. when the load induced the ultimate moment at the mid-span section which is larger than the theoretical ultimate moment. A residual deflection of 2 in. remained at mid-span after the load was released.

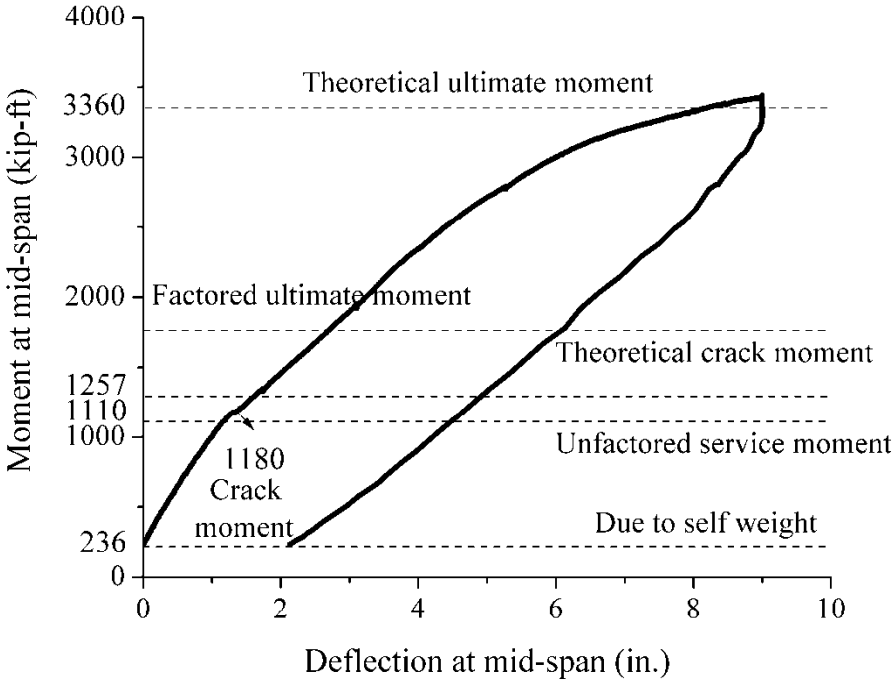

Fig. 6.24 – Moment-deflection Relationship in Flexural Test

The strains at east side of the mid-span section were not acquired. At west side, strains-moment relationship at mid-span section in flexural test is shown in Fig. 6.25. Fig. 6.25 indicated that the strains significantly increased as the crack moment was reached. The maximum strain in the top of deck equals 0.00189, which is less than the ultimate strain of concrete, 0.003. The concrete deck did not crush when theoretical ultimate moment was reached at mid-span section, as shown in Fig. 6.26. At the crack moment,

vertical flexure cracks started to occur in the concrete bottom flange in the middle region of the specimen. Cracks were spaced almost at the same spacing as shown in Fig. 6.27.

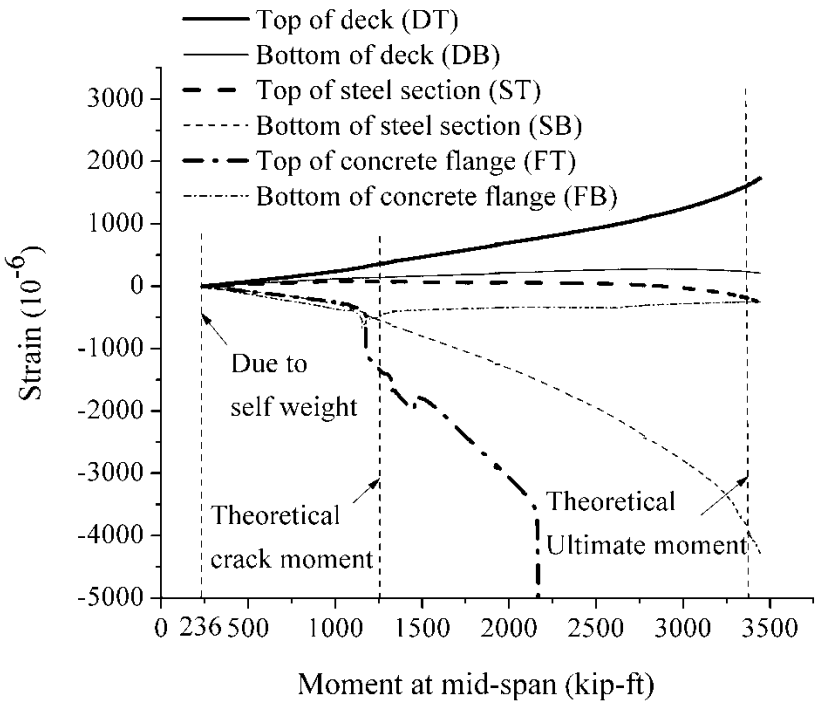

Fig. 6.25 – Strains-Moment Relationship in Flexural Test

Fig. 6.26 – Loading at Theoretical Ultimate Moment

Fig. 6.27 – Flexure Cracks in Flexural Test

As mentioned in Section 6.5, shear tests were conducted at south and north sides of the specimen. The shear-deflection relationships for south and north shear tests are shown in Fig. 6.28. The moment-deflection relationships for south and north shear tests are shown in Fig. 6.29. Fig. 6.28 and Fig. 6.29 indicate that the two shear tests show almost identical shear- and moment-deflection relationships. Note that the initial shear and moment due to self-weight of the specimen is included in Fig. 6.28 and Fig. 6.29, respectively. The failure shear in south and north tests is 324 and 329 kips, respectively, which are both larger than predicted ultimate shear, 256 kip. This is probably due to the pretensioning of strands on the composite section. The specimen suddenly failed at failure shear. The moment at failure in south and north tests is 2918 and 2960 kips, respectively, which are both less than the predicted ultimate moment, 3360 kip-ft. The deflection in failure and residual deflection at mid-span are 4.1 in. and 2 in., and 4.3 in and 1.8 in., for south and north shear tests, respectively. Strains-shear relationships at west and east sides of the section in south shear test are shown in Fig. 6.30(a) and Fig. 6.30(b), respectively. Strains-shear relationships at west and east sides of the section in north shear test are shown in Fig. 6.31(a) and Fig. 6.31(b), respectively.

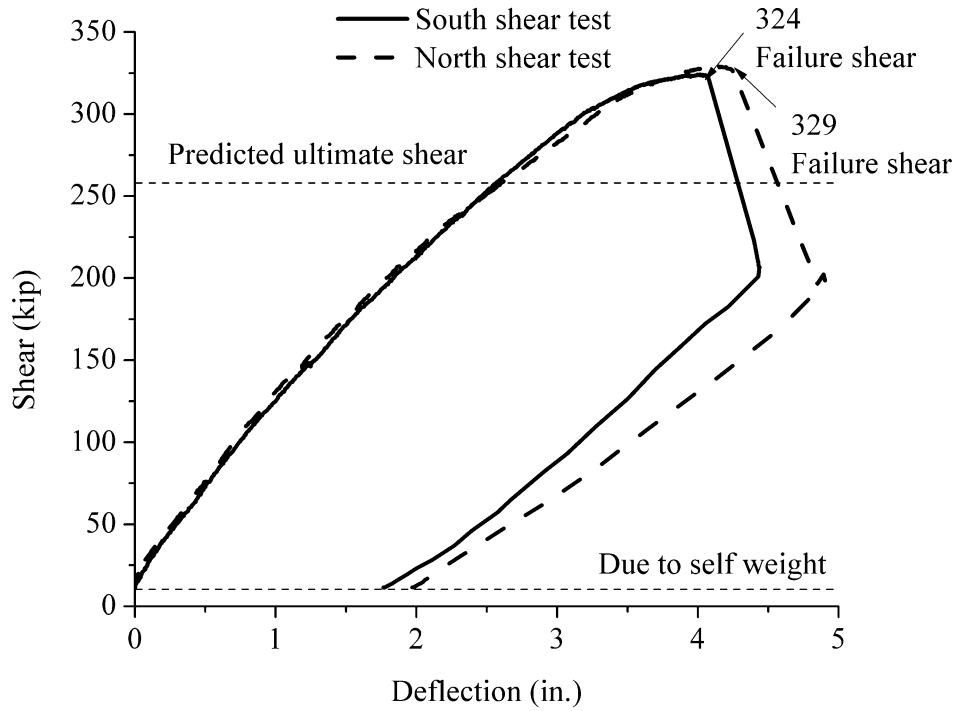

Fig. 6.28 – Shear-Deflection Relationships in South and North Shear Tests

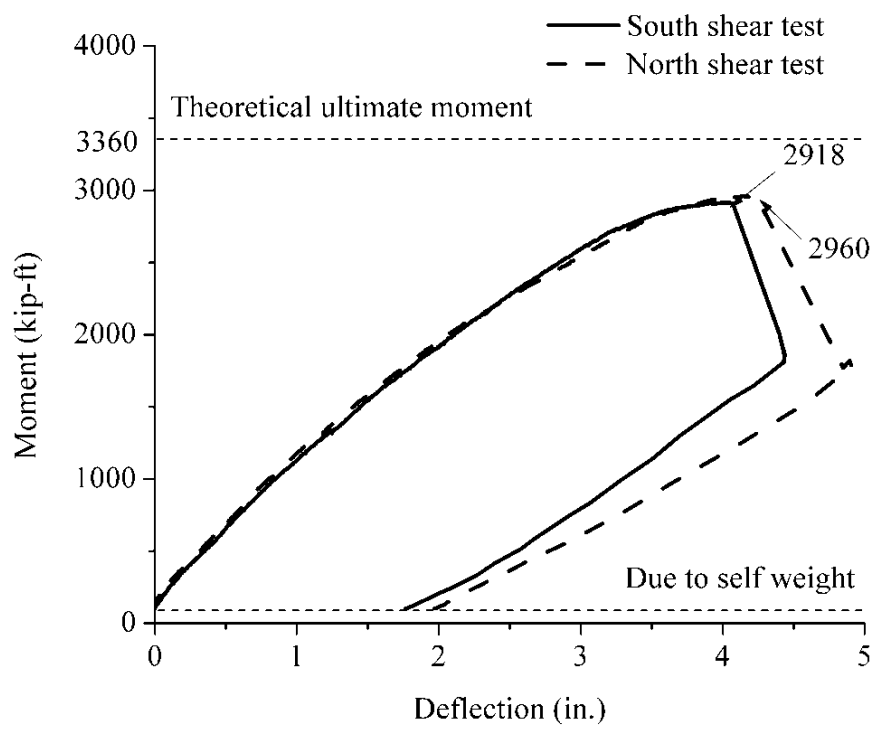

Fig. 6.29 –Moment-Deflection Relationships in South and North Shear Tests

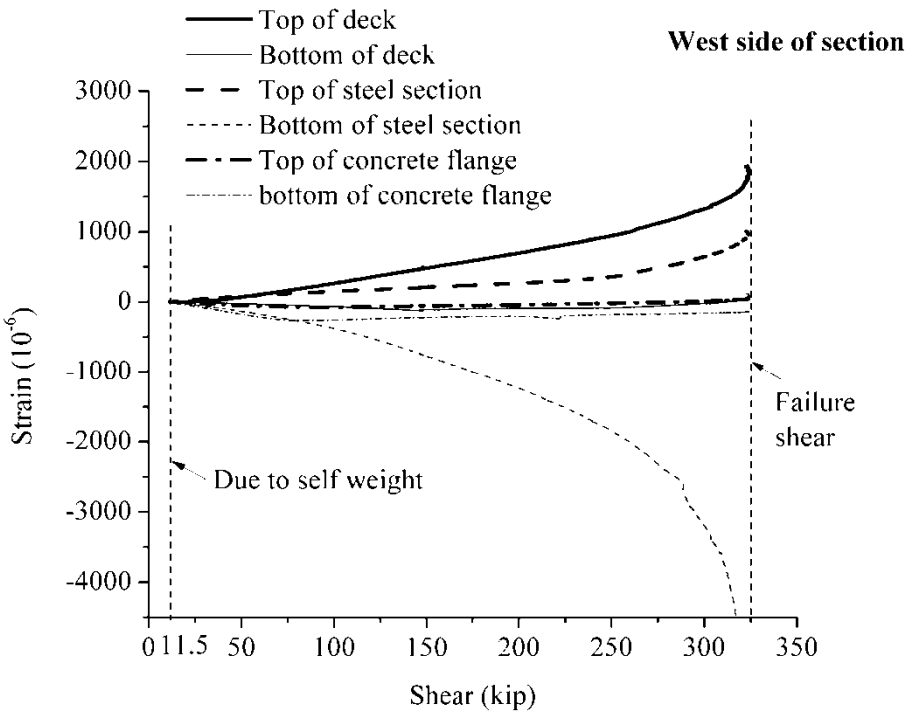

(a) West Side of Section

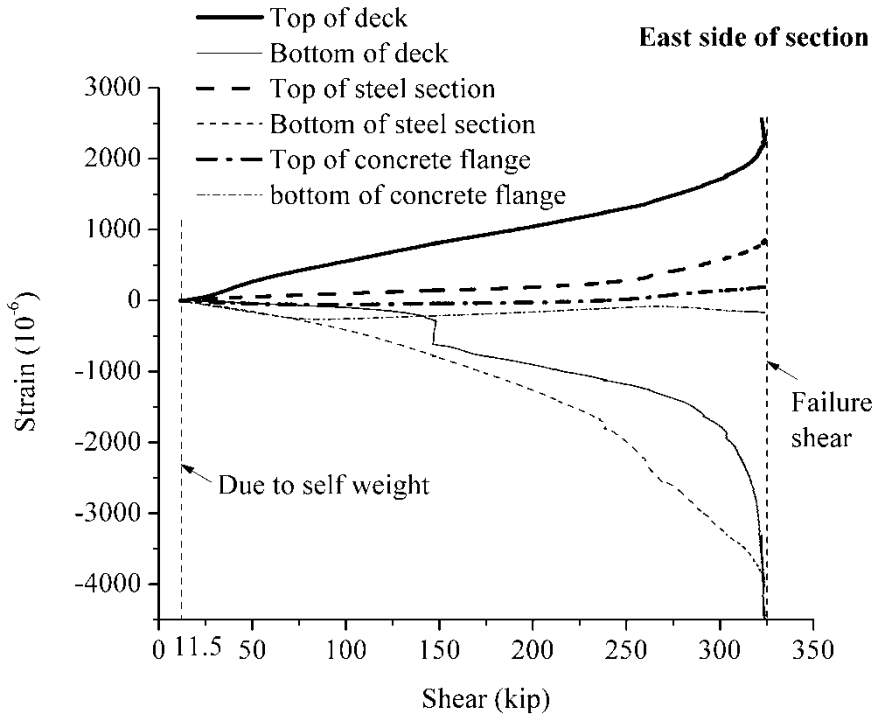

(b) East Side of Section

Fig. 6.30 – Strains-Shear Relationships in South Shear Test

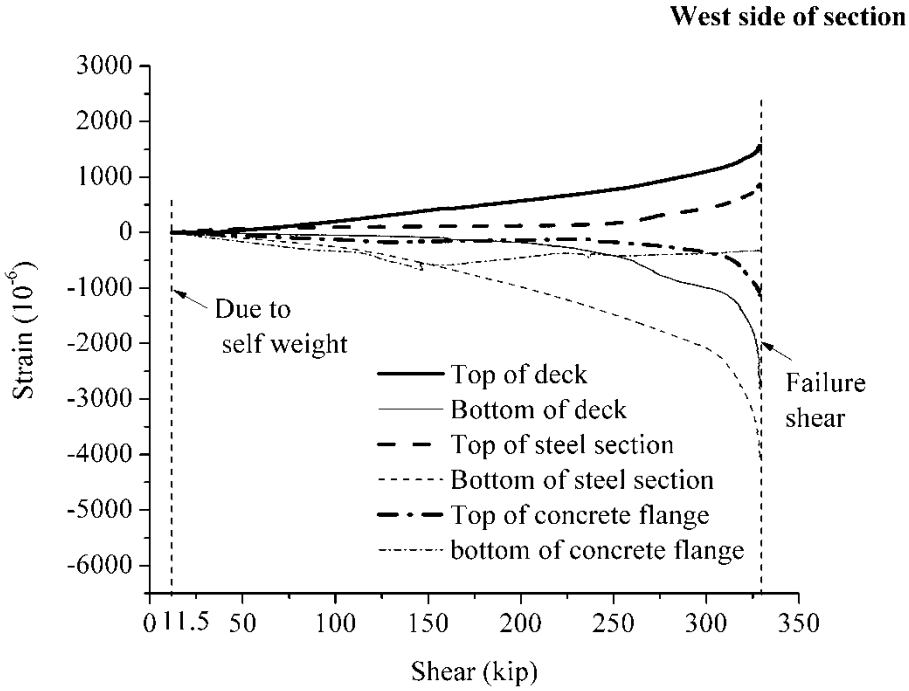

(a) West Side of Section

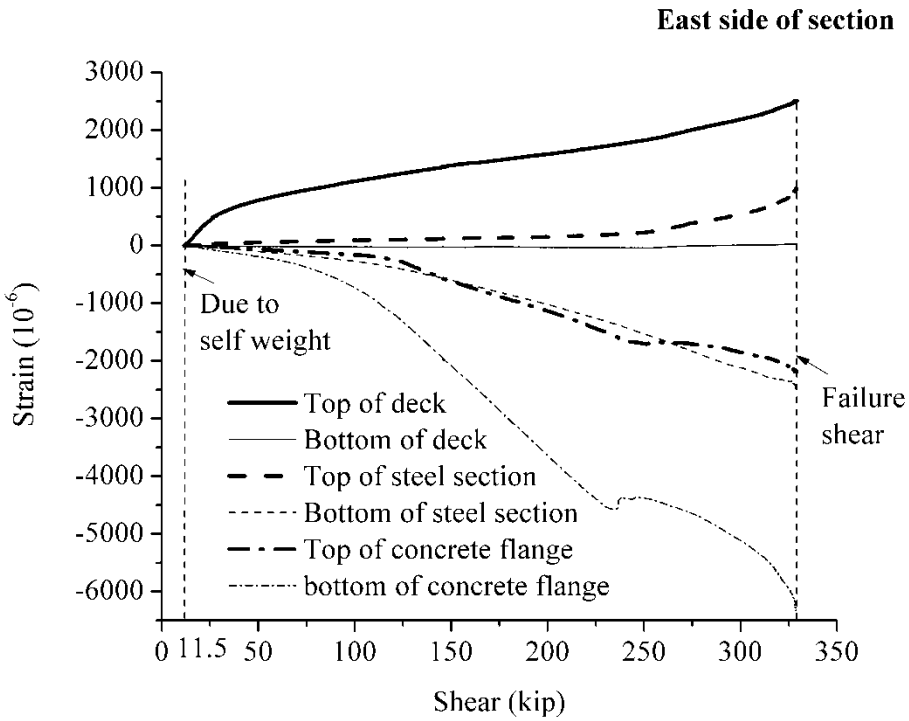

(b) East Side of Section

Fig. 6.31 – Strains-Shear relationships in North Shear Test

The relationships of slip of strands and shear at the sections under loading in south and north shear tests are shown in Fig. 6.32(a) and Fig. 6.32(b), respectively. The slips before reaching the failure shear are less than 0.01 and 0.05 in. in south and north shear tests, respectively. The slips after reaching the failure shear are less than 0.05 and 0.04 in. in south and north shear tests, respectively. In sum, no significant slip of strands was found during the shear tests.

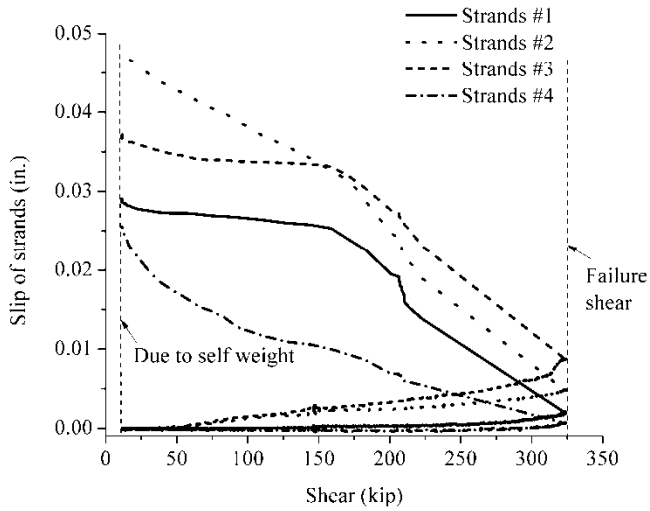

(a) South Shear Test

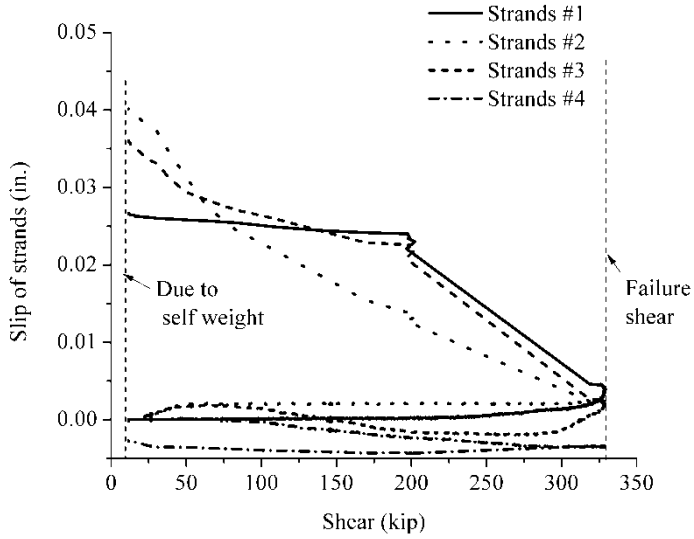

(b) North Shear Test

Fig. 6.32 – Relationships of Slips of Strands and Shear at Sections under Loading

The flexure cracks in concrete bottom flange also started to occur at the crack moment for both south and north shear tests. Vertical flexure cracks in concrete bottom flange under the loading point, spaced almost at the same spacing, was found in south shear test, is shown in Fig. 6.33(a). Inclined flexure shear cracks were also found in concrete bottom flange close to the support as shown in Fig. 6.33(b). The same crack pattern was found in the north shear test.

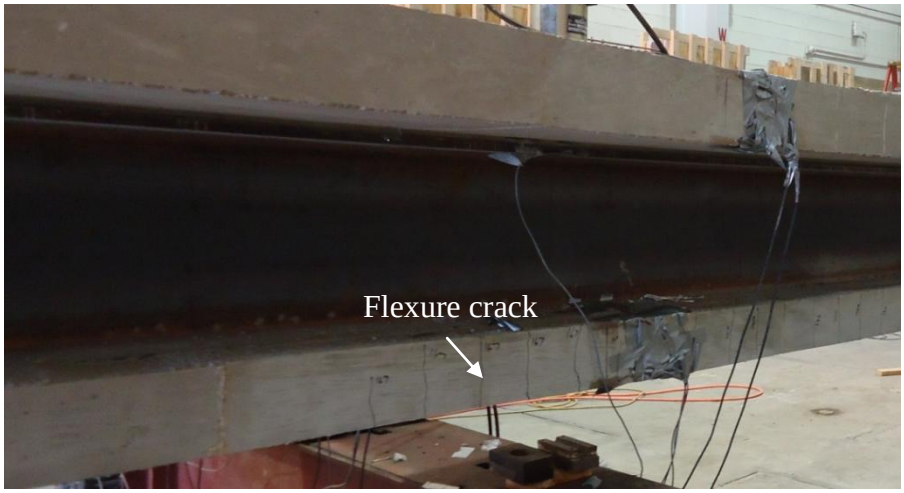

(a) Flexure Cracks

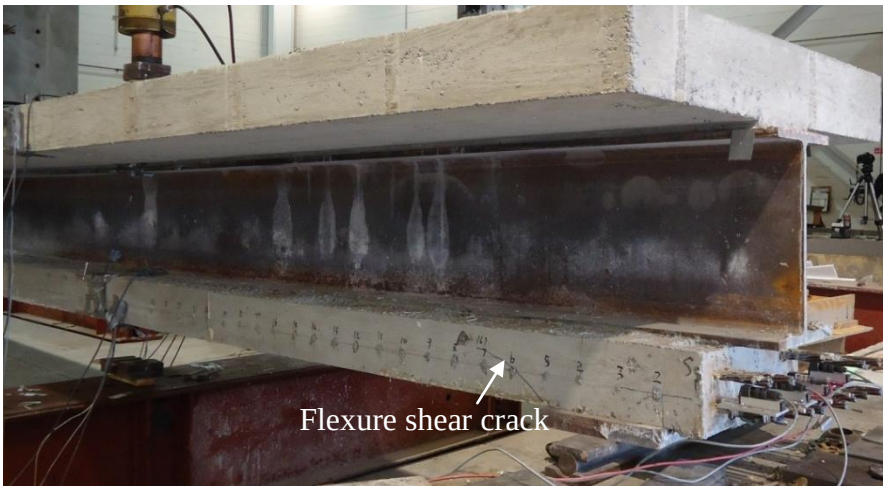

(b) Flexure Shear Cracks

Fig. 6.33 – Cracks at Crack Moment in South Shear Test

The specimen suddenly failed at failure shear and shear failure in the specimen in south and north shear tests are shown in Fig. 6.34(a) and Fig. 6.34(b), respectively. As shown in Fig. 6.34, flexure shear crack extended from concrete bottom flange near support to the top deck, and a significant diagonal shear crack formed in the top deck and rebar was buckled. Shear failures in the top of deck in south and north shear tests are shown in Fig. 6.35(a) and Fig. 6.35(b), respectively. As shown in Fig. 6.35, crushing of concrete was found in the top of deck. It can be concluded that the type of failure is the shear-compression failure. Shear failure in steel beam in south and north shear tests are shown in Fig. 6.36(a) and Fig. 6.36(b), respectively. As shown in Fig. 6.35, buckling was found in both the flange and the web.

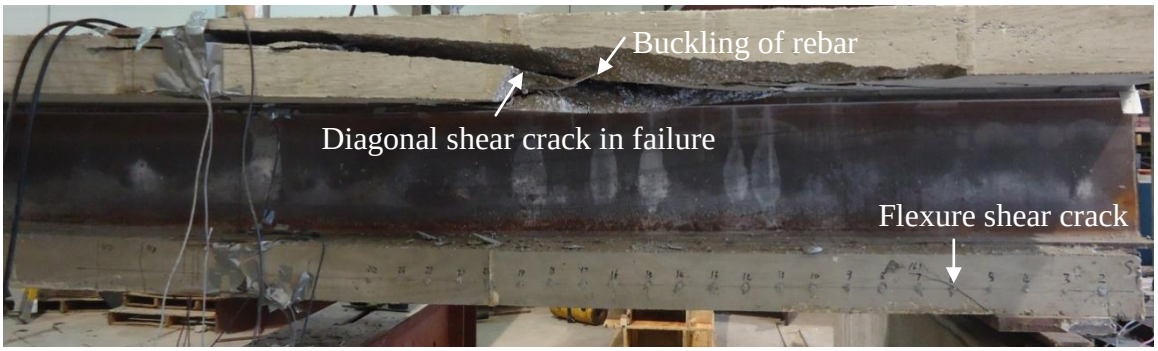

(a) South Shear Test

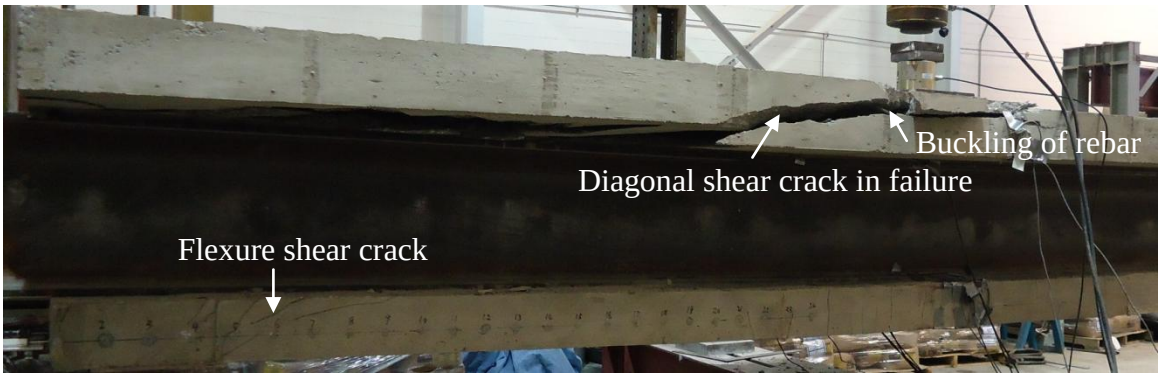

(b) North Shear Test

Fig. 6.34 – Shear Failure in the Specimen

(c)Top of Deck in South Shear Test

(d) Top of Deck in North Shear Test

Fig. 6.35 – Shear Failure in the Top of Deck

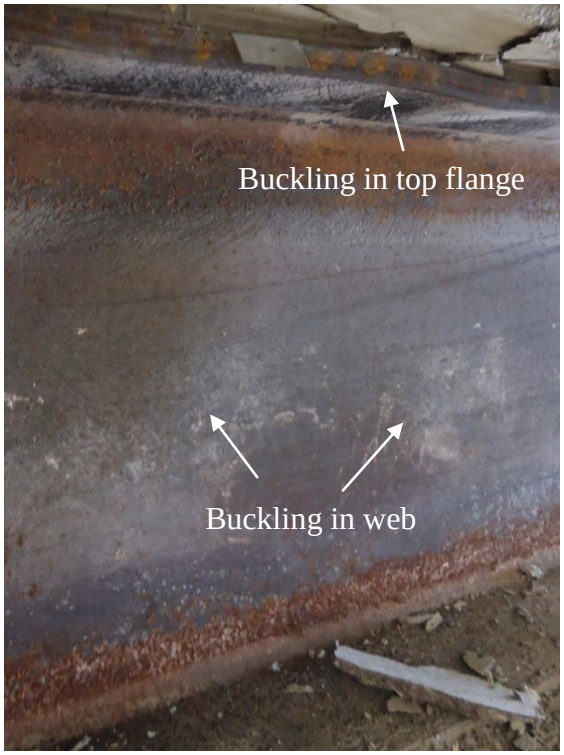

(a) South Shear Test

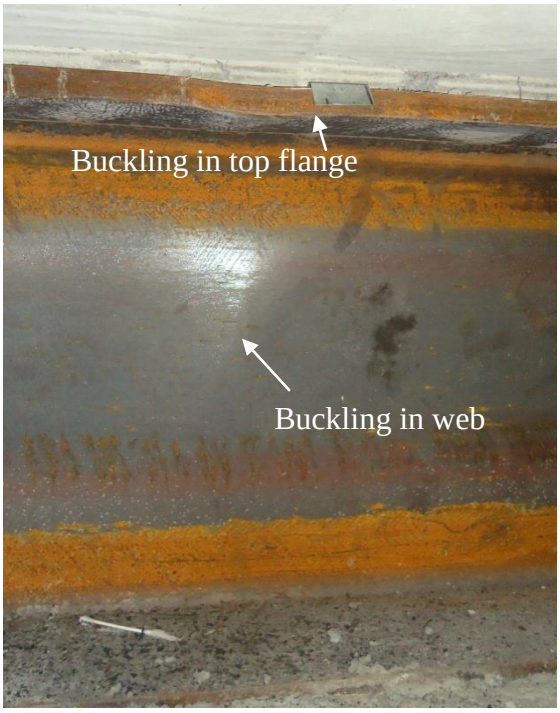

(b) North Shear Test

Fig. 6.36 – Shear Failure in Steel Beam

6.6 *Summary and Conclusions*

A PCSC girder specimen was designed using the introduced design procedures. The specimen was fabricated in the prestressing system following the proposed procedure of five steps along with measurements of strains and camber at different stages. Differences between the designed section and the as-built section encompass the depth of concrete bottom flange, the width of deck and the concrete strengths of the concrete bottom flange and concrete deck. Some conclusions can be drawn as follows:

- Proposed fabrication procedure was successfully achieved in the lab test.
- Immediately after prestress release, design calculations and FEA were validated against the strain profiles measured in sections at mid-span and 48 in. from end.
- The transfer lengths were estimated based on concrete surface strains at 7-day and 28-day monitored at south and north sides of the specimen, using a modified 95% Average Maximum Strain (AMS) method. The transfer length for 0.7 strands is over-estimated using ACI and AASHTO equations due to high concrete strength and corrosion of strands.
- Concrete surface strains at the same level of strands at 7-day were also predicted using FEA and design calculations. The adequacy of FEA is thus validated due to that strains predicted using FEA follow exactly the same order as those obtained from tests at south and north sides. Strains are not well predicted using design calculations until the locations after transfer length.
- Concrete surface strains at the same level of centroid of strands and the camber of the specimen at mid-span were continuously monitored from 7-day at release to 60-day. The initial camber at mid-span at prestress release was well predicted using design

calculations and FEA. The time histories of strains and camber predicted using Age-adjusted Elasticity Modulus Method (AEMM) compare fairly with those obtained from the tests.

- End zone cracking including vertical and inclined cracks was found at end of the specimen due to that the stirrups were placed in the concrete bottom flange at 4 in. from the ends and bearing plates with embedded studs were not used at ends.

Flexural and shear tests were conducted to evaluate the flexural and shear capacities of the fabricated specimen. Test setups for flexural and shear tests were introduced in detail, and measurements of loads, strains, deflection, slip of strands were also performed. Some conclusions can be drawn as follows:

- The crack moment in flexural test has the factor of safety, 1.06, and the ultimate moment in flexural test and ultimate shear in shear tests both have the factor of safety of around 1.9, compared to the demand of bridge girders.
- The crack moment and ultimate moment were well predicted but the deflection at crack moment was not accurately predicted.
- The concrete deck did not crush when theoretical ultimate moment was reached at mid-span section. At the crack moment, vertical flexure cracks spaced almost at the same spacing started to occur in the concrete bottom flange in the middle region of the specimen.
- The two shear tests at south and north sides of the specimen show almost identical shear- and moment-deflection relationships. Ultimate shear is underestimated by only considering the shear strength based on AASHTO LRFD Bridge Specifications

(AASHTO, 2007). The specimen failed suddenly at failure shear. The moment at failure in south and north tests are both less than the predicted ultimate moment.

- No significant slip of strands was found during the shear tests.
- Vertical flexure cracks in concrete bottom flange under the loading point, spaced almost at the same spacing, were found in south and north shear tests. Inclined flexure shear cracks were also found in concrete bottom flange close to the support.
- The specimen suddenly failed at failure shear. Flexure shear crack extended from concrete bottom flange near support to the top deck, a significant diagonal shear crack formed in the top deck and rebar was buckled. Crushing of concrete was found in the top of deck and the type of failure was the shear-compression failure. Buckling was found in both the flange and the web of the steel beam.

Chapter 7 Summary, Conclusions and Recommendations

7.1 *Summary*

In this study, a new Prestressed Concrete-Steel Composite (PCSC) girder system was introduced. The PCSC girder was composed of a pre-tensioned concrete bottom flange, a rolled steel section and reinforced concrete deck. The studs were used to connect the rolled steel section to the concrete bottom flange and later to deck creating a fully composite section. To prove its feasibility and potential, this study was conducted to investigate design and fabrication issues associated with the PCSC girder.

A design procedure was proposed using Age-adjusted Elasticity Modulus Method (AEMM) to evaluate the time-dependent stresses and strains in the PCSC girder due to creep and shrinkage effects of concrete and relaxation of strands. Design examples were presented for bridges with different spans and a design summary chart showing the maximum attainable span versus girder spacing was developed for different girder sections. The strength design method, as a rational approach replacing the current working stress method, was proposed for the design of PCSC girders at prestress release, to assist engineers to accomplish economic design and production of PCSC girders. The design equations were formulated for strength design at release using the strain compatibility approach and based on all the assumptions of the ultimate strength design of reinforced concrete members. A design procedure was proposed for applying the strength design method in an efficient and accurate manner and design examples were developed for different PCSC girder sections of bridges with different spans. Finite Element Analysis of PCSC girders at prestress release was performed to understand the transfer of the prestressing force from the strands to the composite section and stress

distribution at prestress release, and to investigate the impact of stud distribution on the stresses in the concrete bottom flange. The model included the steel beam, prestressed concrete flange including the concrete flange and prestressing strands, the bond between the concrete and strands, and shear studs between the steel beam and the concrete flange, but the stirrups were ignored. FEA predictions were compared with design calculations and then parameter studies were performed to investigate the influences of studs on the stresses in concrete bottom flange. A fabrication procedure of five steps, which was simple, convenient, and similar to that of producing prestressed concrete girders, was proposed for fabricating PCSC girders. A PCSC girder specimen was successfully fabricated in the structural lab along with test measurement following the proposed fabrication procedure of five steps. Flexural and shear tests were conducted to evaluate the flexural and shear capacities of the fabricated specimen and measurements of loads, strains, deflection, slip of strands were also performed.

7.2 *Conclusions*

The following conclusions are drawn in this study:

- The PCSC girder is a viable alternative for steel and prestressed concrete I-girders in bridges that is lightweight, economical, durable and easy to produce.
- The PCSC girder can be designed using AASHTO LRFD Bridge Specifications, Age-adjusted Elasticity Modulus Method (AEMM) for Service III, and strength design method at release. Service III design is always dominant over other design considerations due to the significant tensile stress generated in the concrete bottom flange due to the effects of creep and shrinkage.

- The proposed PCSC girder fabrication procedure is simple and follows the standard procedure of fabricating prestressed concrete girders without the need for specialized equipment, materials, or forms.
- The amount and distribution of shear studs have no significant influences on the stresses in the concrete bottom flange as long as the required amount of studs is determined according to AASHTO LRFD Bridge specifications.
- Stresses and strains in concrete and steel sections and camber at mid-span of the PCSC girder can be accurately predicted using design calculations and FEA.
- The crack moment and ultimate moment of the PCSC girder can be accurately predicted using design calculations.
- The ultimate shear of the PCSC girder is underestimated by only considering shear strength of the steel beam based on AASHTO LRFD Bridge Specifications.

7.3 *Recommendations*

The recommendations for future studies of PCSC girders are suggested as follows:

- In order to avoid end zone crack in concrete bottom flange, confinement stirrups in concrete bottom flange should be well designed at the ends and bearing plates with embedded studs should be used at ends.
- Experimental tests should be conducted to investigate fatigue strength of PCSC girders.
- Girder continuity detail can be further designed for PCSC girders applied in bridges with continuous spans. Their structural performance should be well studied experimentally and analytically.

- Curved and non-prismatic PCSC girders need to be investigated.

References

American Association of State Highway and Transportation Officials (AASHTO). (2007). *AASHTO LRFD Bridge Design Specifications, 4th Edition with 2008 Interim Revisions*, Washington, DC.

American Concrete Institute (ACI) Committee 318. (2011). *Building Code Requirements for Structural Concrete (ACI 318-11) and Commentary (ACI 318R-11)*, Farmington Hills, MI, 503 pp.

American Institute of Steel Construction (AISC). (2010). *Load and resistance factor design specification for structural steel buildings*, Chicago.

ANSYS. Release 11.0 Documentation for ANSYS, ANSYS help, 2009.

Badie S. S., Tadros M. K., Kakish H. F., Splittgerber D. L., and Baishya M. C. (2002). "Large shear studs for composite action in steel bridge girders." *Journal of Bridge Engineering*, 7(3), 195-203.

Balázs, GL (1992). "Transfer control of prestressing strands." *PCI journal*, 37(6), 60–71.

Basu, P. K., Sharif, A. M., and Ahmed, N. U. (1987a). "Partially Prestressed Composite Beams. I." *Journal of Structural Engineering*, ASCE, 113(9), 1909-1925.

Basu, P. K., Sharif, A. M., and Ahmed, N. U. (1987b). "Partially Prestressed Composite Beams. II." *Journal of Structural Engineering*, ASCE, 113(9), 1926-1938.

Bonenfant, R. R. JR. (2009). "How to Estimate the Cost of Structural Steel." *Estimating Today*, January 09, 15-23.

Bozzo L. M. and Torres L. (2004) "A proposed semi-prefabricated prestressed composite steel–concrete slab." Proceedings of the Institution of Civil Engineers, *Structures and Buildings*, 157(5), 309-318.

Carroll, J. C. (2009). Grade 300 Prestressing Strand and the Effect of Vertical Casting Position. *PhD thesis*, Virginia Polytechnic Institute and State University, Blacksburg, Virginia.

Chen S. (2005). "Experimental study of prestressed steel–concrete composite beams with external tendons for negative moments." *Journal of Constructional Steel Research*, 61(12), 1613-1630.

Chen S. and Gu P. (2005) "Load carrying capacity of composite beams prestressed with external tendons under positive moment." *Journal of Constructional Steel Research*, 61(4), 515-530.

Chen S., Wang X. and Jia Y. (2009) "A comparative study of continuous steel–concrete composite beams prestressed with external tendons: Experimental investigation." *Journal of Constructional Steel Research*, 65(7), 1480-1489.

Ding Y., Jiang K., and Liu Y. (2012). "Nonlinear analysis for PC box-girder with corrugated steel webs under pure torsion." *Thin-Walled Structures*, 51, 167-173.

Fédération Internationale du Béton, fib CEB-FIP (2001). *Model Code for Concrete Structures*, Vol. 1.

Florida Department of Transportation (FDOT). (2012). *FDOT Structures Manual, Volume 2, Structures Design Guidelines, Topic No. 625-020-018*, Tallahassee, Florida.

fib-CEB-FIP (1999). Structural concrete. Bull, fib 1999, 1(1), 244.

Gattesco N. (1999). "Analytical modeling of nonlinear behavior of composite beams with deformable connection." *Journal of Constructional Steel Research*, 52, 195-218.

Ghali A., Favre R., and Elbadry M. (2012). *Concrete Structures: Stresses and Deformations (4rd edn)*. Spon Press: London and New York, 646pp.

Hanswille I.G. (2011). “Composite bridges in Germany – State of the Art.” *Workshop on Eurocode 4-2, Composite Bridges*, Stockholm, March 17th.

Hatami, A., Morcous, G., Hanna, K., Tadros, M. K. (2011) “Evaluating the Bond of 0.7 in. Diameter Prestressing Stands for Concrete Bridge Girders.” *Proceedings of the 2011 Annual Meeting of Transportation Research Board*.

Huang L., Hikosaka H., and Komine K. (2004). “Simulation of accordion effect in corrugated steel web with concrete flanges.” *Computers and Structures*, 82, 2061-2069.

Jung K., Yi J. and Kim J.J. (2010). “Structural safety and serviceability evaluations of prestressed concrete hybrid bridge girders with corrugated or steel truss web members.” *Engineering Structures*, 32(12), 3866-3878.

Jung K., Kim K., Sim C., and Kim J.J. (2011). “Verification of Incremental Launching Construction Safety for the Ilsun Bridge: the World’s Longest and Widest Prestressed Concrete Box Girder with Corrugated Steel Web Section.” *Journal of Bridge Engineering*, 16(3), 453-460.

Kim K.S., Lee D.H., Choi S.M., Choi Y.H., and Jung S.H. (2011). “Flexural behavior of prestressed composite beams with corrugated web: Part I. Development and analysis.” *Composites: Part B*, 42, 1603-1616.

Kim K.S. and Lee D.H. (2011). “Flexural behavior of prestressed composite beams with corrugated web: Part II. Experiment and verification.” *Composites: Part B*, 42, 1617-1629.

Kose, M. M., and Burkett W. R. (2005). “Evaluation of code requirement for 0.6 in. (15 mm) prestressing strand.” *ACI Structural Journal*, 3, 422-428.

Lam D. and El-Lobody E. (2005). “Behavior of Headed Stud Shear Connectors in Composite Beam.” *Journal of Structural Engineering*, 131(1), 96-107.

Lorenc W. and Kubica E. (2006). “Behavior of composite beams prestressed with external tendons: Experimental study.” *Journal of Constructional Steel Research*, 62(12), 1353-1366.

Morano, G.S., and Mannini, C. (2006). ‘‘Preflex Beams: A Method of Calculation of Creep and Shrinkage Effects.’’ *Journal of Bridge Engineering*, 21(1), 48-58.

Morcous, G., Hanna K., and Tadros M. K. (2011). “Impact of 0.7 Inch Diameter Strands on NU I-Girders.” *Final Report to Nebraska Department of Roads (NDOR), No. SPR-1(08) P311*, University of Nebraska Lincoln, Omaha, NE.

Nilson, A.H., Darwin D and C.W. Dolan. (2010). *Design of Concrete Structures, 14th* edition. McGraw-Hill Higher Education, New York.

Noppakunwijai P., Al-Omaishi N., Tadros M. K., Krause G. L. (2002). “Elimination of Prestressed Concrete Compression Limits at Service Load.” *PCI Journal*, 47(6), 2-19.

Noppakunwijai, P., Tadros, M. K., Ma, Z., and Mast, R. F. (2001). “Strength Design of Pretensioned Flexural Concrete Members at Prestress Transfer.” *PCI Journal*, 46(1), 34-52.

Noppakunwijai, P., Tadros, M. K., and Sun, C. (2003). “Application of the Strength Design Method for Flexural Members at Prestress Transfer.” *PCI Journal*, 48(5), 62-75.

Ollgard, J. G., Slutter, R. G., and Fischer, J. W. (1971). “Shear strength of stud connectors in lightweight and normal concrete.” *AISC Engineering Journal*, 8, 55-64.

Oswald, U. (2009). *The Cubic Equation*, www.ursoswald.ch/download/CUBIC.pdf, 8 pp.

Patzlaff, Q., Morcous, G., Hanna, K., and Tadros, M. K. (2009) "Transfer and Development of 0.7 inch Strands in Precast/Prestressed Concrete Bridge Girders." *PCI National Bridge Conference*, San Antonio, TX, Sept.

Portela G., Barajas U., and Albarran-Garcia J.A. (2011). "Analysis and Load Rating of Pre-flex Composite Beams." *Engineer Research and Development Center*, Vicksburg, MS. Geotechnical and Structures Lab.

Pozolo, A. M. (2010). Transfer and Development Lengths of Steel Strands in Full-Scale Prestressed Self-Consolidating Concrete Bridge Girders. *Master's thesis*, University of Illinois at Urbana-Champaign, Urbana, Chicago.

Precast/Prestressed Concrete Institute (PCI) Industry Handbook Committee. (2010). *PCI Design Handbook – Precast/Prestressed Concrete, 7th Edition,* Chicago, IL, 804 pp.

Precst/Prestressed Concrete institute (PCI). (2011*). Precast Prestressed Concrete Bridge Design Manual, Third Edition, First Release,* Chicago, IL.

Queiroz F.D., Vellasco P.C.G.S., Nethercot D.A. (2007). "Finite element modeling of composite beams with full and partial shear connection." *Journal of Constructional Steel Research*, 63(4), 505-521.

Saadatmanesh H, Albrecht P. and Ayyub B.M. (1989a) "Experimental study of prestressed composite beams." *Journal of Structural Engineering*, 115(9), 2348–2363.

Saadatmanesh H, Albrecht P and Ayyub BM. (1989b). "Analytical study of prestressed composite beams." *Journal of Structural Engineering*, 115(9), 2364-81.

Staquet S, Espion B., and Toutlemonde F. (2010). "Innovation for Railway Bridge Decks: A Prebent Steel-VHPC Beam." *Structural Engineering International*, 20(2), 134-137(4).

Staquet, S., Rigot, G., Detandt, H. and Espion, B. (2004). “Innovative composite precast precambered U-shaped concrete deck for Belgium’s high speed railway trains”, *PCI Journal*, 49(6), 94-113.

Staquet S, and Toutlemonde F. (2007). “Test up to ultimate limit state and failure of innovative prebended steel-VHPC beams for railway bridges decks.” *Proceedings of the 6th International Conference on Fracture Mechanics of Concrete and Concrete Structures FRAMCOS-6*, Catania, Italy, 929-937.

Toutlemonde F. and Staquet S. (2007). “Fatigue Response of VHPC for Innovative Composite Pre-bended Beams in Railway Bridges.” *Concrete under Severe Conditions: Environment & Loading, CONSEC’07 Tours*, France, 1181-1190.

United States Department of Transportation – Federal Highway Administration (FHWA). (2011). *National Bridge Inventory (NBI) – Count of Bridges by Structure Type*. http://www.fhwa.dot.gov/bridge/struct.cfm.

Wee T. H., Chin M. S., and Mansur M. A. (1996). “Stress-Strain Relationship of High-Strength Concrete in Compression.” *Journal of Materials in Civil Engineering*, 8(70), 70-76.

Willam, K. J. and Warnke E. D. (1975). “Constitutive Model for the Triaxial Behavior of Concrete.” *Proceedings, International Association for Bridge and Structural Engineering*, 19, 1-30.

Yazeed Z. and Ahmed S. (2001) “Behaviour of steel and (or) composite girders with corrugated steel webs.” *Canadian Journal of Civil Engineering*, 28(4), 656-672.

Table of Contents for Appendices

Appendix A – Design Example of the PCSC-36 Girder for a Bridge 174

A.1 Calculations of Properties, Loads and Coefficients.....174

A.1.1 Section Properties and Materials 175

A.1.2 Calculating Loads.....177

A.1.3 Relaxation of Strands, Creep Coefficient, Shrinkage and Aging Coefficient ..178

A.2 Girder design 185

A.2.1 Service Strength Design.....185

A.2.2 Ultimate Strength Design.....206

A.2.3 Horizontal Shear Design 209

A.3 Deck Design.....211

A.4 Deflection Criteria.....211

Appendix B – Strength Design Example of the PCSC-36 Girder at Release 213

B.1 Strength Design at Release 214

B.2 Service Design at Release.....220

Appendix A – Design Example of the PCSC-36 Girder for a Bridge

A.1 Calculations of Properties, Loads and Coefficients

An 80 ft long simple span bridge has a width of 38′8″ and is composed of five girders with the center-to-center spacing of 8 ft and 7 in thick deck. For the PCSC girder, the concrete bottom flange has dimension of 24″×6.5″, and 18-0.7″ diameter strands, and the steel beam has the W30×90 rolled section.

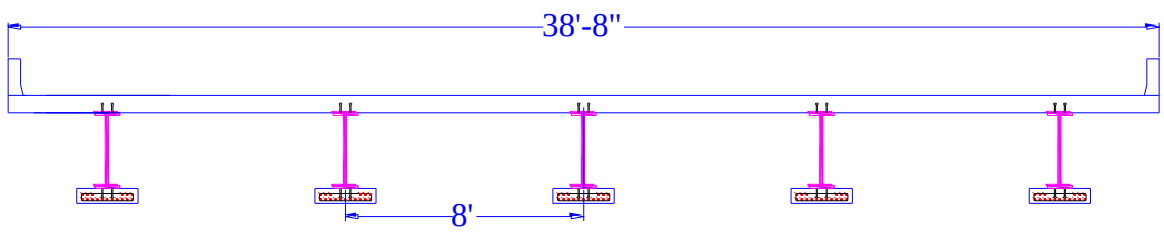

Cross-section of the Bridge

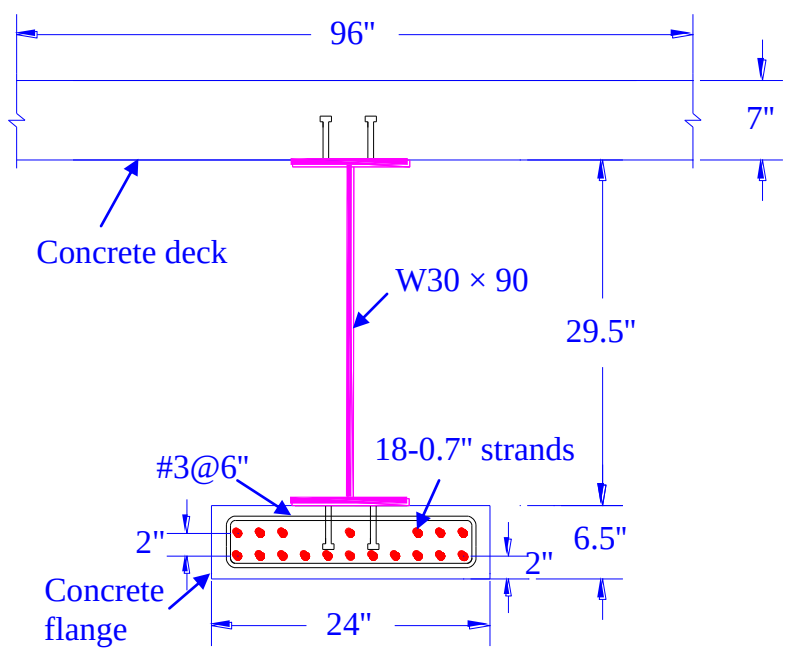

Cross-section of PCSC Girder (PCSC-36)

A.1.1 Section Properties and Materials

Steel beam

Yielding strength: $f_y := 50ksi$

Modulus of elasticity: $E_s := 29000ksi$

Moment of inertia: $I_{sg} := 3610 \cdot in^4$

Area of cross-section: $A_{sg} := 26.4 \cdot in^2$

Depth: $h_s := 29.5in$

Width of flange: $b_f := 10.4in$

Thickness of web: $t_w := 0.47 \cdot in$

Thickness of flange: $t_f := 0.61in$

Strands

$E_{ps} := 28800 \cdot ksi$

Area of cross-section of one strand: $A_s := 0.294 \cdot in^2$

Bottom layer of strands: $n_1 := 11$

Top layer of strands: $n_2 := 7$

Total strands: $n_{str} := n_1 + n_2 = 18$

Total area of strands: $A_{ps} := n_{str} \cdot A_s = 5.292 \cdot in^2$

Strands: $y_{ps} := \dfrac{n_1 \cdot 2 \cdot in + n_2 \cdot 4 \cdot in}{n_{str}} = 2.778 \cdot in$

Momoent of inertia of stands: $I_{ps} := n_1 \cdot A_s \cdot (2in - y_{ps})^2 + n_2 \cdot A_s \cdot (4in - y_{ps})^2 = 5 \cdot in^4$

Concrete bottom flange

Concrete strength: at release (girder): $f'_{c.i} := 8ksi$

28-day (girder): $f'_c := 10 \cdot ksi$

$E_{ci} := 33000 \cdot (0.15)^{1.5} ksi \cdot \dfrac{(f'_{c.i})^{0.5}}{ksi^{0.5}} = 5422 \cdot ksi$

$E_c := 33000 \cdot (0.15)^{1.5} ksi \cdot \dfrac{(f'_c)^{0.5}}{ksi^{0.5}} = 6062 \cdot ks$

$n_{si} := \dfrac{E_s}{E_{ci}} = 5.348$

$n_s := \dfrac{E_s}{E_c} = 4.784$

$n_{psi} := \dfrac{E_{ps}}{E_{ci}} - 1 = 4.311$

$n_{ps} := \dfrac{E_{ps}}{E_c} - 1 = 3.751$

Width of flange: $b_c := 24in$

Depth of flange: $h_c := 6.5in$

Moment of inertia: $I_c := \dfrac{1}{12} \cdot b_c \cdot h_c^3 = 549.25 \cdot in^4$

Net Area of cross-section: $A_c := b_c \cdot h_c = 156 \cdot in^2$

Composite girder

Depth: $h_g := h_c + h_s = 36 \cdot in$

Centroidal distance to bottom fiber: Steel beam: $y_{sg} := \frac{h_s}{2} + h_c$

Concrete bottom flange: $y_c := h_c \cdot 0.5 = 3.25 \cdot in$

Strands: $y_{ps} = 2.778 \cdot in$

Transformed area: At release: $A_{gi} := A_c + n_{si} \cdot A_{sg} + n_{psi} \cdot A_{ps} = 320 \cdot in^2$

At final: $A_g := A_c + n_s \cdot A_{sg} + n_{ps} \cdot A_{ps} = 302.1 \cdot in^2$

Neutral axis: At release: Bottom: $y_{gbi} := \frac{\left(n_{si} \cdot A_{sg} \cdot y_{sg} + A_c \cdot y_c + n_{psi} \cdot A_{ps} \cdot y_{ps}\right)}{A_{gi}} = 11.158 \cdot in$

Top: $y_{gti} := h_g - y_{gbi} = 24.842 \cdot in$

At Final: Bottom: $y_{gb} := \frac{\left(n_s \cdot A_{sg} \cdot y_{sg} + A_c \cdot y_c + n_{ps} \cdot A_{ps} \cdot y_{ps}\right)}{A_g} = 10.743 \cdot in$

Top: $y_{gt} := h_g - y_{gb} = 25.257 \cdot in$

Eccentricity of strands: $e_{mi} := y_{gbi} - y_{ps} = 8.38 \cdot in$ $e_m := y_{gb} - y_{ps} = 7.965 \cdot in$

Moment of inertia:

At release:

$$I_{gi} := n_{si} \cdot I_{sg} + n_{si} \cdot A_{sg} \cdot \left(y_{gbi} - y_{sg}\right)^2 + I_c + A_c \cdot \left(y_{gbi} - y_c\right)^2 + n_{psi} \cdot I_{ps} + n_{psi} \cdot A_{ps} \cdot \left(y_{gbi} - y_{ps}\right)^2 = 45620 \cdot in^4$$

At final:

$$I_g := n_s \cdot I_{sg} + n_s \cdot A_{sg} \cdot \left(y_{gb} - y_{sg}\right)^2 + I_c + A_c \cdot \left(y_{gb} - y_c\right)^2 + n_{ps} \cdot I_{ps} + n_{ps} \cdot A_{ps} \cdot \left(y_{gb} - y_{ps}\right)^2 = 41800 \cdot in^4$$

Composite section with slab

3-day Concrete strength (slab): $f'_{c.slab.i} := 0.75 \cdot 4ksi = 3 \cdot ksi$

$$E_{c.slab.i} := 33000 \cdot (0.15)^{1.5} ksi \cdot \frac{\left(f'_{c.slab.i}\right)^{0.5}}{ksi^{0.5}} = 3321 \cdot ksi$$

28-day Concrete strength (slab): $f'_{c.slab} := 4 \cdot ksi$

$$E_{c.slab} := 33000 \cdot (0.15)^{1.5} ksi \cdot \frac{\left(f'_{c.slab}\right)^{0.5}}{ksi^{0.5}} = 3834 \cdot ksi \qquad n_c := \frac{E_{c.slab}}{E_c} = 0.632$$

Depth of slab: $d_{slab} := 7 \cdot in$ Depth of haunch: $haunch_t := 1 \cdot in$

$span := 80 \cdot ft$ $gird_{spacing} := 96in$ $b_{eff} := gird_{spacing} = 96 \cdot in$

Total depth: $h_{comp} := h_c + h_s + haunch_t + d_{slab} = 44 \cdot in$

Area of slab: $A_d := d_{slab} \cdot gird_{spacing} = 672 \cdot in^2$

Area of composite section: $A_{comp} := A_g + n_c \cdot A_d = 727.1 \cdot in^2$

Moment of inertia of slab: $I_d := \left(\frac{1}{12}\right) \cdot d_{slab}^3 \cdot gird_{spacing} = 2744 \cdot in^4$

$h_{gt} := h_g + haunch_t = 37 \cdot in$

Neutral axis:

Bottom: $$y_{comp.b} := \frac{\left[A_g \cdot y_{gb} + n_c \cdot A_d \cdot \left(h_{gt} + \frac{d_{slab}}{2}\right)\right]}{\left(A_g + n_c \cdot A_d\right)} = 28.14 \cdot in$$

Top: $y_{comp.t} := h_{comp} - y_{comp.b} = 15.86 \cdot in$

Eccentricity of strands: $e_{comp.m} := y_{comp.b} - y_{ps} = 25.358 \cdot in$

Moment of inertia:

$$I_{comp} := I_g + A_g \cdot \left(y_{comp.b} - y_{gb}\right)^2 + n_c \cdot I_d + n_c \cdot A_d \cdot \left(h_{gt} + \frac{d_{slab}}{2} - y_{comp.b}\right)^2 = 199910 \cdot in^4$$

A.1.2 Calculating Loads

Self weight and dead loads

Weight Density of Concrete: $conc := 0.150 \cdot \frac{kip}{ft^3}$

Steel beam: $w_{steel} := 0.090klf$

Concrete flange: $w_c := A_c \cdot conc = 0.162 \cdot klf$

$w_{ow} := w_{steel} + w_c = 0.252 \cdot klf$

Haunch: $w_{haunch} := haunch_t \cdot b_f \cdot conc = 0.0108 \cdot klf$

Wearing surface:

$w_{ws} := 0.02 \cdot ksf \cdot gird_{spacing} = 0.16 \cdot klf$

Barrier:

Use NU 29" Rail: $w_{bar.1} := 0.382klf$

Assume 2 barriers and 5 girders: $w_{bar} := w_{bar.1} \cdot \frac{2}{5} = 0.153 \cdot klf$

Slab: $w_{slab} := d_{slab} \cdot gird_{spacing} \cdot conc = 0.7 \cdot klf$

Moment at mid-span:

Composite section: $M_g := \frac{w_{ow} \cdot span^2}{8} = 202 \cdot ft \cdot kip$

Slab: $M_{slab} := \frac{w_{slab} \cdot span^2}{8} = 560 \cdot ft \cdot kip$

Barrier: $M_{bar} := \frac{w_{bar} \cdot span^2}{8} = 122.24 \cdot ft \cdot kip$

Haunch: $M_{haunch} := \frac{w_{haunch} \cdot span^2}{8} = 8.667 \cdot ft \cdot kip$

Wearing surface: $M_{ws} := \frac{w_{ws} \cdot span^2}{8} = 128 \cdot ft \cdot kip$

Live Loads:

Shear Distribution Factors:

$$VDF_{onelane} := 0.36 + \left(\frac{gird_{spacing}}{25 \cdot ft}\right) = 0.68$$

$$VDF_{twolane} := 0.2 + \left(\frac{gird_{spacing}}{12 \cdot ft}\right) - \left(\frac{gird_{spacing}}{35 \cdot ft}\right)^2 = 0.814$$

$$VDF := \max\left(VDF_{onelane}, VDF_{twolane}\right) = 0.814$$

Moment Distribution Factors

$n' := \frac{1}{n_c} = 1.581 \qquad e_{gc} := y_{gt} + haunch_t + \frac{d_{slab}}{2} = 29.757 \cdot in$

$K_g := n' \cdot \left(I_g + A_g \cdot e_{gc}^2 \right) = 489109 \cdot in^4 \qquad d_{slab} = 7 \cdot in$

$$MDF_{onelane} := 0.06 + \left(\frac{gird_{spacing}}{14 \cdot ft}\right)^{0.4} \cdot \left(\frac{gird_{spacing}}{span}\right)^{0.3} \cdot \left(\frac{K_g}{span \cdot d_{slab}^3}\right)^{0.1} = 0.477$$

$$MDF_{twolane} := 0.075 + \left(\frac{gird_{spacing}}{9.5 \cdot ft}\right)^{0.6} \cdot \left(\frac{gird_{spacing}}{span}\right)^{0.2} \cdot \left[\frac{K_g}{span \cdot \left(d_{slab}\right)^3}\right]^{0.1} = 0.667$$

$MDF := \max\left(MDF_{onelane}, MDF_{twolane}\right) = 0.667$

Live loads calculation:

$w_{lane} := 0.64 \cdot \frac{kip}{ft}$

$M_{lane} := \frac{1}{8} \cdot w_{lane} \cdot span^2 = 512 \cdot kip \cdot ft$

$x := \frac{span}{2} = 40 \cdot ft$

$M_{truck} := \frac{72 \cdot kip \cdot x \cdot [(span - x) - 4.67 \cdot ft]}{span} - 112 \cdot kip \cdot ft = 1160 \cdot kip \cdot ft$

$M_{tandem} := \frac{50 \cdot kip \cdot x \cdot (span - x - 2 \cdot ft)}{span} = 950 \cdot kip \cdot ft$

$M_{LL} := M_{lane} + 1.33 \cdot M_{truck} = 2055 \cdot kip \cdot ft$

Top Compression: *Service I:* $M_{LL.I} := MDF \cdot M_{LL} = 1371 \cdot ft \cdot kip$

Bottom Tension: *Service III:* $M_{LL.III} := 0.8 \cdot MDF \cdot M_{LL} = 1097 \cdot ft \cdot kip$

A.1.3 Relaxation of Strands, Creep Coefficient, Shrinkage and Aging Coefficient

<u>Relaxation of strands</u>

For low-relaxation strands: Transfer to deck placement: $\Delta f_{pR.1} := 1.25ksi$

Deck placement to final: $\Delta f_{pR.2} := 1.25ksi$

Creep coefficient, shrinkage and aging coefficient for Concrete flange:

(1) Interval 1: From Stage 1 at release to Stage 2 during construction ($t_{0.f}$= day 7 to $t_{1.f}$= day 30)

$t_{0.f} := 7$ $t_{1.f} := 30$ Humidity: $H := 70$

$V_f := A_c = 156 \cdot in^2$ $S_f := 2(h_c + b_c) = 61 \cdot in$

$k_{s.f} := 1.45 - \frac{0.13}{in}\left(\frac{V_f}{S_f}\right) = 1.118$ $k_{hc} := 1.56 - 0.008 \cdot H = 1$

$k_{f.f} := \frac{5}{\left(1 + \frac{f'_{c.i}}{ksi}\right)} = 0.556$ $k_{td.f} := \frac{t_{1.f} - t_{0.f}}{61 - 4 \cdot \frac{f'_{c.i}}{ksi} + t_{1.f} - t_{0.f}} = 0.442$

$k_{hs} := 2.00 - 0.014H = 1.02$ $h_{0.f} := \frac{2A_c}{2 \cdot (h_c + b_c)} = 5.1 \cdot in$

Creep coefficient: $\psi_{t0.t1.f} := 1.9 \cdot k_{s.f} \cdot k_{hc} \cdot k_{f.f} \cdot k_{td.f} \cdot t_{0.f}^{-0.118} = 0.415$

Srinkage: $\varepsilon_{t0.t1.f} := 0.00048 k_{s.f} \cdot k_{hs} \cdot k_{f.f} \cdot k_{td.f} = 0.000134$

Aging coefficient: $\chi_{t0.t1.f} := 0.82$

(2) Interval 2: From Stage 2 during construction ($t_{1.f}$= day 30) to Stage 3 in service ($t_{2.f}$= day 60)

$t_{1.f} := 30$ $t_{2.f} := 60$

$k_{td.f} := \frac{t_{2.f} - t_{1.f}}{61 - 4 \cdot \frac{f'_{c.i}}{ksi} + t_{2.f} - t_{1.f}} = 0.508$

$\psi_{t1.t2.f} := 1.9 \cdot k_{s.f} \cdot k_{hc} \cdot k_{f.f} \cdot k_{td.f} \cdot t_{1.f}^{-0.118} = 0.4$

$k_{td.f} := \frac{t_{2.f} - t_{0.f}}{61 - 4 \cdot \frac{f'_{c.i}}{ksi} + t_{2.f} - t_{0.f}} = 0.646$

$\varepsilon_{t0.t2.f} := 0.00048 k_{s.f} \cdot k_{hs} \cdot k_{f.f} \cdot k_{td.f} = 0.000196$

$\varepsilon_{t1.t2.f} := \varepsilon_{t0.t2.f} - \varepsilon_{t0.t1.f} = 0.000062$

$\chi_{t1.t2.f} := 0.89$

(3) Interval 3: From Stage 3 in service ($t_{2.f}$= day 60) to time infinity ($t_{3.f}$= 100000)

$t_{2.f} = 60 \qquad t_{3.f} := 100000$

$$k_{td.f} := \frac{t_{3.f} - t_{2.f}}{61 - 4\cdot\frac{f'_{c.i}}{ksi} + t_{3.f} - t_{2.f}} = 1$$

$$\psi_{t2.t3.f} := 1.9\cdot k_{s.f}\cdot k_{hc}\cdot k_{f.f}\cdot k_{td.f}\cdot t_{2.f}^{-0.118} = 0.73$$

$$k_{td.f} := \frac{t_{3.f} - t_{0.f}}{61 - 4\cdot\frac{f'_{c.i}}{ksi} + t_{3.f} - t_{0.f}} = 1$$

$$\varepsilon_{t0.t3.f} := 0.00048 k_{s.f}\cdot k_{hs}\cdot k_{f.f}\cdot k_{td.f} = 0.000304$$

$$\varepsilon_{t2.t3.f} := \varepsilon_{t0.t3.f} - \varepsilon_{t0.t2.f} = 0.000107$$

$$\chi_{t2.t3.f} := 0.87$$

(4) From start of Interval 1 to end of Interval 2 (from $t_{0.f}$ to $t_{2.f}$)

$t_{0.f} = 7 \qquad t_{2.f} := 60$

$$k_{td.f} := \frac{t_{2.f} - t_{0.f}}{61 - 4\cdot\frac{f'_{c.i}}{ksi} + t_{2.f} - t_{0.f}} = 0.646$$

$$\psi_{t0.t2.f} := 1.9\cdot k_{s.f}\cdot k_{hc}\cdot k_{f.f}\cdot k_{td.f}\cdot t_{0.f}^{-0.118} = 0.61$$

$$\chi_{t0.t2.f} := 0.79$$

(5) From middle of Interval 1 to end of Interval 2 [from ($t_{0.f}$+($t_{1.f}$-$t_{0.f}$)/2) to $t_{2.f}$]

$$t_{01.f} := t_{0.f} + \frac{(t_{1.f} - t_{0.f})}{2} = 18.5 \qquad t_{2.f} := 60$$

$$k_{td.f} := \left(\frac{t_{2.f} - t_{01.f}}{61 - 4\cdot\frac{f'_{c.i}}{ksi} + t_{2.f} - t_{01.f}}\right) = 0.589$$

$$\psi_{t01.t2.f} := 1.9\cdot k_{s.f}\cdot k_{hc}\cdot k_{f.f}\cdot k_{td.f}\cdot t_{01.f}^{-0.118} = 0.49$$

$$\chi_{t01.t2.f} := 0.87$$

(6) From middle of Interval 1 to end of Interval 1 [from ($t_{0.f}$+($t_{1.f}$-$t_{0.f}$)/2) to $t_{1.f}$]

$$t_{01.f} := t_{0.f} + \frac{(t_{1.f} - t_{0.f})}{2} = 18.5 \qquad t_{1.f} := 30$$

$$k_{td.f} := \frac{t_{1.f} - t_{01.f}}{61 - 4\cdot\frac{f'_{c.i}}{ksi} + t_{1.f} - t_{01.f}} = 0.284$$

$$\psi_{t01.t1.f} := 1.9\cdot k_{s.f}\cdot k_{hc}\cdot k_{f.f}\cdot k_{td.f}\cdot t_{01.f}^{-0.118} = 0.24$$

$$\chi_{t01.t1.f} := 0.89$$

(7) From start of Interval 1 to end of Interval 3 (from $t_{0.f}$ to $t_{3.f}$)

$t_{0.f} := 7$ $\quad t_{3.f} := 100000$

$$k_{td.f} := \frac{t_{3.f} - t_{0.f}}{61 - 4\cdot\frac{f'_{c.i}}{ksi} + t_{3.f} - t_{0.f}} = 1$$

$$\psi_{t0.t3.f} := 1.9\cdot k_{s.f}\cdot k_{hc}\cdot k_{f.f}\cdot k_{td.f}\cdot t_{0.f}^{-0.118} = 0.94$$

$$\chi_{t0.t3.f} := 0.697$$

(8) From middle of Interval 1 to end of Interval 3 [from ($t_{0.f}$+($t_{1.f}$-$t_{0.f}$)/2) to $t_{3.f}$]

$$t_{01.f} := t_{0.f} + \frac{(t_{1.f} - t_{0.f})}{2} = 18.5 \qquad t_{3.f} := 100000$$

$$k_{td.f} := \frac{t_{3.f} - t_{01.f}}{61 - 4\cdot\frac{f'_{c.i}}{ksi} + t_{3.f} - t_{01.f}} = 1$$

$$\psi_{t01.t3.f} := 1.9\cdot k_{s.f}\cdot k_{hc}\cdot k_{f.f}\cdot k_{td.f}\cdot t_{01.f}^{-0.118} = 0.84$$

$$\chi_{t01.t3.f} := 0.793$$

(9) From start of Interval 2 to end of Interval 3 (from $t_{1.f}$ to $t_{3.f}$)

$t_{1.f} = 30$ $\quad t_{3.f} := 100000$

$$k_{td.f} := \frac{t_{3.f} - t_{1.f}}{61 - 4\cdot\frac{f'_{c.i}}{ksi} + t_{3.f} - t_{1.f}} = 1$$

$$\psi_{t1.t3.f} := 1.9\cdot k_{s.f}\cdot k_{hc}\cdot k_{f.f}\cdot k_{td.f}\cdot t_{1.f}^{-0.118} = 0.79$$

$$\chi_{t1.t3.f} := 0.821$$

(10) From middle of Interval 2 to end of Interval 3 [from ($t_{1.f}$+($t_{2.f}$-$t_{1.f}$)/2) to $t_{3.f}$]

$$t_{12.f} := t_{1.f} + \frac{(t_{2.f} - t_{1.f})}{2} = 45 \qquad t_{3.f} := 100000$$

$$k_{td.f} := \frac{t_{3.f} - t_{12.f}}{61 - 4\cdot\frac{f'_{c.i}}{ksi} + t_{3.f} - t_{12.f}} = 1$$

$$\psi_{t12.t3.f} := 1.9\cdot k_{s.f}\cdot k_{hc}\cdot k_{f.f}\cdot k_{td.f}\cdot t_{12.f}^{-0.118} = 0.75$$

$$\chi_{t12.t3.f} := 0.845$$

(11) From middle of Interval 2 to end of Interval 2 [from ($t_{1.f}$+($t_{2.f}$-$t_{1.f}$)/2) to $t2_{.f}$]

$$t_{12.f} := t_{1.f} + \frac{(t_{2.f} - t_{1.f})}{2} = 45 \qquad t_{2.f} = 60$$

$$k_{td.f} := \frac{t_{2.f} - t_{12.f}}{61 - 4\cdot\frac{f'_{c.i}}{ksi} + t_{2.f} - t_{12.f}} = 0.341$$

$$\psi_{t12.t2.f} := 1.9\cdot k_{s.f}\cdot k_{hc}\cdot k_{f.f}\cdot k_{td.f}\cdot t_{12.f}^{-0.118} = 0.26$$

$$\chi_{t12.t2.f} := 0.845$$

Creep coefficient, shrinkage and aging coefficient for Deck

(1) From stage 2 during construction ($t_{0.d}$ = day 1) to stage 3 in service ($t_{1.d}$ = day 30)

$$t_{0.d} := 3 \qquad t_{1.d} := 30$$

$$V_d := 8ft\cdot 7in = 672\cdot in^2 \qquad S_d := 2\cdot 8ft = 192\cdot in$$

$$k_{s.d} := 1.45 - \frac{0.13}{in}\left(\frac{V_d}{S_d}\right) = 0.995 \qquad k_{hc} := 1.56 - 0.008\cdot H = 1$$

$$k_{f.d} := \frac{5}{1 + \frac{0.8\cdot f'_{c.slab}}{ksi}} = 1.19 \qquad h_{0.d} := \frac{2(8ft\cdot 7in)}{2\cdot(8ft + 7in)} = 7\cdot in$$

$$k_{td.d} := \frac{t_{1.d} - t_{0.d}}{61 - 4\cdot\frac{0.8\cdot f'_{c.i}}{ksi} + t_{1.d} - t_{0.d}} = 0.433 \qquad k_{hs} := 2.00 - 0.014H = 1.02$$

$\varepsilon_{t0.t1.d} := 0.00048 k_{s.d} \cdot k_{hs} \cdot k_{f.d} \cdot k_{td.d} = 2.509 \times 10^{-4}$

$\psi_{t0.t1.d} := 1.9 \cdot k_{s.d} \cdot k_{hc} \cdot k_{f.d} \cdot k_{td.d} \cdot t_{0.d}^{-0.118} = 0.86$

$\chi_{t0.t1.d} := 0.75$

(2) From the middle of interval 2 to time infinity ($t_{2.d}$ = 100000)

$t_{0.d} := 3$ $\quad t_{1.d} := 30$ $\quad t_{2.d} := 1000000$

$$t_{01.d} := t_{0.d} + \frac{(t_{1.d} - t_{0.d})}{2} = 16.5$$

$$k_{td.d} := \frac{t_{2.d} - t_{01.d}}{61 - 4 \cdot \frac{0.8 \cdot f'_{c.i}}{ksi} + t_{2.d} - t_{01.d}} = 1$$

$\psi_{t01.t2.d} := 1.9 \cdot k_{s.d} \cdot k_{hc} \cdot k_{f.d} \cdot k_{td.d} \cdot t_{01.d}^{-0.118} = 1.62$

$\chi_{t01.t2.d} := 0.79$

(3) From the middle of interval 2 to stage 3 in service ($t_{1.d}$ = day 30)

$t_{0.d} := 3$ $\quad t_{1.d} := 30$

$$t_{01.d} := t_{0.d} + \frac{(t_{1.d} - t_{0.d})}{2} = 16.5$$

$$k_{td.d} := \frac{t_{1.d} - t_{01.d}}{61 - 4 \cdot \frac{0.8 \cdot f'_{c.i}}{ksi} + t_{1.d} - t_{01.d}} = 0.276$$

$\psi_{t01.t1.d} := 1.9 \cdot k_{s.d} \cdot k_{hc} \cdot k_{f.d} \cdot k_{td.d} \cdot t_{01.d}^{-0.118} = 0.45$

$\chi_{t01.t1.d} := 0.79$

(4) From Stage 3 in service ($t_{1.d}$ = day 30) to time infinity ($t_{2.d}$ = 1000000)

$t_{1.d} := 30$ $\quad t_{2.d} := 1000000$

$$k_{td.d} := \frac{t_{2.d} - t_{1.d}}{61 - 4 \cdot \frac{0.8 \cdot f'_{c.i}}{ksi} + t_{2.d} - t_{1.d}} = 1$$

$\psi_{t1.t2.d} := 1.9 \cdot k_{s.d} \cdot k_{hc} \cdot k_{f.d} \cdot k_{td.d} \cdot t_{1.d}^{-0.118} = 1.51$

$$k_{td.d} := \frac{t_{2.d} - t_{0.d}}{61 - 4 \cdot \frac{0.8 \cdot f'_{c.i}}{ksi} + t_{2.d} - t_{0.d}} = 1$$

$\varepsilon_{t0.t2.d} := 0.00048 k_{s.d} \cdot k_{hs} \cdot k_{f.d} \cdot k_{td.d} = 5.799 \times 10^{-4}$

$\varepsilon_{t1.t2.d} := \varepsilon_{t0.t2.d} - \varepsilon_{t0.t1.d} = 3.29 \times 10^{-4}$

$\chi_{t1.t2.d} := 0.83$

A.2 Girder design

A.2.1 Service Strength Design

Interval 1: From Stage 1 at release to Stage 2 during construction ($t_{0.f}$ = day 7 to $t_{1.f}$ = day 30)

$t_{0.f} := 7 \qquad t_{1.f} := 30$

Moment at mid-span: $M_1 := M_g = 2424 \cdot kip \cdot in$

Jacking stress in strands: $f_{pi} := 202.5ksi$

Jacking Prestress force at release: $P_i := f_{pi} \cdot A_{ps} = 1072 \cdot kip \qquad e_{mi} = 8.38 \cdot in$

Step 1:

Stress/strain in bottom fiber of concrete flange:

$$f_{f.b.1} := \frac{P_i}{A_{gi}} + \frac{P_i \cdot e_{mi} \cdot y_{gbi}}{I_{gi}} - \frac{M_1 \cdot y_{gbi}}{I_{gi}} = 4.952 \cdot ksi \text{ Less than } 0.6 \cdot f'_{c.i} = 4.8 \cdot ksi \quad \text{NG}$$

$$\varepsilon_{f.b.1} := \frac{f_{f.b.1}}{E_{ci}} = 9.133 \times 10^{-4}$$

No compressive stress limit at prestrtess release, use strength design method at release instead.

Stress/strain in top fiber of concrete flange:

$$f_{f.t.1} := \frac{P_i}{A_{gi}} + \frac{P_i \cdot e_{mi} \cdot (y_{gbi} - h_c)}{I_{gi}} - \frac{M_1 \cdot (y_{gbi} - h_c)}{I_{gi}} = 4.02 \cdot ksi \text{ Less than } 0.6 \cdot f'_{c.i} = 4.8 \cdot ksi \quad \text{OK}$$

$$\varepsilon_{f.t.1} := \frac{f_{f.t.1}}{E_{ci}} = 7.41 \times 10^{-4}$$

Axial strain in concrete flange only due to creep and shrinkage:

$$\varepsilon_{1.f} := \frac{f_{f.b.1} + f_{f.t.1}}{2E_{ci}} \cdot \psi_{t0.t1.f} + \varepsilon_{t0.t1.f} = 4.775 \times 10^{-4}$$

Curvature in in concrete flange only due to creep and shrinkage:

$$\phi_{1.f} := \frac{f_{f.b.1} - f_{f.t.1}}{E_{ci} \cdot h_c} \cdot \psi_{t0.t1.f} = 1.099 \times 10^{-5} \cdot \frac{1}{in}$$

Strain in bottom/top fibers of concrete flange only due to creep and shrinkage: :

$$\varepsilon_{f.b.1.cs} := \varepsilon_{1.f} + \phi_{1.f} \cdot \frac{h_c}{2} = 5.132 \times 10^{-4}$$

$$\varepsilon_{f.t.1.cs} := \varepsilon_{1.f} - \phi_{1.f} \cdot \frac{h_c}{2} = 4.418 \times 10^{-4}$$

Stress/strain in bottom of steel section:

$$f_{s.b.1} := \left[\frac{P_i}{A_{gi}} + \frac{P_i \cdot e_{mi} \cdot (y_{gbi} - h_c - t_f)}{I_{gi}} - \frac{M_1 \cdot (y_{gbi} - h_c - t_f)}{I_{gi}} \right] \cdot n_s = 18.8 \cdot ksi$$

Less than $0.7f_y = 35 \cdot ksi$ OK

$$\varepsilon_{s.b.1} := \frac{f_{s.b.1}}{E_s} = 6.483 \times 10^{-4}$$

Stress/strain in top of steel section:

$$f_{s.t.1} := \left(\frac{P_i}{A_{gi}} - \frac{P_i \cdot e_{mi} \cdot y_{gti}}{I_{gi}} + \frac{M_1 \cdot y_{gti}}{I_{gi}} \right) \cdot n_s = -1.06 \cdot ksi$$

Less than $-0.7f_y = -35 \cdot ksi$ OK

$$\varepsilon_{s.t.1} := \frac{f_{s.t.1}}{E_s} = -3.655 \times 10^{-5}$$

Elastic shortening losses in strands:

$$f_{ps.1} := \left[\frac{P_i}{A_{gi}} + \frac{P_i \cdot e_{mi} \cdot (y_{gbi} - y_{ps})}{I_{gi}} - \frac{M_1 \cdot (y_{gbi} - y_{ps})}{I_{gi}} \right] \cdot n_{psi} = 19.63 \cdot ksi$$

Initial prestress immediately after prestress release:

$$f_{pe.1.0} := f_{pi} - f_{ps.1} = 182.9 \cdot ksi$$

No strain or curvature due to creep and shrinkage of steel section

Step 2:

Calculate the forces and corresponding stresses in each component that cancel the deformation in Step 1.

Age adjusted effective modulus for concrete flange:

$$E_f := E_{ci} = 5422 \cdot ksi$$

$$E'_f := \frac{E_f}{1 + \chi_{t0.t1.f} \cdot \psi_{t0.t1.f}} = 4046 \cdot ksi$$

Axial restraining force in concrete flange:

$$F_f := -E'_f \cdot A_c \cdot \varepsilon_{1.f} = -301.4 \cdot kip$$

Corresponding stress in concrete flange:

$$f_{f.i} := \frac{F_f}{A_c} = -1.932 \cdot ksi$$

Moment in concrete flange:

$$M_f := -E'_f \cdot I_c \cdot \phi_{1.f} = -24.43 \cdot in \cdot kip$$

Corresponding stress in concrete flange:

$$f_{f.b.i} := \frac{M_f \cdot y_c}{I_c} = -0.145 \cdot ksi$$

$$f_{f.t.i} := -f_{f.b.i} = 0.145 \cdot ksi$$

None for steel section.

Step 3:

$$n'_s := \frac{E_s}{E'_f} = 7.167 \qquad n'_{ps} := \frac{E_{ps}}{E'_f} = 7.117$$

Depth: $h_g := h_c + h_s = 36 \cdot in$

Centroidal distance to bottom fiber: Steel beam: $y_{sg} := \frac{h_s}{2} + h_c$

Concrete bottom flange: $y_c := h_c \cdot 0.5 = 3.25 \cdot in$

Strands: $y_{ps} = 2.778 \cdot in$

Transformed area: $A_{g.1} := A_c + n'_s \cdot A_{sg} + n'_{ps} \cdot A_{ps} = 382.87 \cdot in^2$

Neutral axis: At release: Bottom: $y_{gb.1} := \frac{\left(n'_s \cdot A_{sg} \cdot y_{sg} + A_c \cdot y_c + n'_{ps} \cdot A_{ps} \cdot y_{ps}\right)}{A_{g.1}} = 12.099 \cdot in$

Top: $y_{gt.1} := h_g - y_{gb.1} = 23.901 \cdot in$

Moment of inertia:

$$I_{g.1} := n'_s \cdot I_{sg} + n'_s \cdot A_{sg} \cdot \left(y_{gb.1} - y_{sg}\right)^2 + I_c + A_c \cdot \left(y_{gb.1} - y_c\right)^2 + n'_{ps} \cdot I_{ps} + n'_{ps} \cdot A_{ps} \cdot \left(y_{gb.1} - y_{ps}\right)^2 = 57797 \cdot in^4$$

Bottom of concrete flange:

$$f_{f.b.c} := \frac{-F_f}{A_{g.1}} + \frac{-F_f \cdot (y_{gb.1} - y_c) - M_f \cdot y_{gb.1}}{I_{g.1}} = 1.351 \cdot ksi$$

Top of concrete flange:

$$f_{f.t.c} := \frac{-F_f}{A_{g.1}} + \frac{-F_f \cdot (y_{gb.1} - y_c) - M_f \cdot (y_{gb.1} - h_c)}{I_{g.1}} = 1.048 \cdot ksi$$

Bottom of steel section:

$$f_{s.b.c} := f_{f.t.c} \cdot n'_s = 7.511 \cdot ksi$$

Top of steel section

$$f_{s.t.c} := \left[\frac{-F_f}{A_{g.1}} - \frac{-F_f \cdot (y_{gb.1} - y_c) - M_f \cdot y_{gt.1}}{I_{g.1}} \right] \cdot n'_s = -2.335 \cdot ksi$$

Strands:

$$f_{ps.c} := \left[\frac{-F_f}{A_{g.1}} + \frac{-F_f \cdot (y_{gb.1} - y_c) - M_f \cdot (y_{gb.1} - y_{ps})}{I_{g.1}} \right] \cdot n'_s = 8.753 \cdot ksi$$

Step 4:

Summation of all time-dependent stresses/strains in Step 1-3

Bottom of concrete flange:

$$\Delta f_{f.b.1} := f_{f.i} + f_{f.b.i} + f_{f.b.c} = -0.726 \cdot ksi$$

$$\Delta \varepsilon_{f.b.1} := \varepsilon_{f.b.1.cs} + \frac{\Delta f_{f.b.1}}{E'_f} = 3.338 \times 10^{-4}$$

Top of concrete flange:

$$\Delta f_{f.t.1} := f_{f.i} + f_{f.t.i} + f_{f.t.c} = -0.74 \cdot ksi$$

$$\Delta \varepsilon_{f.t.1} := \varepsilon_{f.t.1.cs} + \frac{\Delta f_{f.t.1}}{E'_f} = 2.59 \times 10^{-4}$$

Bottom of steel section:

$$\Delta f_{s.b.1} := f_{s.b.c} = 7.511 \cdot ksi$$

$$\Delta \varepsilon_{s.b.1} := \frac{\Delta f_{s.b.1}}{E_s} = 2.59 \times 10^{-4}$$

Top of steel section

$\Delta f_{s.t.1} := f_{s.t.c} = -2.335 \cdot ksi$

$\Delta \varepsilon_{s.t.1} := \frac{\Delta f_{s.t.1}}{E_s} = -8.052 \times 10^{-5}$

Losses in strands:

$\Delta f_{ps.1} := f_{ps.c} = 8.753 \cdot ksi$

Final stresses/strains just before stage 2:

Bottom of concrete flange:

$f_{f.b.1} + \Delta f_{f.b.1} = 4.226 \cdot ksi$

$\varepsilon_{f.b.1} + \Delta \varepsilon_{f.b.1} = 1.247 \times 10^{-3}$

Top of concrete flange:

$f_{f.t.1} + \Delta f_{f.t.1} = 3.279 \cdot ksi$

$\varepsilon_{f.t.1} + \Delta \varepsilon_{f.t.1} = 1 \times 10^{-3}$

Bottom of steel section:

$f_{s.b.1} + \Delta f_{s.b.1} = 26.313 \cdot ksi$

$\varepsilon_{s.b.1} + \Delta \varepsilon_{s.b.1} = 9.073 \times 10^{-4}$

Top of steel section

$f_{s.t.1} + \Delta f_{s.t.1} = -3.395 \cdot ksi$

$\varepsilon_{s.t.1} + \Delta \varepsilon_{s.t.1} = -1.171 \times 10^{-4}$

Effective prestress for statge 2:

$f_{pe.1.1} := f_{pi} - f_{ps.1} - \Delta f_{ps.1} - \Delta f_{pR.1} = 172.9 \cdot ksi$

Interval 2: From Stage 2 during construction ($t_{1.f} = 30$) to Stage 3 in service ($t_{2.f} = 60$)

Dead loads: $M_2 := \frac{1}{8} \cdot \left(w_{slab} + w_{haunch}\right) (span)^2 = 6824 \cdot kip \cdot in$

Load due to low-relaxation strands: $\Delta P_1 := \Delta f_{pR.1} \cdot A_{ps} = 6.615 \cdot kip$

Step 1:

Stress/strain in bottom of concrete flange:

$$f_{f.b.2} := \frac{-\Delta P_1}{A_g} + \frac{-\Delta P_1 \cdot e_m \cdot y_{gb}}{I_g} + \frac{-M_2 \cdot y_{gb}}{I_g} = -1.789 \cdot ksi$$

$$\varepsilon_{f.b.2} := \frac{f_{f.b.2}}{E_c} = -2.951 \times 10^{-4}$$

$f_{f.b.1} + \Delta f_{f.b.1} + f_{f.b.2} = 2.437 \cdot ksi$ Less than $0.45 \cdot f'_c = 4.5 \cdot ksi$ OK

Stress/strain in top of concrete flange:

$$f_{f.t.2} := \frac{-\Delta P_1}{A_g} + \frac{-\Delta P_1 \cdot e_m \cdot (y_{gb} - h_c)}{I_g} + \frac{-M_2 \cdot (y_{gb} - h_c)}{I_g} = -0.72 \cdot ksi$$

$$\varepsilon_{f.t.2} := \frac{f_{f.t.2}}{E_c} = -1.187 \times 10^{-4}$$

$f_{f.t.1} + \Delta f_{f.t.1} + f_{f.t.2} = 2.559 \cdot ksi$ Less than $0.45 \cdot f'_c = 4.5 \cdot ksi$ OK

Axial strain in concrete flange only due to creep and shrinkage:

$$\varepsilon_1 := \frac{f_{f.b.1} + f_{f.t.1}}{2E_{ci}} \cdot (\psi_{t0.t2.f} - \psi_{t0.t1.f}) + \frac{\Delta f_{f.b.1} + \Delta f_{f.t.1}}{2 \cdot \frac{(E_{ci} + E_c)}{2}} \cdot (\psi_{t01.t2.f} - \psi_{t01.t1.f}) = 1.257 \times 10^{-4}$$

$$\varepsilon_{2.f} := \varepsilon_1 + \frac{f_{f.b.2} + f_{f.t.2}}{2E_c} \cdot \psi_{t1.t2.f} + \varepsilon_{t1.t2.f} = 1.047 \times 10^{-4}$$

Curvature in concrete flange only due to creep and shrinkage:

$$\phi_1 := \frac{f_{f.b.1} - f_{f.t.1}}{2E_{ci} \cdot h_c} \cdot (\psi_{t0.t2.f} - \psi_{t0.t1.f}) + \frac{\Delta f_{f.b.1} - \Delta f_{f.t.1}}{2 \cdot \frac{(E_{ci} + E_c)}{2} \cdot h_c} \cdot (\psi_{t01.t2.f} - \psi_{t01.t1.f}) = 2.582 \times 10^{-6} \cdot \frac{1}{in}$$

$$\phi_{2.f} := \phi_1 + \frac{f_{f.b.2} - f_{f.t.2}}{E_c \cdot h_c} \cdot \psi_{t1.t2.f} = -8.314 \times 10^{-6} \cdot \frac{1}{in}$$

Strain in bottom/top fibers of concrete flange only due to creep and shrinkage: :

$$\varepsilon_{f.b.2.cs} := \varepsilon_{2.f} + \phi_{2.f} \cdot \frac{h_c}{2} = 7.765 \times 10^{-5}$$

$$\varepsilon_{f.t.2.cs} := \varepsilon_{2.f} - \phi_{2.f} \cdot \frac{h_c}{2} = 1.317 \times 10^{-4}$$

Stress/strain in bottom of steel section:

$$f_{s.b.2} := \left[\frac{-\Delta P_1}{A_g} + \frac{-\Delta P_1 \cdot e_m \cdot (y_{gb} - h_c)}{I_g} + \frac{-M_2 \cdot (y_{gb} - h_c)}{I_g}\right] \cdot n_s = -3.443 \cdot ksi$$

$$\varepsilon_{s.b.2} := \frac{f_{s.b.2}}{E_s} = -1.187 \times 10^{-4}$$

$f_{s.b.1} + \Delta f_{s.b.1} + f_{s.b.2} = 22.869 \cdot ksi$ Less than $-0.7f_y = -35 \cdot ksi$ OK

Stress/strain in top of steel section:

$$f_{s.t.2} := \left(\frac{-\Delta P_1}{A_g} + \frac{\Delta P_1 \cdot e_m \cdot y_{gt}}{I_g} + \frac{M_2 \cdot y_{gt}}{I_g}\right) \cdot n_s = 19.77 \cdot ksi$$

$$\varepsilon_{s.t.2} := \frac{f_{s.t.2}}{E_s} = 6.818 \times 10^{-4}$$

$f_{s.t.1} + \Delta f_{s.t.1} + f_{s.t.2} = 16.377 \cdot ksi$ Less than $0.7f_y = 35 \cdot ksi$ OK

Prestress gain:

$$f_{ps.2} := \frac{n_{ps} \cdot M_2 \cdot (y_{gb} - y_{ps})}{I_g} = 4.877 \cdot ksi$$

Prestress immediately after deck placement:

$$f_{pe.2.0} := f_{pi} - f_{ps.1} - \Delta f_{ps.1} - \Delta f_{pR.1} + f_{ps.2} = 177.744 \cdot ksi$$

No strain or curvature due to creep and shrinkage of steel section

Axial strain in slab:

$$\varepsilon_d := \varepsilon_{t0.t1.d} = 2.509 \times 10^{-4}$$

Strain in bottom/top fibers of concrete flange only due to creep and shrinkage: :

$$\varepsilon_{d.b.2.cs} := \varepsilon_d = 2.509 \times 10^{-4}$$

$$\varepsilon_{d.t.2.cs} := \varepsilon_d = 2.509 \times 10^{-4}$$

Step 2:

Calculate the forces and corresponding stresses in each component that cancel the deformation in Step 1.

Age adjusted effective modulus for concrete flange:

$$E_f := E_c = 6062 \cdot ksi$$

$$E'_f := \frac{E_f}{1 + \chi_{t1.t2.f} \cdot \psi_{t1.t2.f}} = 4466 \cdot ksi$$

Axial restraining force in concrete flange:

$$F_f := -E'_f \cdot A_c \cdot \varepsilon_{2.f} = -72.9 \cdot kip$$

Corresponding stress in concrete flange:

$$f_{f.i} := \frac{F_f}{A_c} = -0.467 \cdot ksi$$

Moment in concrete flange:

$$M_f := -E'_f \cdot I_c \cdot \phi_{2.f} = 20.4 \cdot in \cdot kip$$

Corresponding stress in concrete flange:

$$f_{f.b.i} := \frac{M_f \cdot y_c}{I_c} = 0.121 \cdot ksi$$

$$f_{f.t.i} := -f_{f.b.i} = -0.121 \cdot ksi$$

None for steel section.

Age adjusted effective modulus for deck:

$$E_d := E_{c.slab.i} = 3321 \cdot ksi$$

$$E'_d := \frac{E_d}{1 + \chi_{t0.t1.d} \cdot \psi_{t0.t1.d}} = 2023 \cdot ksi$$

Axial restraining force in deck:

$$A_d = 672 \cdot in^2 \qquad I_d = 2744 \cdot in^4$$

$$F_d := -E'_d \cdot A_d \cdot \varepsilon_d = -341.1 \cdot kip$$

Corresponding stress in deck:

$$f_{d.i} := \frac{F_d}{A_d} = -0.508 \cdot ksi$$

Step 3:

$$n'_s := \frac{E_s}{E'_f} = 6.493 \qquad n'_{ps} := \frac{E_{ps}}{E'_f} = 6.448$$

Depth: $h_g := h_c + h_s = 36 \cdot in$

Centroidal distance to bottom fiber: Steel beam: $y_{sg} := \frac{h_s}{2} + h_c$

Concrete bottom flange: $y_c := h_c \cdot 0.5 = 3.25 \cdot in$

Strands: $y_{ps} = 2.778 \cdot in$

Transformed area: $A_{g.2} := A_c + n'_s \cdot A_{sg} + n'_{ps} \cdot A_{ps} = 361.537 \cdot in^2$

Neutral axis: At release: Bottom: $y_{gb.2} := \frac{\left(n'_s \cdot A_{sg} \cdot y_{sg} + A_c \cdot y_c + n'_{ps} \cdot A_{ps} \cdot y_{ps}\right)}{A_{g.2}} = 11.74 \cdot in$

Top: $y_{gt.2} := h_g - y_{gb.2} = 24.26 \cdot in$

Moment of inertia:

$$I_{g.2} := n'_s \cdot I_{sg} + n'_s \cdot A_{sg} \cdot \left(y_{gb.2} - y_{sg}\right)^2 + I_c + A_c \cdot \left(y_{gb.2} - y_c\right)^2 + n'_{ps} \cdot I_{ps} + n'_{ps} \cdot A_{ps} \cdot \left(y_{gb.2} - y_{ps}\right)^2 = 53516 \cdot in^4$$

Composite section with slab

$$n_{d.f} := \frac{E'_d}{E'_f} = 0.453$$

Area of slab: $A_d := d_{slab} \cdot gird_{spacing} = 672 \cdot in^2$ $\quad y_d := \frac{d_{slab}}{2} = 3.5 \cdot in$

Moment of inertia of slab: $I_d := \left(\frac{1}{12}\right) \cdot d_{slab}^3 \cdot gird_{spacing} = 2744 \cdot in^4$

$h_{gt} := h_g + haunch_t = 37 \cdot in$

Neutral axis:

Bottom: $$y'_{comp.b} := \frac{\left[A_{g.2} \cdot y_{gb.2} + n_{d.f} \cdot A_d \cdot \left(h_{gt} + \frac{d_{slab}}{2}\right)\right]}{\left(A_{g.2} + n_{d.f} \cdot A_d\right)} = 24.88 \cdot in$$

Top: $y'_{comp.t} := h_{comp} - y'_{comp.b} = 19.12 \cdot in$

Area: $A'_{comp} := \left(A_{g.2} + n_{d.f} \cdot A_d\right) = 666 \cdot in^2$

Moment of inertia:

$$I'_{comp} := I_{g.2} + A_{g.2} \cdot \left(y'_{comp.b} - y_{gb.2}\right)^2 + n_{d.f} \cdot I_d + n_{d.f} \cdot A_d \cdot \left(h_{gt} + \frac{d_{slab}}{2} - y'_{comp.b}\right)^2 = 191440 \cdot in^4$$

Bottom of concrete flange:

$$f_{f.b.c} := \frac{-F_f - F_d}{A'_{comp}} + \frac{-F_f \cdot \left(y'_{comp.b} - y_c\right) + F_d \cdot \left(y'_{comp.t} - y_d\right) - M_f \cdot y'_{comp.b}}{I'_{comp}} = 0.132 \cdot ksi$$

Top of concrete flange:

$$f_{f.t.c} := \frac{-F_f - F_d}{A'_{comp}} + \frac{-F_f \cdot (y'_{comp.b} - y_c) + F_d \cdot (y'_{comp.t} - y_d) - M_f \cdot (y'_{comp.b} - h_c)}{I'_{comp}} = 0.26 \cdot ksi$$

Bottom of steel section:

$$f_{s.b.c} := f_{f.t.c} \cdot n'_s = 1.687 \cdot ksi$$

Top of steel section

$$f_{s.t.c} := \left[\frac{-F_f - F_d}{A'_{comp}} - \frac{-F_f \cdot (y'_{comp.b} - y_c) + F_d \cdot (y'_{comp.t} - y_d) - M_f \cdot (y'_{comp.t} - d_{slab} - haunch_t)}{I'_{comp}} \right] \cdot n'_s = 5.458 \cdot ksi$$

Strands:

$$f_{ps.c} := \left[\frac{-F_f - F_d}{A'_{comp}} + \frac{-F_f \cdot (y'_{comp.b} - y_c) + F_d \cdot (y'_{comp.t} - y_d) - M_f \cdot (y'_{comp.b} - y_{ps})}{I'_{comp}} \right] \cdot n'_{ps} = 1.203 \cdot ksi$$

Bottom of deck:

$$f_{d.b.c} := \left[\frac{-F_f - F_d}{A'_{comp}} - \frac{-F_f \cdot (y'_{comp.b} - y_c) + F_d \cdot (y'_{comp.t} - y_d) - M_f \cdot (y'_{comp.t} - d_{slab})}{I'_{comp}} \right] \cdot n_{d.f} = 0.39 \cdot ksi$$

Top of deck:

$$f_{d.t.c} := \left[\frac{-F_f - F_d}{A'_{comp}} - \frac{-F_f \cdot (y'_{comp.b} - y_c) + F_d \cdot (y'_{comp.t} - y_d) - M_f \cdot y'_{comp.t}}{I'_{comp}} \right] \cdot n_{d.f} = 0.452 \cdot ksi$$

Step 4:

Summation of all time-dependent stresses/strains in Step 1-3

Bottom of concrete flange:

$$\Delta f_{f.b.2} := f_{f.i} + f_{f.b.i} + f_{f.b.c} = -0.215 \cdot ksi$$

$$\Delta \varepsilon_{f.b.2} := \varepsilon_{f.b.2.cs} + \frac{\Delta f_{f.b.2}}{E'_f} = 2.952 \times 10^{-5}$$

Top of concrete flange:

$$\Delta f_{f.t.2} := f_{f.i} + f_{f.t.i} + f_{f.t.c} = -0.328 \cdot ksi$$

$$\Delta \varepsilon_{f.t.2} := \varepsilon_{f.t.2.cs} + \frac{\Delta f_{f.t.2}}{E'_f} = 5.817 \times 10^{-5}$$

Bottom of steel section:

$$\Delta f_{s.b.2} := f_{s.b.c} = 1.687 \cdot ksi$$

$$\Delta \varepsilon_{s.b.2} := \frac{\Delta f_{s.b.2}}{E_s} = 5.817 \times 10^{-5}$$

Top of steel section

$$\Delta f_{s.t.2} := f_{s.t.c} = 5.458 \cdot ksi$$

$$\Delta \varepsilon_{s.t.2} := \frac{\Delta f_{s.t.2}}{E_s} = 1.882 \times 10^{-4}$$

Losses in strands:

$$\Delta f_{ps.2} := f_{ps.c} = 1.203 \cdot ksi$$

Bottom of deck:

$$\Delta f_{d.b.2} := f_{d.i} + f_{d.b.c} = -0.118 \cdot ksi$$

$$\Delta \varepsilon_{d.b.2} := \varepsilon_{d.b.2.cs} + \frac{\Delta f_{d.b.2}}{E'_d} = 1.926 \times 10^{-4}$$

Top of deck:

$$\Delta f_{d.t.2} := f_{d.i} + f_{d.t.c} = -0.056 \cdot ksi$$

$$\Delta \varepsilon_{d.t.2} := \varepsilon_{d.t.2.cs} + \frac{\Delta f_{d.t.2}}{E'_d} = 2.235 \times 10^{-4}$$

Final stresses/strains just before stage 3:

Bottom of concrete flange:

$$f_{f.b.1} + \Delta f_{f.b.1} + f_{f.b.2} + \Delta f_{f.b.2} = 2.222 \cdot ksi$$

$$\varepsilon_{f.b.1} + \Delta \varepsilon_{f.b.1} + \varepsilon_{f.b.2} + \Delta \varepsilon_{f.b.2} = 9.815 \times 10^{-4}$$

Top of concrete flange:

$$f_{f.t.1} + \Delta f_{f.t.1} + f_{f.t.2} + \Delta f_{f.t.2} = 2.23 \cdot ksi$$

$$\varepsilon_{f.t.1} + \Delta \varepsilon_{f.t.1} + \varepsilon_{f.t.2} + \Delta \varepsilon_{f.t.2} = 9.395 \times 10^{-4}$$

Bottom of steel section:

$f_{s.b.1} + \Delta f_{s.b.1} + f_{s.b.2} + \Delta f_{s.b.2} = 24.556 \cdot ksi$

$\varepsilon_{s.b.1} + \Delta\varepsilon_{s.b.1} + \varepsilon_{s.b.2} + \Delta\varepsilon_{s.b.2} = 8.468 \times 10^{-4}$

Top of steel section

$f_{s.t.1} + \Delta f_{s.t.1} + f_{s.t.2} + \Delta f_{s.t.2} = 21.835 \cdot ksi$

$\varepsilon_{s.t.1} + \Delta\varepsilon_{s.t.1} + \varepsilon_{s.t.2} + \Delta\varepsilon_{s.t.2} = 7.529 \times 10^{-4}$

Effective prestress for statge 2:

$f_{pe.2.1} := f_{pi} - f_{ps.1} - \Delta f_{ps.1} - \Delta f_{pR.1} + f_{ps.2} - \Delta f_{ps.2} = 176.541 \cdot ksi$

Bottom of slab:

$\Delta f_{d.b.2} = -0.12 \cdot ksi$

$\Delta\varepsilon_{d.b.2} = 1.926 \times 10^{-4}$

Top of slab:

$\Delta f_{d.t.2} = -0.06 \cdot ksi$

$\Delta\varepsilon_{d.b.2} = 1.926 \times 10^{-4}$

<u>Interval 3: From Stage 3 in service (t2.f = day 60) to time infinity (t3.f = 100000)</u>

Wearing Surface and Barrier: $M_{ws.bar} := \frac{1}{8} \cdot \left(w_{ws} + w_{bar}\right) span^2 = 3003 \cdot in \cdot kip$

Step 1

Stress/strain in bottom of concrete flange:

$$f_{f.b.3} := \frac{-M_{ws.bar} \cdot y_{comp.b}}{I_{comp}} = -0.42 \cdot ksi$$

$$\varepsilon_{f.b.3} := \frac{f_{f.b.3}}{E_c} = -6.971 \times 10^{-5}$$

$f_{f.b.1} + \Delta f_{f.b.1} + f_{f.b.2} + \Delta f_{f.b.2} + f_{f.b.3} = 1.8 \cdot ksi$

Stress/strain in top of concrete flange:

$$f_{f.t.3} := \frac{-M_{ws.bar} \cdot \left(y_{comp.b} - h_c\right)}{I_{comp}} = -0.32 \cdot ksi$$

$$\varepsilon_{f.t.3} := \frac{f_{f.t.3}}{E_c} = -5.361 \times 10^{-5}$$

$$f_{f.t.1} + \Delta f_{f.t.1} + f_{f.t.2} + \Delta f_{f.t.2} + f_{f.t.3} = 1.905 \cdot ksi$$

Axial strain in concrete flange:

$$\varepsilon_{1.c} := \frac{f_{f.b.1} + f_{f.t.1}}{2E_{ci}} \cdot \left(\psi_{t0.t3.f} - \psi_{t0.t2.f}\right) + \frac{\Delta f_{f.b.1} + \Delta f_{f.t.1}}{2\,\frac{\left(E_{ci} + E_c\right)}{2}} \cdot \left(\psi_{t01.t3.f} - \psi_{t01.t2.f}\right) = 2.302 \times 10^{-4}$$

$$\varepsilon_{2.c} := \frac{f_{f.b.2} + f_{f.t.2}}{2E_c} \cdot \left(\psi_{t1.t3.f} - \psi_{t1.t2.f}\right) + \frac{\Delta f_{f.b.2} + \Delta f_{f.t.2}}{2E_c} \cdot \left(\psi_{t12.t3.f} - \psi_{t12.t2.f}\right) = -1.025 \times 10^{-4}$$

$$\varepsilon_{3.f} := \varepsilon_{1.c} + \varepsilon_{2.c} + \frac{f_{f.b.3} + f_{f.t.3}}{2E_c} \cdot \psi_{t2.t3.f} + \varepsilon_{t2.t3.f} = 1.903 \times 10^{-4}$$

Curvature in in concrete flange:

$$\phi_{1.c} := \frac{f_{f.b.1} - f_{f.t.1}}{2E_{ci} \cdot h_c} \cdot \left(\psi_{t0.t3.f} - \psi_{t0.t2.f}\right) + \frac{\Delta f_{f.b.1} - \Delta f_{f.t.1}}{2\,\frac{\left(E_{ci} + E_c\right)}{2} \cdot h_c} \cdot \left(\psi_{t01.t3.f} - \psi_{t0.t2.f}\right) = 4.433 \times 10^{-6} \cdot \frac{1}{in}$$

$$\phi_{2.c} := \frac{f_{f.b.2} + f_{f.t.2}}{2E_c \cdot h_c} \cdot \left(\psi_{t1.t3.f} - \psi_{t1.t2.f}\right) + \frac{\Delta f_{f.b.2} - \Delta f_{f.t.2}}{2E_c \cdot h_c} \cdot \left(\psi_{t12.t3.f} - \psi_{t12.t2.f}\right) = -1.164 \times 10^{-5} \cdot \frac{1}{in}$$

$$\phi_{3.f} := \phi_{1.c} + \phi_{2.c} + \frac{f_{f.b.3} - f_{f.t.3}}{E_c \cdot h_c} \cdot \psi_{t2.t3.f} = -9.006 \times 10^{-6} \cdot \frac{1}{in}$$

Strain in bottom/top fibers of concrete flange only due to creep and shrinkage: :

$$\varepsilon_{f.b.3.cs} := \varepsilon_{2.f} + \phi_{2.f} \cdot \frac{h_c}{2} = 7.765 \times 10^{-5}$$

$$\varepsilon_{f.t.3.cs} := \varepsilon_{2.f} - \phi_{2.f} \cdot \frac{h_c}{2} = 1.317 \times 10^{-4}$$

Bottom of steel section:

$$f_{s.b.3} := \frac{-n_s \cdot M_{ws.bar} \cdot (y_{comp.b} - h_c)}{I_{comp}} = -1.55 \cdot ksi$$

$$\varepsilon_{s.b.3} := \frac{f_{s.b.3}}{E_s} = -5.361 \times 10^{-5}$$

$$f_{s.b.1} + \Delta f_{s.b.1} + f_{s.b.2} + \Delta f_{s.b.2} + f_{s.b.3} = 23.002 \cdot ksi$$

Top of steel section:

$$f_{s.t.3} := \frac{n_s \cdot M_{ws.bar} \cdot (y_{comp.t} - 7in)}{I_{comp}} = 0.64 \cdot ksi$$

$$\varepsilon_{s.t.3} := \frac{f_{s.b.3}}{E_s} = -5.361 \times 10^{-5}$$

$$f_{s.t.1} + \Delta f_{s.t.1} + f_{s.t.2} + \Delta f_{s.t.2} + f_{s.t.3} = 22.472 \cdot ksi$$

No strain or curvature due to creep and shrinkage of steel section

Prestress gain:

$$f_{ps.3} := \frac{M_{ws.bar} \cdot (y_{comp.b} - y_{ps})}{I_{comp}} \cdot n_{ps} = 1.429 \cdot ksi$$

$$f_{pe.3.0} := f_{pi} - f_{ps.1} - \Delta f_{ps.1} - \Delta f_{pR.1} + f_{ps.2} - \Delta f_{ps.2} + f_{ps.3} = 177.969 \cdot ksi$$

Bottom of slab:

$$f_{d.b.3} := \frac{n_c \cdot M_{ws.bar} \cdot (y_{comp.t} - d_{slab})}{I_{comp}} = 0.08 \cdot ksi$$

$f_{d.b.3} + \Delta f_{d.b.2} = -0.034 \cdot ksi$ Less than $0.6 \cdot f'_{c.slab} = 2.4 \cdot ksi$ OK

$$\varepsilon_{d.b.3} := \frac{f_{d.b.3}}{E_{c.slab}} = 2.196 \times 10^{-5}$$

Top of slab:

$$f_{d.t.3} := \frac{n_c \cdot M_{ws.bar} \cdot y_{comp.t}}{I_{comp}} = 0.15 \cdot ksi$$

$f_{d.t.3} + \Delta f_{d.t.2} = 0.095 \cdot ksi$ Less than $0.6 \cdot f'_{c.slab} = 2.4 \cdot ksi$ OK

$$\varepsilon_{d.t.3} := \frac{f_{d.t.3}}{E_{c.slab}} = 3.931 \times 10^{-5}$$

Axial strain in slab:

$$\varepsilon_d := \frac{f_{d.t.3} + f_{d.b.3}}{2E_{c.slab}} \cdot \psi_{t1.t2.d} + \frac{\Delta f_{d.b.2} + \Delta f_{d.t.2}}{2 \cdot E_{c.slab}} \cdot \left(\psi_{t01.t2.d} - \psi_{t01.t1.d}\right) + \varepsilon_{t1.t2.d} = 3.487 \times 10^{-4}$$

Curvature in in concrete flange:

$$\phi_d := \frac{f_{d.b.3} - f_{d.t.3}}{E_{c.slab} \cdot h_c} \cdot \psi_{t1.t2.d} + \frac{\Delta f_{d.b.2} - \Delta f_{d.t.2}}{E_{c.slab} \cdot h_c} \cdot \left(\psi_{t01.t2.d} - \psi_{t01.t1.d}\right) = -6.951 \times 10^{-6} \cdot \frac{1}{in}$$

Strain in bottom/top fibers of concrete flange only due to creep and shrinkage: :

$$\varepsilon_{d.b.2.cs} := \varepsilon_d + \phi_d \cdot \frac{d_{slab}}{2} = 3.243 \times 10^{-4}$$

$$\varepsilon_{d.t.2.cs} := \varepsilon_d - \phi_d \cdot \frac{d_{slab}}{2} = 3.73 \times 10^{-4}$$

Step 2

Calculate the forces and corresponding stresses in each component that cancel the deformation in Step 1.

Age adjusted effective modulus for concrete flange:

$$E_f := E_c = 6062 \cdot ksi$$

$$E'_f := \frac{E_f}{1 + \chi_{t2.t3.f} \cdot \psi_{t2.t3.f}} = 3713 \cdot ksi$$

Axial restraining force in concrete flange:

$$F_f := -E'_f \cdot A_c \cdot \varepsilon_{3.f} = -110.207 \cdot kip$$

Corresponding stress in concrete flange:

$$f_{f.i} := \frac{F_f}{A_c} = -0.706 \cdot ksi$$

Moment in concrete flange:

$$M_f := -E'_f \cdot I_c \cdot \phi_{3.f} = 18.365 \cdot in \cdot kip$$

Corresponding stress in concrete flange:

$$f_{f.b.i} := \frac{M_f \cdot y_c}{I_c} = 0.109 \cdot ksi$$

$$f_{f.t.i} := -f_{f.b.i} = -0.109 \cdot ksi$$

Age adjusted effective modulus for deck:

$$E_d := E_{c.slab} = 3834 \cdot ksi$$

$$E'_d := \frac{E_d}{1 + \chi_{t1.t2.d} \cdot \psi_{t1.t2.d}} = 1704 \cdot ksi$$

Axial restraining force in deck:

$$A_d = 672 \cdot in^2 \qquad I_d = 2744 \cdot in^4$$

$$F_d := -E'_d \cdot A_d \cdot \varepsilon_d = -399.2 \cdot kip$$

Corresponding stress in deck:

$$f_{d.i} := \frac{F_d}{A_d} = -0.594 \cdot ksi$$

Moment in deck:

$$M_d := -E'_d \cdot I_d \cdot \phi_d = 32.5 \cdot in \cdot kip$$

Corresponding stress in deck: $y_d := \frac{d_{slab}}{2} = 3.5 \cdot in$

$$f_{d.b.i} := \frac{M_d \cdot y_d}{I_d} = 0.041 \cdot ksi$$

$$f_{d.t.i} := -\frac{M_d \cdot y_d}{I_d} = -0.041 \cdot ksi$$

Step 3:

Composite girder

$$n'_s := \frac{E_s}{E'_f} = 7.811 \qquad n'_{ps} := \frac{E_{ps}}{E'_f} = 7.757$$

Depth: $h_g := h_c + h_s = 36 \cdot in$

Centroidal distance to bottom fiber: Steel beam: $y_{sg} := \frac{h_s}{2} + h_c$

Concrete bottom flange: $y_c := h_c \cdot 0.5 = 3.25 \cdot in$

Strands: $y_{ps} = 2.778 \cdot in$

Transformed area: $A_{g.3} := A_c + n'_s \cdot A_{sg} + n'_{ps} \cdot A_{ps} = 403.257 \cdot in^2$

Neutral axis: At release: Bottom: $y_{gb.3} := \frac{\left(n'_s \cdot A_{sg} \cdot y_{sg} + A_c \cdot y_c + n'_{ps} \cdot A_{ps} \cdot y_{ps}\right)}{A_{g.3}} = 12.406 \cdot in$

Top: $y_{gt.3} := h_g - y_{gb.3} = 23.594 \cdot in$

Moment of inertia:

$$I_{g.3} := n'_s \cdot I_{sg} + n'_s \cdot A_{sg} \cdot \left(y_{gb.3} - y_{sg}\right)^2 + I_c + A_c \cdot \left(y_{gb.3} - y_c\right)^2 + n'_{ps} \cdot I_{ps} + n'_{ps} \cdot A_{ps} \cdot \left(y_{gb.3} - y_{ps}\right)^2 = 61806 \cdot in^4$$

Composite section with slab

$$n_{d.f} := \frac{E'_d}{E'_f} = 0.459$$

Area of slab: $A_d := d_{slab} \cdot gird_{spacing} = 672 \cdot in^2$

Moment of inertia of slab: $I_d := \left(\frac{1}{12}\right) \cdot d_{slab}^{\ 3} \cdot gird_{spacing} = 2744 \cdot in^4$

$h_{gt} := h_g + haunch_t = 37 \cdot in$

Neutral axis:

Bottom: $$y'_{comp.b} := \frac{\left[A_{g.3} \cdot y_{gb.3} + n_{d.f} \cdot A_d \cdot \left(h_{gt} + \frac{d_{slab}}{2}\right)\right]}{\left(A_{g.3} + n_{d.f} \cdot A_d\right)} = 24.58 \cdot in$$

Top: $y'_{comp.t} := h_{comp} - y'_{comp.b} = 19.42 \cdot in$

Area: $A'_{comp} := \left(A_{g.3} + n_{d.f} \cdot A_d\right) = 712 \cdot in^2$

Moment of inertia:

$$I'_{comp} := I_{g.3} + A_{g.3} \cdot \left(y'_{comp.b} - y_{gb.3}\right)^2 + n_{d.f} \cdot I_d + n_{d.f} \cdot A_d \cdot \left(h_{gt} + \frac{d_{slab}}{2} - y'_{comp.b}\right)^2 = 200985 \cdot in^4$$

Bottom of concrete flange:

$$f_{f.b.c} := \frac{-F_f - F_d}{A'_{comp}} + \frac{-F_f \cdot (y'_{comp.b} - y_c) + F_d \cdot (y'_{comp.t} - y_d) - M_f - M_d \cdot y'_{comp.b}}{I'_{comp}} = 0.22 \cdot ksi$$

Top of concrete flange:

$$f_{f.t.c} := \frac{-F_f - F_d}{A'_{comp}} + \frac{-F_f \cdot (y'_{comp.b} - y_c) + F_d \cdot (y'_{comp.t} - y_d) - M_f - M_d \cdot (y'_{comp.b} - h_c)}{I'_{comp}} = 0.351 \cdot ksi$$

Bottom of steel section

$$f_{s.b.c} := f_{f.t.c} \cdot n'_s = 2.742 \cdot ksi$$

Top of steel section

$$f_{s.t.c} := \left[\frac{-F_f - F_d}{A'_{comp}} - \frac{-F_f \cdot (y'_{comp.b} - y_c) + F_d \cdot (y'_{comp.t} - y_d) - M_f - M_d \cdot (y'_{comp.t} - d_{slab} - haunch_t)}{I'_{comp}} \right] \cdot n'_s = 7.391 \cdot ksi$$

Strands:

$$f_{ps.c} := \left[\frac{-F_f - F_d}{A'_{comp}} + \frac{-F_f \cdot (y'_{comp.b} - y_c) + F_d \cdot (y'_{comp.t} - y_d) - M_f - M_d \cdot (y'_{comp.b} - y_{ps})}{I'_{comp}} \right] \cdot n'_{ps} = 2.14 \cdot ksi$$

Bottom of deck:

$$f_{d.b.c} := \left[\frac{-F_f - F_d}{A'_{comp}} - \frac{-F_f \cdot (y'_{comp.b} - y_c) + F_d \cdot (y'_{comp.t} - y_d) - M_f - M_d \cdot (y'_{comp.t} - d_{slab})}{I'_{comp}} \right] \cdot n_{d.f} = 0.443 \cdot ksi$$

Top of deck:

$$f_{d.t.c} := \left[\frac{-F_f - F_d}{A'_{comp}} - \frac{-F_f \cdot (y'_{comp.b} - y_c) + F_d \cdot (y'_{comp.t} - y_d) - M_f - M_d \cdot y'_{comp.t}}{I'_{comp}} \right] \cdot n_{d.f} = 0.508 \cdot ksi$$

Step 4:

Summation of all time-dependent stresses/strains in Step 1-3

Bottom of concrete flange:

$$\Delta f_{f.b.3} := f_{f.i} + f_{f.b.i} + f_{f.b.c} = -0.378 \cdot ksi$$

$$\Delta \varepsilon_{f.b.3} := \varepsilon_{f.b.3.cs} + \frac{\Delta f_{f.b.3}}{E'_f} = -2.414 \times 10^{-5}$$

Top of concrete flange:

$$\Delta f_{f.t.3} := f_{f.i} + f_{f.t.i} + f_{f.t.c} = -0.464 \cdot ksi$$

$$\Delta\varepsilon_{f.t.3} := \varepsilon_{f.t.3.cs} + \frac{\Delta f_{f.t.3}}{E'_f} = 6.688 \times 10^{-6}$$

Bottom of steel section:

$$\Delta f_{s.b.3} := f_{s.b.c} = 2.742 \cdot ksi$$

$$\Delta\varepsilon_{s.b.3} := \frac{\Delta f_{s.b.3}}{E_s} = 9.454 \times 10^{-5}$$

Top of steel section

$$\Delta f_{s.t.3} := f_{s.t.c} = 7.391 \cdot ksi$$

$$\Delta\varepsilon_{s.t.3} := \frac{\Delta f_{s.t.3}}{E_s} = 2.549 \times 10^{-4}$$

Strands

$$\Delta f_{ps.3} := f_{ps.c} = 2.14 \cdot ksi$$

Bottom of deck:

$$\Delta f_{d.b.3} := f_{d.i} + f_{d.b.i} + f_{d.b.c} = -0.109 \cdot ksi$$

$$\Delta\varepsilon_{d.b.3} := \varepsilon_{d.b.2.cs} + \frac{\Delta f_{d.b.3}}{E'_d} = 2.603 \times 10^{-4}$$

Top of deck:

$$\Delta f_{d.t.3} := f_{d.i} + f_{d.t.i} + f_{d.t.c} = -0.127 \cdot ksi$$

$$\Delta\varepsilon_{d.t.3} := \varepsilon_{d.t.2.cs} + \frac{\Delta f_{d.t.3}}{E'_d} = 2.983 \times 10^{-4}$$

Final stresses/strains in section without live loads:

Bottom of concrete flange:

$$f_{f.b.1} + \Delta f_{f.b.1} + f_{f.b.2} + \Delta f_{f.b.2} + f_{f.b.3} + \Delta f_{f.b.3} = 1.422 \cdot ksi$$

$$\varepsilon_{f.b.1} + \Delta\varepsilon_{f.b.1} + \varepsilon_{f.b.2} + \Delta\varepsilon_{f.b.2} + \varepsilon_{f.b.3} + \Delta\varepsilon_{f.b.3} = 8.877 \times 10^{-4}$$

Top of concrete flange:

$$f_{f.t.1} + \Delta f_{f.t.1} + f_{f.t.2} + \Delta f_{f.t.2} + f_{f.t.3} + \Delta f_{f.t.3} = 1.441 \cdot ksi$$

$$\varepsilon_{f.t.1} + \Delta\varepsilon_{f.t.1} + \varepsilon_{f.t.2} + \Delta\varepsilon_{f.t.2} + \varepsilon_{f.t.3} + \Delta\varepsilon_{f.t.3} = 8.925 \times 10^{-4}$$

Bottom of steel section:

$$f_{s.b.1} + \Delta f_{s.b.1} + f_{s.b.2} + \Delta f_{s.b.2} + f_{s.b.3} + \Delta f_{s.b.3} = 25.743 \cdot ksi$$

$$\varepsilon_{f.b.1} + \Delta\varepsilon_{f.b.1} + \varepsilon_{f.b.2} + \Delta\varepsilon_{f.b.2} + \varepsilon_{f.b.3} + \Delta\varepsilon_{f.b.3} = 8.877 \times 10^{-4}$$

Top of steel section

$$f_{s.t.1} + \Delta f_{s.t.1} + f_{s.t.2} + \Delta f_{s.t.2} + f_{s.t.3} + \Delta f_{s.t.3} = 29.863 \cdot ksi$$

$$\varepsilon_{s.t.1} + \Delta\varepsilon_{s.t.1} + \varepsilon_{s.t.2} + \Delta\varepsilon_{s.t.2} + \varepsilon_{s.t.3} + \Delta\varepsilon_{s.t.3} = 9.542 \times 10^{-4}$$

Effective prestress for statge 2:

$$f_{pe.3.1} := f_{pi} - f_{ps.1} - \Delta f_{ps.1} - \Delta f_{pR.1} + f_{ps.2} - \Delta f_{ps.2} + f_{ps.3} - \Delta f_{ps.3} - \Delta f_{pR.2} = 174.579 \cdot ksi$$

Bottom of slab:

$$f_{d.b.3} + \Delta f_{d.b.3} = -0.02 \cdot ksi$$

$$\varepsilon_{d.b.3} + \Delta\varepsilon_{d.b.3} = 2.823 \times 10^{-4}$$

Top of slab:

$$f_{d.t.3} + \Delta f_{d.t.3} = 0.02 \cdot ksi$$

$$\varepsilon_{d.b.3} + \Delta\varepsilon_{d.b.3} = 2.823 \times 10^{-4}$$

Final stresses/strains including live loads and Load due to low-relaxation strands:

Top Compression: *Service I:* $M_{LL.I} = 1371 \cdot ft \cdot kip$

Bottom Tension: *Service III:* $M_{LL.III} = 1097 \cdot ft \cdot kip$

Load due to low-relaxation strands: $\Delta P_2 := \Delta f_{pR.2} \cdot A_{ps} = 6.615 \cdot kip$

Bottom of concrete flange:

$$f_{f.b.LL} := \frac{-\Delta P_2}{A_{comp}} + \frac{-\Delta P_2 \cdot e_{comp.m} \cdot y_{comp.b}}{I_{comp}} + \frac{-M_{LL.III} \cdot y_{comp.b}}{I_{comp}} = -1.88 \cdot ksi$$

$$\varepsilon_{f.b.LL} := \frac{f_{f.b.LL}}{E_c} = -3.109 \times 10^{-4}$$

$$f_{f.b.1} + \Delta f_{f.b.1} + f_{f.b.2} + \Delta f_{f.b.2} + f_{f.b.3} + \Delta f_{f.b.3} + f_{f.b.LL} = -0.463 \cdot ksi$$

Less than $-0.19 \cdot \sqrt{\frac{f'_c}{ksi}}\, ksi = -0.601 \cdot ksi$ OK

$$\varepsilon_{f.b.1} + \Delta\varepsilon_{f.b.1} + \varepsilon_{f.b.2} + \Delta\varepsilon_{f.b.2} + \varepsilon_{f.b.3} + \Delta\varepsilon_{f.b.3} + \varepsilon_{f.b.LL} = 5.768 \times 10^{-4}$$

Top of concrete flange:

$$f_{f.t.LL} := \frac{-\Delta P_2}{A_{comp}} + \frac{-\Delta P_2 \cdot e_{comp.m} \cdot (y_{comp.b} - h_c)}{I_{comp}} + \frac{-M_{LL.III} \cdot (y_{comp.b} - h_c)}{I_{comp}} = -1.45 \cdot ksi$$

$$\varepsilon_{f.t.LL} := \frac{f_{f.b.LL}}{E_c} = -3.109 \times 10^{-4}$$

$$f_{f.t.1} + \Delta f_{f.t.1} + f_{f.t.2} + \Delta f_{f.t.2} + f_{f.t.3} + \Delta f_{f.t.3} + f_{f.t.LL} = -0.01 \cdot ksi$$

Less than $-0.19 \cdot \sqrt{\frac{f'_c}{ksi}}\, ksi = -0.6 \cdot ksi$ OK

$$\varepsilon_{f.t.1} + \Delta\varepsilon_{f.t.1} + \varepsilon_{f.t.2} + \Delta\varepsilon_{f.t.2} + \varepsilon_{f.t.3} + \Delta\varepsilon_{f.t.3} + \varepsilon_{f.t.LL} = 5.817 \times 10^{-4}$$

Bottom of steel section:

$$f_{s.b.LL} := \left[\frac{-\Delta P_2}{A_{comp}} + \frac{-\Delta P_2 \cdot e_{comp.m} \cdot (y_{comp.b} - h_c)}{I_{comp}} + \frac{-M_{LL.III} \cdot (y_{comp.b} - h_c)}{I_{comp}}\right] \cdot n_s = -6.94 \cdot ksi$$

$$\varepsilon_{s.b.LL} := \frac{f_{s.b.LL}}{E_s} = -2.394 \times 10^{-4}$$

$$f_{s.b.1} + \Delta f_{s.b.1} + f_{s.b.2} + \Delta f_{s.b.2} + f_{s.b.3} + \Delta f_{s.b.3} + f_{s.b.LL} = 18.801 \cdot ksi$$

Less than $0.7 f_y = 35 \cdot ksi$ OK

$$\varepsilon_{s.b.1} + \Delta\varepsilon_{s.b.1} + \varepsilon_{s.b.2} + \Delta\varepsilon_{s.b.2} + \varepsilon_{s.b.3} + \Delta\varepsilon_{s.b.3} + \varepsilon_{s.b.LL} = 6.483 \times 10^{-4}$$

Top of steel section:

$$f_{s.t.LL} := \left[\frac{-\Delta P_2}{A_{comp}} + \frac{\Delta P_2 \cdot e_{comp.m} \cdot (y_{comp.t} - d_{slab} - haunch_t)}{I_{comp}} + \frac{M_{LL.I} \cdot (y_{comp.t} - d_{slab} - haunch_t)}{I_{comp}}\right] \cdot n_s = 3.08 \cdot ksi$$

$$\varepsilon_{s.t.LL} := \frac{f_{s.t.LL}}{E_s} = 1.063 \times 10^{-4}$$

$$f_{s.t.1} + \Delta f_{s.t.1} + f_{s.t.2} + \Delta f_{s.t.2} + f_{s.t.3} + \Delta f_{s.t.3} + f_{s.t.LL} = 32.946 \cdot ksi$$

Less than $0.7 f_y = 35 \cdot ksi$ OK

$$\varepsilon_{s.t.1} + \Delta\varepsilon_{s.t.1} + \varepsilon_{s.t.2} + \Delta\varepsilon_{s.t.2} + \varepsilon_{s.t.3} + \Delta\varepsilon_{s.t.3} + \varepsilon_{s.t.LL} = 1.06 \times 10^{-3}$$

Prestress gain:

$$f_{ps.LL} := \frac{M_{LL.III} \cdot (y_{comp.b} - y_{ps})}{I_{comp}} \cdot n_{ps} = 6.26 \cdot ksi$$

$$f_{pe.final} := f_{pi} - f_{ps.1} - \Delta f_{ps.1} - \Delta f_{pR.1} + f_{ps.2} - \Delta f_{ps.2} + f_{ps.3} - \Delta f_{ps.3} - \Delta f_{pR.2} + f_{ps.LL} = 180.8 \cdot ksi$$

Bottom of slab:

$$f_{d.b.LL} := \frac{n_c \cdot M_{LL.I} \cdot (y_{comp.t} - d_{slab})}{I_{comp}} = 0.46 \cdot ksi$$

$$\varepsilon_{d.b.LL} := \frac{f_{d.b.LL}}{E_d} = 1.203 \times 10^{-4}$$

$f_{d.b.3} := \Delta f_{d.b.2} + f_{d.b.3} + \Delta f_{d.b.3} + f_{d.b.LL} = 0.32 \cdot ksi$ Less than $0.6 \cdot f'_{c.slab} = 2.4 \cdot ksi$ OK

$$\varepsilon_{d.b.3} := \Delta\varepsilon_{d.b.2} + \varepsilon_{d.b.3} + \Delta\varepsilon_{d.b.3} + \varepsilon_{d.b.LL} = 5.952 \times 10^{-4}$$

Top of slab:

$$f_{d.t.LL} := \frac{n_c \cdot M_{LL.I} \cdot y_{comp.t}}{I_{comp}} = 0.83 \cdot ksi$$

$$\varepsilon_{d.t.LL} := \frac{f_{d.t.LL}}{E_d} = 2.153 \times 10^{-4}$$

$f_{d.t.3} := \Delta f_{d.t.2} + f_{d.t.3} + \Delta f_{d.t.3} + f_{d.t.LL} = 0.793 \cdot ksi$ Less than $0.6 \cdot f'_{c.slab} = 2.4 \cdot ksi$ OK

$$\varepsilon_{d.t.3} := \Delta\varepsilon_{d.t.2} + \varepsilon_{d.t.3} + \Delta\varepsilon_{d.t.3} + \varepsilon_{d.t.LL} = 7.764 \times 10^{-4}$$

A.2.2 Ultimate Strength Design

Moment due to unfactored applied loads:

$$M_s := M_g + M_{haunch} + M_{slab} + M_{bar} + M_{ws} + M_{LL.I} = 2391.6 \cdot ft \cdot kip$$

Moment due to factored applied loads:

$$M_{u.s} := 1.25 \cdot (M_g + M_{haunch} + M_{slab} + M_{bar}) + 1.5 \cdot M_{ws} + 1.75 \cdot M_{LL.I} = 3706.8 \cdot ft \cdot kip$$

Flexural Strength

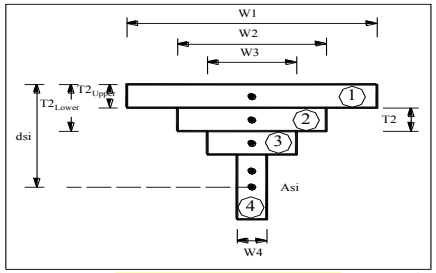

ε_{cu}	0.003
c=	9.922
a	8.434
Sum of forces	0.00
Design	P/C AASHTO
ANSWER:	
ϕ	1.00
ϕM_n kip-in	73748
kip*ft	6145.7

Calculate

Av. β_1 : 0.850

Units in kips and inches

Concrete Layers		f'c	Width, W	Thick., T	Depth, d_c	β_1	T_{upper}	T_{lower}	Revised T	Beta1calcuation				Area	Force	M_n k-in.
	1	4.000	96.000	7.000	3.500	0.850	0.000	7.000	7.000	2284.8	2688			672.000	-2284.80	-7996.80
	2				7.000	0.850	7.000	7.000	0.000	0	0			0.000	0.00	0.00
	3				7.000	0.850	7.000	7.000	0.000	0	0			0.000	0.00	0.00
	4				7.000	0.850	7.000	7.000	0.000	0	0			0.000	0.00	0.00
	5				7.000	0.850	7.000	7.000	0.000	0	0			0.000	0.00	0.00
	6				7.000	0.850	7.000	7.000	0.000	0	0			0.000	0.00	0.00
	7				7.000	0.850	7.000	7.000	0.000	0	0			0.000	0.00	0.00
										2284.8	2688					

Steel Layers		Area A_{si}	Grade	Effective Prest.	Depth d_{si}	E_s	Q	fpy	R	K	ε_{so}	$\Delta\varepsilon$	Total ε_s	Stress	Force	Moment	Modified stress	corresp. f'c
Grade 60 Bars	1	0.6344	50	0	8.531	29000	0	60	100	1.096	0.0000	-0.0004	-0.0004	-12.20	-7.74	-66.04	-12.20	0.00
	2	0.6344	50	0	8.592	29000	0	60	100	1.096	0.0000	-0.0004	-0.0004	-11.67	-7.40	-63.60	-11.67	0.00
0.061	3	0.6344	50	0	8.653	29000	0	60	100	1.096	0.0000	-0.0004	-0.0004	-11.13	-7.06	-61.12	-11.13	0.00
0.61	4	0.6344	50	0	8.714	29000	0	60	100	1.096	0.0000	-0.0004	-0.0004	-10.60	-6.72	-58.59	-10.60	0.00
29.5	5	0.6344	50	0	8.775	29000	0	60	100	1.096	0.0000	-0.0003	-0.0003	-10.06	-6.38	-56.02	-10.06	0.00
28.28	6	0.6344	50	0	8.836	29000	0	60	100	1.096	0.0000	-0.0003	-0.0003	-9.53	-6.05	-53.41	-9.53	0.00
14.14	7	0.6344	50	0	8.897	29000	0	60	100	1.096	0.0000	-0.0003	-0.0003	-8.99	-5.71	-50.76	-8.99	0.00
	8	0.6344	50	0	8.958	29000	0	60	100	1.096	0.0000	-0.0003	-0.0003	-8.46	-5.37	-48.07	-8.46	0.00
10.4	9	0.6344	50	0	9.019	29000	0	60	100	1.096	0.0000	-0.0003	-0.0003	-7.92	-5.03	-45.34	-7.92	0.00
0.47	10	0.6344	50	0	9.080	29000	0	60	100	1.096	0.0000	-0.0003	-0.0003	-7.39	-4.69	-42.57	-7.39	0.00
	11	6.6458	50	0	16.150	29000	0	60	100	1.096	0.0000	0.0019	0.0019	50.00	332.29	5366.32	50.00	0.00
	12	6.6458	50	0	30.290	29000	0	60	100	1.096	0.0000	0.0062	0.0062	50.00	332.29	10064.90	50.00	0.00
	13	6.344	50	0	37.665	29000	0	60	100	1.096	0.0000	0.0084	0.0084	50.00	317.20	11947.18	50.00	0.00
Grade 70 Plate	1		70	0	0.000	29000	0	70	100	1.06	0.0000	0.0000	-0.0030	-70.00	0.00	0.00	-66.60	4.00
Gr. 120 Rods	1		120	0	5.125	29000	0.0217	81.00	4.224	1.01	0.0000	0.0000	-0.0015	-41.50	0.00	0.00	-38.10	4.00
Gr. 150 Rods	1		150	0	5.125	29000	0.0217	120.00	4.224	1.01	0.0000	0.0000	-0.0015	-41.95	0.00	0.00	-38.55	4.00
Gr 270	1	2.058	270	162.64	39.000	28500	0.031	243	7.36	1.043	0.0057	0.0088	0.0145	257.50	529.94	20667.55	257.50	0.00
Gr 270	2	3.234	270	162.64	41.000	28500	0.031	243	7.36	1.043	0.0057	0.0094	0.0151	258.27	835.23	34244.59	258.27	0.00
Gr 270	3	0	270	2.02	9.250	28500	0.031	243	7.36	1.043	0.0001	0.0000	-0.0001	-3.77	0.00	0.00	-3.77	0.00
Gr 270	4	0	270	162.64	7.250	28500	0.031	243	7.36	1.043	0.0057	0.0000	0.0049	139.39	0.00	0.00	139.39	0.00
	5		270	162.64	5.250	28500	0.031	243	7.36	1.043	0.0057	0.0000	0.0043	122.30	0.00	0.00	125.70	4.00
	6		270	162.64	3.250	28500	0.031	243	7.36	1.043	0.0057	0.0000	0.0037	105.12	0.00	0.00	108.52	4.00
	7	0	270	2.02	9.250	28500	0.031	243	7.36	1.043	0.0001	0.0000	-0.0001	-3.77	0.00	0.00	-3.77	0.00
	8		270	160	19.333	28500	0.031	243	7.36	1.043	0.0056	0.0000	0.0085	224.98	0.00	0.00	224.98	0.00
	9		270	160	21.667	28500	0.031	243	7.36	1.043	0.0056	0.0000	0.0092	234.82	0.00	0.00	234.82	0.00
	10		270	160	24.000	28500	0.031	243	7.36	1.043	0.0056	0.0000	0.0099	241.91	0.00	0.00	241.91	0.00
	11		270	160	26.333	28500	0.031	243	7.36	1.043	0.0056	0.0000	0.0106	246.85	0.00	0.00	246.85	0.00
	12		270	160	28.667	28500	0.031	243	7.36	1.043	0.0056	0.0000	0.0113	250.27	0.00	0.00	250.27	0.00
	13		270	160	31.000	28500	0.031	243	7.36	1.043	0.0056	0.0000	0.0120	252.69	0.00	0.00	252.69	0.00
	Sum of M									MAXIMUM	$\Delta\varepsilon$:	0.0094		Moment (	0.00	73748.20	kip*in	
																6145.68	kip*f	

Strain Compatibility Method

Based on spreadsheet, nominal moment is found as $M_{ns} := 6146ft \cdot kip$ $\phi := 1.0$

$\phi \cdot M_{ns} = 6146 \cdot ft \cdot kip$ Larger than $M_{u.s} = 3706.8 \cdot ft \cdot kip$ OK

A.2.3 Vertical Shear Design:

<u>Shear force at critical section:</u>

Dead loads: $w_{DL} := w_{ow} + w_{slab} + w_{haunch} = 0.963 \cdot klf$

$$V_{DL} := w_{DL} \cdot \left(\frac{span}{2}\right) = 38.533 \cdot kip$$

Barrier load:

$$V_{bar} := w_{bar} \cdot \left(\frac{span}{2}\right) = 6.112 \cdot kip$$

Wearing Surface:

$$V_{ws} := w_{ws} \cdot \left(\frac{span}{2}\right) = 6.4 \cdot kip$$

Lane Load:

$$V_{lane} := VDF \cdot w_{lane} \cdot \left(\frac{span^2}{2 \cdot span}\right) = 20.849 \cdot kip$$

Truck Load:

$$V_{truck} := VDF \cdot \left[\frac{72 \cdot kip \cdot (span - 9.33 \cdot ft)}{span}\right] = 51.8 \cdot kip$$

Tandem Load:

$$V_{tandem} := VDF \cdot 50 \cdot kip \cdot \frac{(span - 2 \cdot ft)}{span} = 39.703 \cdot kip$$

Live Load:

$$V_{LL} := V_{lane} + 1.33 \cdot V_{truck} = 89.743 \cdot kip$$

Total Dead Load (without load factor):

$$V_d := V_{DL} + V_{bar} + V_{ws} = 51.045 \cdot kip$$

$$V_u := 1.25 \cdot V_{DL} + 1.25 \cdot V_{bar} + 1.5 \cdot V_{ws} + 1.75 \cdot V_{LL} = 222.456 \cdot kip$$

Vertical shear checks

Rolled I-shaped member $\phi_v := 1.0$ $k_v := 5$

$D := t_w \cdot 33.4 = 15.698 \cdot in$ $E_s = 29000 \cdot ksi$

$\frac{D}{t_w} = 33.4 < 1.10 \cdot \sqrt{\frac{k_v \cdot E_s}{f_y}} = 59.237$ $C_v := 1.0$

$A_w := h_s t_w = 13.865 \cdot in^2$

$V_n := 0.58 \cdot f_y \cdot A_w \cdot C_v = 402.085 \cdot kip$ $> V_u = 222.456 \cdot kip$

A.2.3 Horizontal Shear Design

Composite action for deck

Use studs with 7/8 in diameter and 4 in hight, and Fu=60 ksi for studs

$d_{stud} := \frac{7}{8} \cdot in$ $h_{stud} := 4in$

Cover and penetration

$Cover_c := d_{slab} + haunch_t - h_{stud} = 4 \cdot in$ > 2 in OK

$Pen := h_{stud} - haunch_t = 3 \cdot in$ > 2 in OK

Types of shear connectors

$ratio := \frac{h_{stud}}{d_{stud}} = 4.571$ > 4.0 OK

Transverse spacing

Three 7/8 in. studs side by side

$2 \cdot 1in + d_{stud} + 2 \cdot 4d_{stud} = 9.875 \cdot in$ $< b_f = 10.4 \cdot in$

Therefore, use three 7/8 in. stud connectors at each transverse direction.

Nominal horizontal shear force:

$V_{deck} := 0.85 f'_{c.slab} \cdot gird_{spacing} \cdot d_{slab} = 2284.8 \cdot kip$ $f_{pu} := 270ksi$

$T_d := f_{pu} \cdot A_{ps} + f_y \cdot A_{sg} = 2748.84 \cdot kip$

$V_h := \min(V_{deck}, T_d) = 2284.8 \cdot kip$

$Q_n = 0.5 A_{sc} \cdot \sqrt{f_c \cdot E_c} \le A_{sc} \cdot F_u$ $\qquad F_u := 60ksi$

$A_{sc} := \pi \cdot \frac{d_{stud}^2}{4} = 0.601 \cdot in^2$

$Q_n := 0.5 \cdot A_{sc} \cdot \sqrt{f'_{c.i} \cdot E_{ci}} = 62.621 \cdot kip$ $\qquad A_{sc} \cdot F_u = 36.079 \cdot kip$

Thus, $Q_n := 36.08kip$

$\phi_{sc} := 0.85$ $\qquad Q_r := \phi_{sc} \cdot Q_n = 30.668 \cdot kip$

Number of studs: $N_h := \frac{V_h}{Q_r} = 74.501$ $\qquad$ Use 2 studs per row

Spacing of studs < $\frac{\frac{span}{2}}{\frac{75}{2}} = 12.8 \cdot in$

Use 150 - 7/8 in. stud connectors @ 12 in. and 2 studs per row

Composite action for concrete flange

Cover and penetration

$Cover_b := h_c - h_{stud} = 2.5 \cdot in$ $\qquad > 2$ in $\qquad$ OK

$Pen_{b.} := h_{stud} = 4 \cdot in$ $\qquad > 2$ in $\qquad$ OK

Types of shear connectors

$ratio_b := \frac{h_{stud}}{d_{stud}} = 4.571 > 4.0$ $\qquad$ OK

Transverse spacing

Two 7/8 in. studs side by side

$2 \cdot 1in + d_{stud} + 4in = 6.875 \cdot in$ $\qquad < \qquad b_f = 10.4 \cdot in$

Therefore, use two 7/8 in. stud connectors at each transverse direction.

Prestress stress at ultimate strength design:

Maximum transferred shear force: $f_{ps} := 260ksi$ $T_{str} := f_{ps} \cdot A_{ps} = 1.376 \times 10^3 \cdot kip$

Number of studs: $N_{bh} := \frac{T_{str}}{2Q_r} = 22.433$ Use 2 studs per row

Spacing of studs < $\frac{\frac{span}{2}}{\frac{22}{2}} = 43.6 \cdot in$

Use 44 - 7/8 in. stud connectors @ 12 in. and use 2 studs per row

A.3 Deck Design

Empirical method

Use #4@12 in. for top layer bars and #4@12 in. for bottom layer bars.

The clear cover is 2 in. at top and 1 in. at bottom.

A.4 Deflection Criteria

Live Load Deflection must be Less than $\Delta_{LL} := \frac{span}{800} = 1.2 \cdot in$

Live Load Deflections:

The Δ_{LL} is found by using Δ_{truck} * Impact Factor (1.33) * Distribution Factor for Moment

$$\Delta_{Lane} := \frac{5 \cdot \left(\frac{0.64}{12} \frac{kip}{in}\right) \cdot (span)^4}{384 \cdot E_c \cdot I_{comp}} = 0.487 \cdot in \qquad MDF = 0.667$$

$$\Delta_{truck.1} := \frac{32 \cdot kip \cdot span^3}{48 \cdot E_c \cdot I_{comp}} = 0.487 \cdot in \qquad a_x := \frac{span}{2} - 14ft = 26 \cdot ft$$

$$\Delta_{truck.2} := (32 \cdot kip + 8 \cdot kip) \cdot \frac{a_x \cdot \frac{span}{2}}{6 \cdot E_c \cdot I_{comp} \cdot span} \cdot \left[span^2 - (a_x)^2 - \left(\frac{span}{2}\right)^2 \right] = 0.51 \cdot in$$

$\Delta_{truck} := \Delta_{truck.1} + \Delta_{truck.2} = 0.996 \cdot in$

$\Delta_{LL.I} := MDF \cdot \left(\Delta_{truck} \cdot 1.33\right) = 0.884 \cdot in$

$\Delta_{LL.II} := MDF \cdot \left(25\% \, \Delta_{truck} \cdot 1.33 + \Delta_{Lane}\right) = 0.546 \cdot in$

$\Delta_{LL.c} := \Delta_{LL.I} = 0.884 \cdot in$

$$LiveLoad_{Deflection} := \begin{cases} \text{"Deflection limits are satisfied!"} & \text{if } \Delta_{LL.c} < \Delta_{LL} \\ \text{"Deflection limit exceeded... Check Design"} & \text{otherwise} \end{cases}$$

$LiveLoad_{Deflection} = \text{"Deflection limits are satisfied!"}$

Appendix B – Strength Design Example of the PCSC-36 Girder at Release

A design example is developed using the PCSC-36 girder section. The girder is designed using strength design method with simplified solutions and closed form solutions and working stress design method. Note that the detailed calculations of section properties and materials were presented in Section A.1.1 of Appendix A.

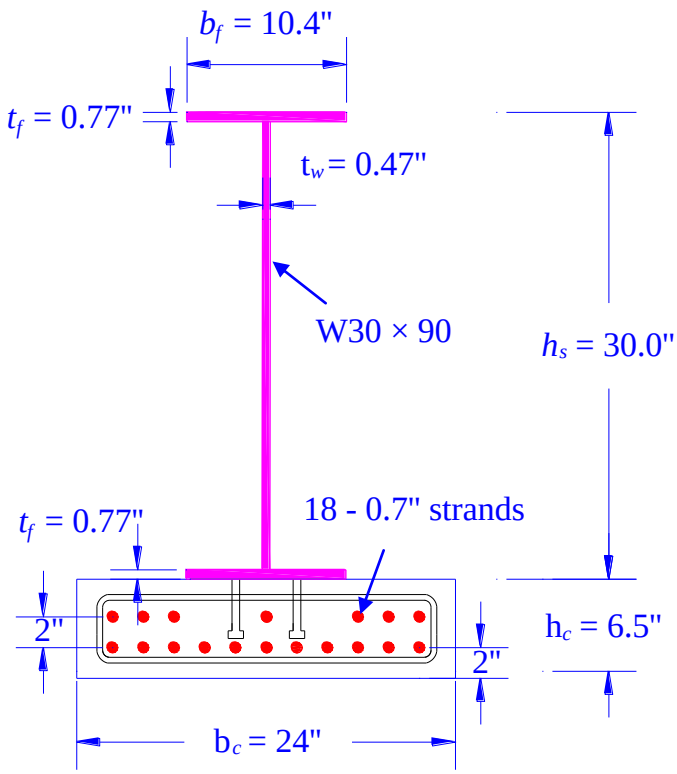

Cross-section of the PCSC-36 Girder (Span = 80 ft)

B.1 Strength Design at Release

(1) Determine the design parameters:

Steel beam:

Yielding strength: $f_y := 50ksi$ Modulus of elasticity: $E_s := 29000ksi$

Depth: $h_s := 29.5in$ Width of flange: $b_f := 10.4in$

Thickness of web: $t_w := 0.47 \cdot in$ Thickness of flange: $t_f := 0.61in$

Self weight: $w_{steel} := 0.090klf$

Strands

Area of cross-section of one strand: $A_s := 0.294 \cdot in^2$

Bottom layer of strands: $n_1 := 11$ Top layer of strands: $n_2 := 7$

Total strands: $n_{str} := n_1 + n_2 = 18$

Total area of strands: $A_{ps} := n_{str} \cdot A_s = 5.292 \cdot in^2$

$$d_p := \frac{n_1 \cdot 2in + n_2 \cdot 4in}{n_{str}} = 2.778 \cdot in$$

$f_{pj} := 202.5ksi$ $E_{ps} := 28800 \cdot ksi$

Concrete bottom flange

$b_c := 24in$ $h_c := 6.5in$ $A_c := b_c \cdot h_c = 156 \cdot in^2$

$conc := 0.150 \cdot \frac{kip}{ft^3}$ $w_c := A_c \cdot conc = 0.162 \cdot klf$

PCSC girder:

Self weight: $w_{ow} := w_{steel} + w_c = 0.252 \cdot klf$

Span: $L := 80ft$

Transfer length: $l_1 := 0.7 \cdot 60in = 3.5 \cdot ft$

(2) Calculate self-weight moment and determine the value of load factor.

$$M_{sw} := \frac{1}{2}\cdot w_{ow}\cdot l_1\left(L - l_1\right) = 405.6\cdot kip\cdot in$$

M_{sw} counteracts the moment due to prestress: $\gamma_m := 0.9$ $\gamma_p := 1.2$

The concrete strength at release should be larger than 5 ksi: $\phi := 0.7$ $\alpha := 0.85$

(3) Start to design

- *Simplified method:*

Neutral axis should be located in the range: $h_c + t_f = 7.11\,in < c < h_c + h_s - t_f = 35.39\,in$

Try #1: $c := 29in$

$\varepsilon_{cu} := 0.003$ $\varepsilon_s := \frac{f_y}{E_s} = 0.00172$

$$\Delta\varepsilon_{ps} := \frac{c - d_p}{c}\cdot\varepsilon_{cu} = 0.00271$$

$$\varepsilon_{s1} := \frac{h_s + h_c - c}{c}\cdot\varepsilon_{cu} = 0.000724 < \varepsilon_s = 0.00172 \qquad d_{s1} := h_s + h_c - \frac{t_f}{2} = 35.695\cdot in$$

$$\varepsilon_{s2} := \frac{h_s + h_c - c - t_f}{c}\cdot\varepsilon_{cu} = 0.000661 < \varepsilon_s = 0.00172 \qquad d_{s2} := \frac{2\left(h_s + h_c - t_f\right) + c}{3} = 33.26\cdot in$$

$$\varepsilon_{s3} := \frac{c - h_c - t_f}{c}\cdot\varepsilon_{cu} = 0.002264 > \varepsilon_s = 0.00172 \qquad d_{s3} := \frac{c + 2\cdot\left(h_c + t_f\right)}{3} = 14.407\cdot in$$

$$\varepsilon_{s4} := \frac{c - h_c}{c}\cdot\varepsilon_{cu} = 0.002328 > \varepsilon_s = 0.00172 \qquad d_{s4} := h_c + \frac{t_f}{2} = 6.805\cdot in$$

$$f'_{cia} := \frac{A_{ps}\cdot\left(\frac{\gamma_p}{\phi}\cdot f_{pj} - \Delta\varepsilon_{ps}\cdot E_{ps}\right) - \frac{E_s\cdot t_w}{2}\cdot\left[\left(c - h_c - t_f\right)\cdot\varepsilon_s - \left(h_s + h_c - c - t_f\right)\cdot\varepsilon_{s2} + \frac{\left(b_f\cdot t_f\right)}{t_w}\cdot\left(2\cdot\varepsilon_s - \varepsilon_{s1} - \varepsilon_{s2}\right)\right]}{0.85\left(h_c\cdot b_c - A_{ps}\right)} = 7.85\cdot ksi$$

$$f'_{cib} := \frac{A_{ps}\cdot d_p\cdot\left(\frac{\gamma_p}{\phi}\cdot f_{pj} - \Delta\varepsilon_{ps}\cdot E_{ps}\right) + \frac{\gamma_m\cdot M_{sw}}{\phi} - \left[\frac{E_s\cdot t_w}{2}\cdot\left[\left(c - h_c - t_f\right)\cdot\varepsilon_s\cdot d_{s3} - \left(h_s + h_c - c - t_f\right)\cdot\varepsilon_{s2}\cdot d_{s2} + \frac{\left(b_f\cdot t_f\right)}{t_w}\cdot 2\cdot\varepsilon_s\cdot d_{s4} - \left(\varepsilon_{s1} + \varepsilon_{s2}\right)\cdot d_{s1}\right]\right]}{0.85\left(h_c\cdot b_c\cdot\frac{h_c}{2} - A_{ps}\cdot d_p\right)} = 9.84\cdot ksi$$

Try #2: $c := 29.7\cdot in$

$$\Delta\varepsilon_{ps} := \frac{c - d_p}{c}\cdot\varepsilon_{cu} = 0.00272$$

$\varepsilon_{s1} := \frac{h_s + h_c - c}{c} \cdot \varepsilon_{cu} = 0.000636$ $\quad < \quad \varepsilon_s = 0.00172$ $\quad d_{s1} := h_s + h_c - \frac{t_f}{2} = 35.695 \cdot in$

$\varepsilon_{s2} := \frac{h_s + h_c - c - t_f}{c} \cdot \varepsilon_{cu} = 0.000575$ $\quad < \quad \varepsilon_s = 0.00172$ $\quad d_{s2} := \frac{2(h_s + h_c - t_f) + c}{3} = 33.493333 \cdot in$

$\varepsilon_{s3} := \frac{c - h_c - t_f}{c} \cdot \varepsilon_{cu} = 0.002282$ $\quad > \quad \varepsilon_s = 0.00172$ $\quad d_{s3} := \frac{c + 2 \cdot (h_c + t_f)}{3} = 14.64 \cdot in$

$\varepsilon_{s4} := \frac{c - h_c}{c} \cdot \varepsilon_{cu} = 0.002343$ $\quad > \quad \varepsilon_s = 0.00172$ $\quad d_{s4} := h_c + \frac{t_f}{2} = 6.805 \cdot in$

$$f'_{cia} := \frac{A_{ps} \cdot \left(\frac{\gamma_p}{\phi} \cdot f_{pj} - \Delta\varepsilon_{ps} \cdot E_{ps}\right) - \frac{E_s \cdot t_w}{2} \cdot \left[(c - h_c - t_f) \cdot \varepsilon_s - (h_s + h_c - c - t_f) \cdot \varepsilon_{s2} + \frac{(b_f \cdot t_f)}{t_w} \cdot (2 \cdot \varepsilon_s - \varepsilon_{s1} - \varepsilon_{s2})\right]}{0.85(h_c \cdot b_c - A_{ps})} = 7.6 \cdot ksi$$

$$f'_{cib} := \frac{A_{ps} \cdot d_p \cdot \left(\frac{\gamma_p}{\phi} \cdot f_{pj} - \Delta\varepsilon_{ps} \cdot E_{ps}\right) + \frac{\gamma_m \cdot M_{sw}}{\phi} - \left[\frac{E_s \cdot t_w}{2} \cdot \left[(c - h_c - t_f) \cdot \varepsilon_s \cdot d_{s3} - (h_s + h_c - c - t_f) \cdot \varepsilon_{s2} \cdot d_{s2} + \frac{(b_f \cdot t_f)}{t_w} \cdot 2 \cdot \varepsilon_s \cdot d_{s4} - (\varepsilon_{s1} + \varepsilon_{s2}) \cdot d_{s1}\right]\right]}{0.85\left(h_c \cdot b_c \cdot \frac{h_c}{2} - A_{ps} \cdot d_p\right)} = 7.53 \cdot ksi$$

Try #3: $c := 29.675in$

$\Delta\varepsilon_{ps} := \frac{c - d_p}{c} \cdot \varepsilon_{cu} = 0.00272$

$\varepsilon_{s1} := \frac{h_s + h_c - c}{c} \cdot \varepsilon_{cu} = 0.000639$ $\quad < \quad \varepsilon_s = 0.00172$ $\quad d_{s1} := h_s + h_c - \frac{t_f}{2} = 35.695 \cdot in$

$\varepsilon_{s2} := \frac{h_s + h_c - c - t_f}{c} \cdot \varepsilon_{cu} = 0.000578$ $\quad < \quad \varepsilon_s = 0.00172$ $\quad d_{s2} := \frac{2(h_s + h_c - t_f) + c}{3} = 33.485 \cdot in$

$\varepsilon_{s3} := \frac{c - h_c - t_f}{c} \cdot \varepsilon_{cu} = 0.002281$ $\quad > \quad \varepsilon_s = 0.00172$ $\quad d_{s3} := \frac{c + 2 \cdot (h_c + t_f)}{3} = 14.632 \cdot in$

$\varepsilon_{s4} := \frac{c - h_c}{c} \cdot \varepsilon_{cu} = 0.002343$ $\quad > \quad \varepsilon_s = 0.00172$ $\quad d_{s4} := h_c + \frac{t_f}{2} = 6.805 \cdot in$

$$f'_{cia} := \frac{A_{ps} \cdot \left(\frac{\gamma_p}{\phi} \cdot f_{pj} - \Delta\varepsilon_{ps} \cdot E_{ps}\right) - \frac{E_s \cdot t_w}{2} \cdot \left[(c - h_c - t_f) \cdot \varepsilon_s - (h_s + h_c - c - t_f) \cdot \varepsilon_{s2} + \frac{(b_f \cdot t_f)}{t_w} \cdot (2 \cdot \varepsilon_s - \varepsilon_{s1} - \varepsilon_{s2})\right]}{0.85(h_c \cdot b_c - A_{ps})} = 7.61 \cdot ksi$$

$$f'_{cib} := \frac{A_{ps} \cdot d_p \cdot \left(\frac{\gamma_p}{\phi} \cdot f_{pj} - \Delta\varepsilon_{ps} \cdot E_{ps}\right) + \frac{\gamma_m \cdot M_{sw}}{\phi} - \left[\frac{E_s \cdot t_w}{2} \cdot \left[(c - h_c - t_f) \cdot \varepsilon_s \cdot d_{s3} - (h_s + h_c - c - t_f) \cdot \varepsilon_{s2} \cdot d_{s2} + \frac{(b_f \cdot t_f)}{t_w} \cdot 2 \cdot \varepsilon_s \cdot d_{s4} - (\varepsilon_{s1} + \varepsilon_{s2}) \cdot d_{s1}\right]\right]}{0.85\left(h_c \cdot b_c \cdot \frac{h_c}{2} - A_{ps} \cdot d_p\right)} = 7.61 \cdot ksi$$

Concrete strength at release: $\quad f'_{ci} := \frac{(f'_{cia} + f'_{cib})}{2} = 7.61 \cdot ksi$

- *Closed form method:*

$\varepsilon_{cu} := 0.003$ $\qquad$ $\varepsilon_s := \frac{f_y}{E_s} = 0.00172$

$w_1 := h_c \cdot b_c - A_{ps} = 150.708 \cdot in^2$

$w_2 := \frac{1}{2} \cdot h_c^{\,2} \cdot b_c - A_{ps} \cdot d_p = 492.3 \cdot in^3$

$r_1 := A_{ps} \cdot E_{ps} \cdot \varepsilon_{cu} \cdot h_c \cdot b_c \cdot d_p \cdot \left(d_p - \frac{1}{2} \cdot h_c\right) = -93562.6 \cdot kip \cdot in^4$

$r_2 := \frac{1}{2} \cdot E_s \cdot \varepsilon_{cu} \cdot t_w \cdot \left[w_2 \cdot t_f \cdot (2 \cdot h_c + 2h_s - t_f) - (h_c + h_s)^2 + w_1 \cdot \left[\frac{2}{3} \cdot h_c^{\,3} + h_s^{\,3} - t_f^{\,3} + (h_c + h_s) \cdot 2h_c \cdot h_s + 2 \cdot t_f^{\,2} - 2\, t_f \cdot (h_c + h_s)^2\right]\right] = 7.84 \times 10^7 \cdot kip \cdot in$

$r_3 := \frac{1}{2} \cdot E_s \cdot \varepsilon_{cu} \cdot b_f \cdot t_f \cdot \left[w_2 \cdot (-2 \cdot h_c - 2 \cdot h_s + t_f) + w_1 \cdot \left[2 \cdot (h_c + h_s)^2 - t_f \cdot \left(2h_c + 2 \cdot h_s - \frac{1}{2} \cdot t_f\right)\right]\right] = 9.628 \times 10^7 \cdot kip \cdot in^4$

$r_4 := \frac{1}{2} \cdot E_s \cdot t_w \cdot \left[w_2 \cdot 2 \cdot \varepsilon_{cu} \cdot (h_c + h_s - t_f) - \varepsilon_s \cdot (h_c + t_f) + w_1 \cdot \left[\varepsilon_{cu} \cdot -(h_c + h_s)^2 + t_f \cdot (2 \cdot h_c + 2 \cdot h_s - t_f) + \frac{2}{3} \cdot \varepsilon_s \cdot (h_c + t_f)^2\right]\right] = -3.128 \times 10^6 \cdot kip \cdot in^3$

$r_5 := \frac{-r_1}{d_p} + \frac{1}{2} \cdot E_s \cdot b_f \cdot t_f \cdot 2 \cdot w_2 \cdot (\varepsilon_{cu} + \varepsilon_s) + w_1 \cdot -2 \cdot h_c \cdot (\varepsilon_{cu} + \varepsilon_s) - 2 \cdot h_s \cdot \varepsilon_{cu} + t_f \cdot (\varepsilon_{cu} - \varepsilon_s) = -2.833 \times 10^6 \cdot kip \cdot in^3$

$A := \frac{1}{6} \cdot w_1 \cdot E_s \cdot t_w \cdot (\varepsilon_{cu} - \varepsilon_s) = 436.802 \cdot kip \cdot in$

$B := -\frac{1}{2} \cdot E_s \cdot t_w \cdot \left[w_2 \cdot (\varepsilon_{cu} - \varepsilon_s) + \frac{1}{3} \cdot w_1 \cdot \varepsilon_s \cdot (h_c + t_f)\right] = -8.477 \times 10^3 \cdot kip \cdot in^2$

$C := r_4 + r_5 - w_2 \cdot \frac{\gamma_p \cdot A_{ps} \cdot f_{pj}}{\phi} + w_1 \cdot \frac{\gamma_p \cdot A_{ps} \cdot f_{pj} \cdot d_p + \gamma_m \cdot M_{sw}}{\phi} = -6.018 \times 10^6 \cdot kip \cdot in^3$

$D := r_1 + r_2 + r_3 = 1.746 \times 10^8 \cdot kip \cdot in^4$

$p := 9 \cdot A \cdot C - 3B^2 = -2.387 \times 10^{10} \cdot in^4 kip^2$

$q := 2B^3 - 9A \cdot B \cdot C + 27A^2 \cdot D = 6.979 \times 10^{14} \cdot in^6 \cdot kip^3$

$U := \frac{-q}{2} \cdot \sqrt{\left(\frac{3}{-p}\right)^3} = -0.492$

Due to $p < 0$ and $U = 0.492$ <1 Use Eq. (5.50d) to calculate *c*.

$$c_1 := \frac{1}{3A}\cdot\left(2\cdot\sqrt{\frac{p}{3}}\cdot\cos\left(\frac{1}{3}\cdot\mathrm{acos}(U)\right) - B\right) = 111.049\cdot in \quad < \quad h := h_s + h_c = 36\cdot in \quad \text{NG}$$

$$c_2 := \frac{1}{3A}\cdot\left(2\cdot\sqrt{\frac{p}{3}}\cdot\cos\left(\frac{1}{3}\cdot\mathrm{acos}(U) + \frac{2\pi}{3}\right) - B\right) = -121.317\cdot in \quad >0 \quad \text{OK}$$

$$c_3 := \frac{1}{3A}\cdot\left(2\cdot\sqrt{\frac{p}{3}}\cdot\cos\left(\frac{1}{3}\cdot\mathrm{acos}(U) + 2\cdot\frac{2\pi}{3}\right) - B\right) = 29.68\cdot in \quad < \quad h := h_s + h_c = 36\cdot in$$

$$c := c_3 = 29.676\cdot in$$

$$\Delta\varepsilon_{ps} := \frac{c - d_p}{c}\cdot\varepsilon_{cu} = 0.00272$$

$$\varepsilon_{s1} := \frac{h_s + h_c - c}{c}\cdot\varepsilon_{cu} = 0.000639 \quad < \quad \varepsilon_s = 0.00172 \qquad d_{s1} := h_s + h_c - \frac{t_f}{2} = 35.695\cdot in$$

$$\varepsilon_{s2} := \frac{h_s + h_c - c - t_f}{c}\cdot\varepsilon_{cu} = 0.000578 \quad < \quad \varepsilon_s = 0.00172 \qquad d_{s2} := \frac{2\left(h_s + h_c - t_f\right) + c}{3} = 33.485365\cdot in$$

$$\varepsilon_{s3} := \frac{c - h_c - t_f}{c}\cdot\varepsilon_{cu} = 0.002281 \quad > \quad \varepsilon_s = 0.00172 \qquad d_{s3} := \frac{c + 2\cdot\left(h_c + t_f\right)}{3} = 14.632\cdot in$$

$$\varepsilon_{s4} := \frac{c - h_c}{c}\cdot\varepsilon_{cu} = 0.002343 \quad > \quad \varepsilon_s = 0.00172 \qquad d_{s4} := h_c + \frac{t_f}{2} = 6.805\cdot in$$

$$f'_{ci} := \frac{\frac{\gamma_p}{\phi}\cdot A_{ps}\cdot f_{pj} - A_{ps}\cdot\Delta\varepsilon_{ps}\cdot E_{ps} - E_s\cdot t_w\cdot\left[\left(c - h_c - t_f\right)\cdot\frac{\varepsilon_s}{2} - \left(h_s + h_c - c - t_f\right)\cdot\frac{\varepsilon_{s2}}{2} + \frac{b_f\cdot t_f}{t_w}\cdot\frac{\left(\varepsilon_s + \varepsilon_s - \varepsilon_{s1} - \varepsilon_{s2}\right)}{2}\right]}{0.85\cdot\left(h_c\cdot b_c - A_{ps}\right)} = 7.61\cdot ksi$$

Thus, the two methods give identical concrete strength at release:

$$f'_{ci} = 7.61\ ksi$$

(4) Design shear studs from end to transfer length

$f_p := 202.5ksi$

$P_i := f_p \cdot A_{ps} = 1071.6 \cdot kip$

$V_h := 1.2 \cdot P_i - \alpha \cdot f'_{ci} \cdot b_c \cdot h_c = 276.996\ kip$

7/8" shear studs: $Q_n := 36.08kip$

$\phi_{sc} := 0.85$ $Q_r := \phi_{sc} \cdot Q_n = 30.668 \cdot kip$

Number of studs: $N_h := \frac{V_h}{Q_r} = 9.032$ Transfer length: $l_1 = 3.5\,ft$

10 studs are required from end to transfer length.

(5) Check the design results:

$T_{s1} := b_f \cdot t_f \cdot E_s \cdot \frac{(\varepsilon_{s1} + \varepsilon_{s2})}{2} = 111.942 \cdot kip$

$C_{s3} := t_w \cdot (c - h_c - t_f) E_s \cdot \frac{\varepsilon_s}{2} = 265.152 \cdot kip$

$C_{s4} := b_f \cdot t_f \cdot E_s \cdot \varepsilon_s = 317.2 \cdot kip$

$C_c := 0.85 \cdot f'_{ci} \cdot h_c \cdot b_c = 1009 \cdot kip$

$C_{ps} := A_{ps} \cdot (\Delta\varepsilon_{ps} \cdot E_{ps} - 0.9 \cdot f'_{ci}) = 378.19 \cdot kip$

$R_P := \phi \cdot (C_c + C_{ps} + C_{s3} + C_{s4} - T_{s1} - T_{s2}) = 1285 \cdot kip$

$R_M := \phi \cdot \left(C_c \cdot \frac{h_c}{2} + C_{ps} \cdot d_p + C_{s3} \cdot d_{s3} + C_{s4} \cdot d_{s4} - T_{s1} \cdot d_{s1} - T_{s2} \cdot d_{s2} \right) = 328 \cdot kip \cdot ft$

$Q_{sP} := A_{ps} \cdot f_{pj} = 1071.6 \cdot kip$

$Q_{sM} := A_{ps} \cdot f_{pj} \cdot d_p = 2976.8 \cdot kip \cdot in$

$Q_{swM} := M_{sw} = 405.6 \cdot kip \cdot in$

$Q_{Pu} := \gamma_p \cdot Q_{sP} = 1286 \cdot kip$ equal to $R_P = 1285 \cdot kip$

$Q_{Mu} := \gamma_p \cdot Q_{sM} + \gamma_m \cdot Q_{swM} = 328 \cdot kip \cdot ft$ equal to $R_M = 328 \cdot kip \cdot ft$

Thus, the design is OK.

B.2 Service Design at Release

$y_{gbi} := 11.158in$ $\quad y_{gt} := 24.842in$ $\quad I_{gi} := 45620in^4$ $\quad A_{gi} := 320in^2$

$e_{mi} := y_{gbi} - d_p = 8.38 \cdot in$ $\quad y_{gs} := y_{gbi} - h_c = 4.658 \cdot in$ $\quad n_s := 4.784$

Stage 1 (At Release):

$M_{sw} = 405.641 \cdot kip \cdot in$ $\quad f_p := 202.5ksi$ $\quad P_i := f_p \cdot A_{ps} = 1071.6 \cdot kip$

For section at transfer length:

$$f_{bc} := \frac{P_i}{A_{gi}} + \frac{P_i \cdot e_{mi} \cdot y_{gbi}}{I_{gi}} - \frac{M_{sw} \cdot y_{gbi}}{I_{gi}} = 5.45 \cdot ksi \qquad < \quad 0.7f'_{ci} \quad \text{or} \quad 0.6f'_{ci}$$

$0.7f'_{ci}$: $\quad f'_{ci..} := \frac{f_{bc}}{0.7} = 7.8 \cdot ksi$ $\qquad 0.6f'_{ci}$: $\quad f'_{ci.} := \frac{f_{bc}}{0.6} = 9.1 ksi$

$$f_{bs} := n_s \cdot \left(\frac{P_i}{A_{gi}} + \frac{P_i \cdot e_{mi} \cdot y_{gs}}{I_{gi}} - \frac{M_{sw} \cdot y_{gs}}{I_{gi}} \right) = 20.21 \cdot ksi \qquad < \quad 0.7f_y = 35 \cdot ksi$$

$$f_t := \frac{P_i}{A_{gi}} - \frac{P_i \cdot e_{mi} \cdot y_{gt}}{I_{gi}} + \frac{M_{sw} \cdot y_{gt}}{I_{gi}} = -1.32 \cdot ksi \qquad < \quad 0.7f_y = 35 \cdot ksi$$